Chapter 7

Late-Stage Halogenation by MalA Experimental Section

7.1 Experimental Methods

7.1.1 M. graminicola *Genomic DNA Extraction and Sequencing*

The filamentous fungal strain *Malbranchea graminicola* was cultivated on a static 100 mL potato dextrose broth (PBD) medium for 10 days at 26ºC. The gDNA extraction and sequencing protocols are the same for that used in Li, et al.[2] and the Solexa genome sequencing was performed at the University of Michigan DNA Sequencing Core.

7.1.2 M. aurantiaca *cDNA Preparation*

Malbranchea aurantiaca was cultured for 15 days in PDB shaking at 160 rpm at 28°C. The Invitrogen Purelink RNA Mini Kit was used with the Plant and Fungal Tissue Processing protocol from the associated Rneasy Mini Handbook (2010) to isolate the RNA prior to treatment with Dnase. Invitrogen Superscript first strand synthesis was used with the Protoscript M-MuLV First Strand cDNA Synthesis Kit and protocol to generate the cDNA. malA was amplified from the cDNA template by PCR using the primers below and the following PCR cycle: (1) 94ºC for 2 minutes, (2) 98ºC for 10 seconds, (3) 66.3ºC for 30 seconds, (4) 68ºC for 2 minutes, repeating steps 2-4 40 times.

Primers

5′-GAGAGCTAGCATGGCGCCGACACCAAAGTATACGT-3′

5′-CATTAAGCTTCTATGCAGCTGGCCTGGTAGGGGTT-3′

7.1.3 Cloning of malA-pMCSG7

The *malA* PCR product was inserted into the *pMCSG7* vector by ligation independent cloning (LIC).[212] *Escherichia coli* XL1Blue cells were transformed with *malA-pMCSG7* for screening and plasmid maintenance. *malA*' – *pMCSG7* was prepared though site-directed mutagenesis as described below. The HpaC flavin reductase (*phaC* plasmid*)* was obtained from Prof. David Ballou (University of Michigan).[213]

7.1.4 M. aurantiaca *Growth and Extraction of Malbrancheamides*

The isolation and purification procedure was adapted from Martínez-Luis, et al.[5] Individual flasks of 75 mL potato dextrose broth were inoculated with 100 µL spore stock of *M. aurantiaca* and grown for three weeks, or until a white fungal mat was produced. Prior to the noticeably orange sporulation, the cultures were pulverized and extracted with dichloromethane. The crude extract was acid-base purified first with 1 M HCl, then neutralized with 2 M ammonium hydroxide to pH 9, and back extracted with dichloromethane. The extract was then purified by chiral HPLC on a Phenomenex Lux 5 µm Cellulose-3 250 x 10 mm column. The following HPLC time program was used for separation and purification of the malbrancheamide compounds: 50% acetonitrile for 18 minutes, gradient to 55% acetonitrile over 2 minutes, 55% acetonitrile for 2 minutes, gradient to 40% acetonitrile over 2 minutes, 40% acetonitrile for 5 minutes, at a flow rate of 4 mL/min. The mobile phase consisted of water and acetonitrile. From a 1.5 L growth of *M. aurantiaca*, we obtained the following yields of the naturally occurring malbrancheamides: 1.6 mg/L premalbrancheamide (^{1}H-NMR, 400 MHz, CD_3OD, ∂ 1.24 (s, 3H), 1.34 (s, 3H), 1.42 (m, 1H), 1.85 (m, 3H), 1.94 (d, J = 11.3 Hz, 1H), 1.99 (d, J = 12.8 Hz, 1H), 2.14 (m, 2H), 2.21 (d, J = 10.2 Hz, 1H), 2.78 (d, J = 15.2 Hz, 1H), 2.89 (d, J = 15.3 Hz, 1H), 3.01 (m, 1H), 3.42 (d, J = 10.4 Hz, 1H), 7.02 (t, J = 7.5 Hz, 1H), 7.07 (t, J = 7.6 Hz, 1H), 7.25 (d, J = 8.1 Hz, 1H), 7.35 (d, J = 7.7 Hz,

1H), 2.6 mg/L isomalbrancheamide B, 4.4 mg/L malbrancheamide B, and 5.8 mg/L malbrancheamide. NMR data tables for all compounds are included below.

7.1.5 Expression and Purification

7.1.5.1 Expression of malA, malA', malA/A' Mutants, and phaC

E. coli strain BL21 (DE3) was transformed with *malA-pMCSG7* and the *pGro7* chaperone plasmid set (GroEL/GroES) from Takara. Ampicillin (0.1 mg/mL), chloramphenicol (35 µg/mL), and L-arabinose (0.5 mg/mL) were added to 1 L of Terrific Broth (TB) media, which was then inoculated with the transformed *E. coli* cells. The 1 L cultures were grown at 37°C until an OD_{600} of 0.8 – 1.0 was reached, cooled at 20°C for one hour, induced with 0.1 mM isopropyl β-D-1-thiogalactopyranoside (IPTG), and expressed for 18 hours at 20°C.

E. coli strain BL21 (DE3) containing *pRARE* was transformed with *phaC-pET11a7*. Ampicillin (0.05 mg/mL) and spectinomycin (0.1 mg/mL) were added to 1 L of Terrific Broth (TB) media, which was then inoculated with the transformed *E. coli* cells. The 1 L cultures were grown at 37°C until an OD_{600} of 0.8 – 1.0 was reached, cooled at 20°C for one hour, induced with 0.2 mM isopropyl β-D-1-thiogalactopyranoside (IPTG), supplemented with 50 µM riboflavin and expressed for 18 hours at 20°C.

7.1.5.2 Expression of malA' for Selenomethionyl MalA'

450 mL selenomethionine medium (AthenaES) was supplemented with 25 mL TB media, and 150 µg/mL seleno-DL-methionine. Ampicillin (0.1 mg/mL), chloramphenicol (35 µg/mL), and L-arabinose (0.5 mg/mL) were added to the medium, which was then inoculated with the transformed *E. coli* cells. The cell cultures were grown at 37°C until an OD_{600} of 0.6 was reached, cooled at 20°C for one hour, induced with 0.1mM IPTG, and expressed for 18 hours at 20°C.

7.1.5.3 Protein Purification for Chlorination Assays and Large-Scale Reactions

The cell pellet from a 500 mL culture was re-suspended in 30 mL lysis $buffer_{NaCl}$ (10% (v/v) glycerol, 500 mM NaCl, 20 mM imidazole pH 7, 20 mM HEPES pH 7). The cell suspension was supplemented with 50 μM flavin adenine dinucleotide (FAD) and cells were lysed with 5 mg lysozyme, 2 mg Dnase, and 3 mM $MgSO_4$. Cell lysis was completed through sonication and cell waste was cleared through centrifugation (18,000 rpm for 25 minutes). The supernatant was filtered and MalA was purified through metal affinity chromatography on a 5 mL His-trap column (GE Healthcare) with a 10-column volume gradient of elution $buffer_{NaCl}$ (10% glycerol, 500 mM NaCl, 30-560mM imidazole pH 7, 20 mM HEPES pH 7). The protein was incubated on ice with 2mM ATP and 50 μM FAD and further purified by size exclusion chromatography on a Superdex S200 16/60 HiLoad column with storage $buffer_{NaCl}$ (10% glycerol, 300 mM NaCl, 20 mM HEPES pH 7) to remove the chaperone proteins. 20 mg purified MalA were obtained per 1 L of cell culture.

7.1.5.4 Protein Purification for Bromination Assays and Large-Scale Reactions

A cell pellet from a 500 mL expression culture was re-suspended in 30 mL lysis $buffer_{NaBr}$ (50 mM NaH_2PO_4, 10 mM imidazole pH 7, 300 mM NaBr, 10% glycerol) and supplemented with 50 μM FAD. Cell lysis was accomplished through addition of 5 mg lysozyme, 2 mg Dnase, and 3 mM $MgSO_4$ and sonication. Cell waste was cleared through centrifugation (18,000 rpm for 25 minutes), and the protein was purified through batch binding with 10 mL Ni-NTA Superflow resin (Qiagen). The resin-bound protein was washed with wash $buffer_{NaBr}$ (50 mM NaH_2PO_4, 20 mM imidazole pH 7, 300 mM NaBr, 10% glycerol) and the protein was eluted with elution $buffer_{NaBr}$ (50 mM NaH_2PO_4, 250 mM imidazole pH 7, 100 mM NaBr, 10% glycerol, 0.2 mM TCEP). Bromide-bound MalA was exchanged into storage $buffer_{NaBr}$ (50 mM NaH_2PO_4, 1 mM EDTA, 0.2 mM DTT, 10% glycerol, pH 7.3) on a PD-10 column (GE Healthcare).

7.1.5.5 Protein Purification for Crystallography

The initial steps of the purification were identical to those for the purification of MalA for chlorination assays. The His-tag was cleaved by TEV protease (1 mg protease/50 mg MalA) in an overnight dialysis with storage buffer$_{NaCl}$, supplemented with 50 μM FAD and 2 mM DTT. Tag-free MalA was separated from TEV protease and any remaining His$_6$-MalA by metal affinity chromatography, and purified by size exclusion chromatography with storage buffer$_{NaCl}$. 10 mg of pure MalA were obtained per 1 L of cell culture.

7.1.6 MalA Biochemical Activity Assays

Biochemical activity assays were performed in a 100 μL volume with the following components: 18 μM MalA, 54 μM HpaC flavin reductase,[213] 100 μM FAD, 50 mM NaCl, 250 μM substrate, 5 mM NADH, and filled to the total volume with reaction buffer (same as storage buffer$_{NaBr}$). The chlorination reactions proceeded for 20 minutes and the bromination reactions proceeded overnight. The reactions were extracted with ethyl acetate (200 μL, in triplicate) and dried down under nitrogen gas. The dried extract was re-suspended in LC/MS grade methanol to a concentration of around 10 μM for LC/MS analysis. High resolution mass spectrometry was performed using electrospray ionization on an Agilent quadrupole time-of-flight spectrometer (Q-TOF 6500 series). Biochemical activity was monitored via the following HPLC method using acetonitrile and water: 65% acetonitrile for 5 minutes, gradient over 10 minutes to 95% acetonitrile, 95% acetonitrile for 5 minutes, gradient over 2 minutes to 65% acetonitrile, 65% acetonitrile for 11 minutes to reequilibrate with a flow rate of 0.3 mL/min, monitoring at 240nm on a Phenomenex Lux cellulose-3, cellulose Tris (4-methylbenzoate) 250x4.6 mm column.

7.1.7 Co-crystallization of MalA'

7.1.7.1 MalA' Crystallization Conditions

MalA from *M. aurantiaca* was recalcitrant to crystallization, but MalA' from *M. graminicola* (generated by Site-directed mutagenesis of *malA*: L276P/R428P) proved optimal for crystallization. The purified MalA' was dialyzed overnight into a 20 mM HEPES pH 7 buffer with 200 mM NaCl or 300 mM NaCl to remove glycerol, and then supplemented with an equimolar quantity of FAD. Pre-incubation of MalA' with an equimolar concentration of isomalbrancheamide B resulted in crystals with the molecule bound in a lattice contact and not in the active site. For active site complexes with premalbrancheamide , malbrancheamide B, and isomalbrancheamide B, MalA' was pre-incubated with a four-fold molar excess of substrate. Crystals were grown by vapor diffusion from 1:2 mixtures of 5 mg/mL MalA' pre-incubated with one of the substrates and a well solution containing 2 M $(NH_4)_2SO_4$, 0.2 M Li_2SO_4, 5 mM $CdCl_2$, and 0.1 M Bis-Tris pH 5.5. Crystals were cryoprotected in well solution augmented with 10% glycerol and flash-cooled in liquid nitrogen.

7.1.7.2 Data Collection of MalA' Crystals

Data were collected at GM/CA beamline 23ID-B at the Advanced Photon Source (APS) at Argonne National Laboratory. For the SeMet-MalA' crystal, 180º of diffraction data were collected in inverse-beam geometry using 30º wedges. All data were processed using XDS.[214] The SeMet MalA' halogenase structure was solved by single-wavelength anomalous diffraction (SAD) using AutoSol in the Phenix suite to locate the Se sites, determine initial phases and perform density modification (figure of merit = 0.236).[215] AutoBuild in the Phenix suite was used to build an 82% complete starting model. The SeMet MalA model was used as a template in molecular replacement to solve the native MalA structure using Phaser in the Phenix suite. A progression of model building and refinement were carried out to complete the models using Coot and Phenix Refine with seven translation/libation/screw groups.[216]

7.1.8 Site-Directed Mutagenesis

7.1.8.1 MalA ‘ (MalA L276P/R428P)

The SDM to prepare the L276P/R428P double substitution was performed sequentially starting with R428P. The reaction included 100 ng *malA-pMCSG7* template, 100 ng each primer ($forward_{L276P}$ and $reverse_{L276P}$) 5 µL 10x Pfu buffer, 0.5 µL dNTPs (250 µM each), and 1 µL PfuTurbo from Agilent in a total of 50 µL. The PCR cycle was 1.) 95°C for 30 seconds, 2.) 95°C for 30 seconds, 3.) 55°C for 1 minute, 4.) 68°C for 8 minutes, and steps 2-4 were repeated for 16 cycles. DpnI digestion contained 0.5 µL 2 U/µL *DpnI* and 25 µL PCR reaction solution for 2 hours at 37°C and was performed prior to plasmid isolation by alkaline lysis (Purelink Quick Plasmid Miniprep Kit from Invitrogen) and sequencing to verify the presence of the mutant performed by the University of Michigan Sequencing Core. The L276P substitution was prepared using single primer SDM with 100 ng *malA* R428P template, 0.2 µM primer, 250 µM dNTPs, 5 µL 10x Pfu buffer, 1 µL Pfu fusion polymerase in a total volume of 50 µL. The PCR time program was as follows: 1.) 95°C for 3 minutes, 2.) 95°C for 35 seconds, 3.) 52°C for 50 seconds, 4.) 65°C for 13 minutes, 5.) 65°C for 15 minutes, steps 2-4 were repeated for 30 cycles. DpnI digestion and sequence analysis was performed in the same manner as described above.

Primers

$forward_{L276P}$ 5’-GCACAGCTTTCGCACCCAATTGTGGAGATTGGG-3’

$reverse_{L276P}$ 5’-CCCAATCTCCACAATTGGGTGCGAAAGCTGTGC-3’

R428P 5’-CGTCTACCCTCTTGGGAAGGGAGCCCCATAGCGAACTTGATGGATATGG-3’

7.1.8.2 MalA K108A

The *malA* K108A mutant was prepared using the *Quikchange Lightning Site-Directed Mutagenesis Kit* and protocol. The PCR time program used was 1.) 95°C for 2 minutes, 2.) 95°C

for 20 seconds, 3.) 55°C for 30 seconds, 4.) 65°C for 6 minutes, 5.) 65°C for 5 minutes, steps 2-4 were repeated for 30 cycles. The QCL DpnI digest and transformation protocol were used with XL10-Gold Ultracompetent cells.

Primer

5'-GTAAAAGCACAGCCCATCCGCGAGTCCGAATAGTCGAAGG-3'

7.1.8.3 All Other malA Mutants

The mutants were prepared using single primer SDM with 100 ng *malA* or *malA*' template, 0.2 µM primer, 250 µM dNTPs, 5 µL 10x Pfu buffer, 1 µL Pfu fusion polymerase in a total volume of 50 µL. The PCR time program was as follows: 1.) 95°C for 3 minutes, 2.) 95°C for 35 seconds, 3.) X°C (see below) for 50 seconds, 4.) 65°C for 13 minutes, 5.) 65°C for 15 minutes, steps 2-4 were repeated for 30 cycles. DpnI digestion and sequence analysis was performed in the same manner as described above.

Primers

Mutant	**Primer**	**X (°C)**
S409A	5'-GGTTTCACCAACCCGCTCTATGCCCCGGGGATTAATGTTGG-3'	50.0
S82A	5'-CCTGGTTACAAGATTGGCGAGGCGACTCTACCTATCTTTTACACCTGG-3'	50.8
E494A	5'-GGCAGTTTTTCGCTGGCATAGCGCGATATTTGTCAGATGTTAACATTGAAACC-3'	49.0
E494Q	5'-GGCAGTTTTTCGCTGGCATACAGCGATATTTGTCAGATGTTAACATTGAAACC-3'	49.0
W263A	5'-CCACCTGTGTTTTCCGGAAGGTGCTGTCTGGGTTATTCGTCTACCCTCTTGGG-3'	55.0
W265A	5'-CCACCTGTGTTTTCCGGAAGGTTGGGTCGCGGTTATTCGTCTACCCTCTTGGG-3'	55.0
H253A	5'-CCCTTTGATCTCTATGAAGGTGATGCGACAAACCACCTGTGTTTTCC-3'	48.0
F489H	5'-CCCCAGGTGGCATGCCTCTGGCAGCATTTCGCTGGCATAGAGCG-3'	55.0
C613S/ C616S	5'-CCGCCCAGATTGGAAAAAGTCTCACTCATCTGGTCTTCTGGGCACCG-3'	49.0
C112S	5'- GGACTCAAGGATGGGCTGTCTTTTTACTTTCTTGATCGAGAGAACC-3'	49.6
C128S	5'- GGGGCAGTACACAGACTTCTCTAGTGTTGGGGCTCCAGGTTTGG-3'	53.7
E494D	5'-GGCAGTTTTTCGCTGGCATAGATCGATATTTGTCAGATGTTAACATTGAAACC-3'	50.0
H253F	5'-CCCTTTGATCTCTATGAAGGTGATTTTACAAACCACCTGTGTTTTCC-3'	48.0
S129A	5'-GGGGCAGTACACAGACTTCTGCGCGGTTGGGGCTCCAGGTTTGG-3'	55.0
D129A	5'-CCTTCGACTATTCGGACTCAAGGCGGGGCTGTGCTTTTACTTTCTTGATCG-3'	50.0

7.1.9 MalA Large-Scale Reactions and Isolation of Products

7.1.9.1 Chlorination Reaction Conditions and Extraction

Reactions were run in 1 mL aliquots with 90 µM MalA, 54 µM HpaC flavin reductase, 250 µM **2** 100 µM FAD, 50 mM NaCl, 5 mM NADH, and filled to the total volume with reaction buffer (same as storage $buffer_{NaBr}$). Reactions were extracted after 20 minutes with 2 mL ethyl acetate in triplicate, dried under nitrogen gas, and re-suspended in methanol for HPLC purification. In a 5.1 mg reaction, 1.7 mg malbrancheamide B, 1.3 mg isomalbrancheamide B, and 1.2 mg malbrancheamide were isolated.

7.1.9.2 Bromination Reaction Conditions and Extraction

Reactions were run in 1 mL aliquots with 40 µM MalA, 54 µM HpaC flavin reductase, 250 µM **2**, 100 µM FAD, 50 mM NaBr, 5 mM NADH, and filled to the total volume with reaction buffer (same as storage $buffer_{NaBr}$). Reactions were extracted after 12 hours with 2 mL ethyl acetate in triplicate, dried under nitrogen gas, and resuspended in methanol for HPLC purification. In a 3.7 mg reaction with substrate premalbrancheamide, 0.9 mg malbrancheamide C and 0.7 mg isomalbrancheamide C were isolated. In a 2 mg reaction with malbrancheamide B, 480 µg malbrancheamide D were isolated**.** In a 2 mg reaction of isomalbrancheamide B 300 µg isomalbrancheamide D were isolated.

7.1.9.3 HPLC Purification

The malbrancheamide B, isomalbrancheamide B, and malbrancheamide products were purified using the same chiral HPLC method as for purification of the fungal extract. The malbrancheamide C, isomalbrancheamide C, malbrancheamide D, and isomalbrancheamide D products were isolated using chiral HPLC with the previously mentioned semi-preparative

cellulose column with the following HPLC time program: 70% acetonitrile for 14 minutes, gradient to 60% acetonitrile over 2 minutes at a flowrate of 4 mL/min.

7.1.10 Michaelis-Menten Model Kinetics

7.1.10.1 *Substrates Malbrancheamide B and Isomalbrancheamide B to Product Malbrancheamide*

Reactions were set up in a total volume of 250 µL with the following components: 1.1 µM MalA, 44 µM HpaC flavin reductase, 100 µM FAD, 50 mM NaCl, 3.6 mM NADH, and a variety of substrate concentrations ranging from 1 µM to 60 µM. Reactions were quenched with methanol by removing 50 µL at each time point (2, 5, 10, 15 minutes). Reactions were analyzed on a Schimadzu HPLC with the following LC time program: 40% acetonitrile for 1 minute, gradient over 6 minutes from 40-85% acetonitrile, 85% acetonitrile for 1 minute, gradient over 1 minute to 40% acetonitrile, re-equilibration to 40% acetonitrile for 3 minutes. The absorbance was measured at 240 nm and the mobile phase consisted of water and acetonitrile. A Phenomenex Lux cellulose-3, cellulose Tris (4-methylbenzoate) 250x4.6 mm column was used for separation. GraphPad Prism (Version 6.01) software was used to plot the initial velocities against the substrate concentration and to determine the kinetic constants k_{cat} and K_m.

7.1.10.2 *Substrate Premalbrancheamide toProducts Isomalbrancheamide B and Malbrancheamide B.*

Reactions were set up in a total volume of 250 µL with the following components: 1.8 µM MalA, 44 µM HpaC, 100 µM FAD, 50 mM NaCl, 3.6 mM NADH, and a variety of substrate concentrations ranging from 5 µM to 80 µM. Reactions were quenched with 100 µL methanol by removing 50 µL at each time point (2, 5, 7, 10 minutes). Reactions were analyzed on a Schimadzu HPLC with the following LC time program: 34% acetonitrile for 1 minute, gradient over 11 minutes to 62% acetonitrile, 62% acetonitrile for 30 seconds, gradient over 30 seconds to 34%

acetonitrile, re-equilibration to 34% for 3 minutes. The absorbance was measured at 240 nm and the mobile phase consisted of water and acetonitrile. A Phenomenex Lux cellulose-3 Tris (4-methylbenzoate) 250x4.6 mm column was used for separation.

7.1.11 Density Functional Theory Calculations

DFT calculations were performed using Gaussian 09 (Revision D.01).[217] All geometries were optimized using M06-2X,[218] within the CPCM polarizable conductor model (diethylether, ε = 4),[219, 220] and the 6-31G(d) basis set. Single point energies were calculated using the same DFT functional and solvation model, and the 6-311++G(d,p) basis set. The resulting energies were used to correct the gas phase energies obtained from the M06-2X/6-31G(d) optimizations.[221] Enthalpies and entropies were calculated for 1 atm and 298.15 K. All stationary points were verified as minima or first-order saddle points by a vibrational frequency analysis. The use of a dielectric constant ε=4 has been proved to be a good and general model to account for electronic polarization and small backbone fluctuations in enzyme active sites to have an estimation of the dielectric permittivity in the enzyme active site.[222, 223] Computed structures are illustrated with CYLView.[224]

7.1.12 Molecular Dynamics Simulations

Molecular dynamics (MD) simulations were performed using the GPU code (*pmemd*)[225] of the AMBER 16 package.[226] Parameters for intermediate Cl-K and substrates were generated within the *antechamber* module using the general AMBER force field (*gaff*),[227] with partial charges set to fit the electrostatic potential generated at the HF/6-31G(d) level by the RESP model.[228] The charges were calculated according to the Merz–Singh–Kollman scheme[229, 230] using the Gaussian 09 package.[217] Each protein was immersed in a pre-equilibrated truncated cuboid box with a 10 Å buffer of TIP3P[231] water molecules using the *leap* module, resulting in the addition of around 15,000 solvent molecules. The systems were neutralized by addition of explicit counter ions (Na^+

and Cl^-). All subsequent calculations were done using the widely tested Stony Brook modification of the Amber99 force field (*ff99sb*).[232] A two-stage geometry optimization approach was performed. The first stage minimizes the positions of solvent molecules and ions imposing positional restraints on the solute by a harmonic potential with a force constant of 500 $kcal \cdot mol^{-1} \cdot Å^{-2}$ and the second stage minimizes all the atoms in the simulation cell except those involved in the harmonic distance restraint. The systems were gently heated using six 50 ps steps, incrementing the temperature by 50 K for each step (0–300 K) under constant-volume and periodic-boundary conditions. Water molecules were treated with the SHAKE algorithm such that the angle between the hydrogen atoms was kept fixed. Long-range electrostatic effects were modelled using the particle-mesh-Ewald method.[233] An 8 Å cutoff was applied to Lennard–Jones and electrostatic interactions. Harmonic restraints of 30 $kcal \cdot mol^{-1}$ were applied to the solute and the Andersen equilibration scheme was used to control and equalize the temperature. The time step was kept at 1 fs during the heating stages, allowing potential inhomogeneities to self-adjust. Each system was then equilibrated for 2 ns with a 2 fs time step at a constant volume. Production trajectories were then run for an additional 500 ns under the same simulation conditions.

7.2 Tables

Table 7.1 MalA' crystallographic information.

Data collection	SeMet	Wild-type MalA'			H253A MalA'	
	pH 5.5	Premalbranch-eamide **(1.14)**	Malbranch-eamide B **(1.15)**	Isomalbranch-eamide B (**1.16**)	Premalbranch-eamide **(1.14)**	Malbranch-eamide B **(1.15)**
space group	*I 2 2 2*	*I 2 2 2*	*I 2 2 2*	*I 2 2 2*	*I 2 2 2*	*I 2 2 2*
cell dimensions						
a, b, c (Å)	79.6, 120.6, 170.4	79.3, 120.6, 170.4	79.4, 120.9, 170.9	79.1, 120.7, 170.9	79.2, 120.5, 170.3	79.2, 120.4, 170.2
X-ray source	APS 23ID-B	APS 23ID-B	APS 23ID-B	APS 23ID-B	APS 23ID-B	APS 23ID-B
wavelength (Å)	0.979	1.033	1.033	1.033	1.033	1.033
d_{min} (Å)	2.50 (2.60-2.50)	2.36 (2.45-2.36)	2.09 (2.17-2.09)	2.04 (2.11-2.04)	2.09 (2.17-2.09)	1.97 (2.04-1.97)
R-merge	0.137 (2.057)	0.106 (1.110)	0.088 (1.022)	0.078 (1.234)	0.072 (1.007)	0.081 (1.072)
avg I/σ (I)	15.5 (1.3)	14.1 (1.9)	15.3 (1.9)	15.7 (1.4)	16.6 (1.8)	14.9 (1.8)
completeness (%)	100 (99)	99 (98)	100 (100)	100 (99)	100 (99)	100 (99)
multiplicity	13.5 (13.6)	6.8 (7.1)	6.8 (6.8)	6.7 (6.7)	6.8 (6.6)	6.8 (6.6)
total observations	386,201	230,043	329,858	351,300	327,347	
$CC_{1/2}$	0.999 (0.643)	0.998 (0.690)	0.999 (0.772)	0.999 (0.581)	0.999 (0.703)	0.999 (0.728)
CC*		1 (0.90)	1 (0.93)	1 (0.86)	1 (0.91)	1 (0.92)
refinement						
data range (Å)		39.64-2.36	46.29-2.09	46.18-2.04	46.14-2.09	46.14-1.97
reflections (#)		33,618 (3,260)	48,823 (4,818)	52,106 (5,100)	48,221 (4,699)	57,508 (5,644)
R_{work}/R_{free} (%)		14.9/20.4	16.1/20.2	16.5/20.6	16.2/20.5	16.3/19.8
non-hydrogen atoms (#)		5,785	5,870	5,837	5,827	5,950
macromolecules		5,248	5,248	5,248	5,243	5,243
ligands		139	151	161	144	166
water		397	470	427	439	540
amino acid residues		664	664	664	664	664
deviation from ideality						
bond lengths (Å)		0.006	0.005	0.006	0.006	0.005
bond angles (deg)		0.77	0.72	0.75	0.78	0.74
average B-factor (Å^2)						
protein		49.7	40.5	44.7	45.5	37.1
ligands						
FAD		37.4	28.2	32.6	34.7	27.3
substrate		66.0	55.4	75.4	49.8	40.7
solvent		56.6	45.4	47.9	50.3	44.1
Ramachandran plot						
favored (%)		96.8	97.3	97.1	97.3	97.1
allowed (%)		3.2	2.6	2.9	2.6	2.7
outliers (%)		0	0.1	0	0.1	0.2
PDB		5WGR	5WGW	5WGZ	5WGT	5WGX

Table 7.1 MalA' crystallographic information continued.

Data collection	H253F MalA'	C112S/C128S MalA'		E494D MalA'
	Premalbranch-eamide **(1.14)**	Premalbranch-eamide **(1.14)**	Malbranch-eamide B **(1.15)**	Premalbranch-eamide **(1.14)**
space group	*I 2 2 2*	*I 2 2 2*	*I 2 2 2*	*I 2 2 2*
cell dimensions				
a, b, c (Å)	79.5, 121.2, 170.1	79.4 120.7 170.0	79.3 120.8 170.3	79.6 121.3 170.6
X-ray source	APS 23ID-B	APS 23ID-B	APS 23ID-B	APS 23ID-B
wavelength (Å)	1.033	1.033	1.033	1.033
d_{min} (Å)	2.34 (2.42-2.34)	2.30 (2.38-2.30)	2.00 (2.07-2.00)	2.05 (2.13-2.05)
R-merge	0.159 (1.681)	0.115 (1.227)	0.079 (1.369)	0.110 (1.146)
avg I/σ (I)	11.6 (1.2)	13.4 (1.6)	16.0 (1.4)	12.3 (1.3)
completeness (%)	100 (99)	100 (100)	100 (100)	100 (97)
multiplicity	6.5 (6.9)	6.8 (6.8)	6.8 (6.9)	6.5 (5.7)
total observations	226,608	251,217	378,655	337,456
$CC_{1/2}$	0.997 (0.523)	0.998 (0.665)	0.999 (0.548)	0.998 (0.592)
CC*	1 (0.83)	1 (0.89)	1 (0.84)	1 (0.86)
refinement				
data range (Å)	46.17-2.34	49.21-2.30	46.26-2.00	49.43-2.05
reflections (#)	34,994 (3,426)	36,680 (3,609)	55,522 (5,464)	51,793 (4,956)
R_{work}/R_{free} (%)	17.71/23.32	16.4/21.5	16.1/20.6	16.3/19.8
non-hydrogen atoms (#)	5,722	5,742	5,871	5,871
macromolecules	5,249	5,248	5,248	5,247
ligands	139	138	155	154
water	334	355	467	469
amino acid residues	664	664	664	664
deviation from ideality				
bond lengths (Å)	0.006	0.006	0.012	0.008
bond angles (deg)	0.83	0.77	1.12	0.91
average B-factor (Å^2)				
protein	54.4	52.2	40.9	40.2
ligands				
FAD	38.4	38.3	28.8	27.1
substrate	84.4	84.6	45.2	52.3
solvent	51.2	51.7	45.5	45.2
Ramachandran plot				
favored (%)	96.2	96.5	96.7	97.3
allowed (%)	3.6	3.2	3.1	2.7
outliers (%)	0.2	0.3	0.2	0
PDB	5WGS	5WGV	5WGY	5WGU

Table 7.2 Kinetic parameters and standard deviation for MalA chlorination reactions.

Reaction	k_{cat} **(min^{-1})**	K_m **(μM)**	k_{cat}/K_m **(min^{-1}mM^{-1})**
Premalbrancheamide to malbrancheamide B	0.08 +/- 0.05	7.0 +/- 2.9	11.49 +/- 0.02
premalbrancheamide to isomalbrancheamide B	0.09 +/- 0.05	7.5 +/- 2.9	12.02 +/- 0.02
malbrancheamide B to malbrancheamide	0.12 +/- 0.03	4.4 +/- 1.1	27.33 +/- 0.03
isomalbrancheamide B to malbrancheamide	0.12 +/- 0.03	4.0 +/- 0.8	29.70 +/- 0.04

Table 7.3 ^{1}H-NMR data for malbrancheamide B (**1.15**) fungal and *in vitro* samples. HRMS (ESI-QTOF): *m/z* $[M+H]^+$ calculated for $C_{21}H_{24}ClN_3O$ = 370.1681, experimental (*in vitro*) 370.1675.

Malbrancheamide B $(CD_3)_2SO$-d_6	Fungal	*in vitro*
Position	∂ ^{1}H (*J* [Hz])	∂ ^{1}H (*J* [Hz])
1	2.47m	2.46m
	1.34m	1.33m
2	1.75m	1.74m
3	2.97m	2.95m
	2.43m	2.42m
5	2.16 (d, 9.6)	2.15 (d, 9.9)
	3.29 (d, 9.9)	3.29 (d, 10.0)
6	2.77s	2.76s
7	7.33 (d, 8.4)	7.33 (d, 8.3)
8	6.96 (dd, 8.4, 1.9)	6.96 d (8.3)
10	7.28s	7.27s
12a	1.89 (d, 13.0)	1.90 (d, 12.9)
13	1.83 (dd, 13.0, 4.8)	1.82 (13.0, 4.4)
	1.91m	1.90m
16	1.27s	1.27s
17	1.33s	1.33s

Table 7.4 ^{1}H-NMR data for fungal and *in vitro* isomalbrancheamide B (**1.16**). HRMS (ESI-QTOF): *m/z* $[M+H]^+$ calculated for $C_{21}H_{24}ClN_3O$ = 370.1681, experimental (*in vitro*) 370.1685.

Isomalbrancheamide B $(CD_3)_2SO$-d_6	Fungal	*in vitro*
Position	∂ ^{1}H (*J* [Hz])	∂ ^{1}H (*J* [Hz])
1	2.45m	2.46m
	1.34m	1.34m
2	1.75m	1.74m
3	2.95m	2.95m
	2.42m	2.43m
5	2.16 (d, 10.0)	2.15 (d, 9.3)
	3.29 (10.0)	3.28 (d, 9.9)
6	2.76s	2.76s
7	7.34s	7.34s
9	7.03 (dd, 8.5, 2.0)	7.03 (dd, 8.5, 2.0)
10	7.29 (d, 8.5)	7.28 (d, 8.5)
12a	2.07m	2.05m
13	1.91 (d, 13.0)	1.90 (d, 12.7)
	1.81 (dd, 13.0, 4.9)	1.81 (dd, 13.4, 5.0)
16	1.27s	1.27s
17	1.34s	1.33s

Table 7.5 ^{1}H-NMR data for fungal and *in vitro* malbrancheamide (**1.17**). HRMS (ESI-QTOF): *m/z* $[M+H]^+$ calculated for $C_{21}H_{23}Cl_2N_3O$ = 404.1291, experimental (*in vitro*) 404.1287.

Malbrancheamide CD_3OD	Fungal	*in vitro*
Position	∂ ^{1}H (*J* [Hz])	∂ ^{1}H (*J* [Hz])
1	2.56m	2.54m
	1.49m	1.49m
2	1.87m	1.89m
3	2.03m	2.04m
	2.19m	2.19m
5	2.27 (dd, 10.3, 1.5)	2.28 (d, 10.3)
	3.43 (d, 10.2)	3.45 (d, 10.4)
6	2.84s	2.85 (d, 3.6)
7	7.48	7.49s
10	7.40	7.40s
12a	2.13m	2.15m
13	2.03 (d, 13.1)	2.03 (d, 13.2)
	1.96 (dd, 13.1, 5.2)	1.97 (dd, 13.2, 4.8)
16	1.32s	1.34s
17	1.42s	1.43s

Table 7.6 ^{1}H-NMR and ^{13}C-NMR data for *in vitro* malbrancheamide C (**1.92**). HRMS (ESI-QTOF): *m/z* $[M+H]^{+}$ calculated for $C_{21}H_{24}BrN_3O$ = 414.1176, experimental (*in vitro*) 414.1169.

Malbrancheamide C (*in vitro*) CD_3OD		
Position	∂ ^{13}C	∂ ^{1}H (*J* [Hz])
1	28.3	2.53 (ddd, 12.0, 9.0, 5.5)
		1.47m
2	23.7	1.89m
3	55.5	3.06m
		2.18m
5	59.6	3.45 (d, 9.8)
		2.26 (dd, 11.9, 1.6)
5a	57.7	
6	30.4	2.87 (d, 9.7)
6a	105.1	
6b	127.3	
7	199.9	7.26 (d, 10.4)
8	122.8	7.07 (dd, 11.4, 1.8)
9	115.4	
10	114.6	7.42 (d, 1.8)
10a	139.4	
11		
11a	143.5	
12	35.6	
12a	48.8	2.16m
13	32.7	2.01 (dd, 13.1, 11.1)
		1.96 (dd, 13.3, 5.0)
13a	66.3	
14	176.8	
15		
16	30.9	1.34s
17	24.2	1.43s

Table 7.7 ^{1}H-NMR and ^{13}C-NMR data for *in vitro* isomalbrancheamide C (**1.93**). HRMS (ESI-QTOF): *m/z* $[M+H]^+$ calculated for $C_{21}H_{24}BrN_3O$ = 414.1176, experimental (*in vitro*) 414.1179.

isomalbrancheamide C (*in vitro*) CD_3OD		
position	∂ ^{13}C	∂ ^{1}H (*J* [Hz])
1	28.3	2.56 (ddd, 12.7, 9.1, 5.7)
		1.49m
2	23.7	1.89m
3	55.5	3.08m
		2.19m
5	59.6	3.46 (d, 10.3)
		2.28 (dd, 10.4, 1.8)
5a	57.7	
6	30.3	2.86 (d, 2.2)
6a		
6b	130.2	
7	121.2	7.49 (dd, 1.9, 0.6)
8	112.7	
9	113.4	7.14 (dd, 8.5, 1.9)
10	124.8	7.2 (dd)
10a	137.2	
11a		
12	35.6	
12a		2.17m
13	32.7	2.03 (dd, 13.1, 11.3)
		1.97 (dd, 13.2, 4.8)
13a	66.3	
14	176.8	
16	30.9	1.34s
17	24.4	1.44s

Table 7.8 ^{13}C-NMR, ^{1}H-NMR, gHMBCAD and gCOSY correlations for *in vitro* malbrancheamide D (**1.94**). HRMS (ESI-QTOF): *m/z* $[M+H]^+$ calculated for $C_{21}H_{23}BrClN_3O$ = 448.0786, experimental (*in vitro*) 448.0782.

Malbrancheamide D (*in vitro*) CD_3OD				
Position	∂ ^{13}C	∂ ^{1}H (*J* [Hz])	gHMBCAD	gCOSY
1	28.0	2.54 (ddd, 11.9, 9.0, 5.5)	2, 14	1, 2
		1.47m	14	1
2	23.4	1.89m		1, 3
3	55.3	3.07m		3, 2
		2.16m	2, 5	3
5	59.3	2.27 (dd, 10.1, 1.8)	3, 5, 5a, 12a	
		3.44 (d, 10.1)		5
5a	57.3			
6	29.9	2.85 (d, 5.0)	5, 5a, 6a, 11a, 12a, 6b	
6a	104.6			
6b	128.7			
7	123.0	7.66s	6a, 10a, 8, 9	
8	112.2			
9	126.9			
10	113.0	7.43s	8, 9, 6b	
10a	137.8			
11a	145.0			
12	35.4			
12a	48.4	2.14m		
13	32.4	2 (t, 12.1)	12, 13a, 14	
		1.94m	13a	
13a	66.0			
14	176.7			
16	30.5	1.34s	11a, 17, 12, 12a	
17	24.1	1.43s	11a, 12, 12a, 16	

Table 7.9 ^{13}C-NMR, ^{1}H-NMR, gHMBCAD, gCOSY correlations for *in vitro* isomalbrancheamide D (**1.95**). HRMS (ESI-QTOF): *m/z* $[M+H]^+$ calculated for $C_{21}H_{23}BrClN_3O$ = 448.0786, experimental (*in vitro*) 448.0783.

Isomalbrancheamide D (*in vitro*) CD_3OD				
Position	∂ ^{13}C	∂ ^{1}H (*J* [Hz])	gHMBCAD	gCOSY
1	28.1	2.53 (ddd, 12.2, 9.1, 5.6)	2, 3, 13a, 14	1, 2
		1.46m	13a, 14	1
2	23.6	1.88m		1, 2
3	55.4	3.06m	2, 1	3
		2.16 (q, 8.8)	2, 5	2, 3
5	59.4	2.26 (d, 10.4)	12a, 3,5a	5
		3.43 (d, 10.3)	13a, 3, 5a	5
5a	57.4			
6	30.0	2.85 (d, 4.8)	5a, 5, 12a, 6a, 6b, 11a	
6a	104.8			
6b	128.8			
7	119.5	7.51s	6a, 8, 9, 10a	
8	124.8			
9	114.5			
10	116.3	7.57s	8, 9, 6b	
10a	137.6			
11a	145.2			
12	35.5			
12a	48.5	2.15m	17, 16, 12, 5, 5a	
13	32.5	2.01 (m)	12, 12a, 5a	
		1.94m	12,12a,13a, 5a, 1, 14	
13a	66.9			
14	176.6			
16	30.6	1.33s	17, 12, 12a, 11a	
17	24.2	1.43s	16, 12, 12a, 11a	

7.3 Figures

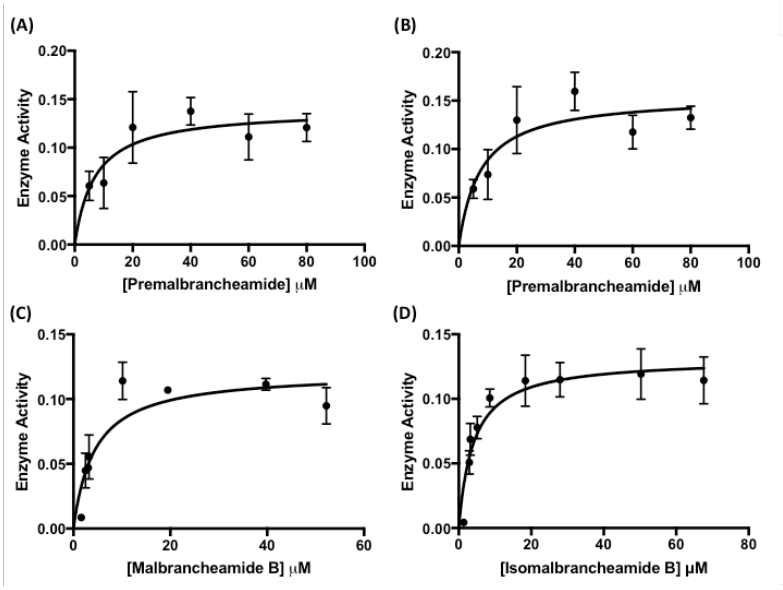

Figure 7.1 MalA kinetics. Kinetic characterization of (A) premalbrancheamide (**1.14**) conversion to malbrancheamide B (**1.15**), (B) premalbrancheamide (**1.14**) conversion to isomalbrancheamide B (**1.16**), (C) malbrancheamide B (**1.15**) conversion to malbrancheamide (**1.17**), (D) isomalbrancheamide B (**1.16**) conversion to malbrancheamide (**1.17**) monitoring enzyme activity (min^{-1}) for each substrate.

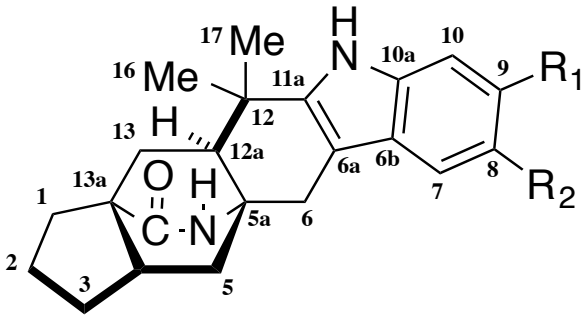

Figure 7.2 Malbrancheamide numbering scheme.

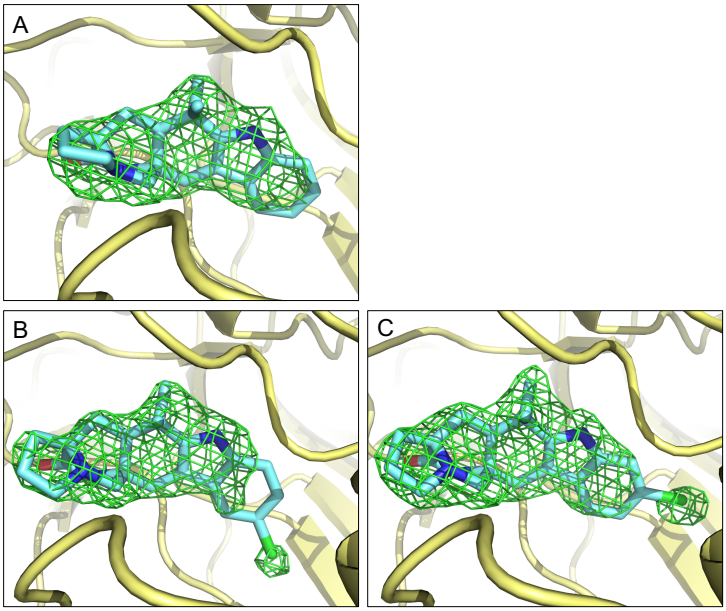

Figure 7.3 MalA' omit maps. mFo-DFc omit maps for MalA' co-crystallized with (A) premalbrancheamide (**1.14**), (B) isomalbrancheamide B (**1.16**), and (C) malbrancheamide B (**1.15**) contoured at 3σ.

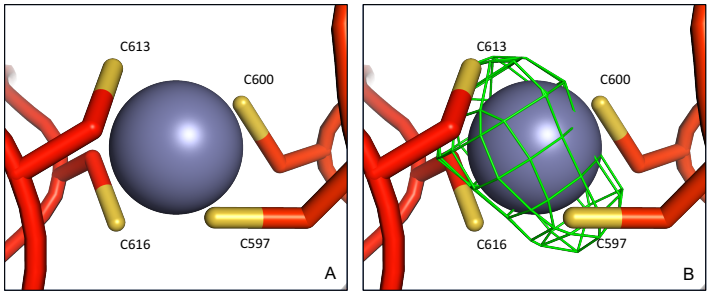

Figure 7.4 Zn^{2+}-binding site of MalA'. Electron density from data collected at (A) 9.1 keV and (B) 9.7 keV is shown contoured at 3σ.

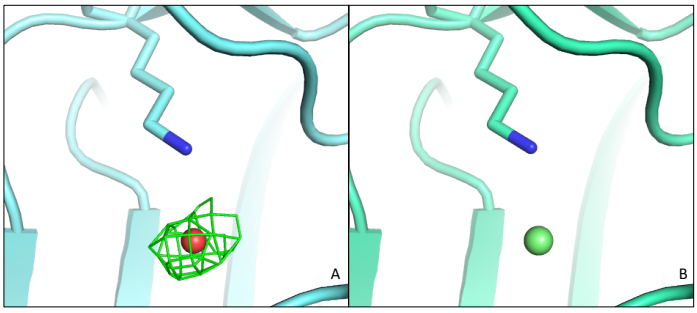

Figure 7.5 Chloride binding site in MalA' active site. (A) Residual difference density when water is modelled into the chloride binding site with mFo-DFc map contoured at 3σ. (B) Chloride ion modelled into active site with no mFo-DFc density observed.

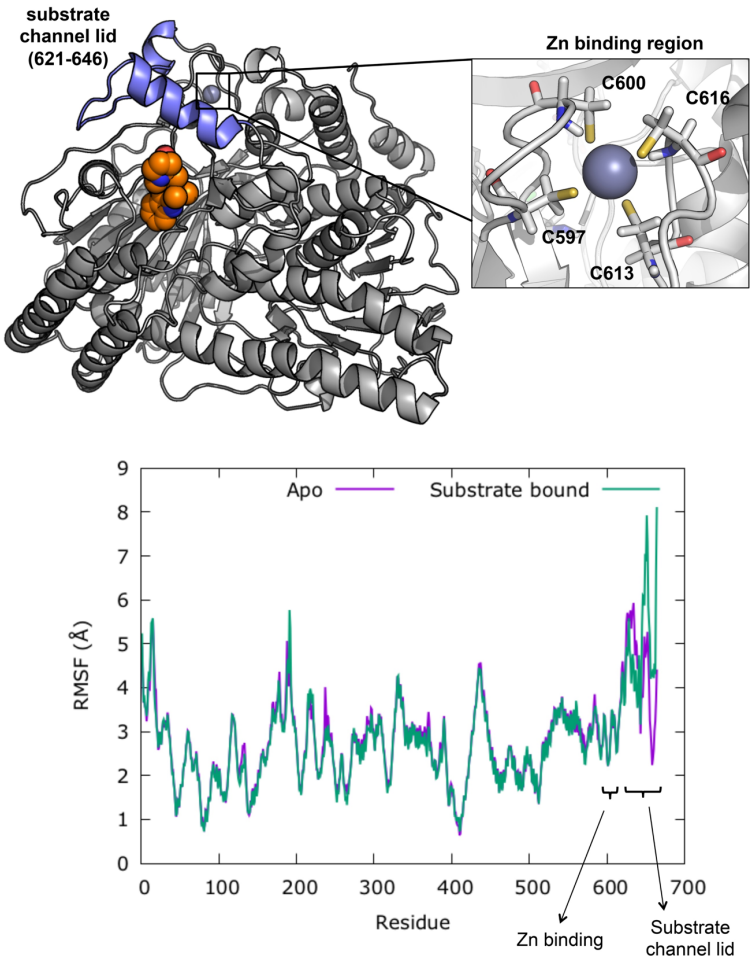

Figure 7.6 RMSF measured along 500 ns MD simulations for the apo and premalbrancheamide bound MalA' systems.

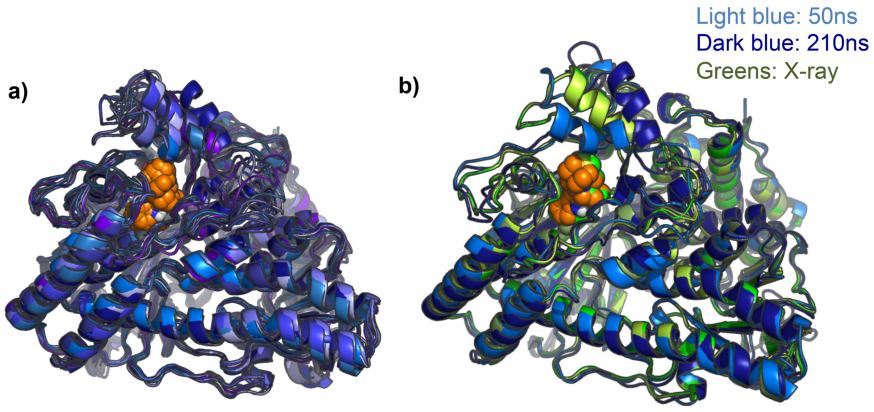

Figure 7.7 MD simulations with MalA complex. (a) Overlay of different snapshots obtained from a 500 ns MD simulation of MalA' substrate complex and (b) overlay of two representative snapshots from the MD trajectory and available X-ray structures.

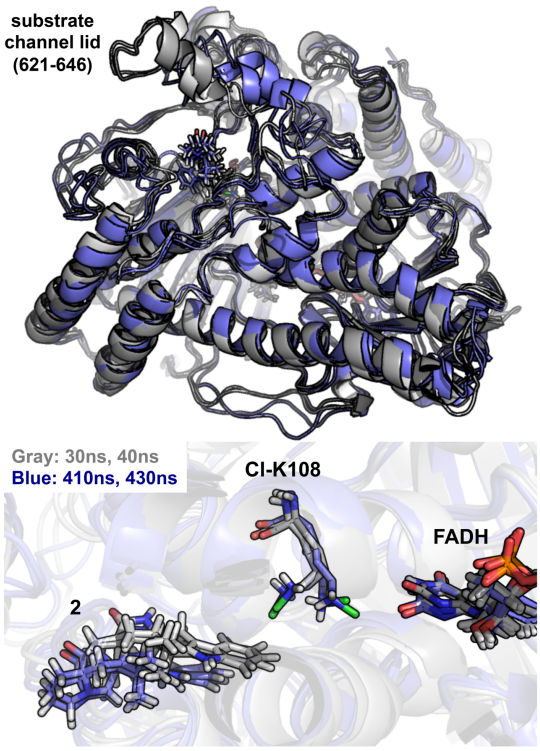

Figure 7.8 Lysine chloramine conformations. Representative snapshots obtained from 500 ns MD trajectory of MalA' premalbrancheamide bound complex to show the two main conformations explored by Cl-Lys108. In grey, the Cl atom is closer to the substrate; in blue, the Cl atom is closer to the FAD cofactor.

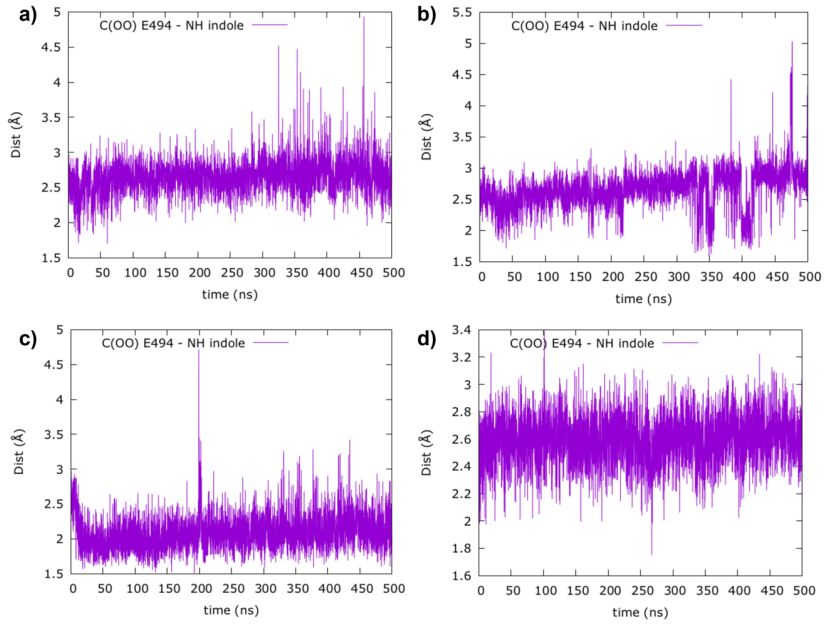

Figure 7.9 Interactions between Glu494 and substrates. Distance between the center of mass of the two oxygen atoms of the Glu494 carboxylate group and the H(N-indole) in a) premalbrancheamide, b) isomalbrancheamide B, c) malbrancheamide B, and d) malbrancheamide. Measurements obtained along the 500 ns MD trajectories are plotted for each system.

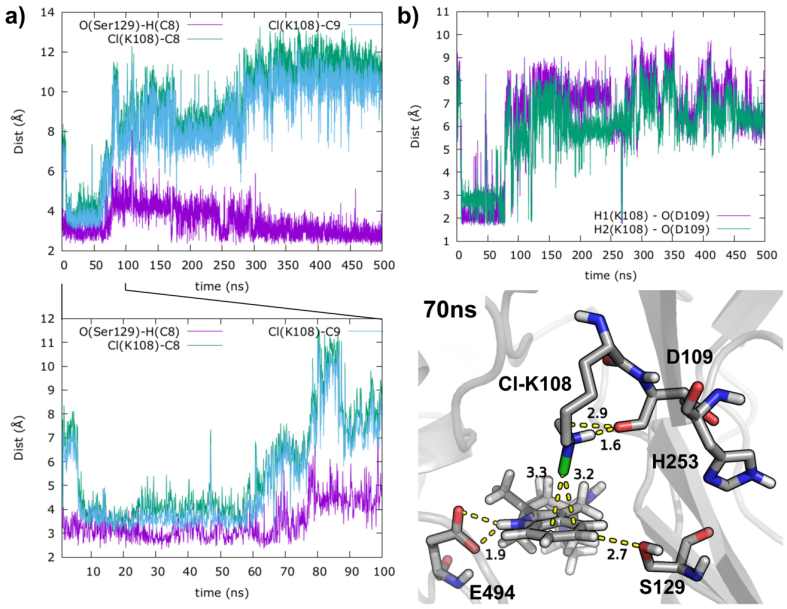

Figure 7.10 Interactions between chloramine and substrates. Distance between Cl atom in Lys108-Cl and C8 / C9 atoms of premalbrancheamide bound in WT MaIA', and between O(Ser129) and H(C8). B) Distance between Cl-Lys108 protons (H1 and H2) and O atom from the carbonyl backbone of Asp109. Measurements obtained along the 500 ns MD trajectory are plotted.

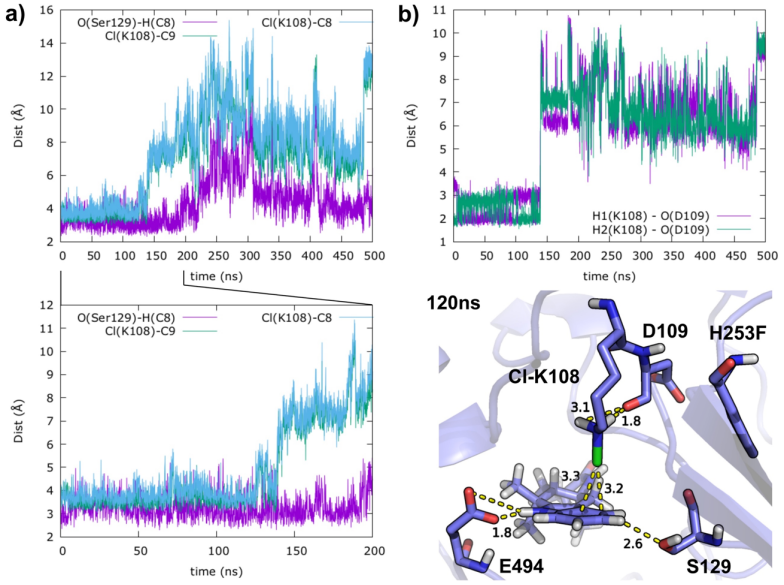

Figure 7.11 Interactions between chloramine and substrates in H253F. Distance between Cl atom in Lys108-Cl and C8 / C9 atoms of premalbrancheamide bound in H253F MaIA', and between O(Ser129) and H(C8). B) Distance between Cl-Lys108 protons (H1 and H2) and O atom from the carbonyl backbone of Asp109. Measurements obtained along the 500 ns MD trajectory are plotted.

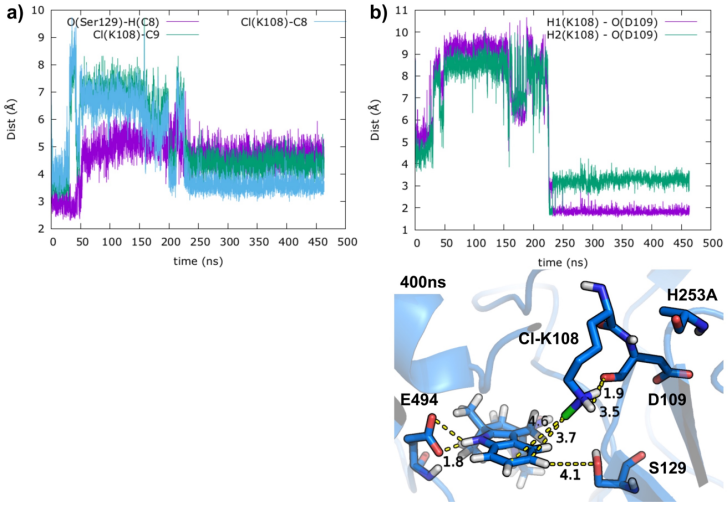

Figure 7.12 Interactions between chloramine and substrates in H253A. Distance between Cl atom in Lys108-Cl and C8 / C9 atoms of premalbrancheamide bound in H253A MaIA', and between O(Ser129) and H(C8). B) Distance between Cl-Lys108 protons (H1 and H2) and O atom from the carbonyl backbone of Asp109. Measurements obtained along the 500 ns MD trajectory are plotted.

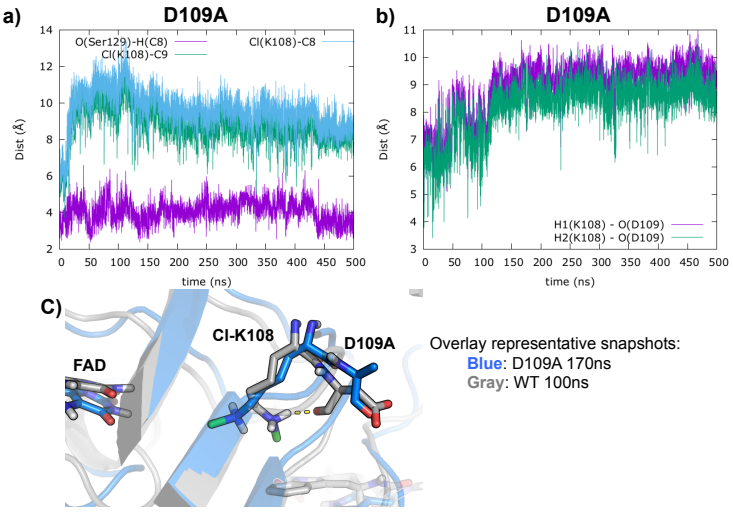

Figure 7.13 Interactions between chloramine and substrates in D109A. Distance between Cl atom in Lys108-Cl and C8 / C9 atoms of premalbrancheamide bound in D109A MaIA', and between O(Ser129) and H(C8). B) Distance between Cl-Lys108 protons (H1 and H2) and O atom from the backbone carbonyl of Asp109. Measurements obtained along the 500 ns MD trajectory. C) Overlay of representative snapshots for WT and D109A MalA' that highlight the rotation of the carbonyl backbone in the D109A mutant and the different position of the side chain, as compared to the original Asp109 residue. Cl-Lys108 cannot H-bond with the D109A carbonyl backbone.

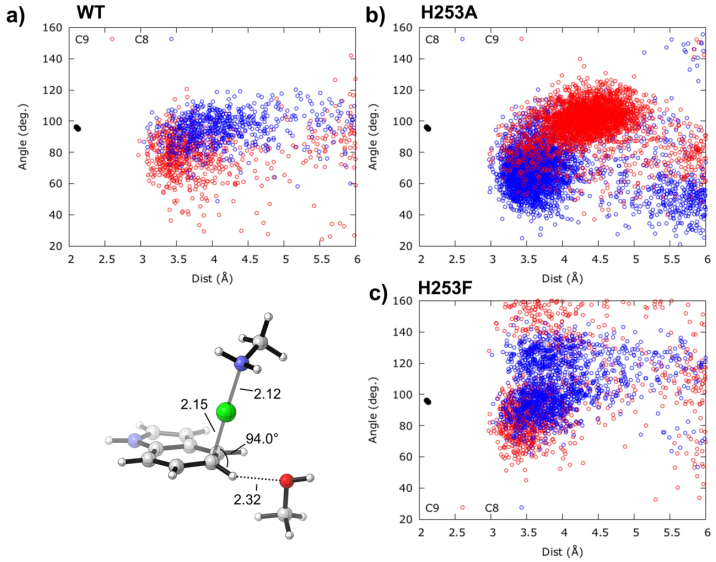

Figure 7.14 Cl-C-H angle and Cl-C distance for WT and H253A/F. Cl-C-H angle and Cl-C distance (as described in the figure) measured along 500 ns of MD simulation are used to describe the orientations explored by Cl-Lys108 with respect to the substrate in: a) WT, b) H253A, and c) H253F. Black dots represent the geometric parameters obtained from DFT optimized transition states TS1c-C8 and TS1c-C9.

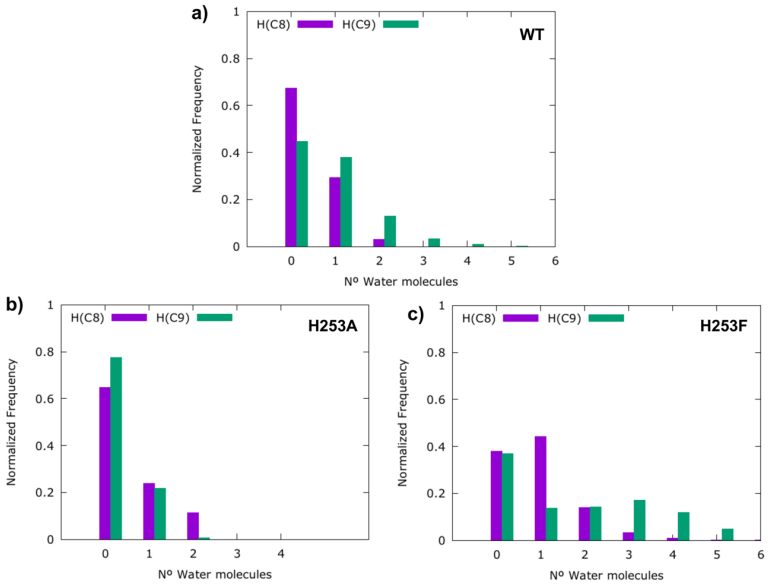

Figure 7.15 Solvation shells in WT and H253A/F. Solvation shell (3.4 Å) around H(C8) and H(C9) observed along the 500 ns of MD simulations in the a) WT; b) H253A; and c) H253F MalA' with bound premalbrancheamide.

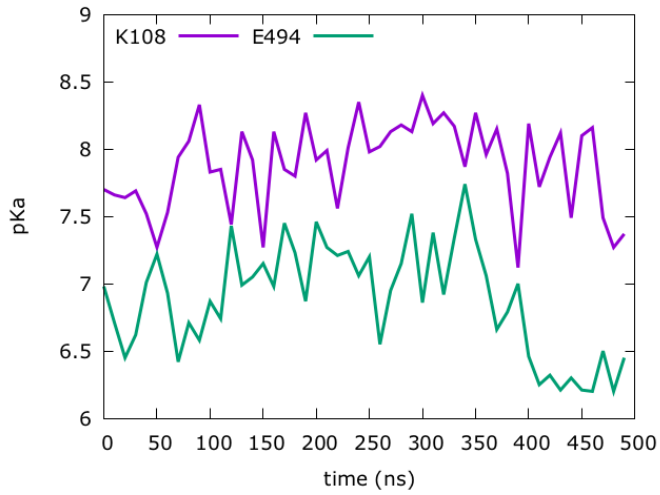

Figure 7.16 pK_a predictions for Lys108 and Glu494 in the apo state of WT MalA'. pK_a estimates obtained from propka3.1 program.[234, 235]

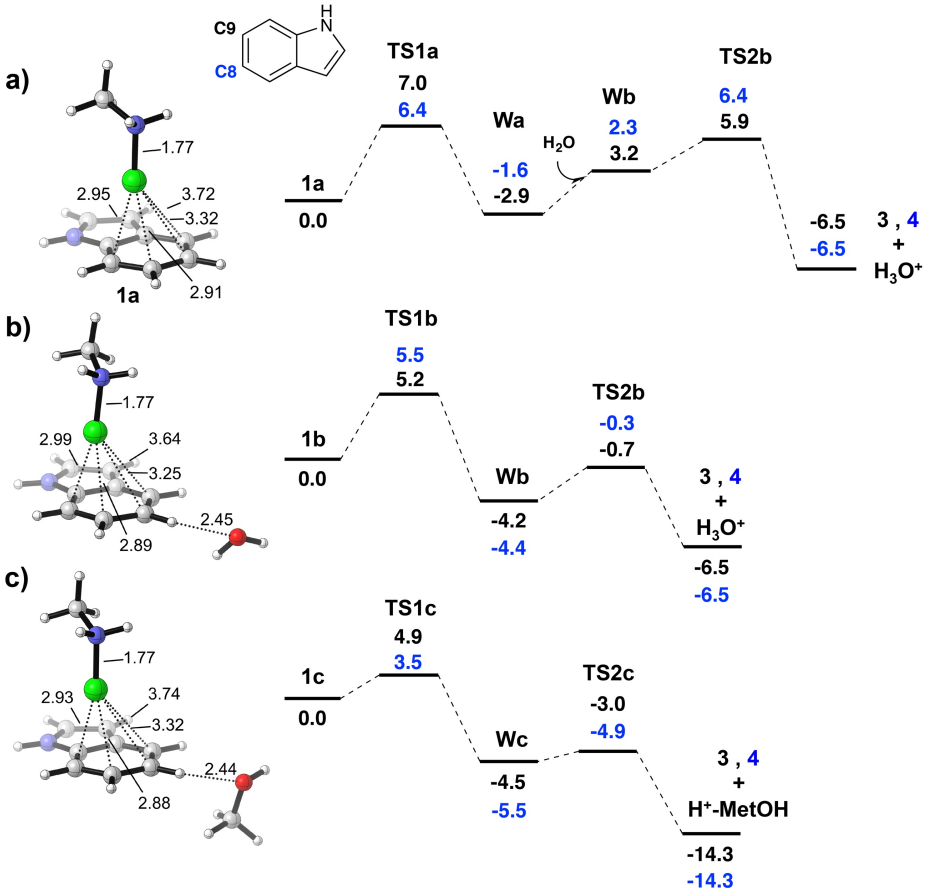

Figure 7.17 DFT optimized reaction pathways. The C8 and C9 chlorination reactions were calculated using three computational models: **a)** an indole ring and methyl chloramine; **b)** an indole ring, methyl chloramine and a water molecule closer to C8- or C9-H respectively; **c)** an indole ring, methyl chloramine and a methanol molecule as a Ser129 model. Relative Gibb's free energies (ΔG, in kcal/mol) are computed at the M06-2x/6-311+G(d,p)/CPCM(Diethylether)//M06-2x/6-31G(d)/CPCM(Diethylether) level. Bond lengths are in Å.

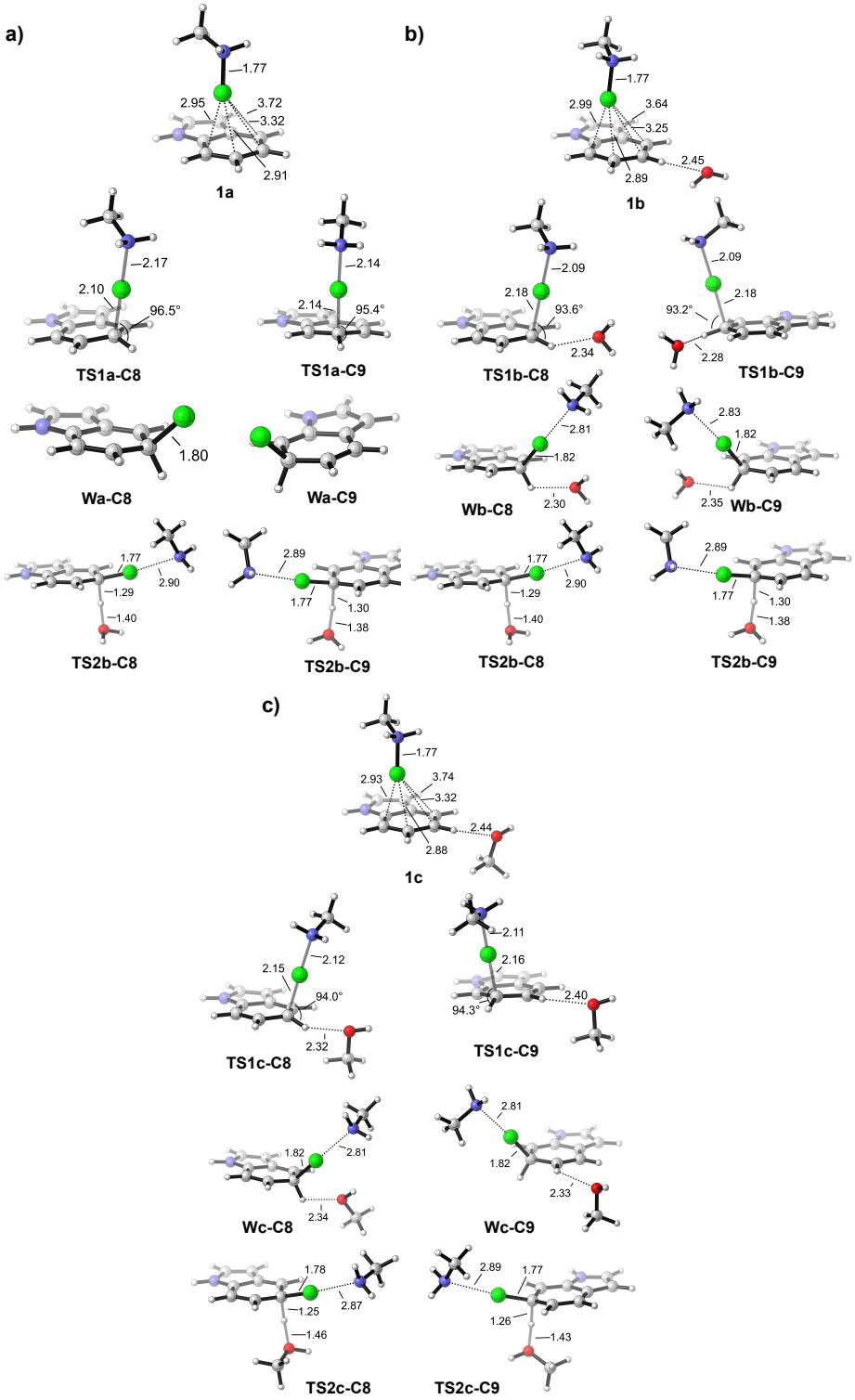

Figure 7.18 Optimized structures for the three computational models. A) an indole ring and a protonated methyl chloramine as an active species; b) addition of a water molecule close to H-C8 or H-C9 positions; c) and addition of a methanol molecule close to H-C8 to mimic Ser129.

7.4 Compound Characterization

7.4.1 Mass Spectrometry Data

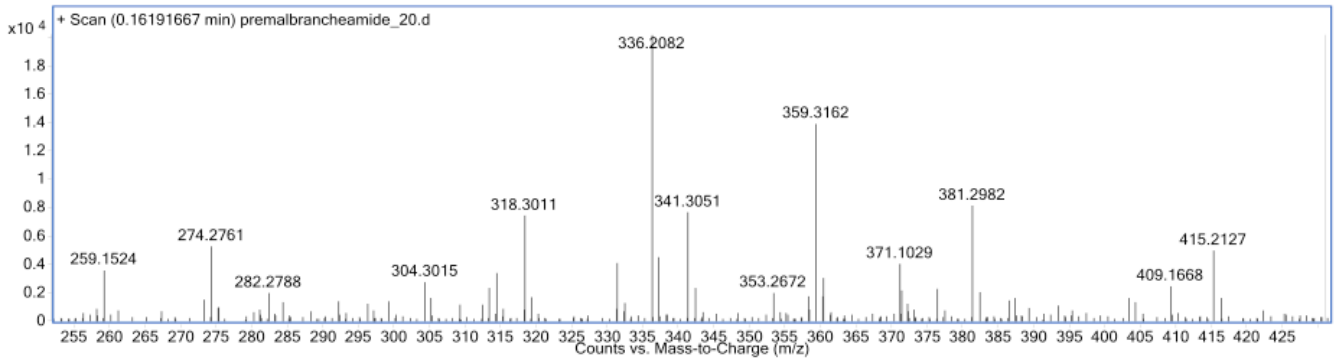

Figure 7.19 Premalbrancheamide (fungal) mass spectrometry data. Calculated mass $[M+H]^+$ = 336.2070, experimental mass $[M+H]^+$ = 336.2082.

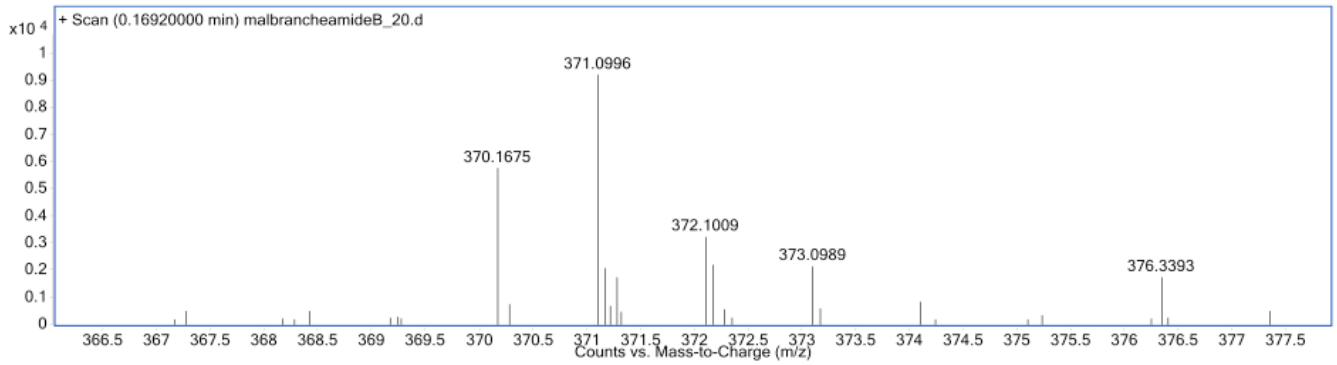

Figure 7.20 Malbrancheamide B (*in vitro* assay) mass spectrometry data. Calculated mass $[M+H]^+$ = 370.1681, experimental mass $[M+H]^+$ = 370.1675.

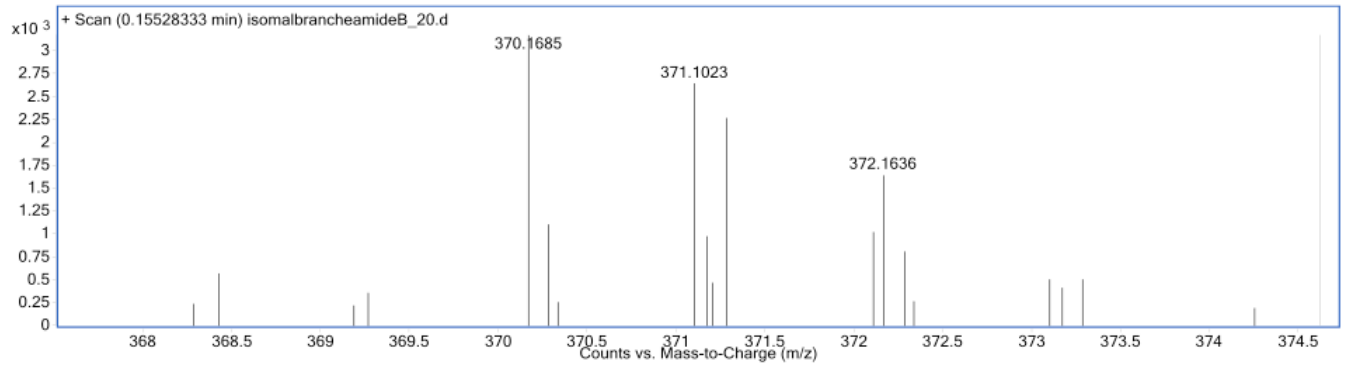

Figure 7.21 Isomalbrancheamide B (*in vitro* assay) mass spectrometry data. Calculated mass $[M+H]^+$ = 370.1681, experimental mass $[M+H]^+$ = 370.1685.

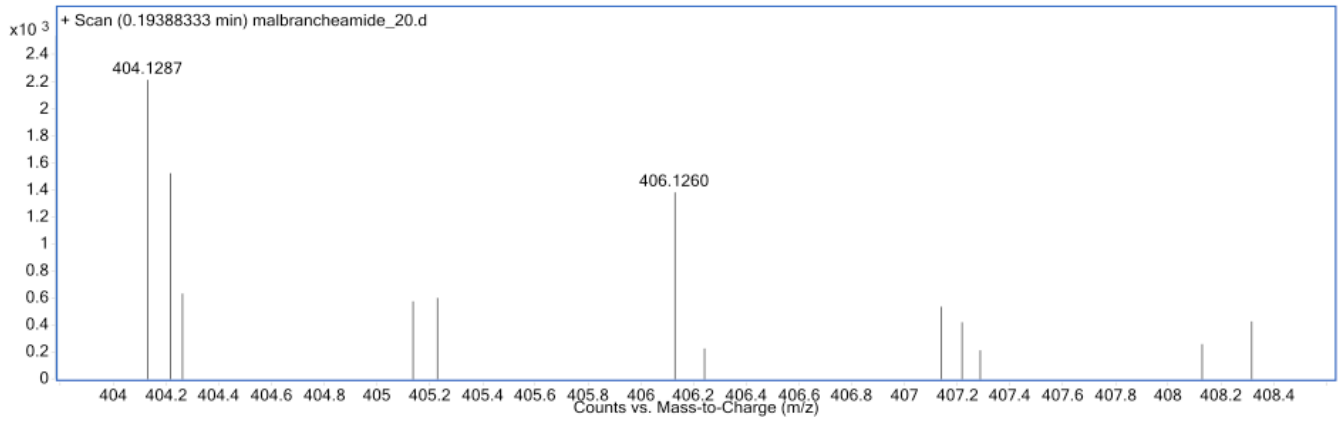

Figure 7.22 Malbrancheamide (*in vitro* assay) mass spectrometry data. Calculated mass $[M+H]^+$ = 404.1291, experimental mass $[M+H]^+$ = 404.1287.

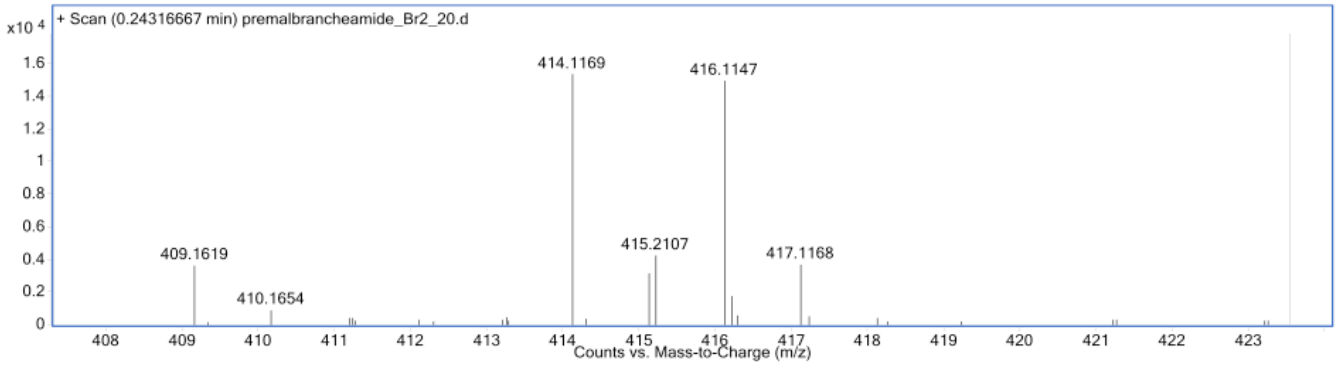

Figure 7.23 Malbrancheamide C (*in vitro* assay) mass spectrometry data. Calculated mass $[M+H]^+$ = 414.1176, experimental mass $[M+H]^+$ = 414.1169.

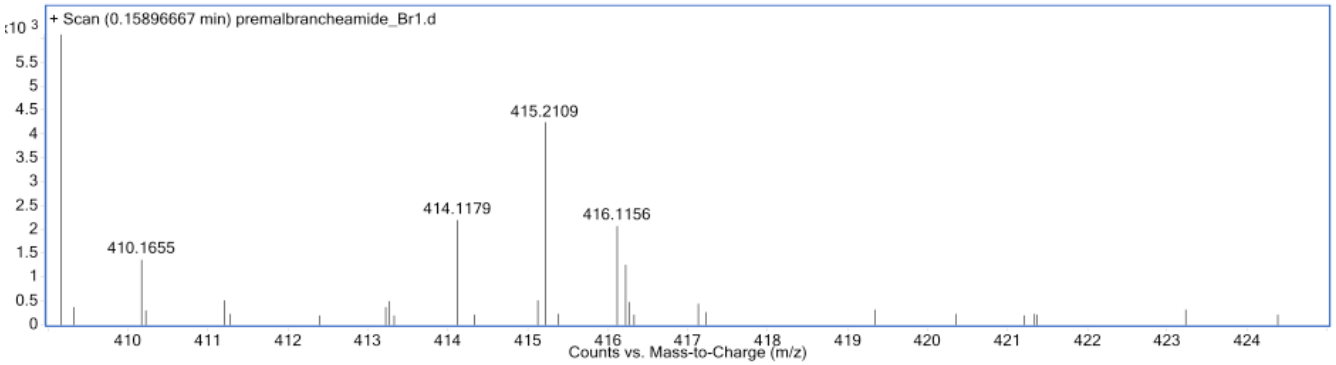

Figure 7.24 Isomalbrancheamide C (*in vitro* assay) mass spectrometry data. Calculated mass $[M+H]^+$ = 414.1176, experimental mass $[M+H]^+$ = 414.1179.

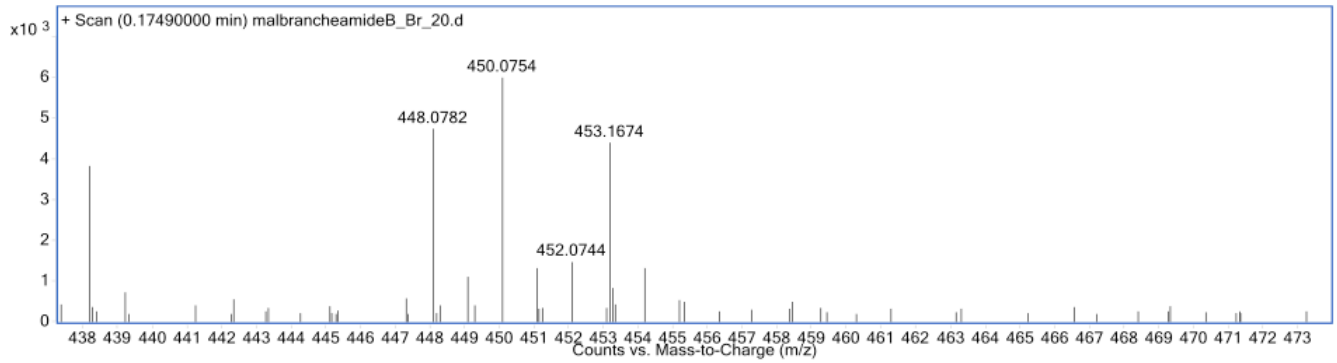

Figure 7.25 Malbrancheamide D (*in vitro* assay) mass spectrometry data. Calculated mass $[M+H]^+$ = 448.0786, experimental mass $[M+H]^+$ = 448.0782.

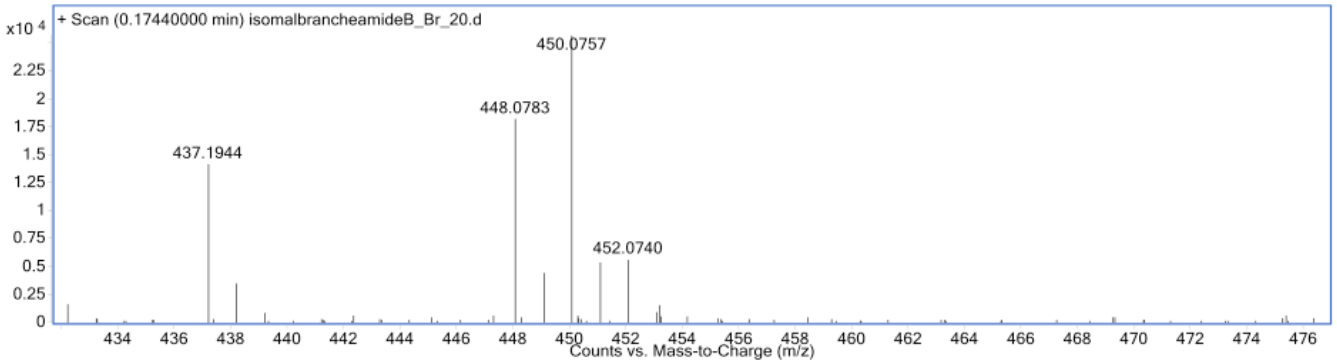

Figure 7.26 Isomalbrancheamide D (*in vitro* assay) mass spectrometry data. Calculated mass $[M+H]^+$ = 448.0786, experimental mass $[M+H]^+$ = 448.0783.

7.4.2 NMR Spectroscopy Data

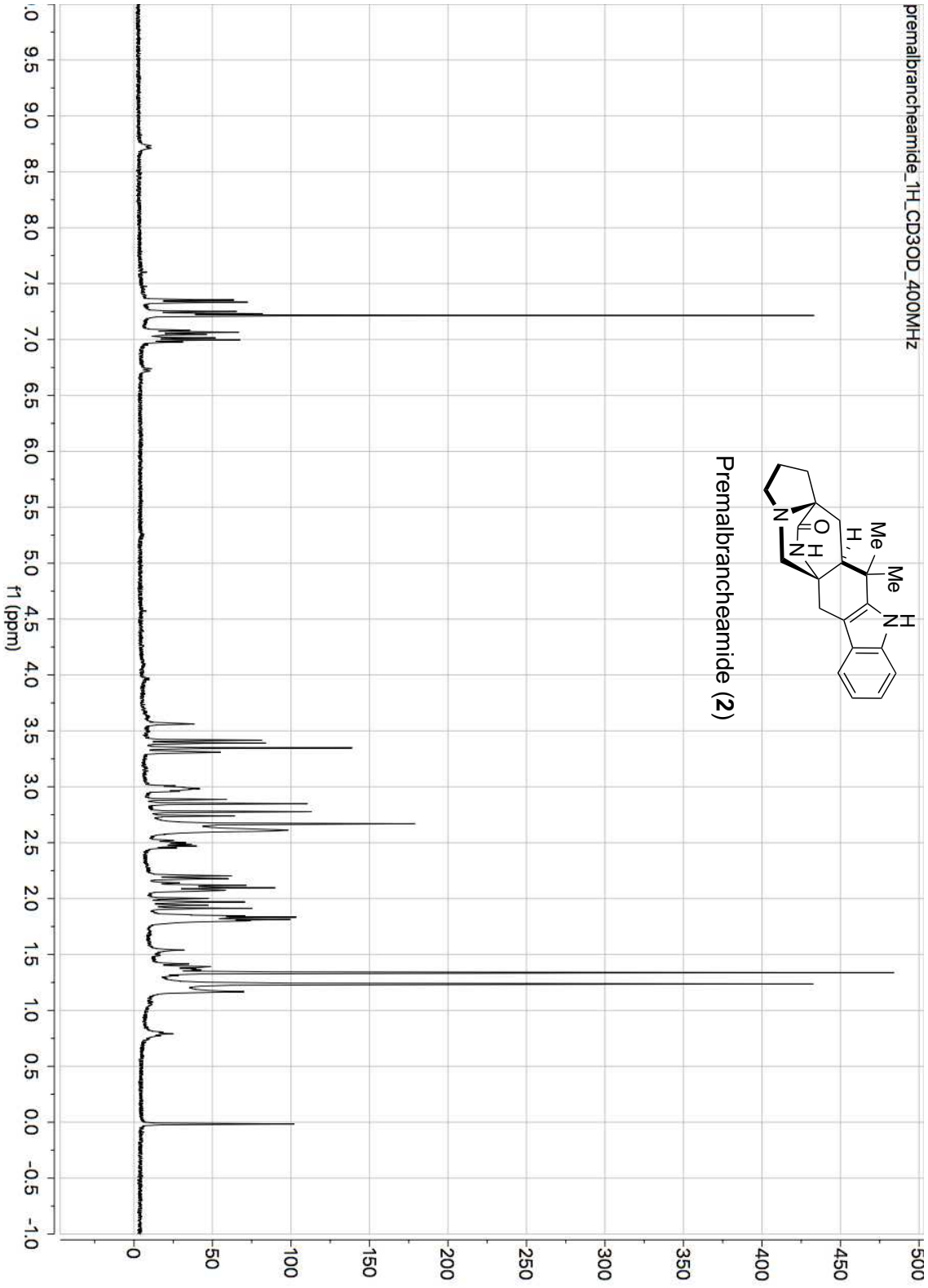

Figure 7.27 ^{1}H-NMR of premalbrancheamide isolated from *M. aurantiaca* (400 MHz, CD_3OD).

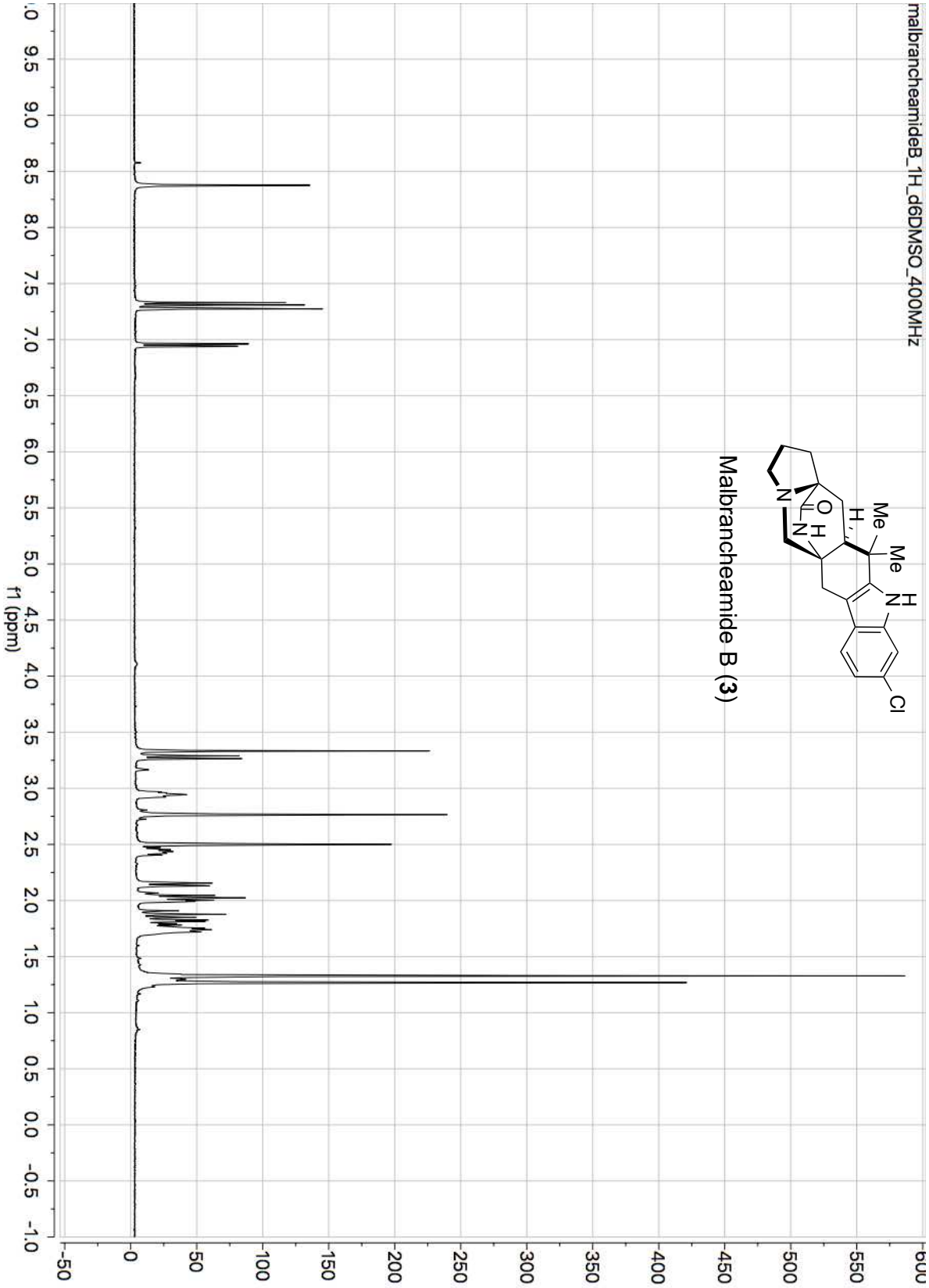

Figure 7.28 ^{1}H-NMR of malbrancheamide B isolated from *M. aurantiaca* (400 MHz, -$(CD_3)_2SO$-d_6).

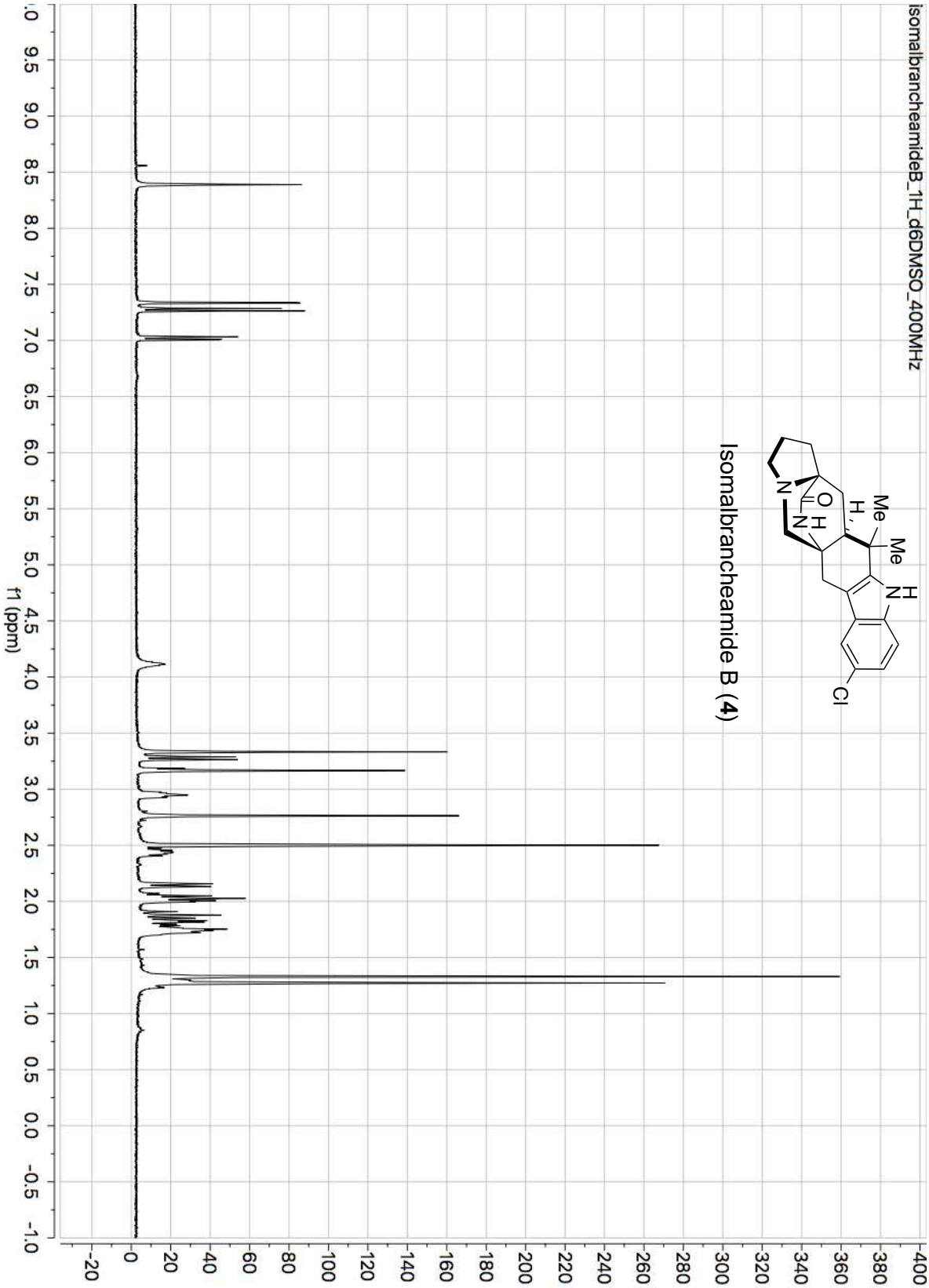

Figure 7.29 ^{1}H-NMR of isomalbrancheamide B from *M. aurantiaca* (400 MHz, $(CD_3)_2SO$-d_6).

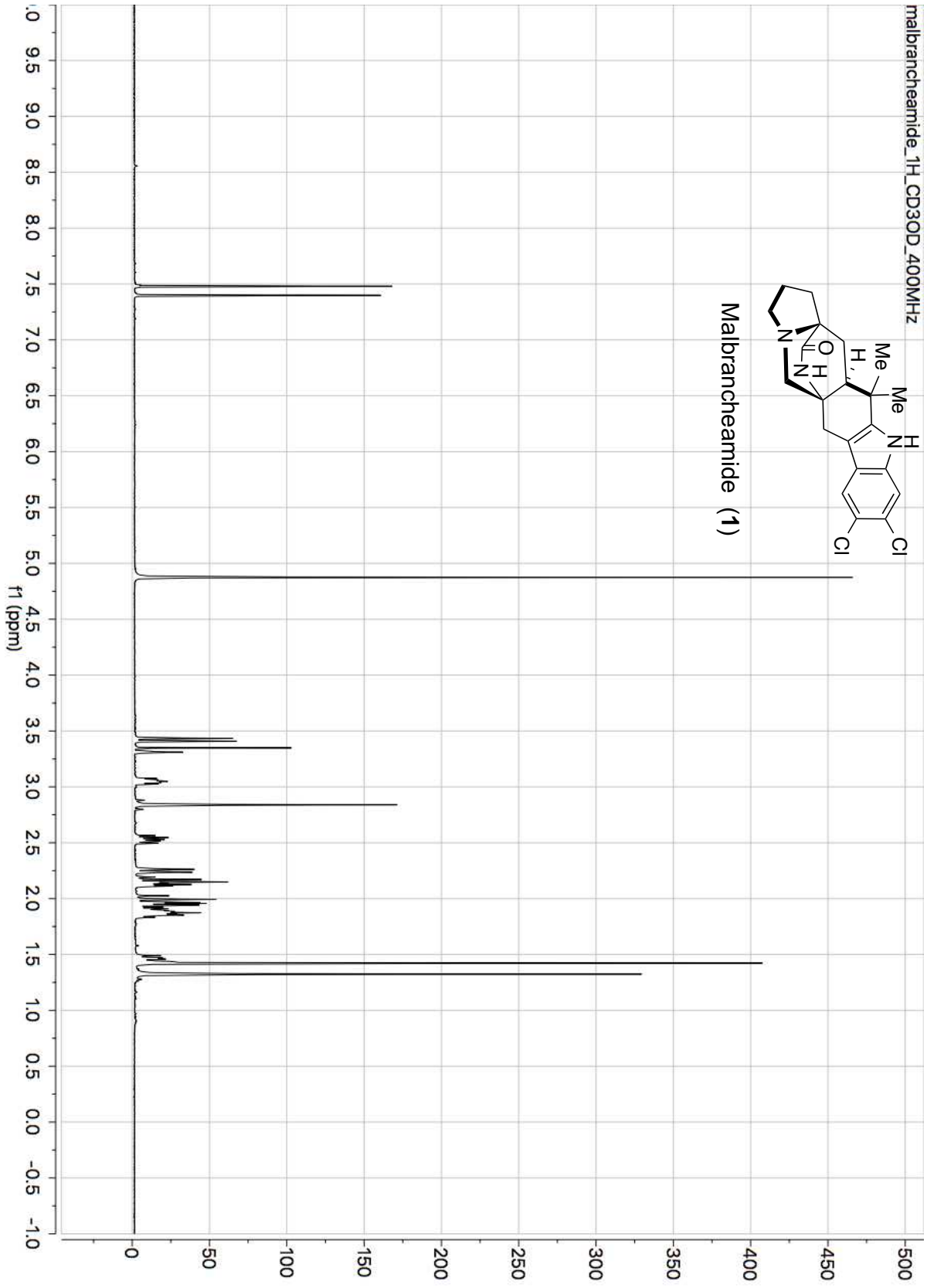

Figure 7.30 ^{1}H-NMR of malbrancheamide isolated from *M. aurantiaca* (400 MHz, CD_3OD).

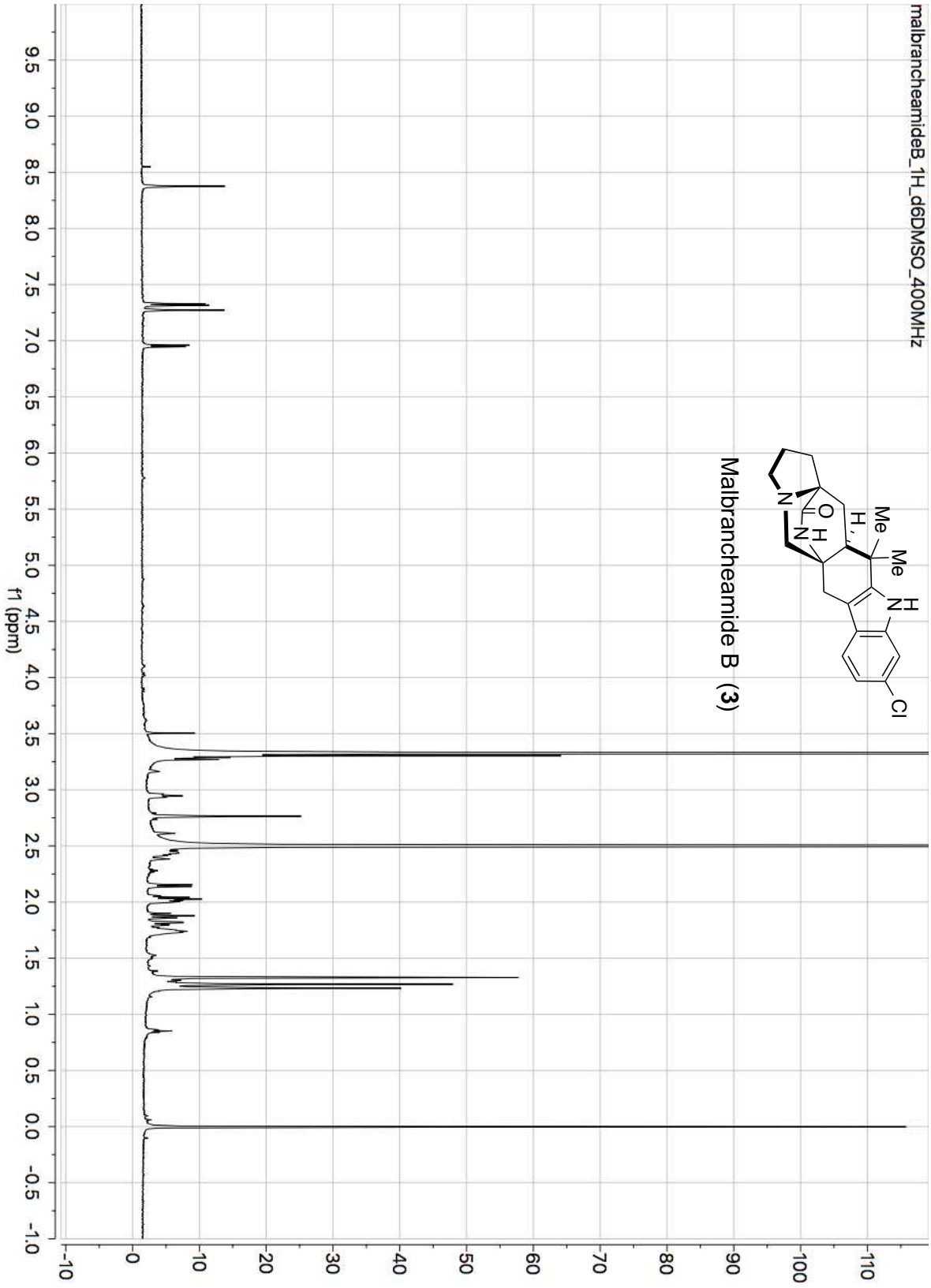

Figure 7.31 ^{1}H-NMR of malbrancheamide B from MalA *in vitro* reaction (400 MHz, $(CD_3)_2SO$-d_6).

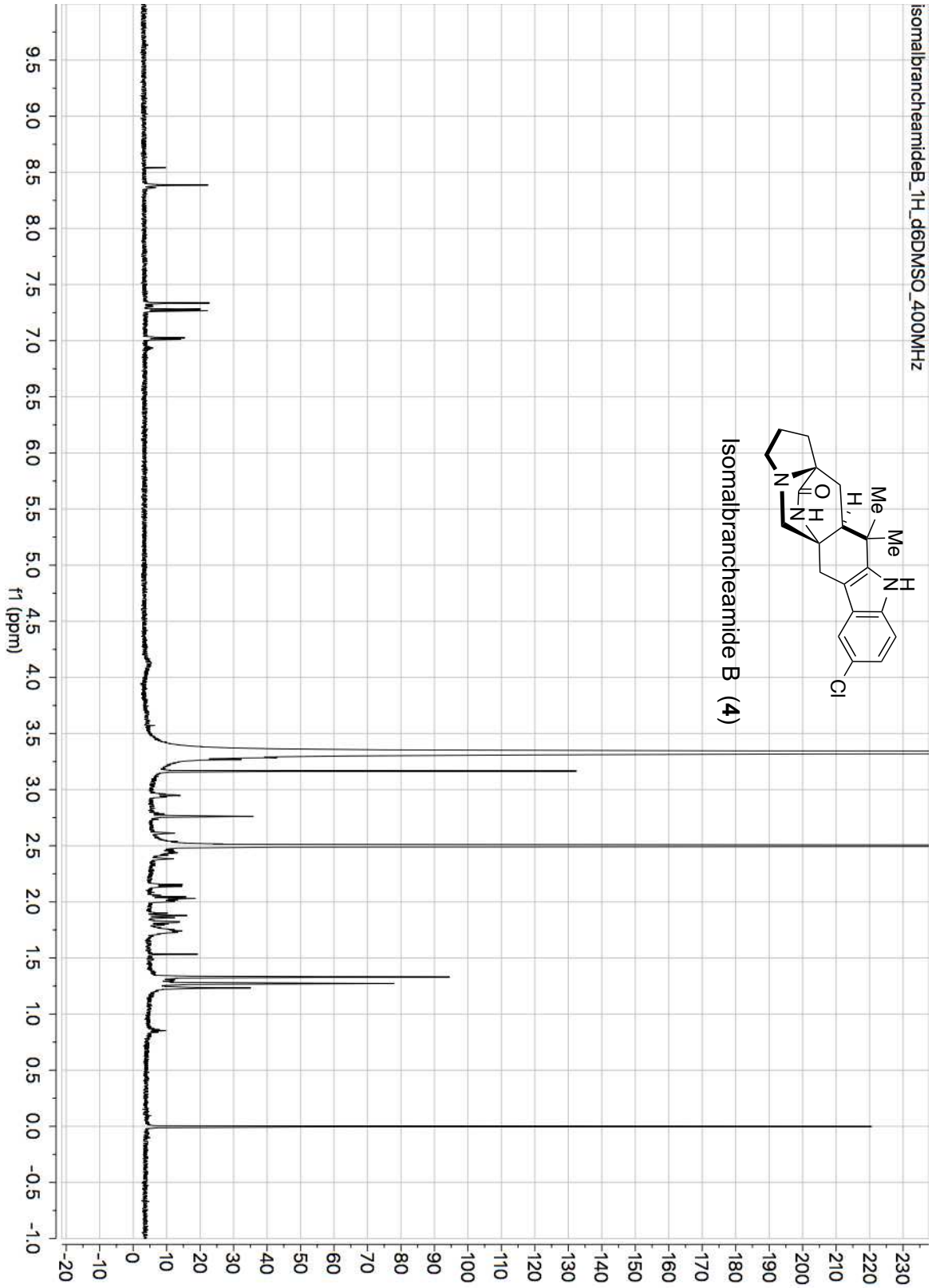

Figure 7.32 ^{1}H-NMR of isomalbrancheamide B from MalA *in vitro* reaction (400 MHz, $(CD_3)_2SO$-d_6).

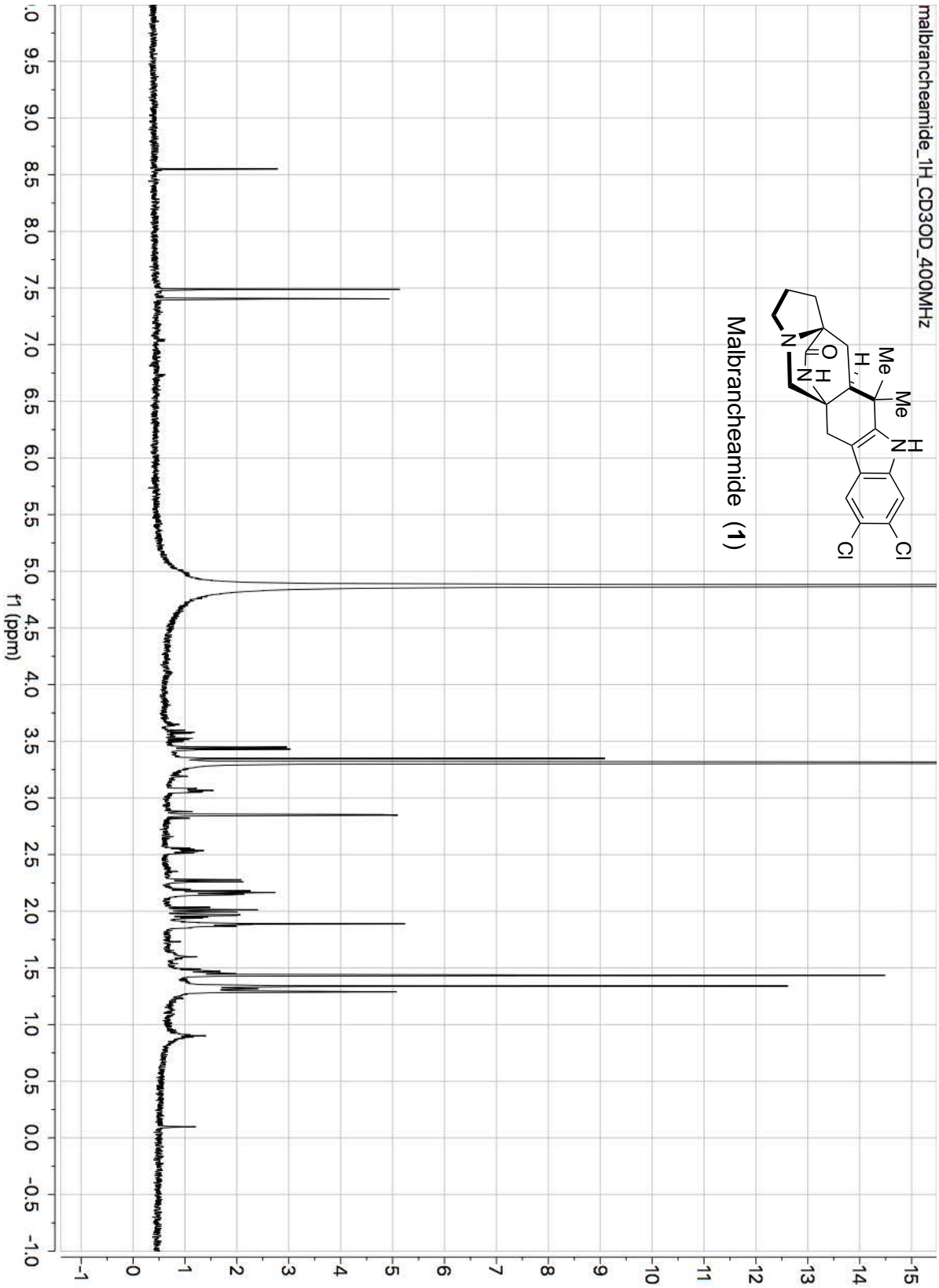

Figure 7.33 ^{1}H-NMR of malbrancheamide from MalA *in vitro* reaction (400 MHz, CD_3OD).

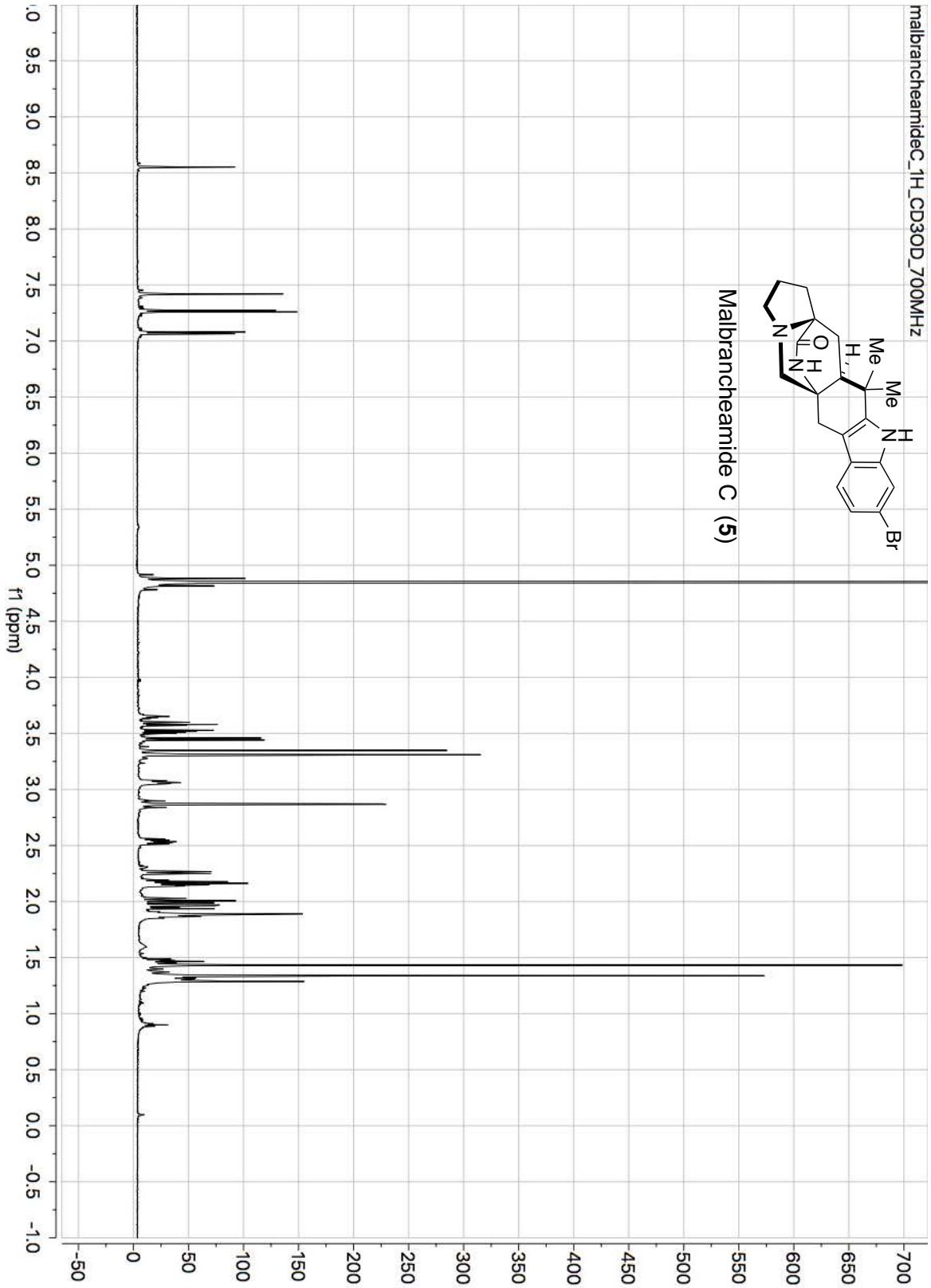

Figure 7.34 ^{1}H-NMR of malbrancheamide C (**5**) from MalA *in vitro* reaction (700 MHz, CD_3OD).

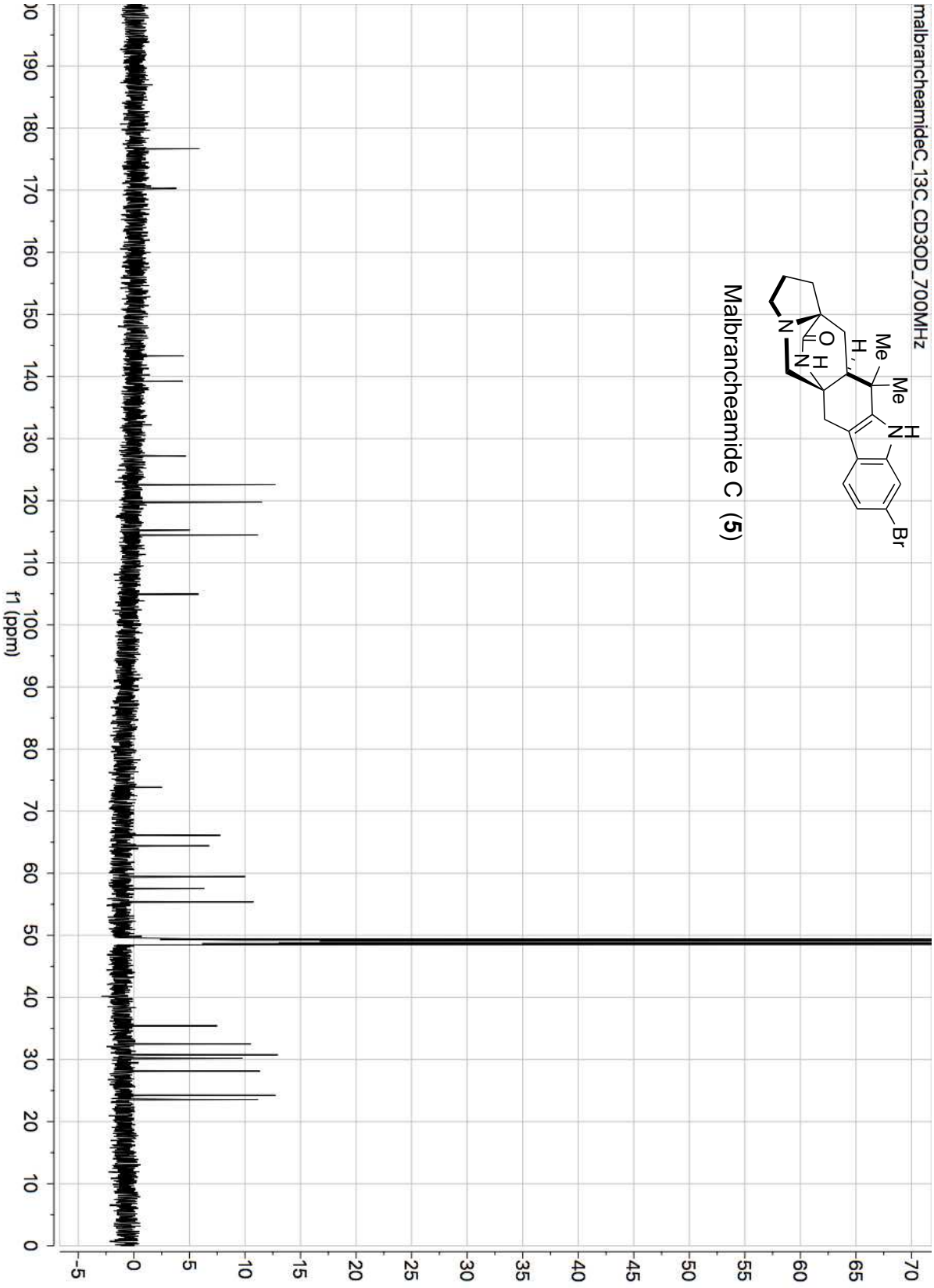

Figure 7.35 ^{13}C-NMR of malbrancheamide C from MalA *in vitro* reaction (176 MHz, CD_3OD).

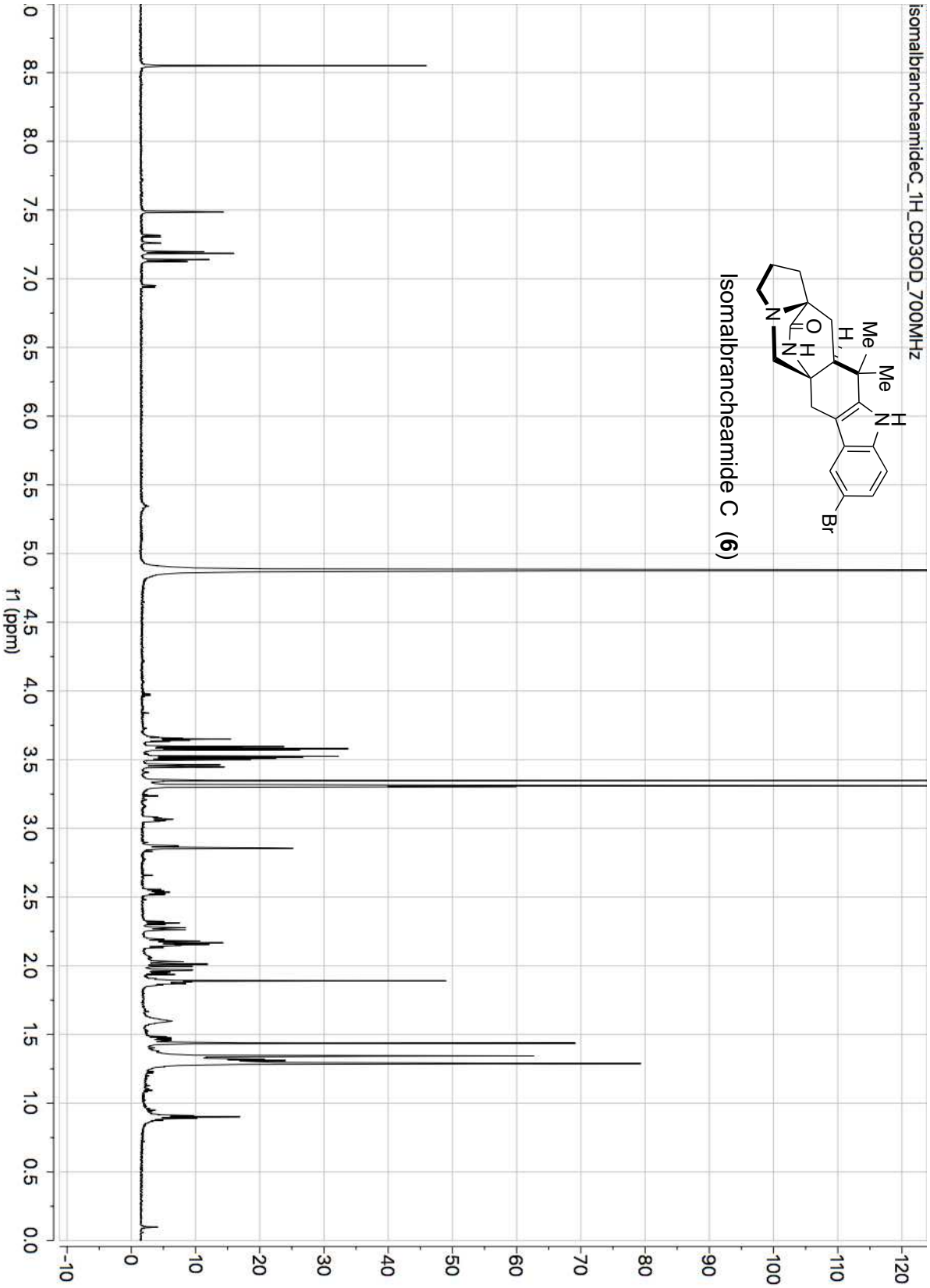

Figure 7.36 ^{1}H-NMR of isomalbrancheamide C from MalA *in vitro* reaction (700 MHz, CD_3OD).

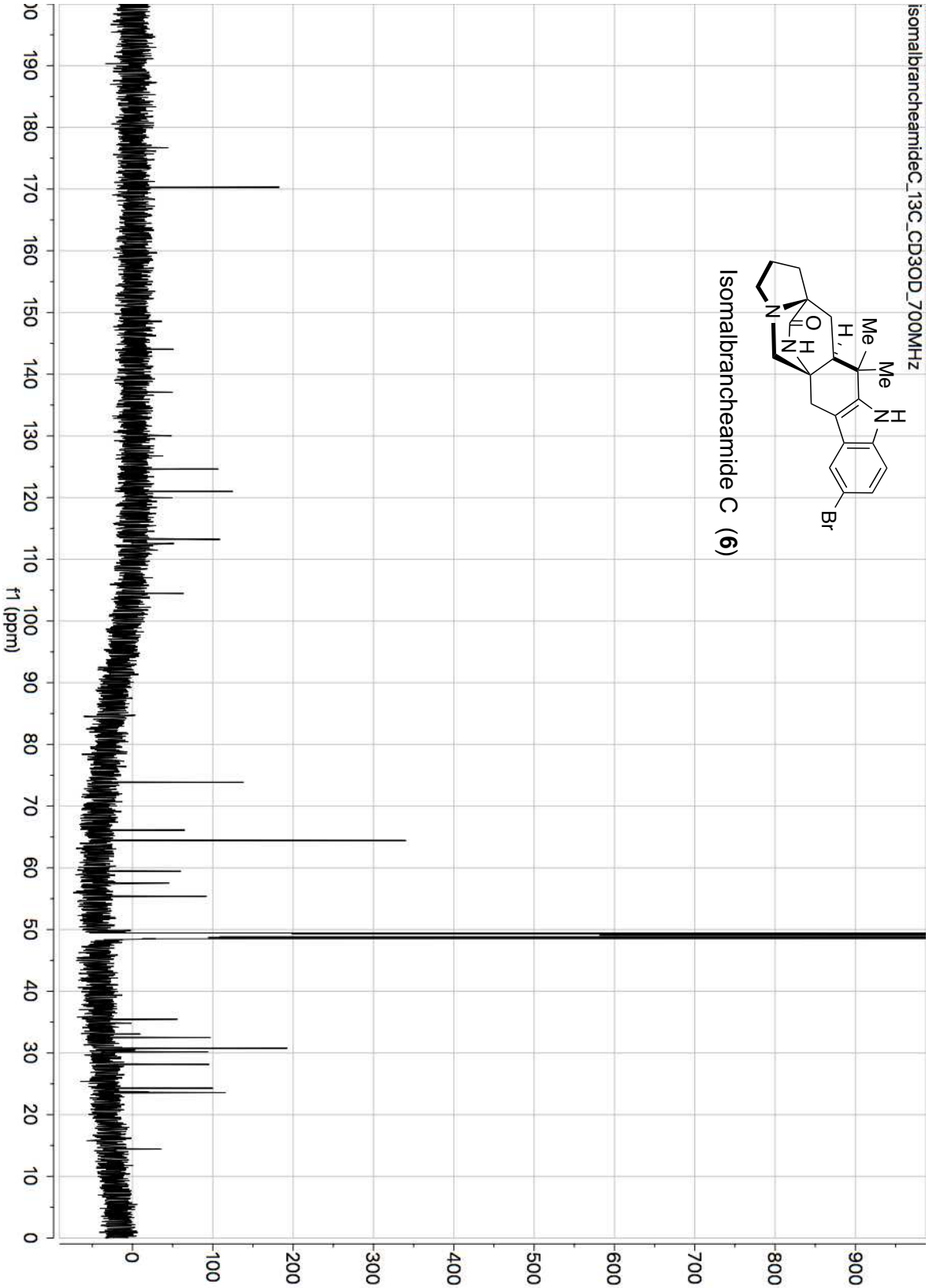

Figure 7.37 ^{13}C-NMR of isomalbrancheamide C from MalA *in vitro* reaction (176 MHz, CD_3OD).

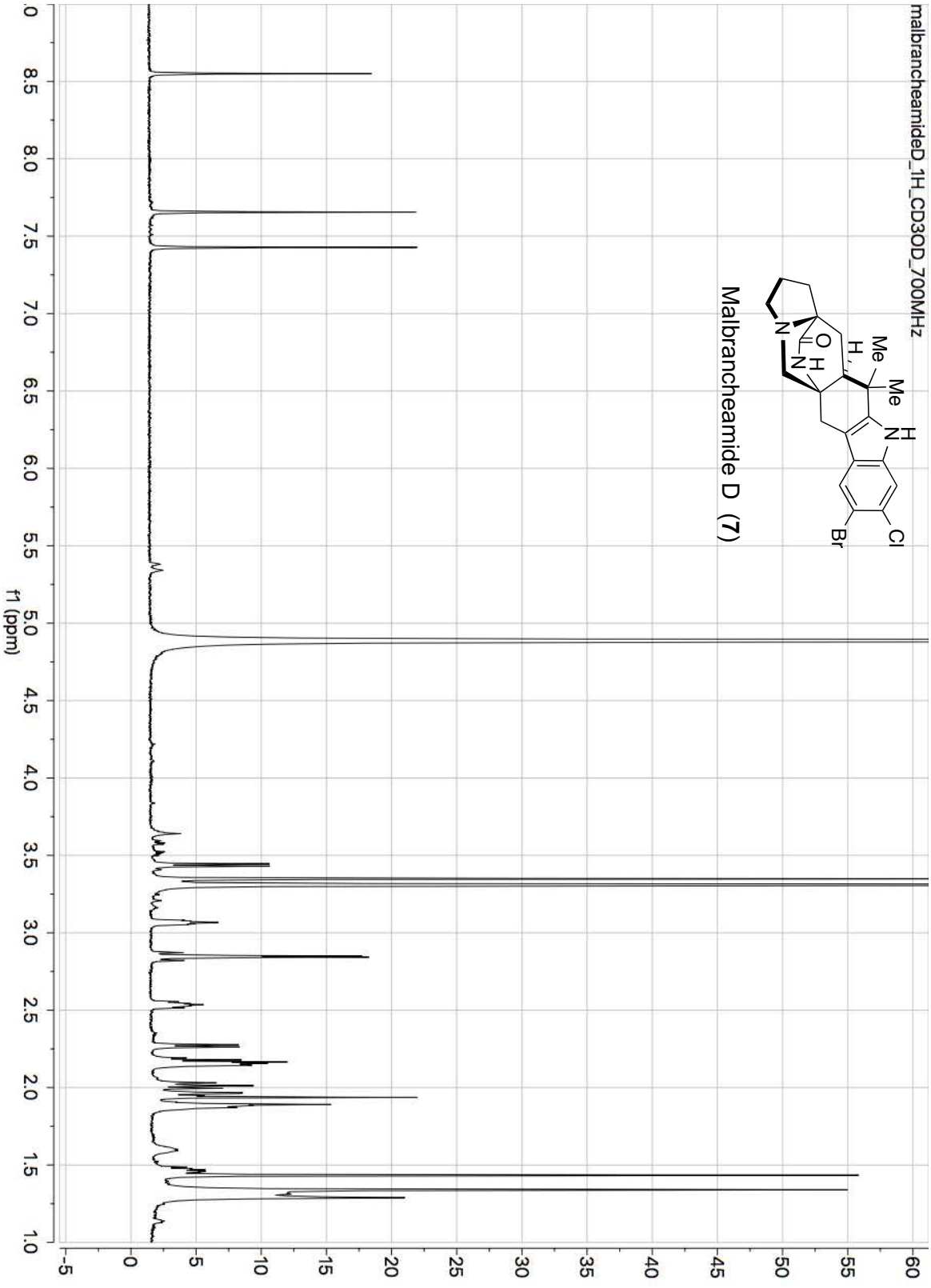

Figure 7.38 ^{1}H-NMR of malbrancheamide D from MalA *in vitro* reaction (700 MHz, CD_3OD).

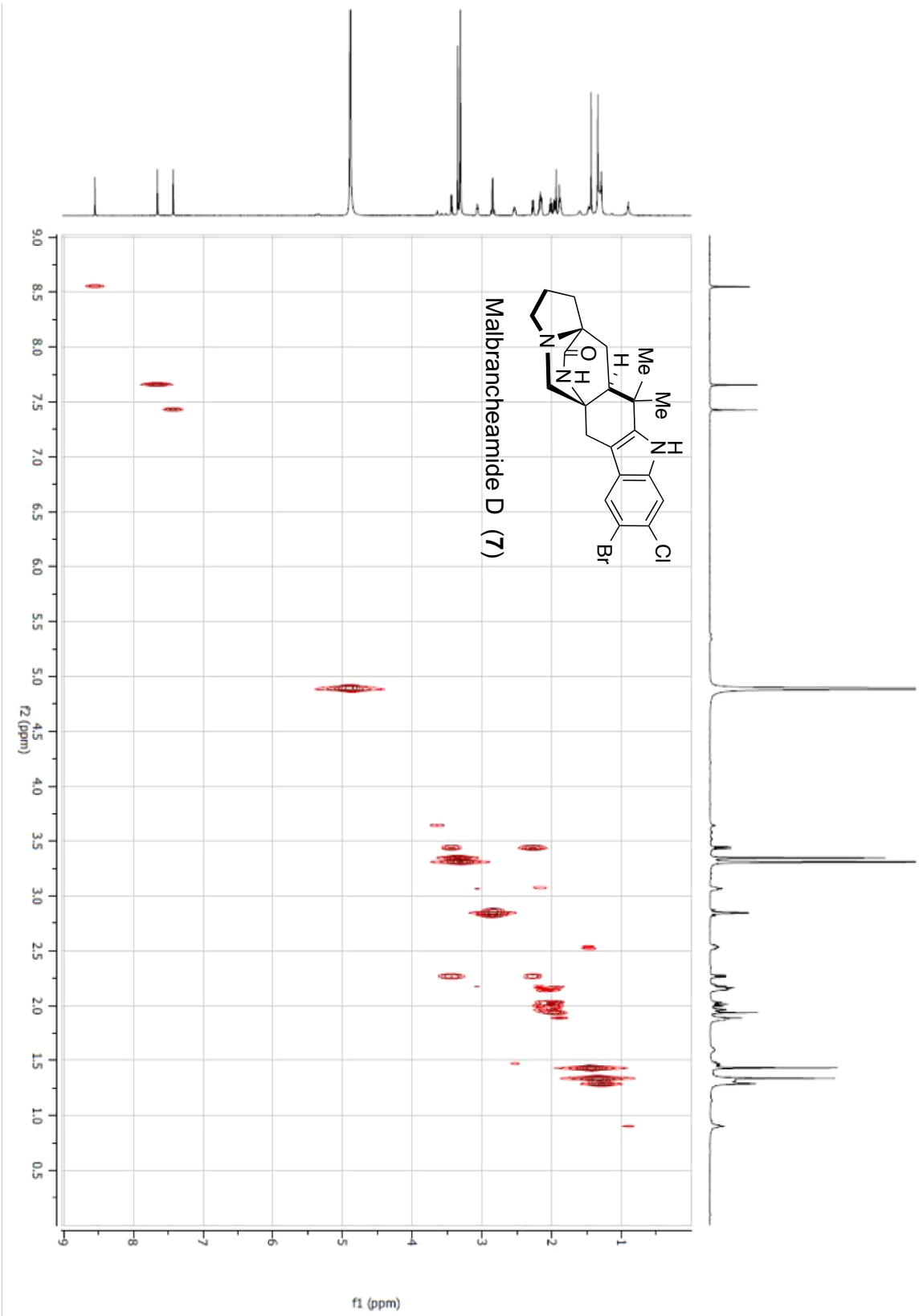

Figure 7.39 gCOSY correlations of malbrancheamide D from *in vitro* reaction with MalA (700 MHz, CD_3OD).

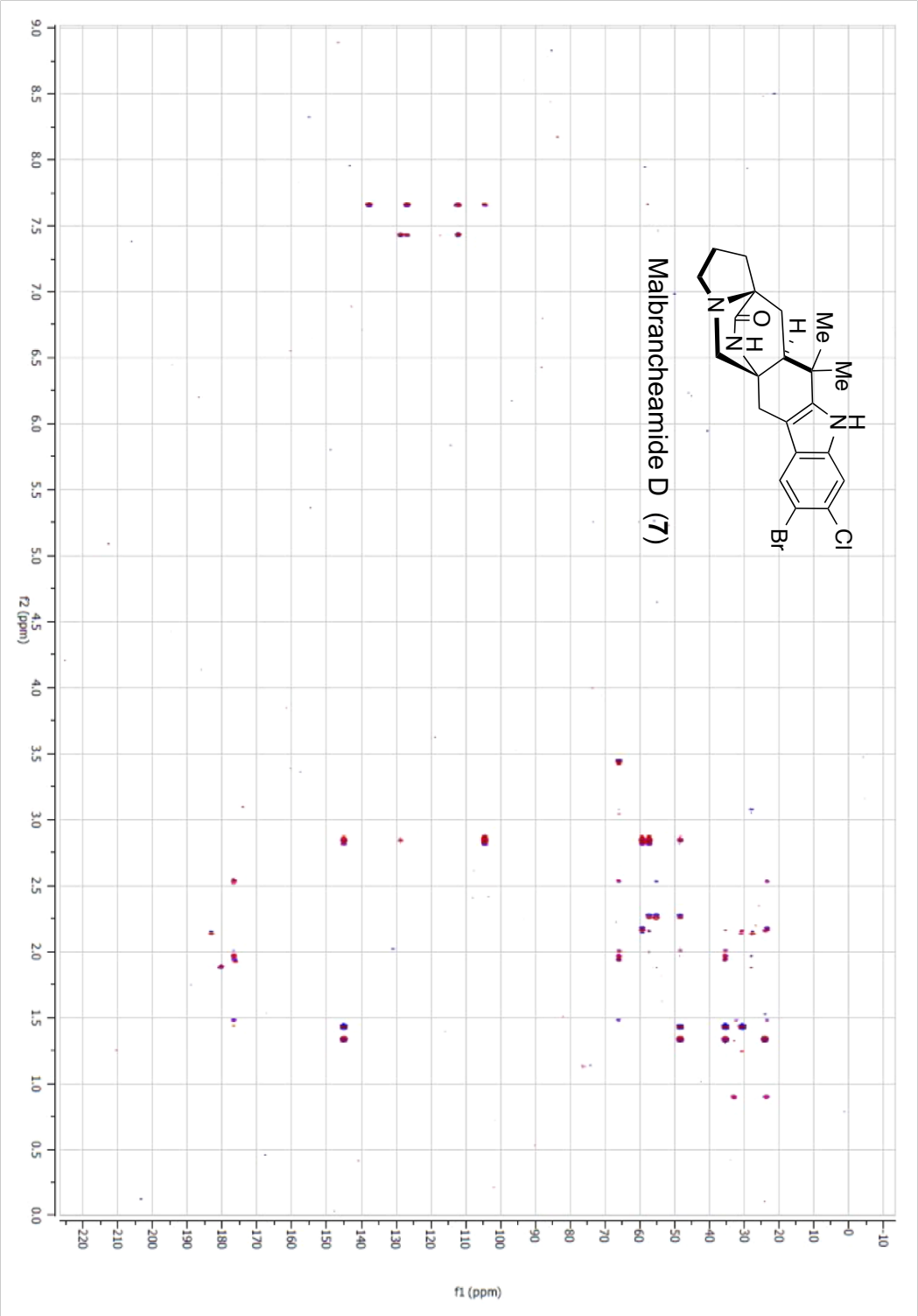

Figure 7.40. gHMBCAD correlations of malbrancheamide D from *in vitro* reaction with MalA (700 MHz, CD_3OD).

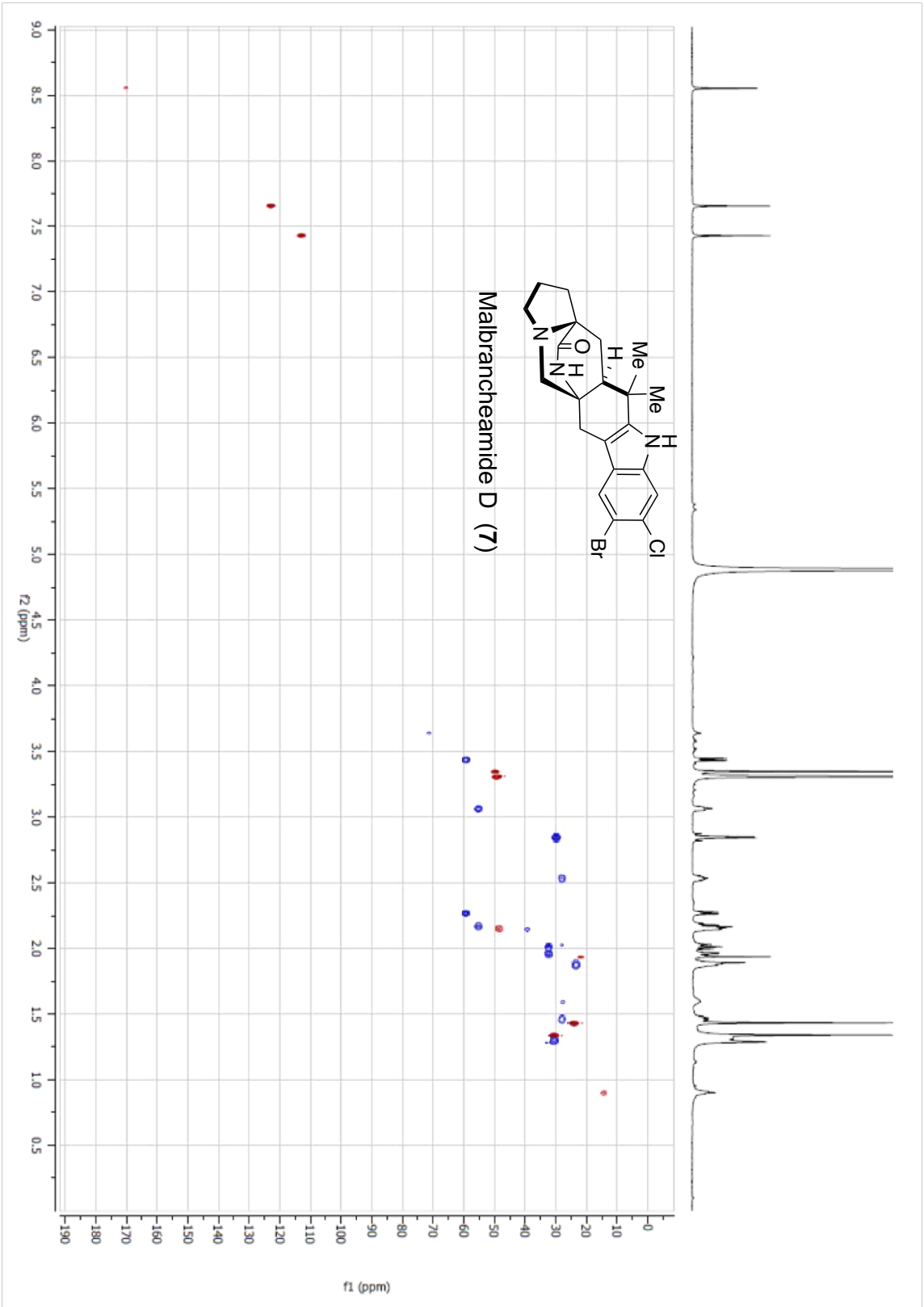

Figure 7.41 gHSQCAD correlations of malbrancheamide D from *in vitro* reaction with MalA (700 MHz, CD_3OD).

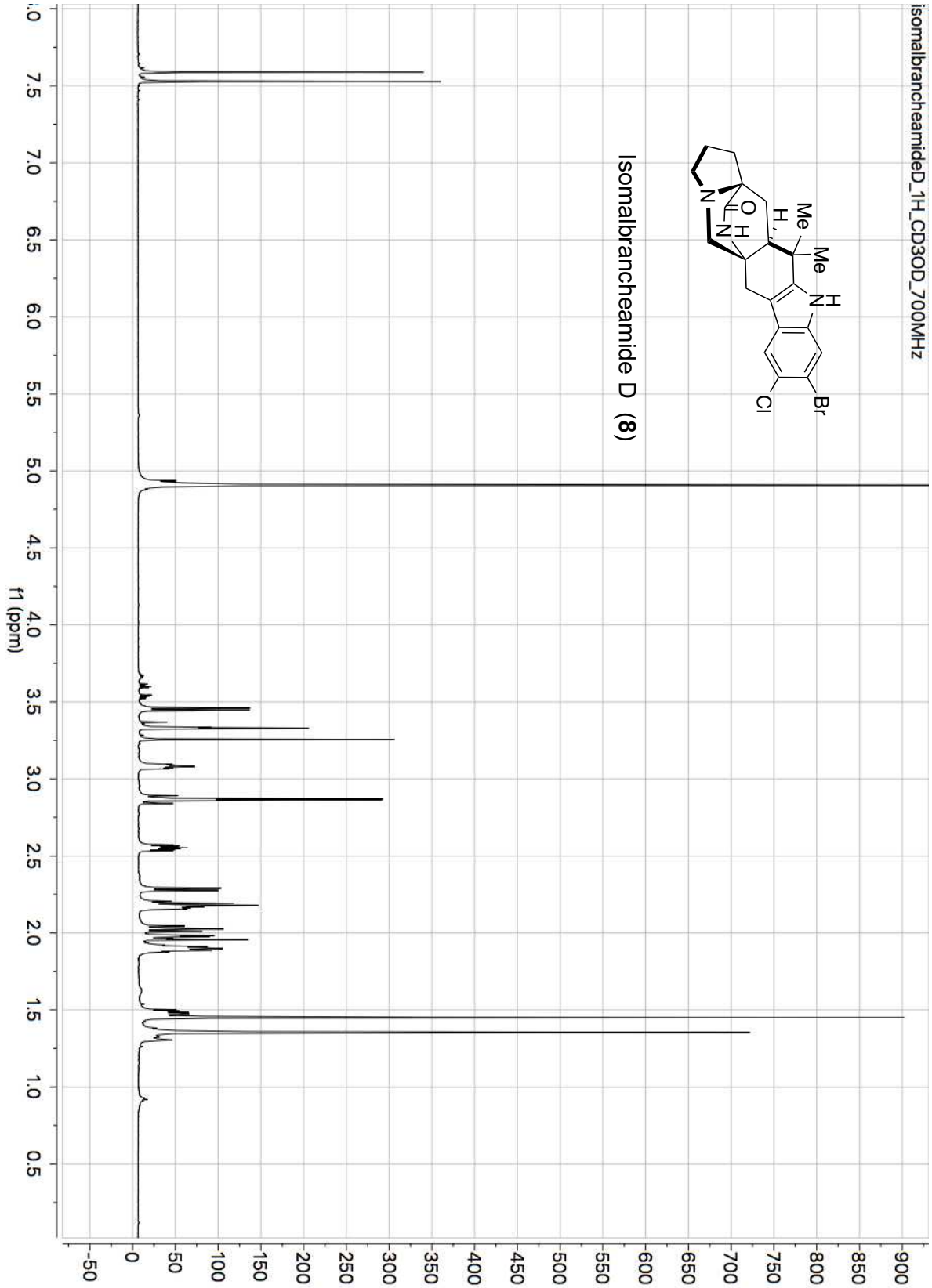

Figure 7.42 ^{1}H-NMR of isomalbrancheamide D from *in vitro* reaction with MalA (700 MHz, CD_3OD).

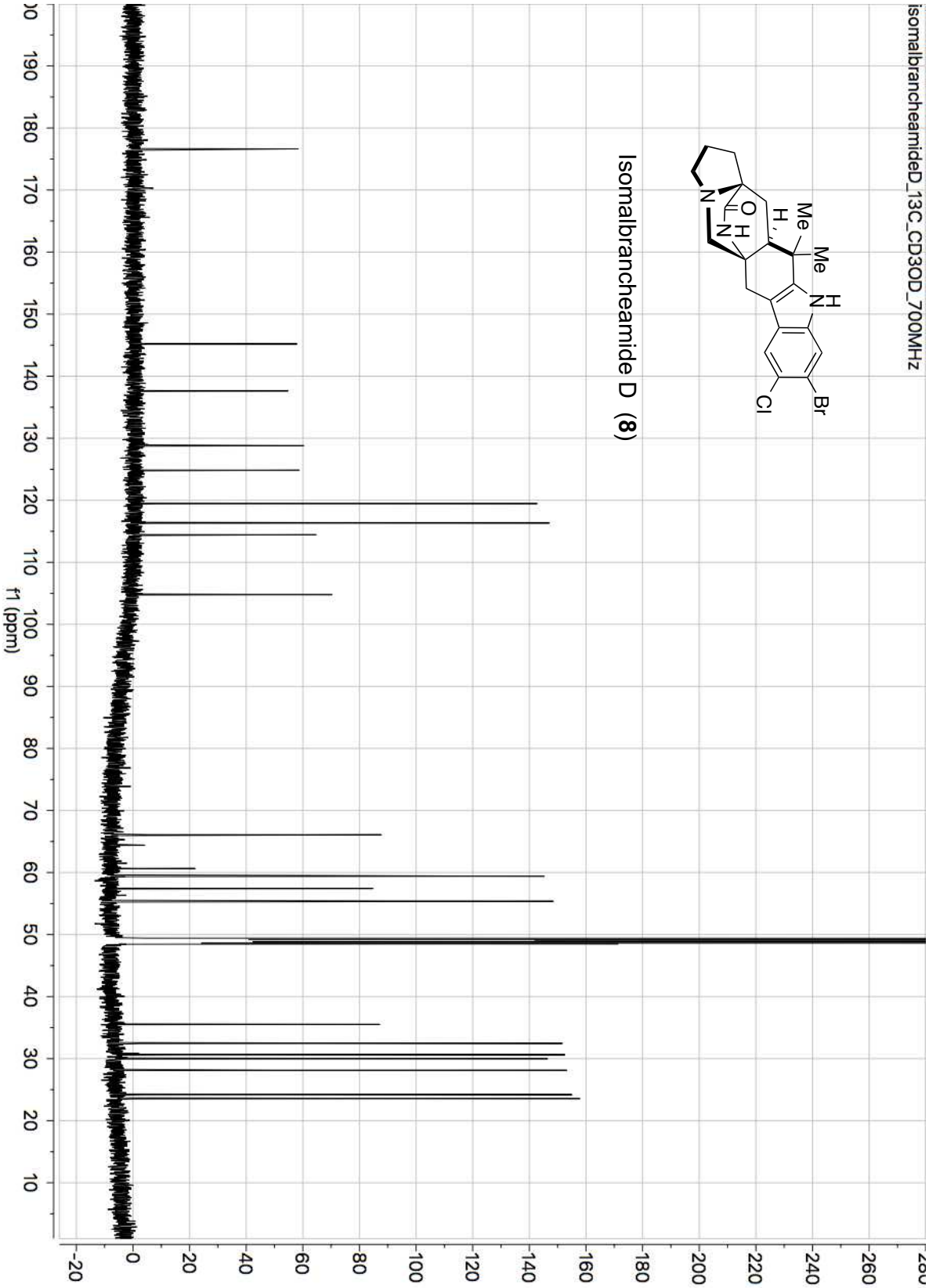

Figure 7.43 ^{13}C-NMR of isomalbrancheamide D from *in vitro* reaction with MalA (176 MHz, CD_3OD).

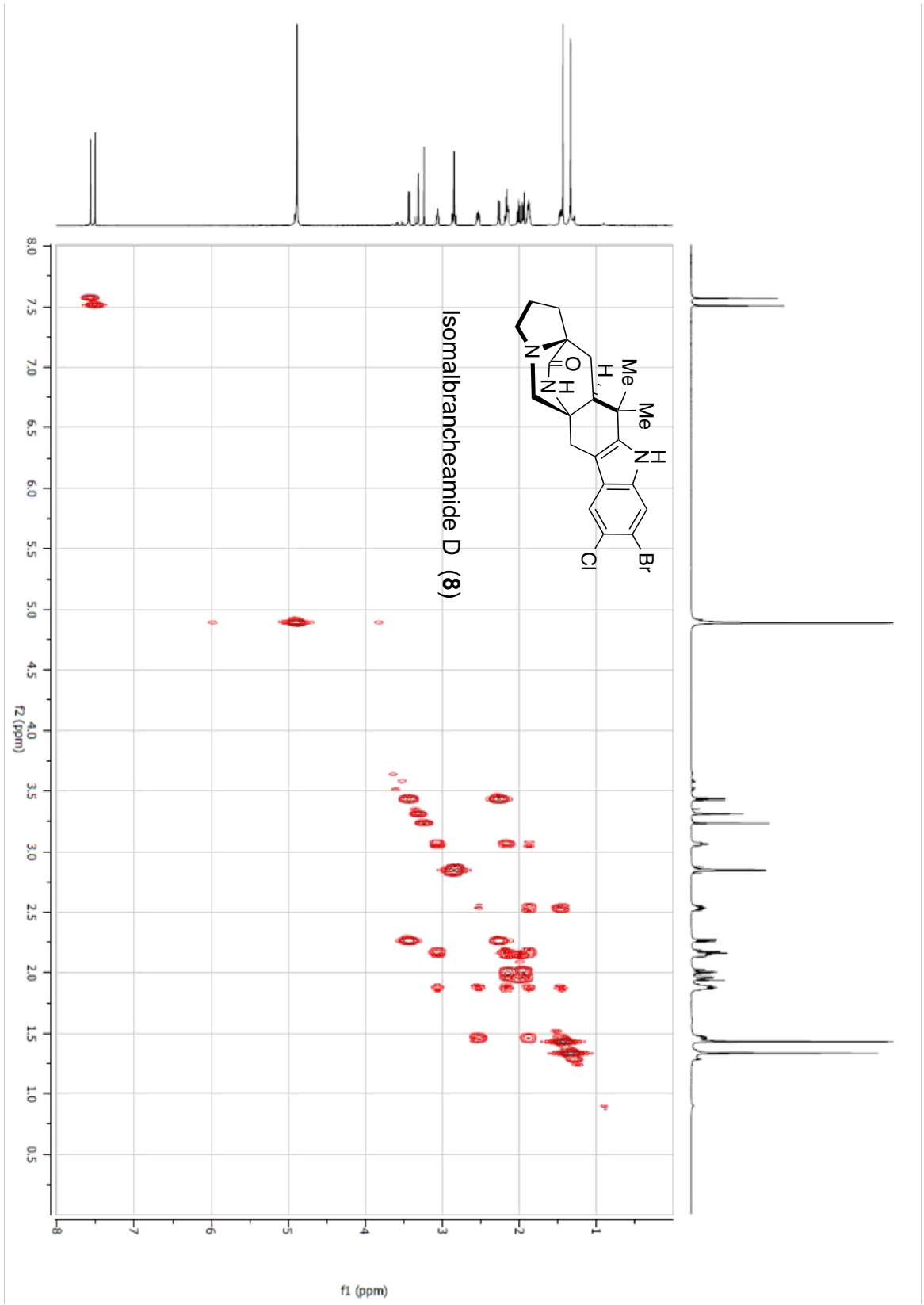

Figure 7.44 gCOSY correlations of isomalbrancheamide D from *in vitro* reaction with MalA (700 MHz, CD_3OD).

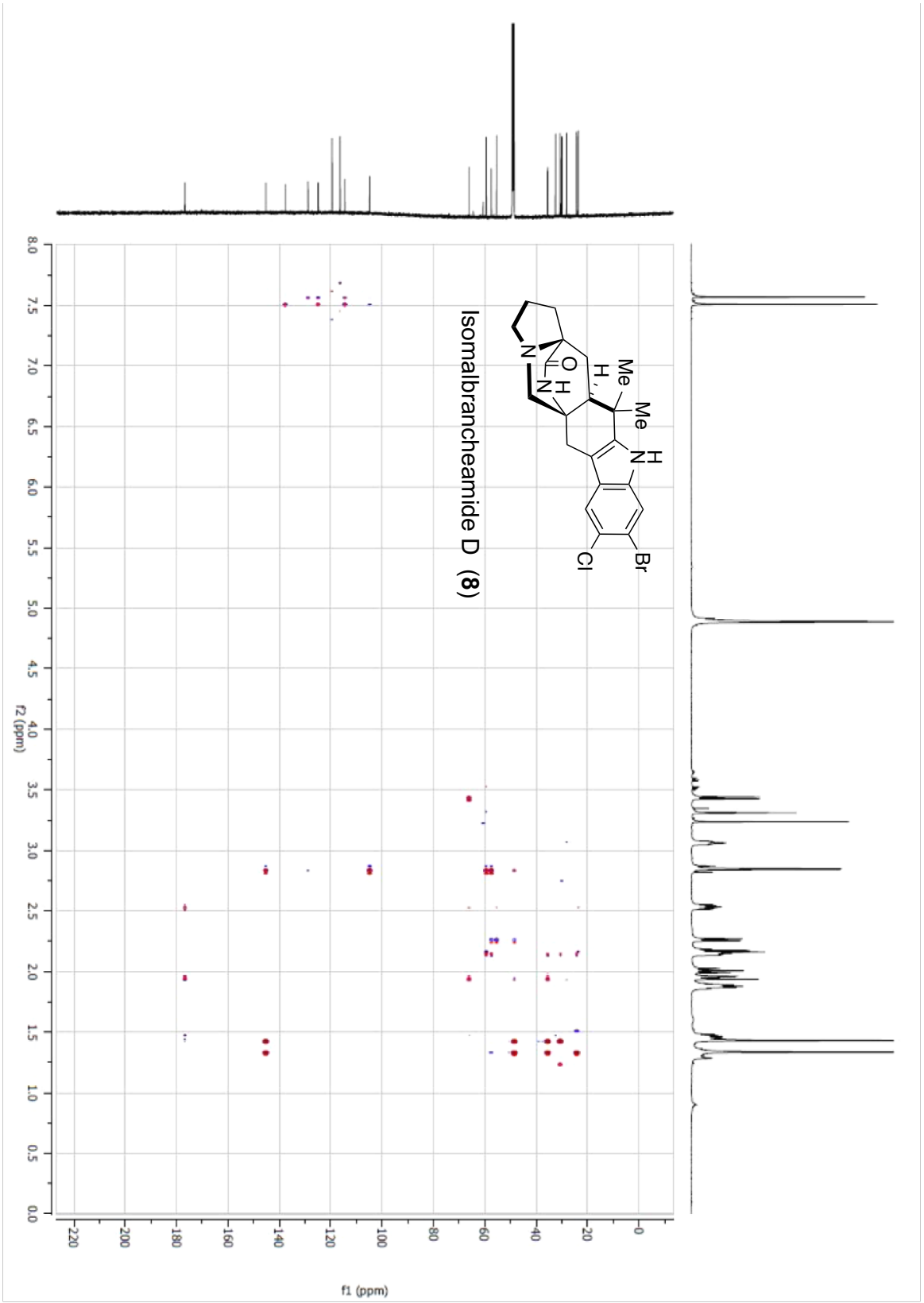

Figure 7.45 gHMBCAD correlations of isomalbrancheamide D from *in vitro* reaction with MalA (700 MHz, CD_3OD).

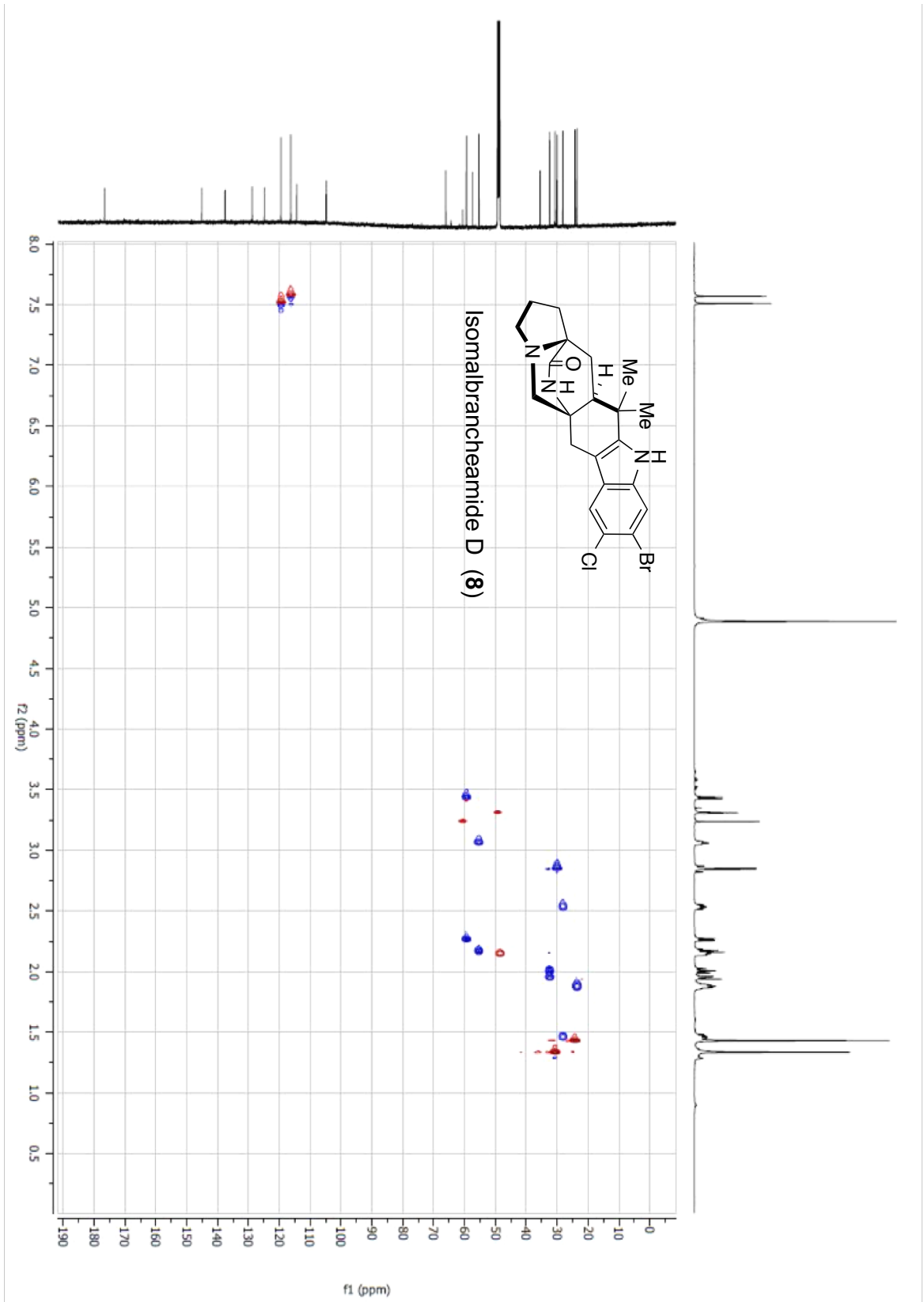

Figure 7.46 gHSQCAD correlations of isomalbrancheamide D from *in vitro* reaction with MalA (700 MHz, CD_3OD).

Chapter 8

Molecular Basis for Spirooxindole Formation in the Paraherquamide Biosynthetic Pathway Experimental Section

8.1 Experimental Methods

8.1.1 Fungal Strains and Culture Conditions

Penicillium fellutanum ATCC 20841 spores were generated on YPD agar plates over the course of 7 days. Spores were harvested into 5 mL sterile water per plate by gently scraping the surface of the culture with a sterile inoculating loop. Spores were stored at -80°C until ready to use. Genomic DNA was harvested using Wizard Genomic DNA Purification Kit from Promega.

8.1.2 cDNA Preparation and Cloning of phqK

Total RNA was extracted from a filter paper dried 17th day mycelia (roughly 500 mg fungal mat) culture of *Aspergillus protuberus* statically cultivated in liquid medium (50% seawater with 2.0% malt extract and 0.5% peptone) at 28°C, using Invitrogen PureLink RNA Mini Kit by following the plant tissue processing protocol. RNA was treated using Dnase I. cDNA was generated using Invitrogen Superscript First Strand Synthesis. PCR was used to amplify NotI from the cDNA template. To generate *phqK*, introns were predicted by analysis using Softberry Fgenesh-M, and the *phqK* gene was amplified from genomic DNA using overlapping PCR using primers in Table S1. Amplified genes were cloned into a *pKLD116* vector using restriction enzyme digest and ligation. Plasmids were transformed into E. coli DH5α for screening and plasmid maintenance.

8.1.3 Overexpression and Purification for Enzymatic Reactions

The *Escherichia coli* BL21 *pRARE* transformant containing *pKDL116-MBP-phqK* was grown at 37°C overnight in LB media containing 50 μg/mL of ampicillin and 100 μg/mL of spectinomycin. 10 mL of culture were used to inoculate 1 L of TB media containing the aforementioned concentrations of antibiotic and 4% glycerol. Cells were grown at 37°C for roughly 4 hours until A_{600} reached 0.6-1.0, and isopropyl β-D-thiogalactoside (IPTG, 0.2 mM) and riboflavin (50 μM) were added to induce protein overexpression overnight at 18°C.

All purification steps were conducted at 4°C. Briefly, 1 L of expression culture was spun down at 5,500 rpm. The harvested cell pellet was resuspended in 35 ml of lysis buffer (10 mM imidazole pH 8, 50 mM NaH_2PO_4, 300 mM NaCl, 10% v/v glycerol, adjusted to pH 8) with the addition of 10mg lysozyme, 4mg Dnase, 50 µM flavin adenine dinucleotide (FAD), 2 mM $MgSO_4$ and lysed by sonication. Insoluble material was removed by centrifugation at 20,000 rpm for 30 min, and the supernatant was filtered. NotI and NotI' were purified through metal affinity chromatography with Ni^{2+}-NTA resin (Novagen) that was equilibrated with lysis buffer. The protein-bound resin was washed with 50 mL of lysis buffer, 50 mL of wash buffer (20 mM imidazole pH 8, 50 mM NaH_2PO_4, 300 mM NaCl, 10% v/v glycerol, adjusted to pH 8), and finally 10 mL of elution buffer (250 mM imidazole pH 8, 50 mM NaH_2PO_4, 300 mM NaCl, 10% v/v glycerol, adjusted to pH 8). Protein in the eluate was exchanged into storage buffer (10 mM HEPES pH 7.6, 50 mM NaCl, 0.1 mM EDTA, 0.2 mM TCEP, 10% v/v glycerol) using a PD-10 column. Samples were then flash frozen with liquid N_2 and stored at -80°C.

8.1.4 Purification of PhqK for Crystallization and Kinetics

A cell pellet from a 1L expression culture was re-suspended in 30 mL lysis buffer (10 mM HEPES pH 8, 10 mM imidazole pH 8, 300 mM NaCl, 10% glycerol) and supplemented with 50 µM FAD. Cell lysis was accomplished through addition of 10 mg lysozyme, 4 mg Dnase, 2 mM $MgSO_4$, and sonication. Cell waste was cleared through centrifugation (18,000 rpm for 25 minutes). The supernatant was filtered and PhqK was purified through metal affinity chromatography on a 5 mL His-Trap column (GE Healthcare) with a 10 column volume gradient of elution buffer (10 mM HEPES pH 8, 280 mM imidazole pH 8, 300 mMM NaCl, 10% glycerol). The MBP and tag-free PhqK was separated from TEV protease and any remaining His_6-MBP-PhqK by metal affinity chromatography, and dialyzed into storage buffer (20mM HEPES pH 7.6, 300 mM NaCl, 10% glycerol).

8.1.5 Crystallization of PhqK

The purified PhqK was dialyzed overnight into 20 mM HEPES pH 7.6 buffer with 300 mM NaCl to remove glycerol and then supplemented with 2x FAD. For active site complexes with malbrancheamide B, paraherquamide K, and paraherquamide L, the protein was incubated with 5x concentration of substrate prior to crystallization. For active site complexes with malbrancheamide C, the protein was incubated with 2x concentration of substrate prior to crystallization. Crystals were grown by vapor diffusion from 1:1 mixture of 8-10 mg/mL PhqK

preincubated with substrate and a well solution containing 25% PEG 3350, 0.2 M ammonium acetate, 0.1 M Bis-Tris pH 5.5, and 2% 2,2,2-trifluoroethanol. Crystals with no substrate bound were produced in a similar manner, except without the addition of substrate. Crystals were cyoprotected in well solution at 30% PEG 3350 and flash-cooled in liquid nitrogen.

8.1.6 Data Collection

Data were collected at GM/CA beamline 23ID-B at the Advanced Photon Source (APS) at Argonne National Laboratory. For the SeMet-PhqK crystal, 360º of diffraction data were collected in inverse-beam geometry using 30º wedges. All data were processed using XDS.[236] The SeMet PhqK monooxygenase structure was solved by single-wavelength anomalous diffraction (SAD) using AutoSol in the Phenix suite to locate the Se sites, determine initial phases and perform density modification (figure of merit = 0.320).[237] AutoBuild in the Phenix suite was used to build an 82% complete starting model. The SeMet PhqK model was used as a template in molecular replacement to solve the native PhqK structures using Phaser in the Phenix suite. A progression of model building and refinement were carried out to complete the models using Coot and Phenix Refine with seven translation/libation/screw groups.[238]

8.1.7 Enzymatic Reactions and HPLC Analysis of PhqK Reactions

The standard enzyme assay containing 200 µM FAD, 200 µM substrate, 5 mM NADH, and 40 µM enzyme in 50 µL reaction buffer (10 mM HEPES pH 7.6, 50 mM NaCl, 0.1 mM EDTA, 0.2 mM TCEP 10% v/v glycerol, pH 7.6) was performed at 28°C for 2 hours. The reactions were quenched with 100µL LC/MS grade methanol and centrifuged to remove solid material. The samples were analyzed on a Schimadzu HPLC using a Phenomenex Lux 5 µm Cellulose-3 LC column 250x4.6mm with the following time program: 30% acetonitrile for 1 minute, 30-95% acetonitrile over 15 minutes, 95% acetonitrile for 1 minute, 95-30% acetonitrile over 1 minute, and 30% acetonitrile for 7 minutes. The flow rate was 1.5 mL/min and the reactions were monitored at 240nm.

8.1.8 Enzymatic Reactions and HPLC analysis of PhqK Kinetics

The standard enzyme assay containing 200 µM FAD, varying concentrations of substrate between 20 and 700 µM, 5 mM NADH, and 1 µM enzyme in 250 µL reaction buffer (10 mM HEPES pH 7.6, 50 mM NaCl, 0.1 mM EDTA, 0.2 mM TCEP 10% v/v glycerol, pH 7.6) was performed at 28°C for varying time points (4, 10, 20, 30 minutes). At each time point, 50 µL of the reaction mix were quenched with 100µL ethyl acetate, vortexed, and extracted. The samples were resuspended

in 50 µL methanol and analyzed on a Schimadzu HPLC using a Phenomenex Lux 5 µm Cellulose-3 LC column 250x4.6mm with the following time program: 15-75% acetonitrile over 7 minutes, 95% acetonitrile for 2.5 minutes, 75-15% acetonitrile over half a minute, and 15% acetonitrile for 5 minutes. The flow rate was 1.4 mL/min and the reactions were monitored at 240nm. Three replicates were performed for each time point.

8.2 Tables

Table 8.1 Primers for *phqK* intron removal and amplification

Name	Sequence
*phqK*_Int1_F	ATGGGCTCTTTAGGTGAAGAAGTTCAAG
*phqK*_Int1_R	GTTGCTTTGAAGACCAATACAGTCTCCGATGGACTTCA GTATATTGCTTTTC
*phqK*_Int2_F	GAAAAGCAATATACTGAAGTCCATCGGAGACTGTATTG GTCTTCAAAGCAAC
*phqK*_Int2_R	CAGACGTCTAGGAGATTTCTTGTATCCTGATGAATGCAG AACCACGAAAAG
*phqK*_Int3_F	CTTTTCGTGGTTCTGCATTCATCAGGATACAAGAAATCT CCTAGACGTCTG
*phqK*_Int3_R	CTAGGGTGACTTGTTCTGCAATGG

Table 8.2 Crystallographic Information

Ligand	Malbrancheamide B (SeMet)	None	Malbrancheamide C	Paraherquamide K	Paraherquamide L
Space Group	*P* 2_1 2_1 2_1	*P* 2_1 2_1 2_1	*P* 2_1 2_1 2_1	*P* 2_1 2_1 2_1	*P* 2_1 2_1 2_1
Cell Dimensions					
a,b,c (Å)	48.0, 82.4, 119.3	47.7, 84.2, 116.4	48.1, 82.8, 120.1	48.2, 83.2, 119.6	64.9, 79.9, 87.7
	90.0, 90.0, 90.0	90.0, 90.0, 90.0	90.0, 90.0, 90.0	90.0, 90.0, 90.0	90.0, 90.0, 90.0
X-ray Source	APS 23ID-B	APS 23ID-B	APS 23ID-B	APS 23ID-B	APS 23ID-B
Wavelength (Å)	0.979	1.033	0.7293	1.033	1.033
d_{min} (Å)	1.69 (1.75 – 1.69)	1.71 (1.77 – 1.71)	1.25 (1.30 – 1.25)	1.89 (1.96 – 1.89)	2.09 (2.17 – 2.09)
R-merge	0.082 (0.948)	0.071 (1.195)	0.069 (1.548)	0.193 (1.463)	0.155 (1.160)
Avg I/σ	21.58 (1.55)	19.97 (1.34)	17.88 (1.11)	10.93 (1.14)	12.08 (1.66)
Completeness (%)	99 (88)	99 (91)	100 (99)	99 (95)	100 (98)
Multiplicity	12.0 (8.0)	12.4 (9.1)	13.0 (10.7)	12.7 (11.8)	12.6 (11.9)
Total Reflections	635,907	630,819	1,725,902	495,499	345,452
$CC_{1/2}$	1.00 (0.72)	1.00 (0.60)	1.00 (0.53)	1.00 (0.56)	1.00 (0.54)
CC*	1 (0.91)	1 (0.87)	1 (0.83)	1 (0.85)	1 (0.84)
Refinement					
Reflections (#)	53,023 (4,655)	50,852 (4,603)	132,940 (13,092)	38,891 (3,628)	27,473 (2,646)
R_{work}/R_{free} (%)	16.9/20.7	16.2/19.2	15.5/17.5	21.5/26.1	20.7/25.6
Number of Non-Hydrogen Atoms	4,077	3,991	4,268	3,823	3,728
Macromolecules	3,522	3,538	3,570	3,517	3,483
Ligands	79	53	79	85	86
Solvent	476	400	619	221	159
Amino Acid Residues	445	445	444	444	440
Deviation From Ideality					
Bond Lengths (Å)	0.007	0.006	0.006	0.007	0.008
Bond Angles (deg)	0.9	0.86	0.87	0.94	1.01
Average B-Factor ($Å^2$)	29.6	37.4	26.2	9	57.9
Macromolecules	28.4	36.6	23.7	39.8	58
FAD	20.6	25.6	19.5	30.1	39.2
Substrate	29.6		20.6	57.3	92.5
Solvent	39.1	46.3	41.3	41	55.6
Ramachandran Plot					
Favored (%)	97.97	97.52	98.19	97.06	96.33
Allowed (%)	2.03	2.48	1.81	2.94	3.67
Outliers (%)	0	0	0	0	0

Table 8.3 NMR data for paraherquamide K (**1.24**). ^{13}C-NMR, ^{1}H-NMR, gHMBCAD, and gCOSY, correlations for paraherquamide K isolated from *phqK* knockout in *P. simplicissimum*. HRMS (ESI-QTOF): m/z $[M+H]^+$ calculated for $C_{27}H_{33}N_3O_2$ = 432.2651, experimental (isolated) = 432.2662.

Paraherquamide K DMSO-d6, 800 MHz

	∂ ^{13}C	∂ ^{1}H (*J* [Hz])	gHMBCAD	gCOSY
1			2, 3, 8, 9	
2	140.09			
3	103.76			
4	117.32	7.01 (8.3)	3, 6, 8	5
5	108.52	6.44 (8.3)	6, 7, 9	4
6	147.43			
7	104.78			
8	132.82			
9	121.51			
10a	28.95	2.65 (d, 15.5)	2, 3, 11, 12a, 20	
10b		2.71 (d, 15.5)	2, 3, 11, 12a,	
11	55.62			
12a	59.53	2.05 (d, 10.2)	11, 16, 20	
12b		3.27 (m)		
13	64.36			
14	39.84	1.85 (dd, 16.6, 9.1)		17
15a	30.18	1.70 (ddd, 21.8, 11.1, 5.4)		16a
15b		1.91 (m)		
16a	53.93	2.14 (m)		15
16b		3.08 (m)		
17	13.13	1.32 (d, 7.0)	13, 14	
18	172.70			
19a	29.34	1.58 (dd, 12.8, 4.0)	13, 18,21	
		2.02 (dd, 12.5)		
20	46.16	1.97 (m)		
21	33.87			
22	30.02	1.28 (s)	2, 20, 21, 23	
23	23.38	1.31 (s)	2, 20, 21, 22	
24	118.13	6.94 (d, 9.8)	6, 26	25
25	128.91	5.72 (d, 9.7)	7, 26	24
26	74.98			
27	27.08	1.36	25, 26, 28	
28	27.08	1.36	25, 26, 27	
29		8.11	10, 11, 13	

Table 8.4 NMR data for paraherquamide L (**1.25**). ^{13}C-NMR, ^{1}H-NMR, gHMBCAD, and gCOSY, correlations for paraherquamide L isolated from *phqK* knockout in *P. simplicissimum*. HRMS (ESI-QTOF): m/z $[M+H]^+$ calculated for $C_{27}H_{33}N_3O_3$ = 448.2600, experimental (isolated) = 448.2612.

Paraherquamide L DMSO-d6, 600 MHz

	∂ ^{13}C	∂ ^{1}H (*J* [Hz])	gHMBCAD	gCOSY
1		10.89 (s)	2, 3, 9, 10	
2	141.57			
3	104.01			
4	112.32	6.92 (d, 8.3)	6, 8	5
5	115.81	6.64 (d, 8.3)	6, 7, 9	4
6	139.58			
7	136.82			
8	127.96			
9	124.69			
10	29.03	2.71 (m)	2, 3, 9, 11, 20	
11	55.6			
12	59.54	2.05 (m)		
		3.28 (d, 9.9)		
13	64.38			
14	39.91	1.85 (m)	18	15
15	30.19	1.68 (ddt, 15.5, 10.5, 5.0)	14, 16, 17	14, 16
		1.90 (m)		
16	53.43	2.14 (td, 10.2, 4.7)		15
		3.08 (q, 8.8)		
17	13.17	1.31 (s)	14	
18	172.72			
19	29.44	1.58 (dd, 12.4, 3.5)	13, 18, 20, 21	
		2.02 (m)		
20	46.2	1.98 (m)		
21	34.07			
22	29.83	1.29 (s)	23	
23	23.22	1.30 (s)	2, 21, 22	
24	139.25	6.51 (d, 7.6)	7, 25, 26	
25	115.35	4.97 (d, 7.6)	24, 26	
26	78.86			
27	29.5	1.35 (s)	25, 26	
28	29.5	1.35 (s)	25, 26	
29		8.13 (s)	10, 11	

Table 8.5 NMR data for paraherquamide M (**1.26**). ^{13}C-NMR, ^{1}H-NMR, gHMBCAD, gCOSY, and NOESY correlations for paraherquamide M isolated from PhqK *in vitro* reaction. HRMS (ESI-QTOF): m/z $[M+H]^+$ calculated for $C_{27}H_{33}N_3O_3$ = 448.2600, experimental (isolated) = 448.2604.

Paraherquamide M DMSO-d6

Position	∂ ^{13}C	∂ ^{1}H (*J* [Hz])	gHMBCAD	gCOSY	NOESY
1		10.61 (s)	8		24
2	183.17				
3	172.02				
4	125.91	7.03 (d, 8.1)	6, 7, 8, 10	5	5, 10a
5	108.02	6.32 (d, 8.1)	6, 7	4	4
6	152.00				
7	104.31				
8	138.35				
9	122.13		5		
10a	38.41	1.78 (d, 14.8)	2, 12, 16		
10b		2.27 (d, 14.8)	2, 21		29
11	61.37				
12	60.15	2.31 (d, 10.5)	16, 18		
		3.58 (d, 10.7)	13, 20		
13	66.96				
14	39.34	1.81 (m)	13		17
15	30.05	1.64 (m)		16	
		1.90 (m)			
16	52.43	2.13 (m)		15	
		3.05 (m)	13		
17	13.06	1.30 (d, 7.0)	13, 16		
18	60.74				
19a	27.06	1.27 (m)	20	20	20
19b		1.88 (m)	3, 17		20
20	52.53	2.84 (t, 10.4	19, 22, 23	19	19b
21	45.21				
22	23.99	0.72 (s)	11, 20, 21, 23		
23	20.24	0.94 (s)	20, 21, 22		
24	116.68	6.57 (d, 9.9)	6, 7, 8, 25, 26	25	
25	130.1	5.73 (d, 9.9)	7, 27	24	
26	75.73				
27	27.52	1.36 (d) 18.5	25, 26, 28		
28	27.52	1.36 (d) 18.5	25, 26, 27		
29		8.47 (s)			

Table 8.6 NMR data for paraherquamide N (**1.27**). ^{13}C-NMR, ^{1}H-NMR, gHMBCAD, gCOSY, and NOESY correlations for paraherquamide N isolated from PhqK *in vitro* reaction. HRMS (ESI-QTOF): m/z $[M+H]^+$ calculated for $C_{27}H_{33}N_3O_4$ = 464.2549, experimental (isolated) = 464.2550.

Paraherquamide N, DMSO-d6

Position	∂ ^{13}C	∂ ^{1}H (*J* [Hz])	gHMBCAD	gCOSY	NOESY
1		10.51	3, 6, 8		
2	182.45				
3	62.03				
4	120.96	6.99 (d, 8.1)	3, 8, 9	5	10a, 23
5	116.17	6.60 (d, 8.0)	6, 7, 9	4	
6	126.22				
7	135.04				
8	133.41				
9	145.61				
10a	38.33	1.82 (s)	2, 21, 16		
10b		2.28 (s)	2, 21		29
11	60.87				
12a	60.14	2.31 (d, 10.7)	13, 16		
12b		3.61 (d, 10.8)	13, 16		
13	66.93				
14	39.46				
15a	30.06	1.64 (m)	14, 16, 17	16	
15b		1.91 (m)	13		
16a	52.45	2.14 (m)	12	15	
16b		3.05 (m)	13, 14, 15		
17	13.03	1.30 (d, 7.0)	13, 14, 15		
18	172.00				
19a	27.05	1.27 (m)	11, 18, 20, 21	20	
19b		1.89 (m)	13, 18		
20	52.45	2.81 (t, 20.5, 10.3)	19, 21, 22, 23	19	19a, 19b
21	45.21				
22	24.11	0.72 (s)	3, 20, 21, 23		
23	20.40	0.95 (s)	3, 20, 21, 23		
24	139.00	6.36 (d, 7.6)	7, 25, 26	25	25
25	115.17	4.97 (d, 7.6)	24, 26, 27, 28	24	24
26	79.28				
27	29.22	1.36 (d, 16.7)	24, 25, 26, 28		
28	29.22	1.36 (d, 16.7)	24, 25, 26, 27		
29		8.50 (s)	10, 13, 11		10b

Table 8.7 ^{1}H-NMR for malbrancheamide isolated from *Malbranchea aurantiaca*. HRMS (ESI-QTOF): m/z $[M+H]^{+}$ calculated for $C_{21}H_{23}Cl_2N_3O$ = 404.1291, experimental (isolated) = 404.1287.

Malbrancheamide, CD_3OD

Position	∂ ^{1}H (*J* [Hz])
1	2.56m
	1.49m
2	1.87m
3	2.03m
	2.19m
5	2.27 (dd, 10.3, 1.5)
	3.43 (d, 10.2)
6	2.84
7	7.48
10	7.40
12a	2.13m
13	2.03 (d, 13.1)
	1.96 (dd, 13.1, 5.2)
16	1.32s
17	1.42s

Table 8.8 ^{13}C-NMR, ^{1}H-NMR, gHMBCAD, gCOSY, and NOESY correlations for spiromalbramide isolated from PhqK *in vitro* reaction. HRMS (ESI-QTOF): m/z $[M+H]^+$ calculated for $C_{27}H_{33}N_3O_4$ = 420.1246, experimental (isolated) = 420.1243.

Spiromalbramide, CD_3OD, 600MHz

Position	∂ ^{13}C	∂ ^{1}H (*J* [Hz])	gHMBCAD	gCOSY	NOESY
1	28.19	2.46 (ddd, 12.8, 9.5, 3.9)	14	2	2
	28.21	1.46 (td, 11.7, 7.1)	13a	2	
2	22.99	1.89 (m)		1, 3	1, 3
3	54.08	3.11 (td, 8.9, 3.0)		2	2
		2.25 (q, 8.9)		2	
5	59.77	3.71 (d, 11.3)	3, 5a, 13a		17
	59.73	2.65 (d, 10.0)			
5a	68.62				
6	39.31	2.39 (d, 15.1)	5, 6a, 6b, 11a, 12, 12a		
	39.24	2.06 (d, 15.2)			
6a	63.75				
6b	131.82				
7	128.72	7.51	6a, 8, 9, 10a		6, 17
8	125.49				
9	132.24				
10	112.12	7.02	8, 9, 10a		
10a	143.75				
11a	184.11				
12	46.97				
12a	55.10	3.05 (t, 10.1)		13	16
13	28.81	1.86 (m)	5a, 14	12a	12a
	28.78	1.71 (dd, 12.7, 10.0)			17
13a	62.60				
14	1756.1				
16	24.40	0.83 (s)	6a, 12, 12a, 17		
17	20.93	1.12 (s)	6a, 12, 12a, 16		5, 13

8.3 Figures

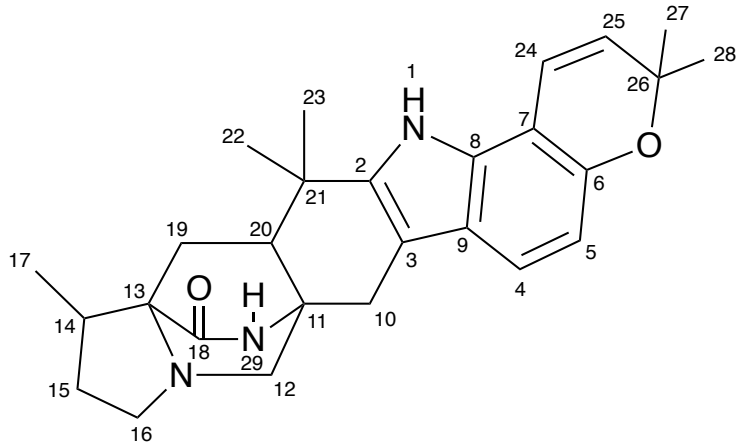

Figure 8.1 Numbering scheme for paraherquamide K (**1.24**).

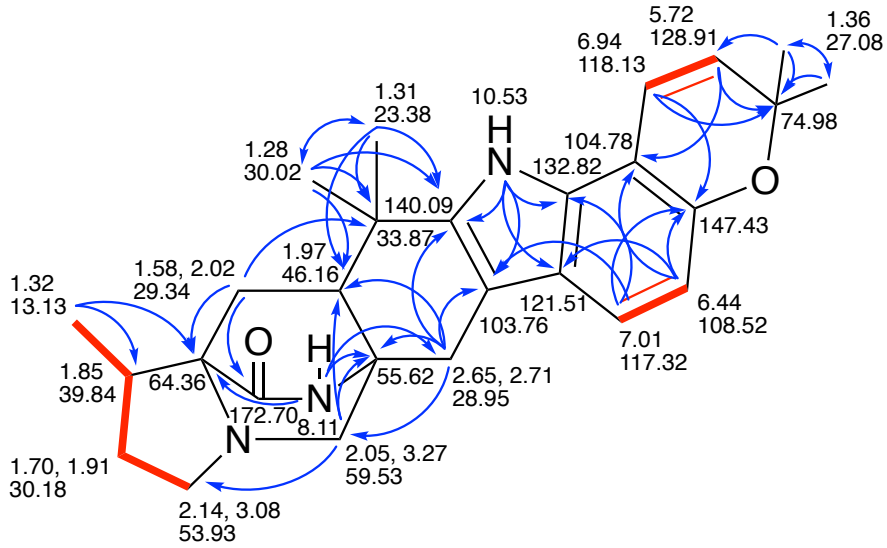

Figure 8.2 gHMBC and gCOSY correlations for paraherquamide K (**1.24**).

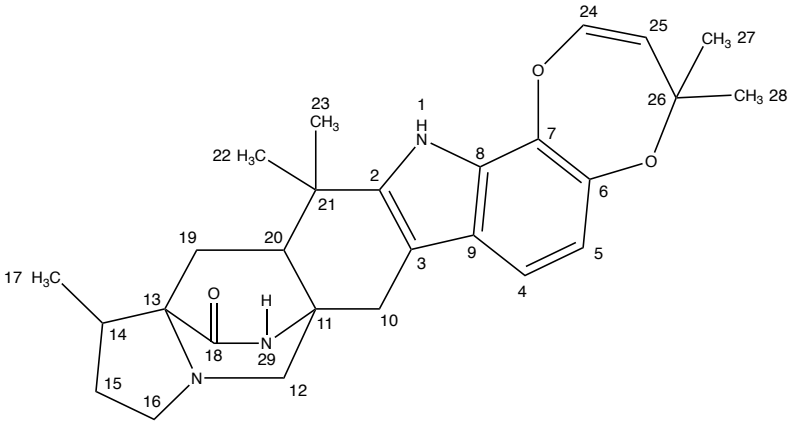

Figure 8.3 Numbering scheme for paraherquamide L (**1.25**).

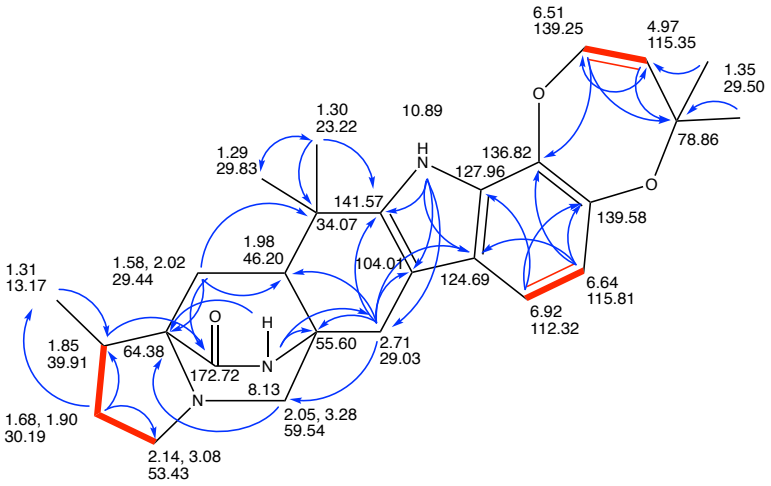

Figure 8.4 gHMBC and gCOSY correlations for paraherquamide L (**1.25**).

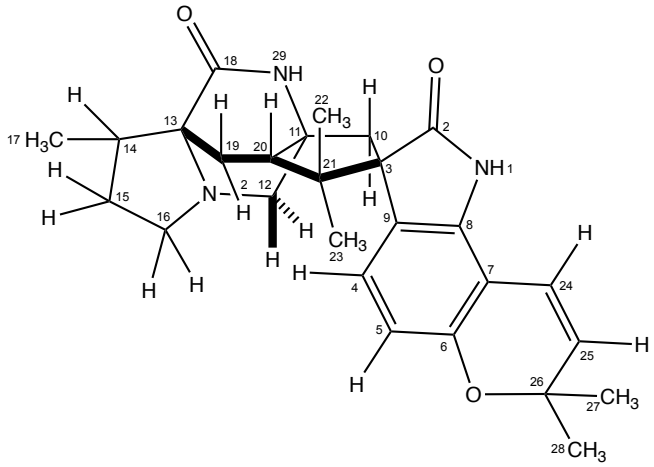

Figure 8.5 Numbering scheme for paraherquamide M (**1.26**).

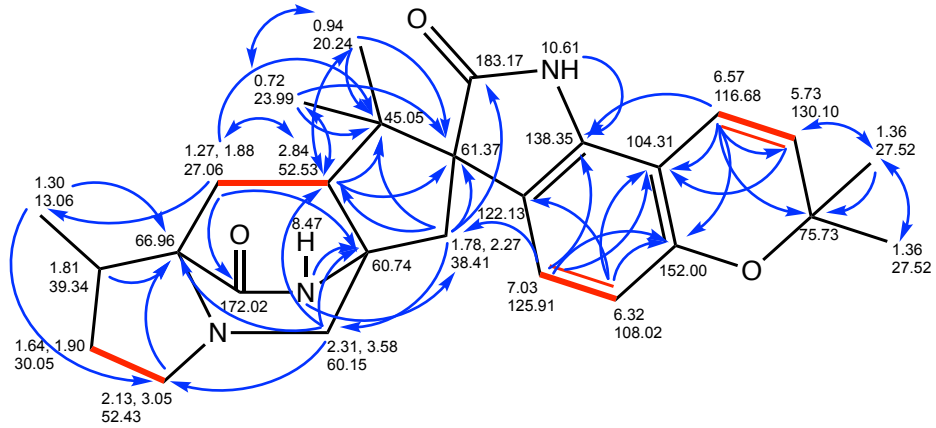

Figure 8.6 gHMBC and gCOSY correlations for paraherquamide M (**1.26**) in DMSO-d_6.

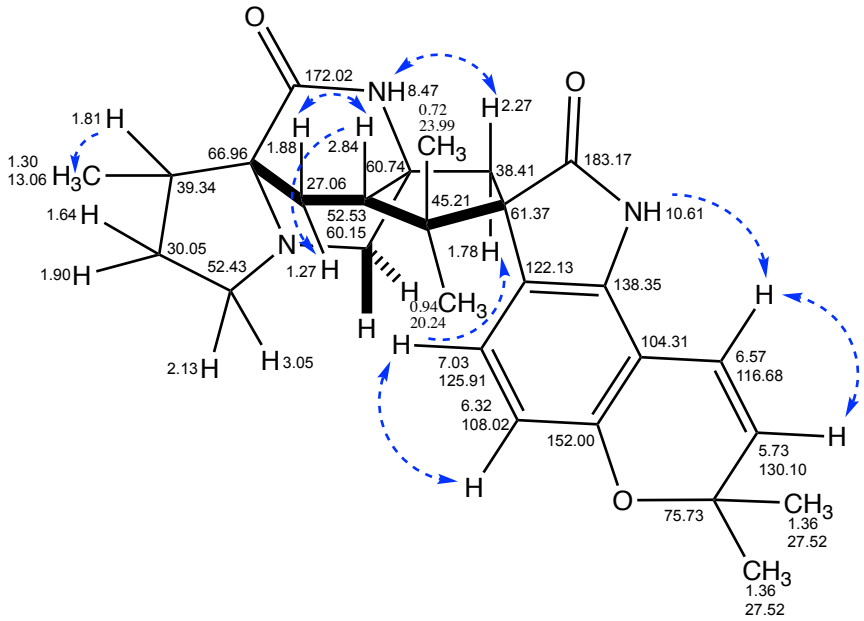

Figure 8.7 NOESY correlations for paraherquamide M (**1.26**) in DMSO-d_6.

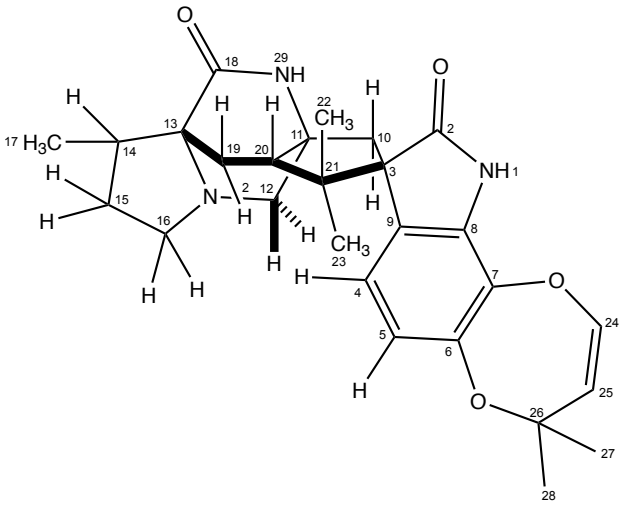

Figure 8.8 Numbering scheme for paraherquamide N (**1.27**).

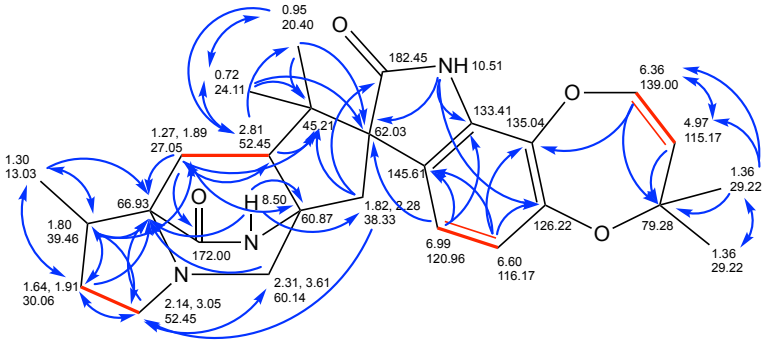

Figure 8.9 gHMBC and gCOSY correlations for paraherquamide N (**1.27**) in DMSO-d_6.

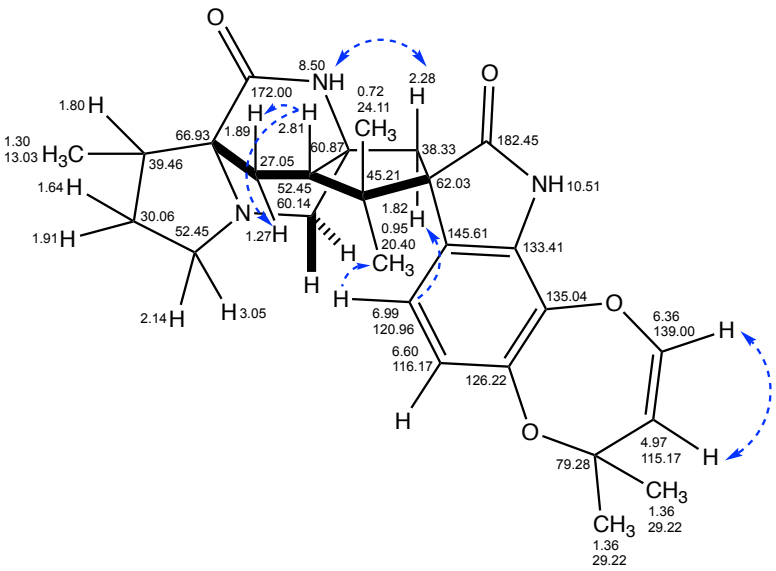

Figure 8.10 NOESY correlations for paraherquamide N (**1.27**) in DMSO-d_6.

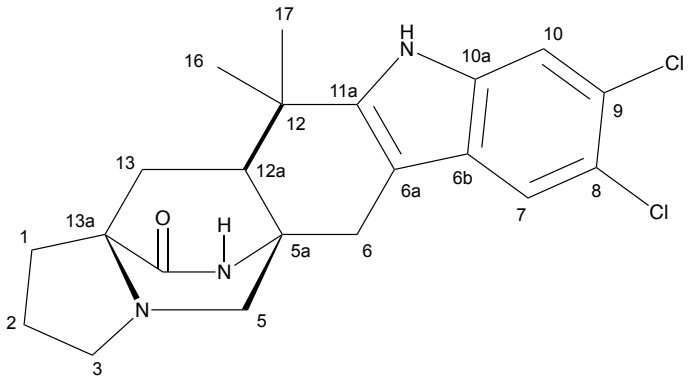

Figure 8.11 Numbering scheme for malbrancheamide (**1.17**).

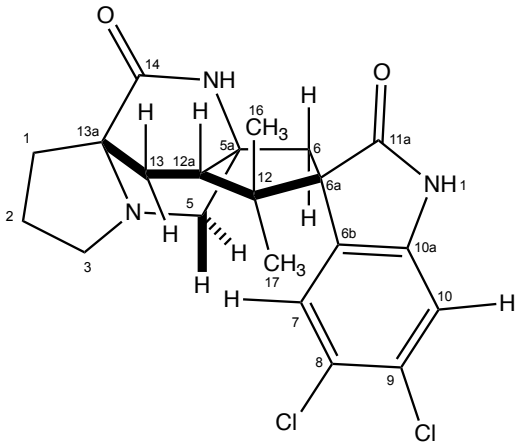

Figure 8.12 Numbering scheme for spiromalbramide (**3.1**).

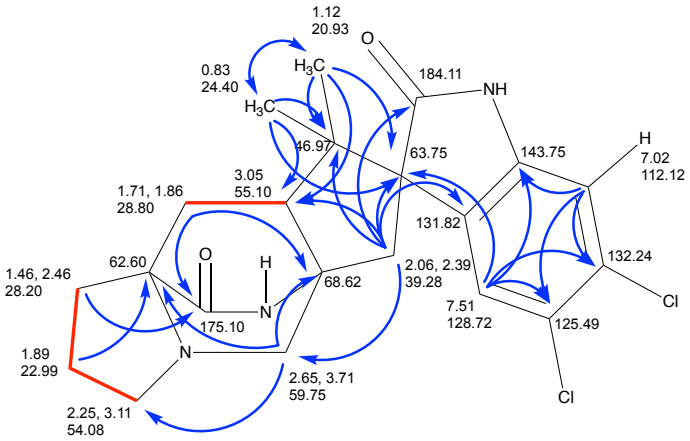

Figure 8.13 gHMBC and gCOSY correlations for spiromalbramide (**3.1**) in CD_3OD.

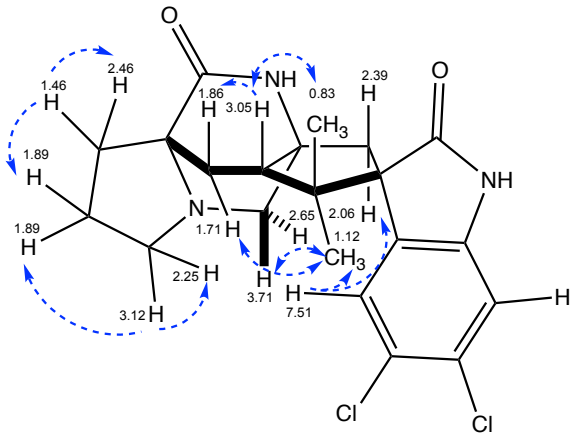

Figure 8.14 NOESY correlations for spiromalbramide (**3.1**) in CD_3OD.

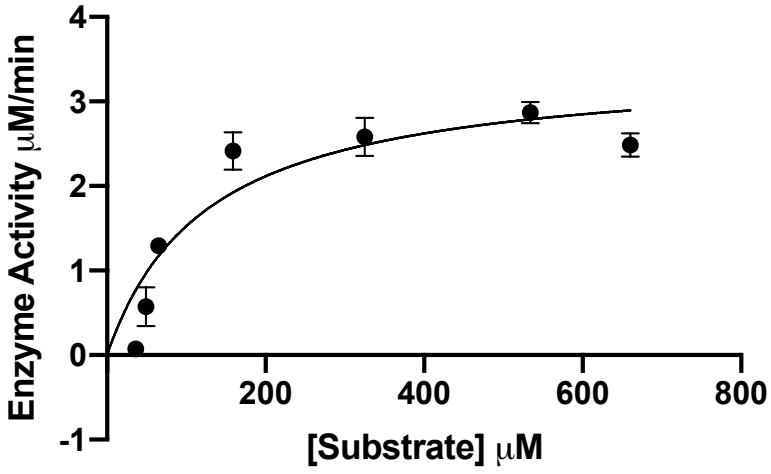

Figure 8.15 Michaelis-Menten model kinetics for paraherquamide K (**1.24**).

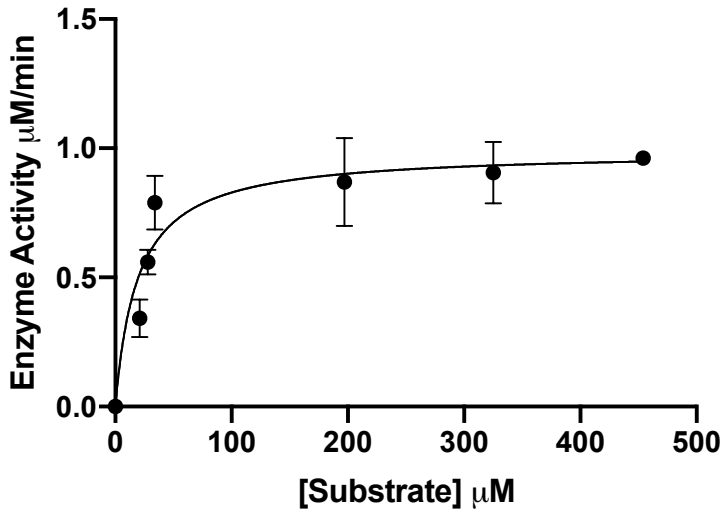

Figure 8.16 Michaelis-Menten model kinetics for paraherquamide L (**1.25**).

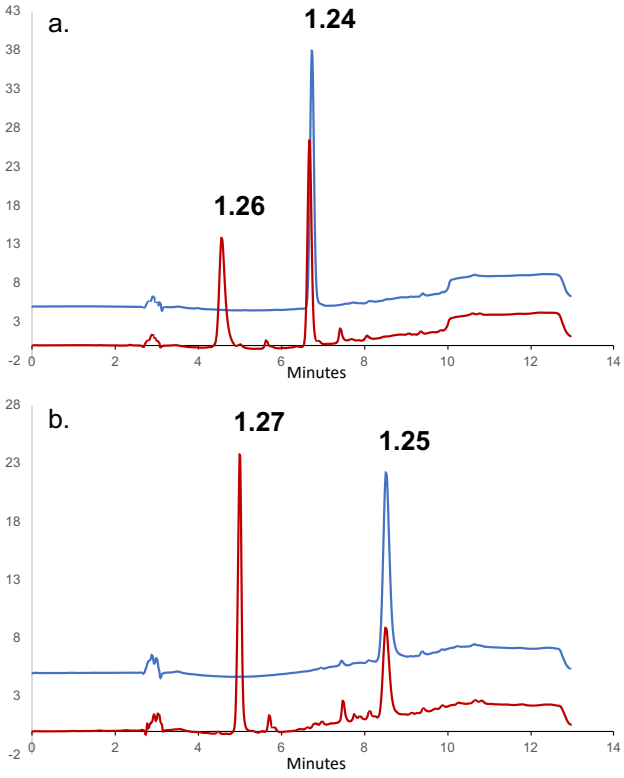

Figure 8.17 PhqK reactions with paraherquamide K **1.24** (a.) and paraherquamide L **1.25** (b.) with no enzyme control in blue and the reaction shown in red.

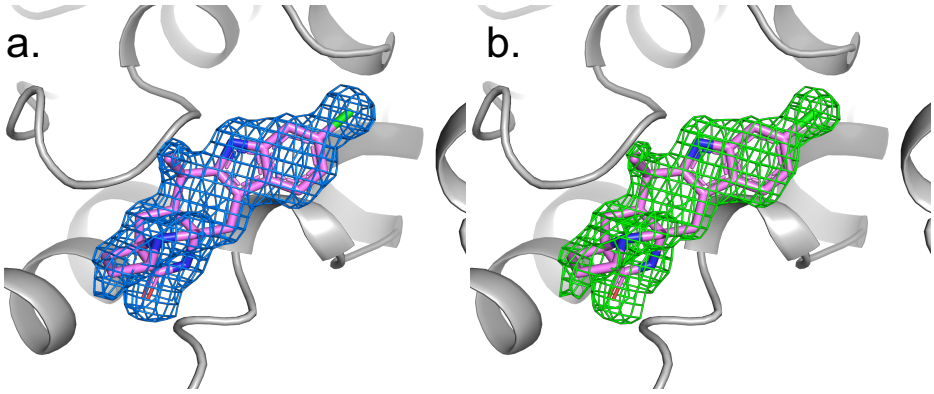

Figure 8.18 a.) Mfo-DFc map contoured at 1σ for malbrancheamide B cocrystal structure. b.) 2Mfo-DFc map contoured at 1σ for malbrancheamide B cocrystal structure.

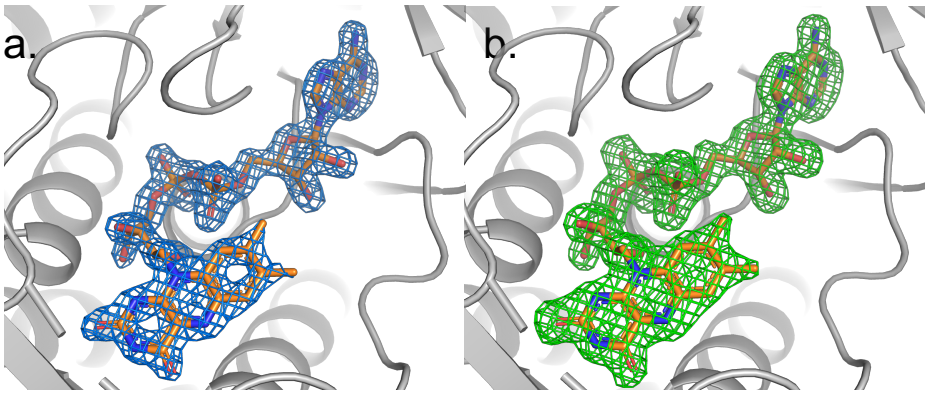

Figure 8.19 a.) Mfo-DFc map contoured at 1σ for FAD in malbrancheamide B cocrystal structure. b.) 2Mfo-DFc map contoured at 1σ for FAD in malbrancheamide B cocrystal structure.

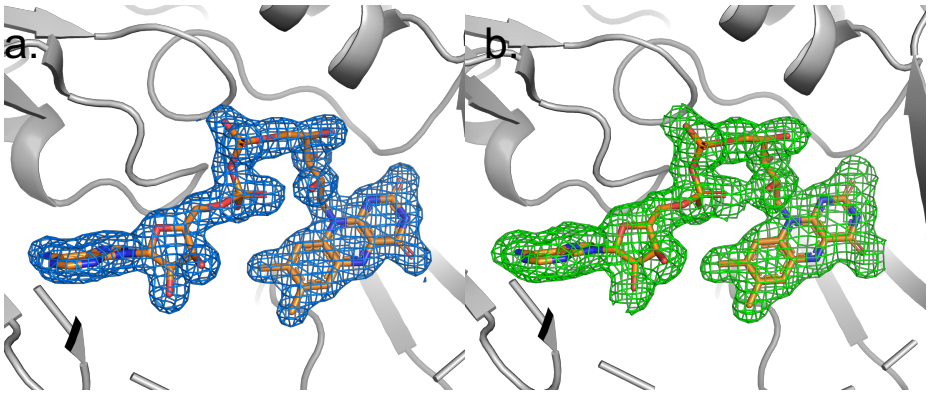

Figure 8.20 a.) Mfo-DFc map contoured at 1σ for FAD cocrystal structure. b. 2Mfo-DFc map contoured at 1σ for FAD cocrystal structure.

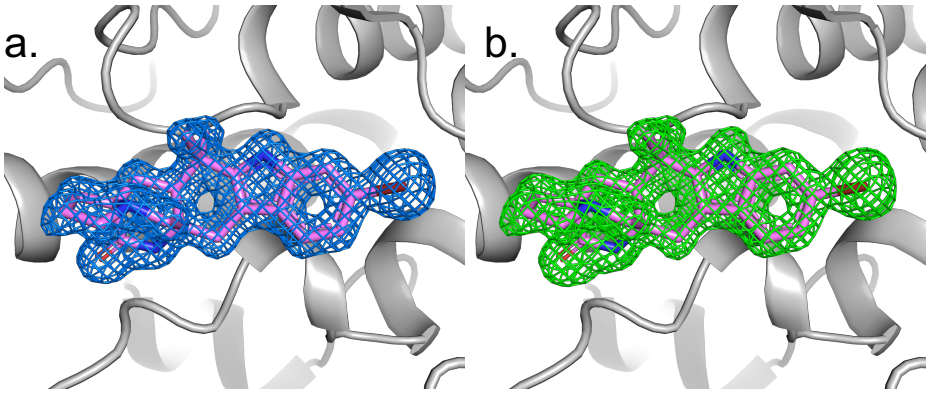

Figure 8.21 a.) Mfo-DFc map contoured at 1σ for malbrancheamide C cocrystal structure. b.) 2Mfo-DFc map contoured at 1σ for malbrancheamide C cocrystal structure.

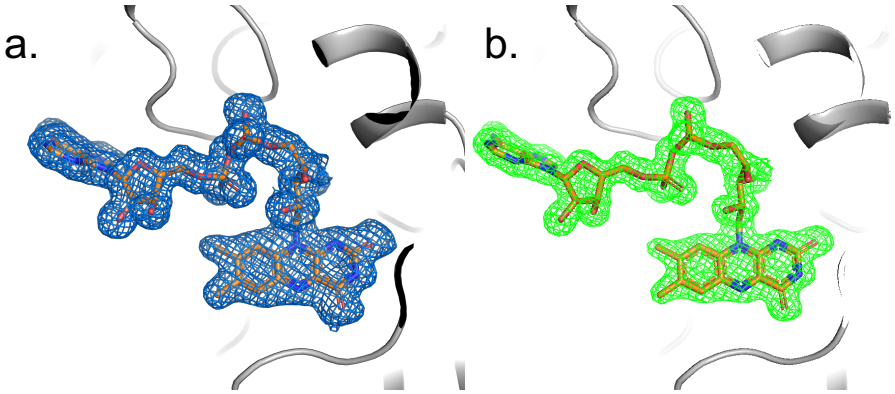

Figure 8.22 a.) Mfo-DFc map contoured at 1σ for FAD in malbrancheamide C cocrystal structure. b.) 2Mfo-DFc map contoured at 1σ for FAD in malbrancheamide C cocrystal structure.

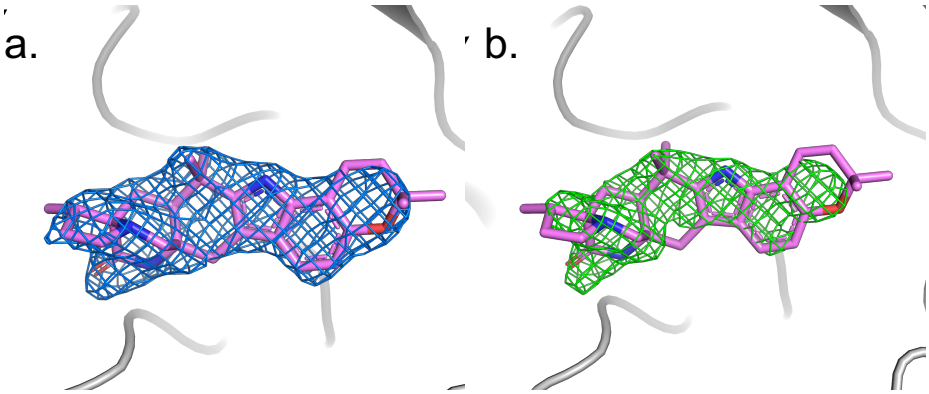

Figure 8.23 a.) Mfo-DFc map contoured at 1σ for paraherquamide K cocrystal structure. b.) 2Mfo-DFc map contoured at 1σ for paraherquamide K cocrystal structure.

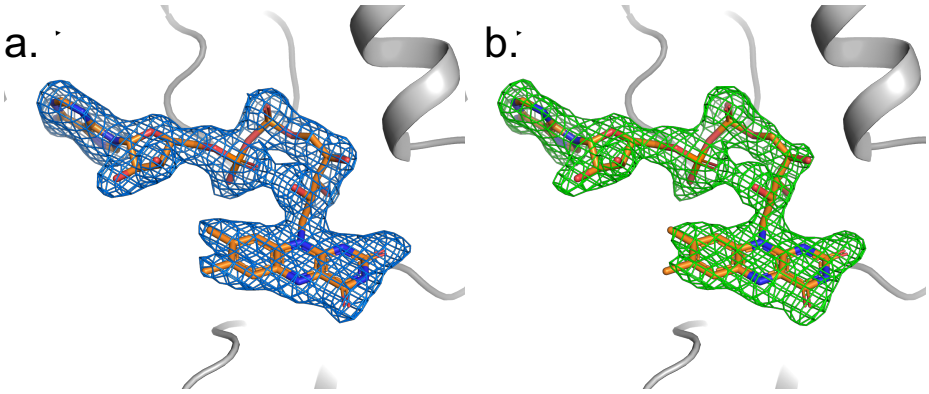

Figure 8.24 a.) Mfo-DFc map contoured at 1σ for FAD in paraherquamide K cocrystal structure. b.) 2Mfo-DFc map contoured at 1σ for FAD in paraherquamide K cocrystal structure.

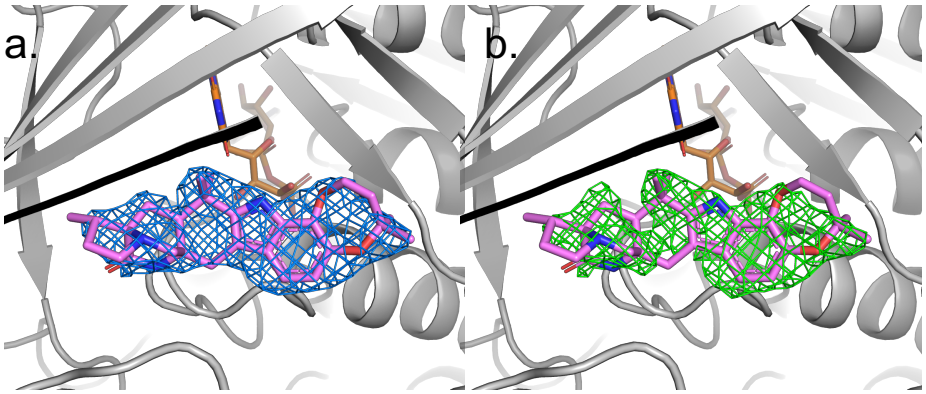

Figure 8.25 a.) MFo-DFc map contoured at 1σ for paraherquamide L cocrystal structure. b.) 2MFo-DFc map contoured at 1σ for paraherquamide L cocrystal structure.

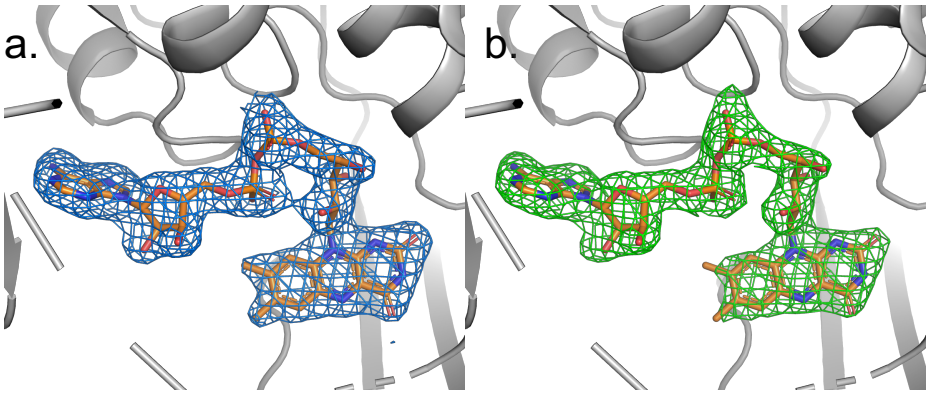

Figure 8.26 a. MFo-DFc map contoured at 1σ for FAD in paraherquamide L cocrystal structure. b. 2MFo-DFc map contoured at 1σ for FAD in paraherquamide L cocrystal structure.

8.4 Compound Characterization

8.4.1 NMR Characterization

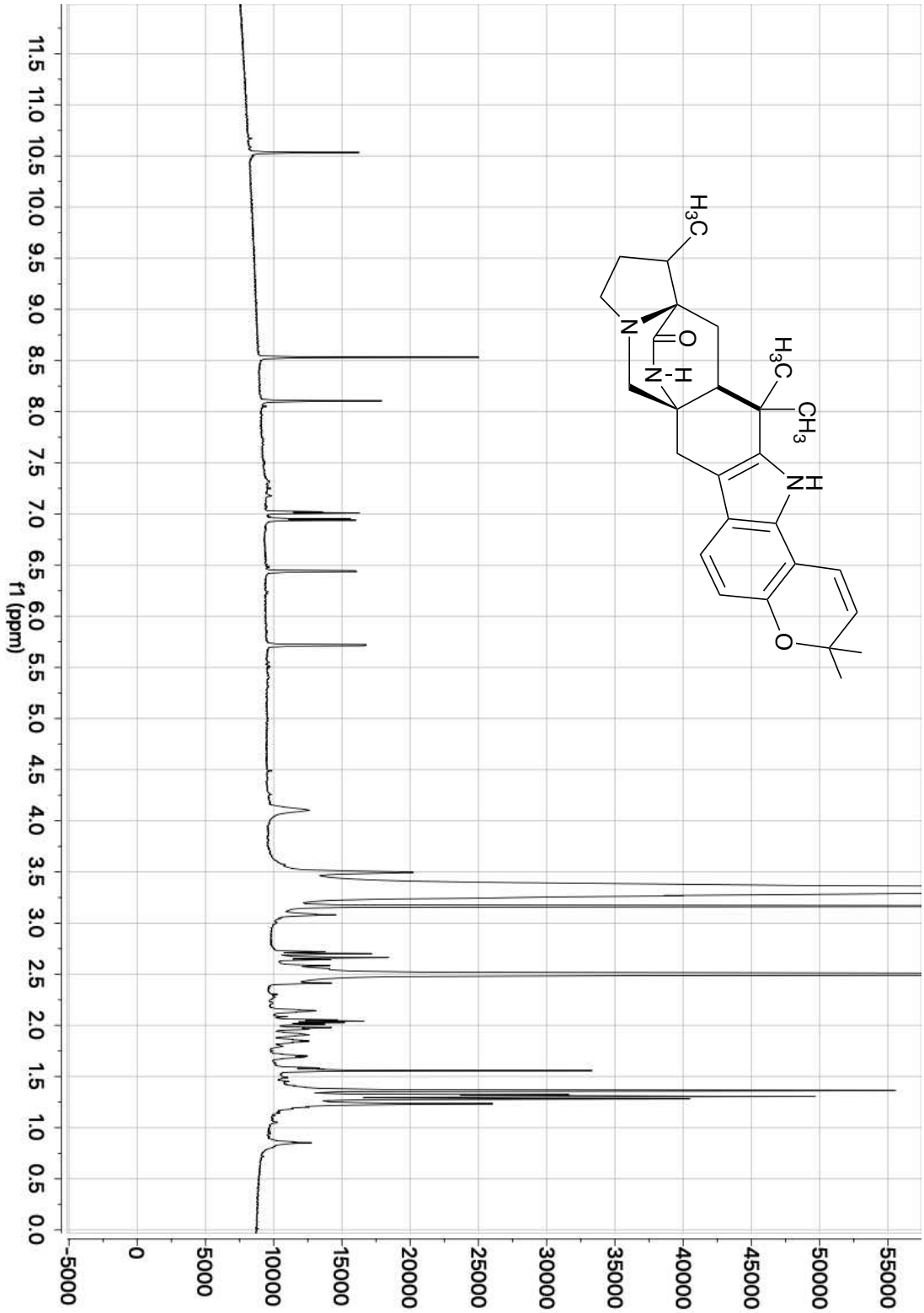

Figure 8.27 ^{1}H-NMR of paraherquamide K (**1.24**) (800 MHz, DMSO-d6).

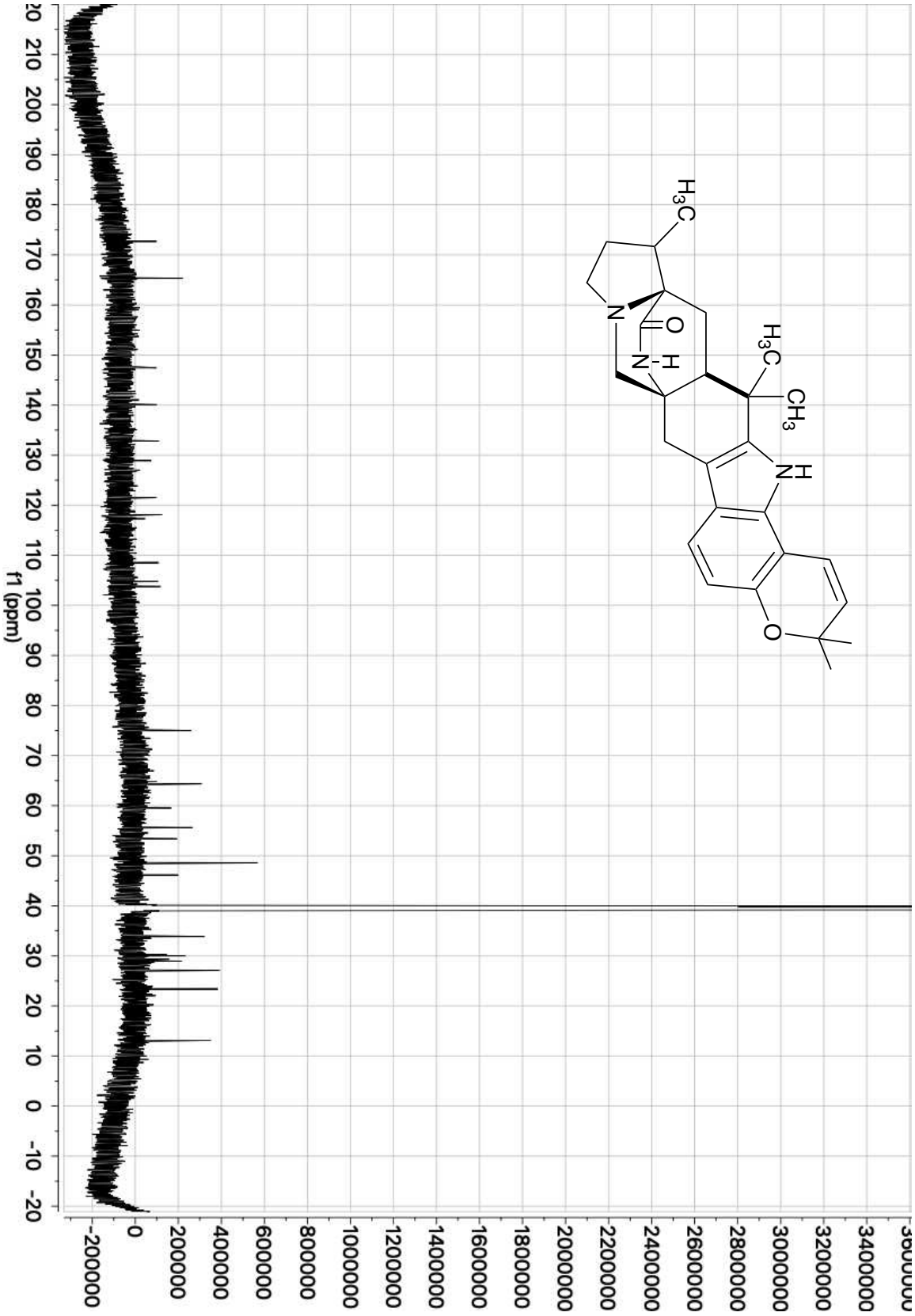

Figure 8.28 ^{13}C-NMR of paraherquamide K (**1.24**) (800 MHz, DMSO-d6).

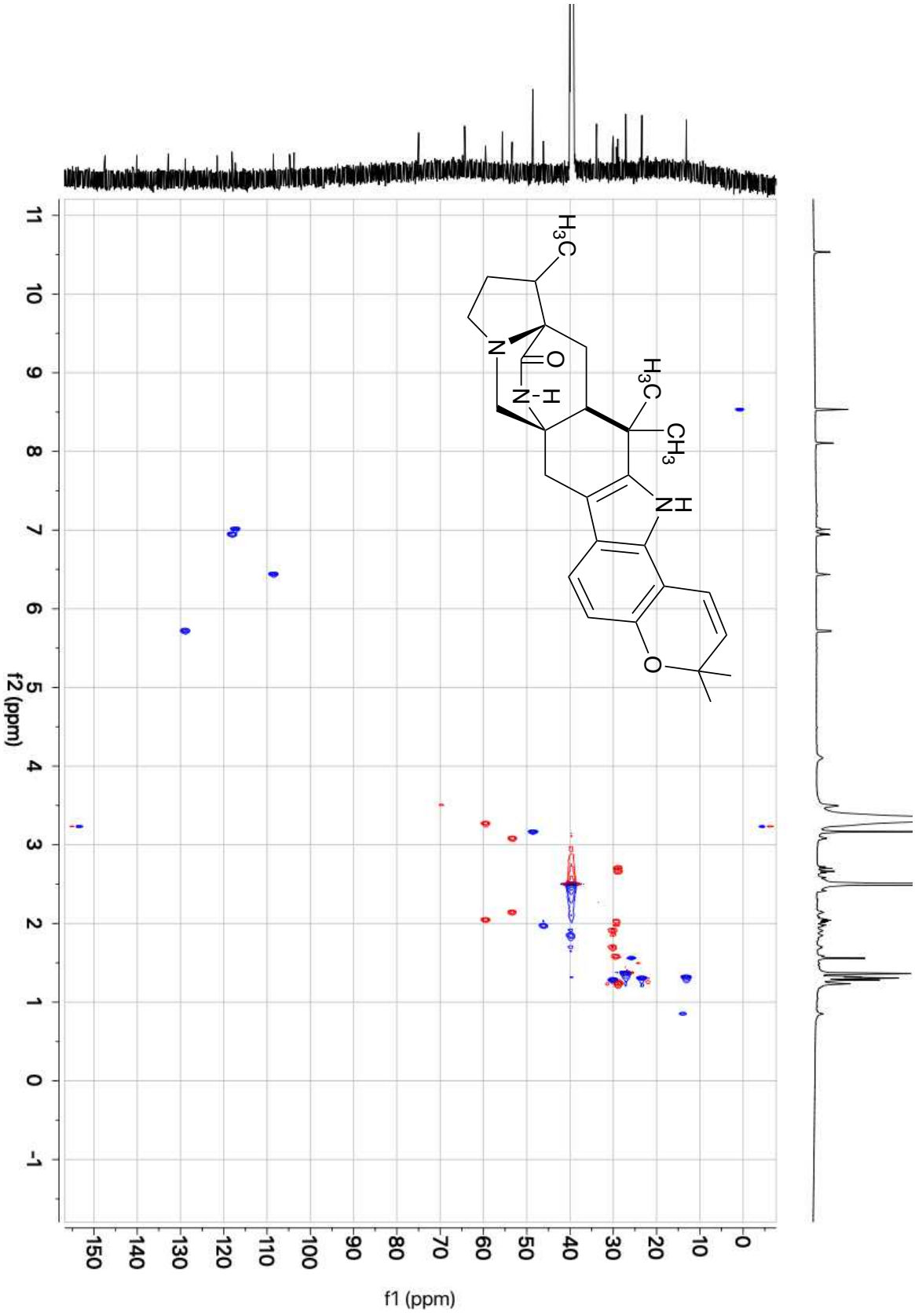

Figure 8.29 gHSQCAD correlations of paraherquamide K (**1.24**) (800 MHz, DMSO-d6).

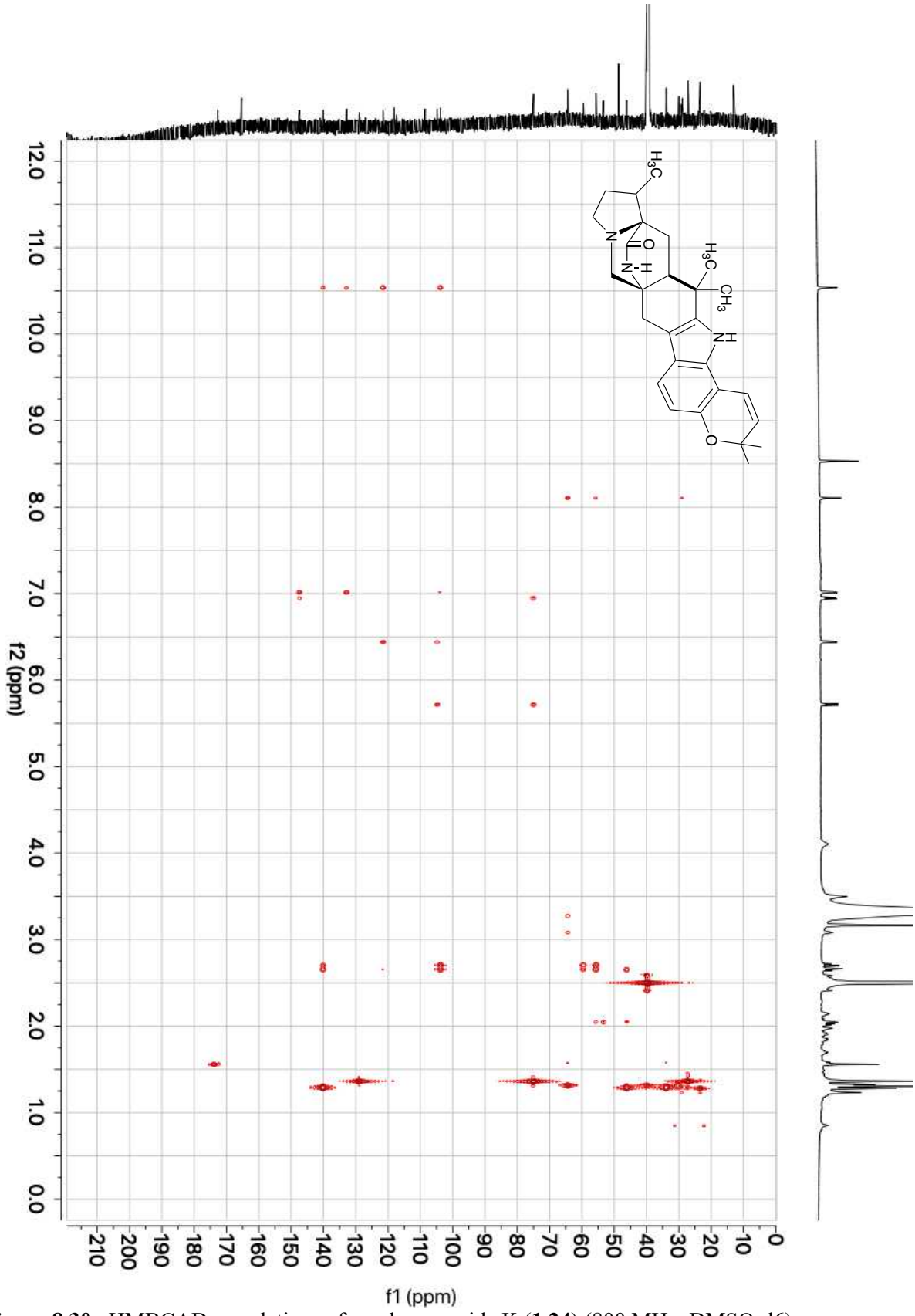

Figure 8.30 gHMBCAD correlations of paraherquamide K (**1.24**) (800 MHz, DMSO-d6).

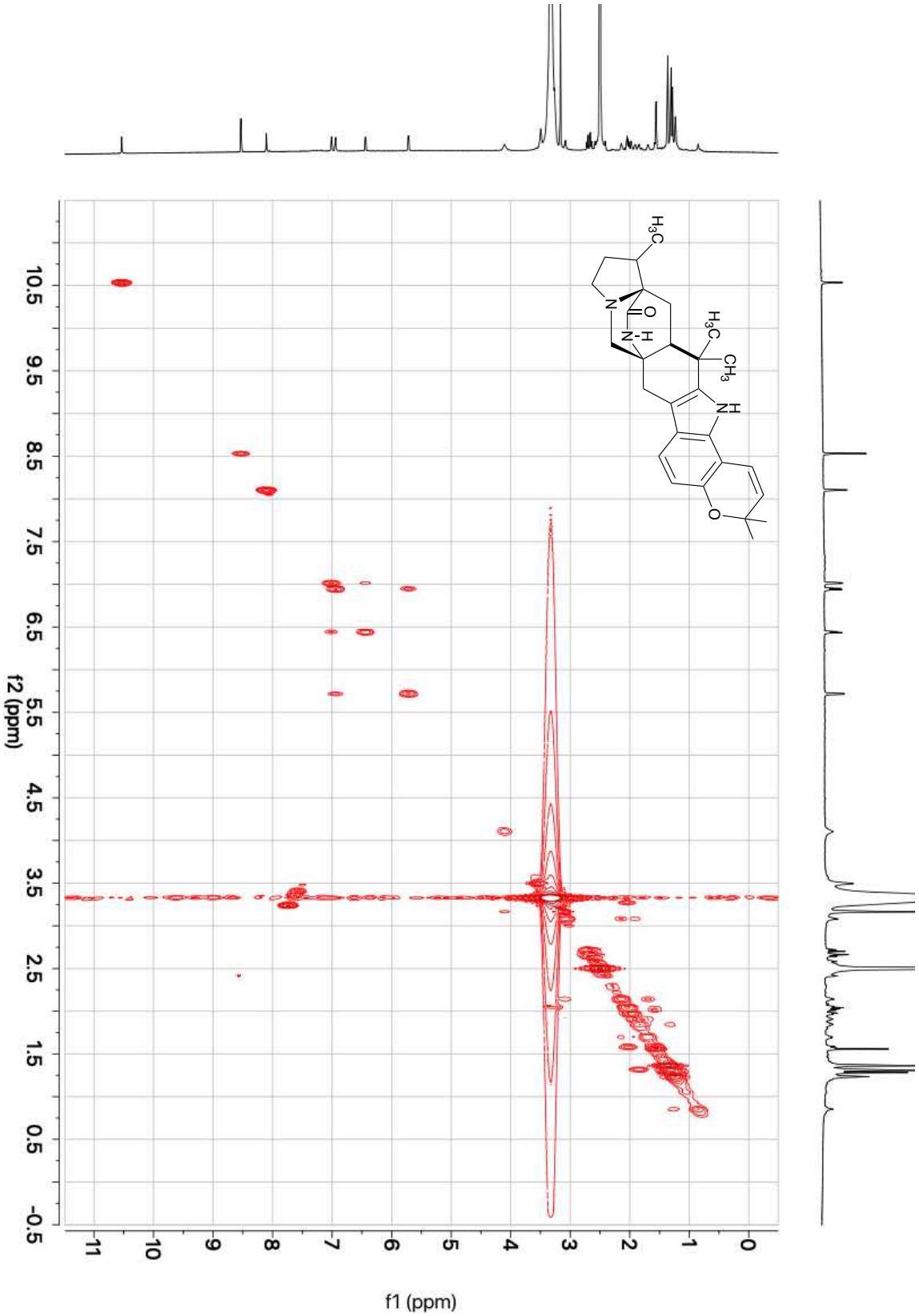

Figure 8.31 gCOSY correlations of paraherquamide K (**1.24**) (800 MHz, DMSO-d6).

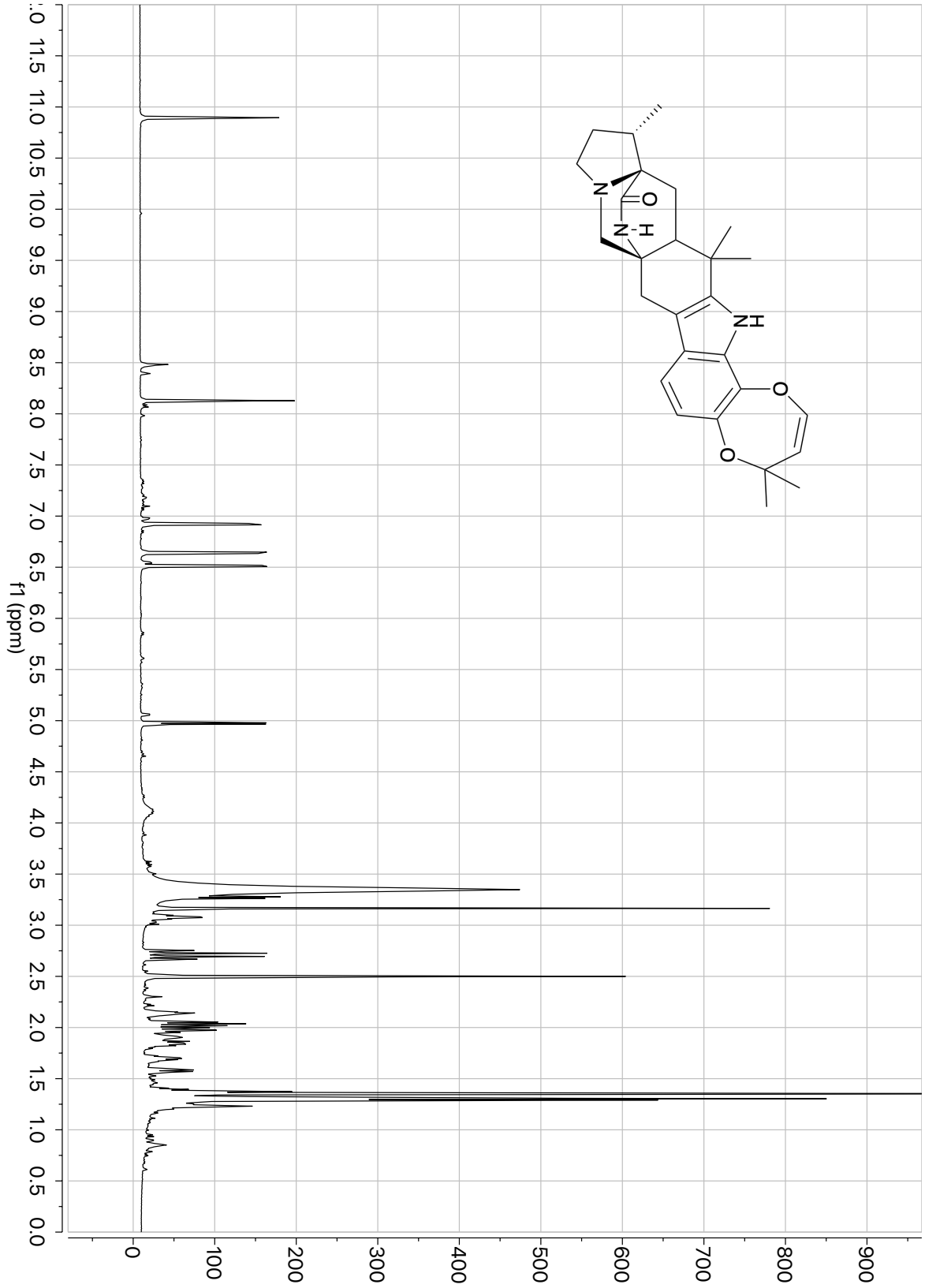

Figure 8.32 [1]H-NMR of paraherquamide L (**1.25**) (600 MHz, DMSO-d6).

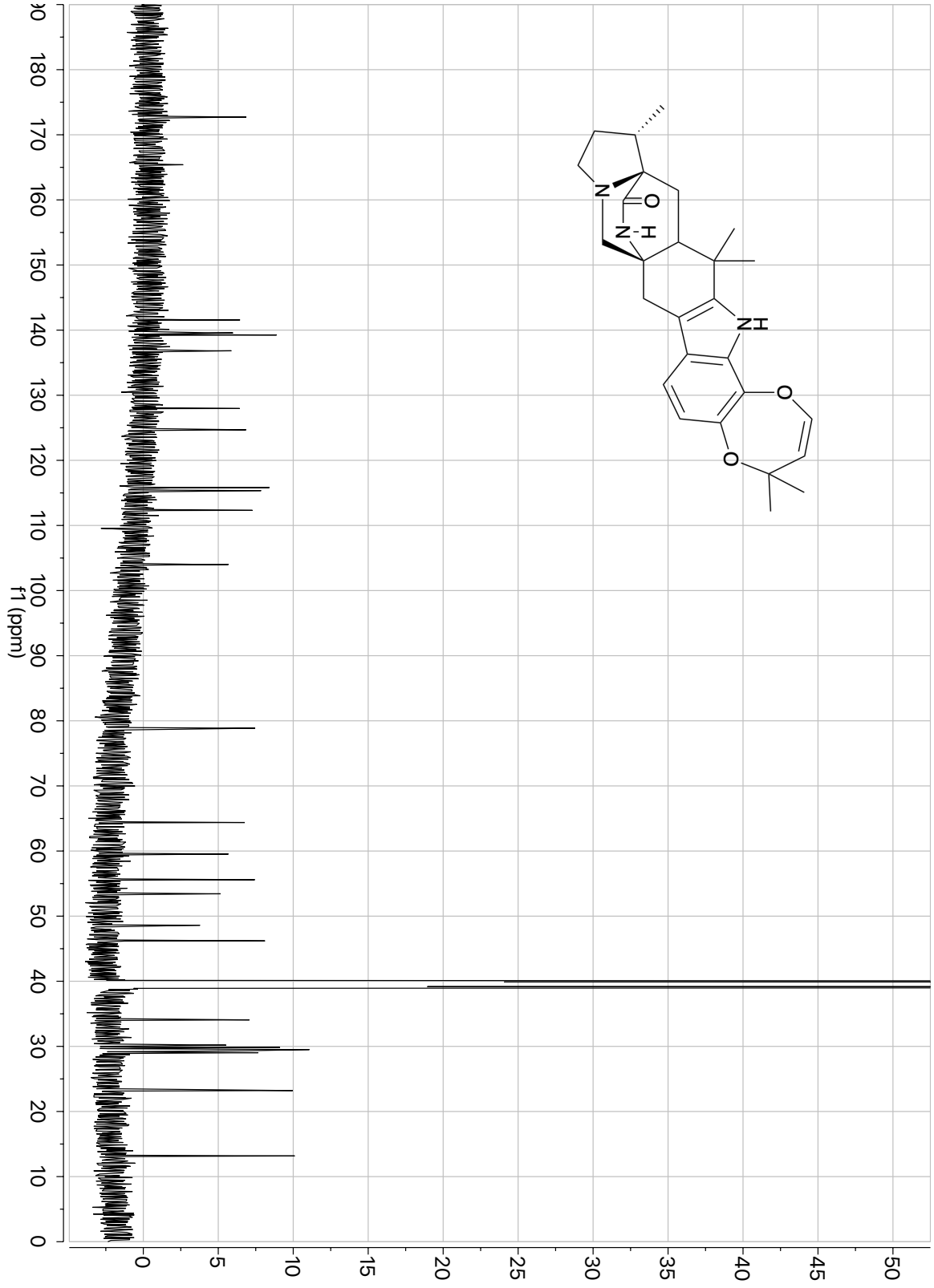

Figure 8.33 ^{13}C-NMR of paraherquamide L (**1.25**) (600 MHz, DMSO-d6).

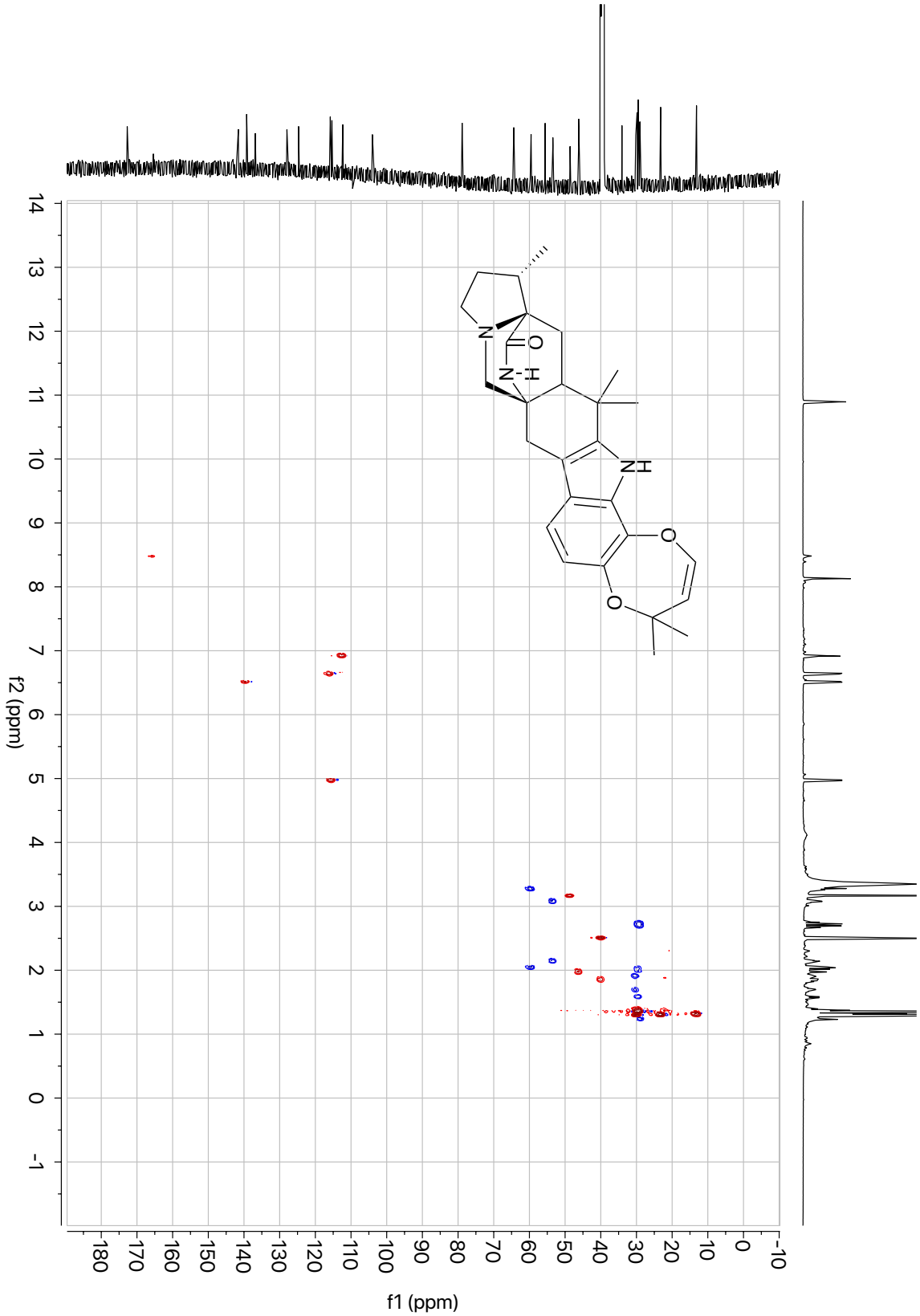

Figure 8.34 gHSQCAD correlations of paraherquamide L (**1.25**) (600 MHz, DMSO-d6).

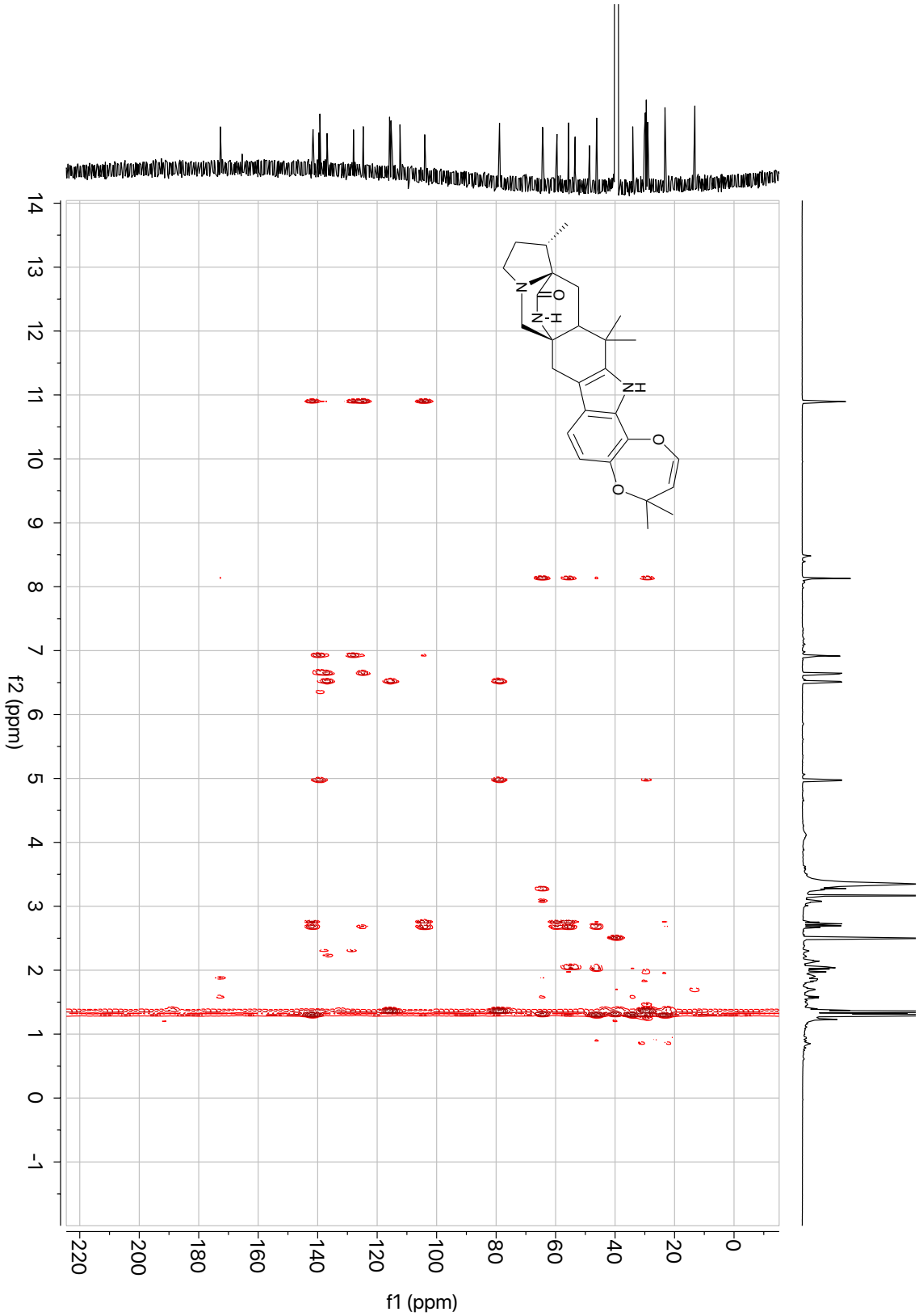

Figure 8.35 gHMBCAD correlations of paraherquamide L (**1.25**) (600 MHz, DMSO-d6).

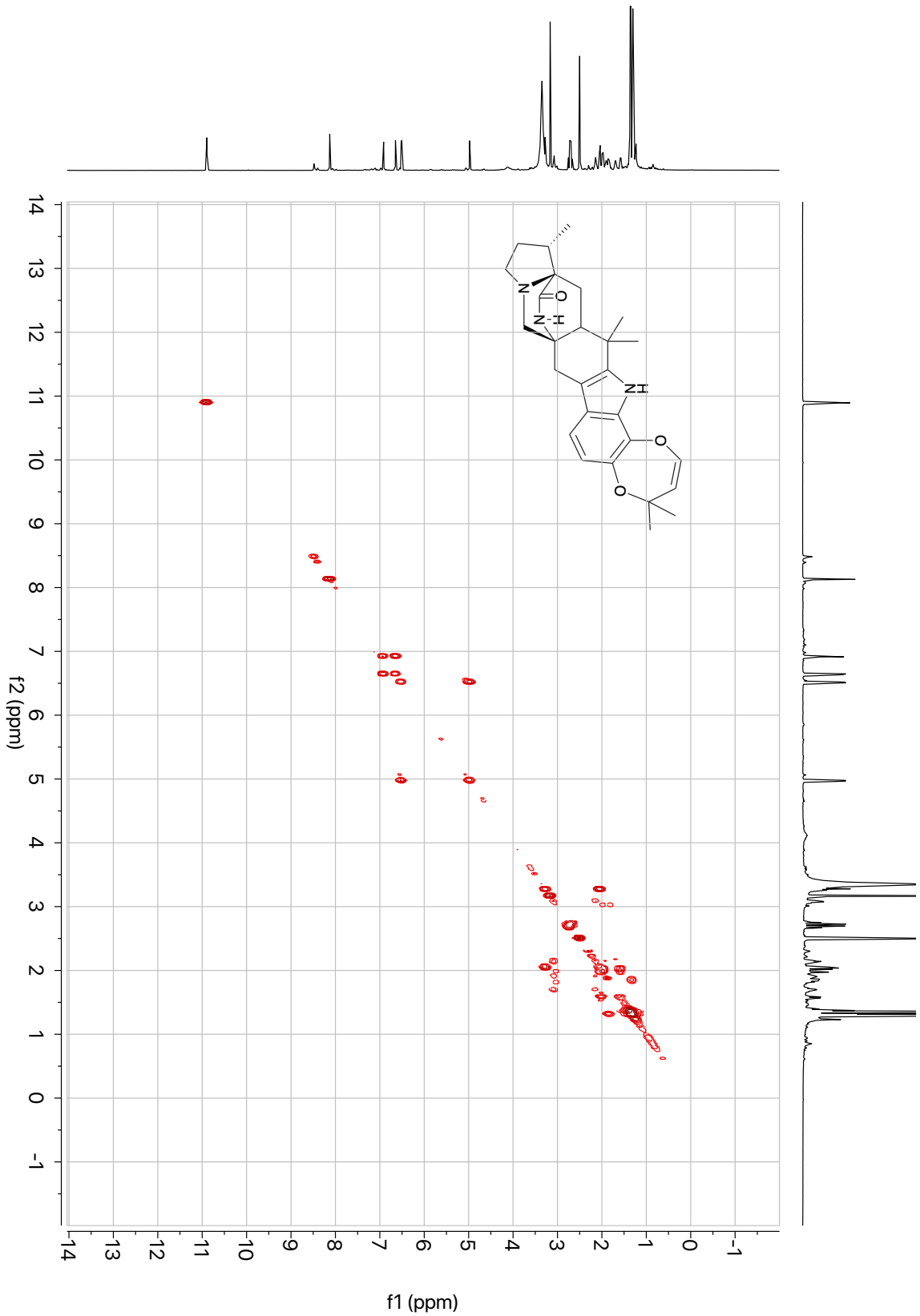

Figure 8.36 gCOSY correlations of paraherquamide L (**1.25**) (600 MHz, DMSO-d6).

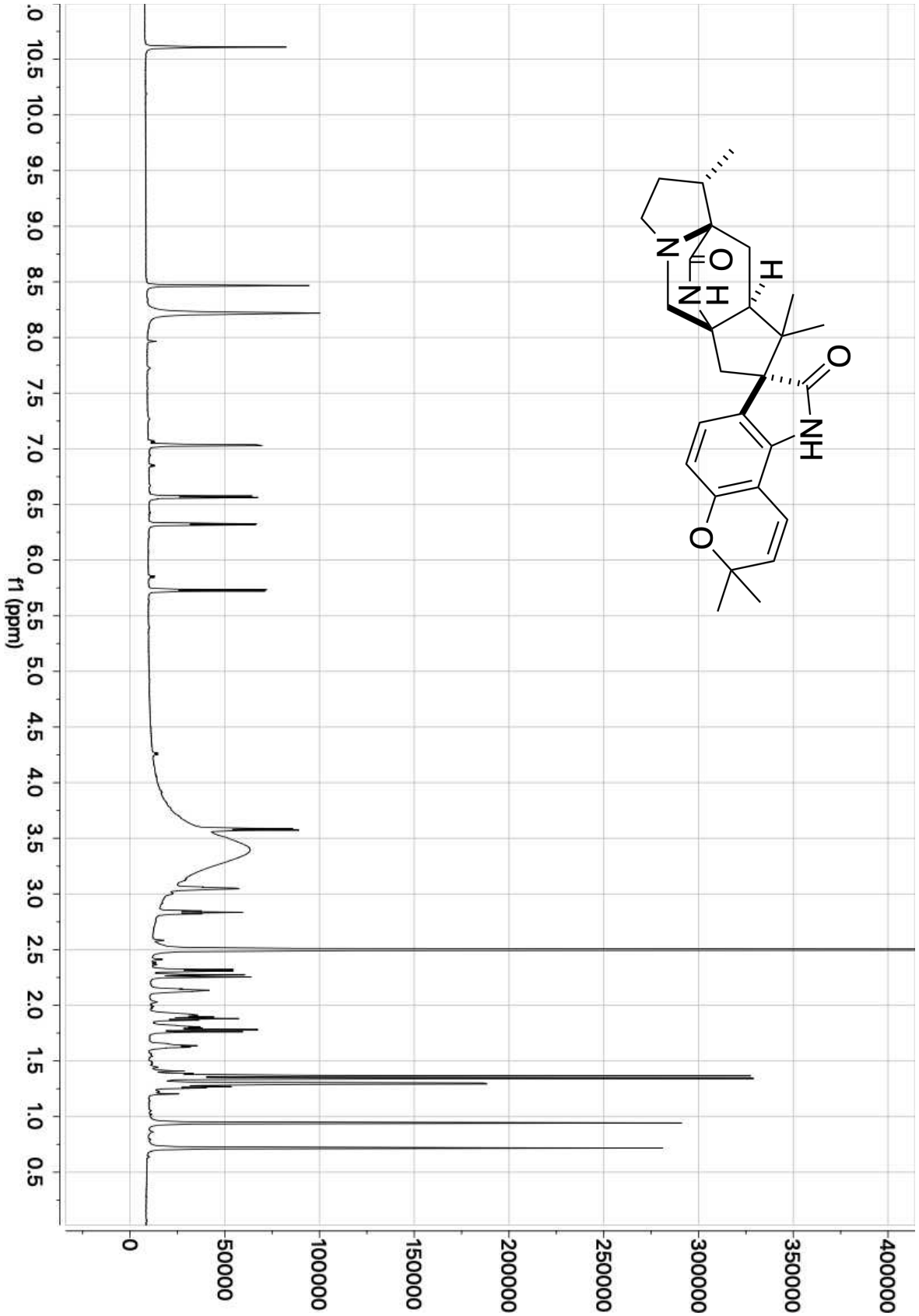

Figure 8.37 ^{1}H-NMR of paraherquamide M (**1.26**) (800 MHz, DMSO-d_6).

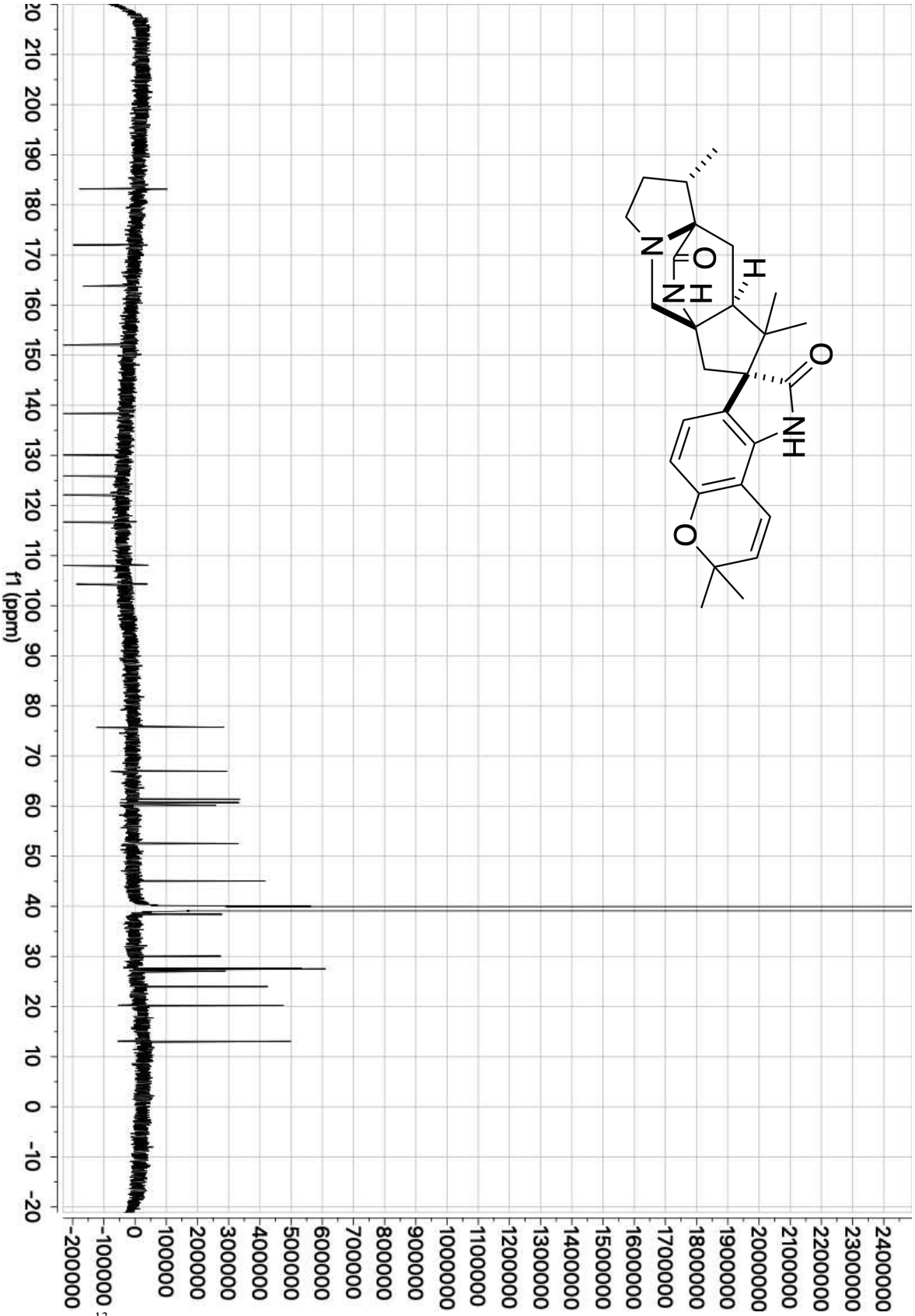

Figure 8.38 ^{13}C-NMR of paraherquamide M (**1.26**) (800 MHz, DMSO-d_6).

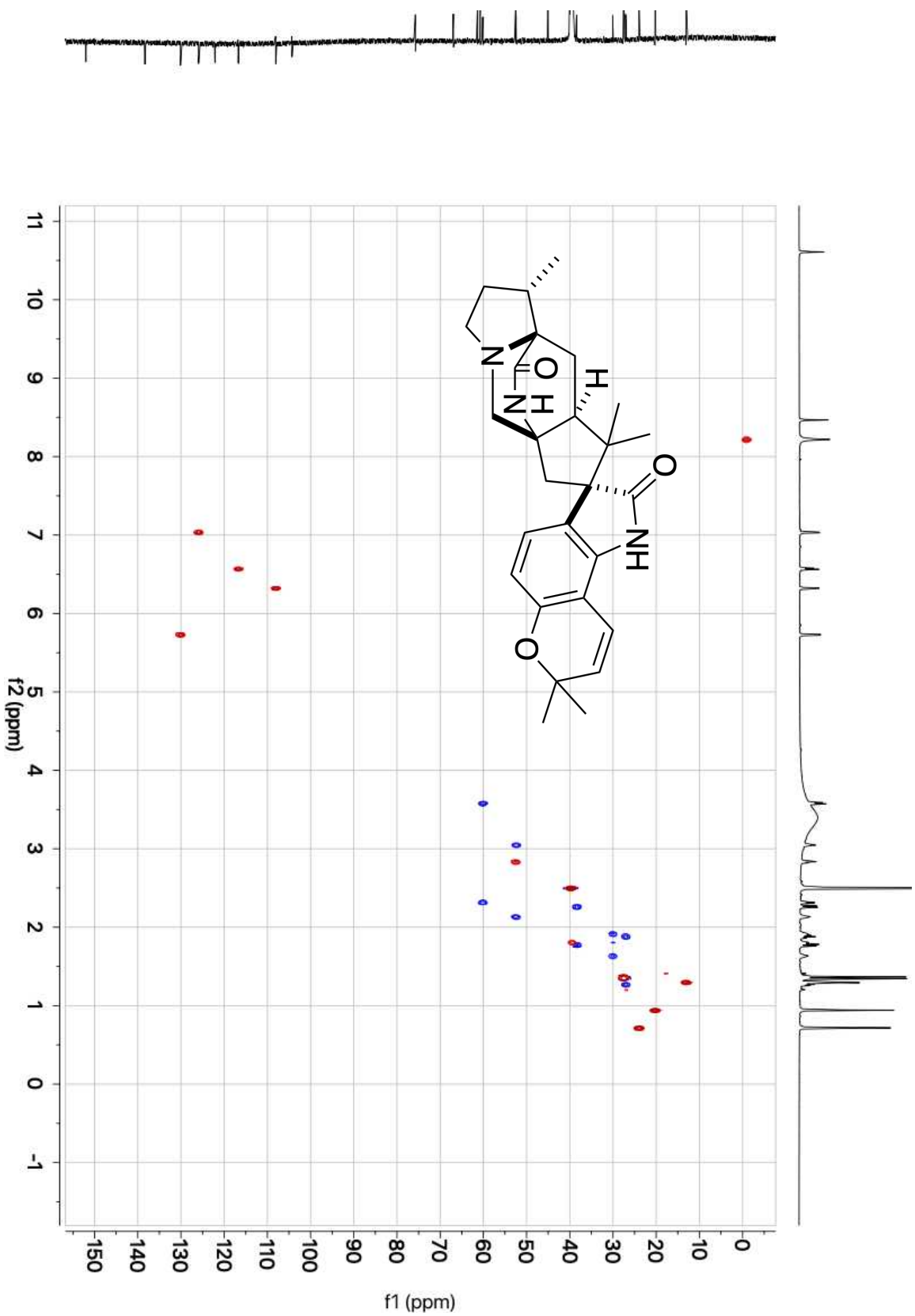

Figure 8.39 gHSQCAD correlations of paraherquamide M (**1.26**) (800 MHz, DMSO-d_6).

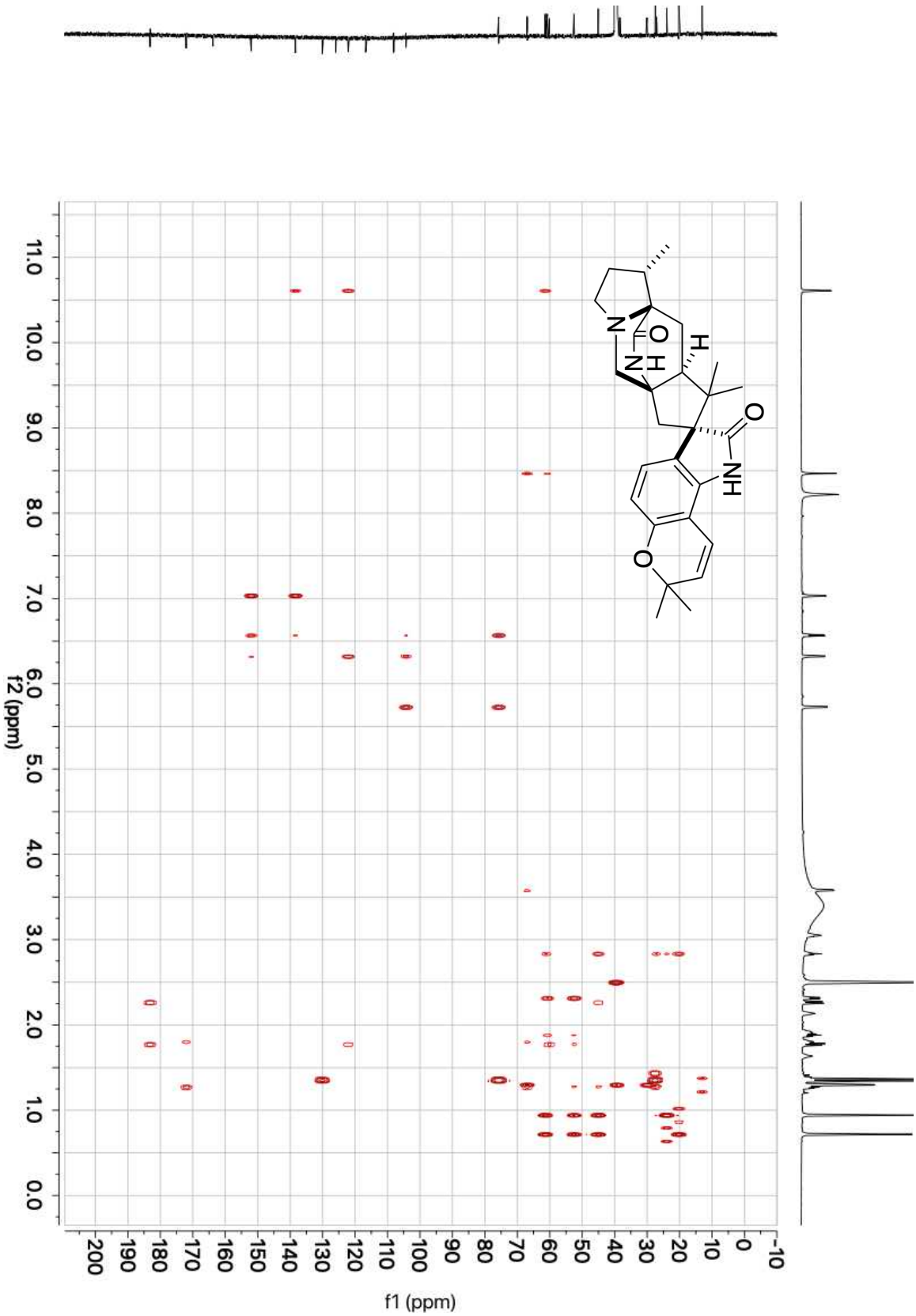

Figure 8.40 gHMBCAD correlations of paraherquamide M (**1.26**) (800 MHz, DMSO-d_6).

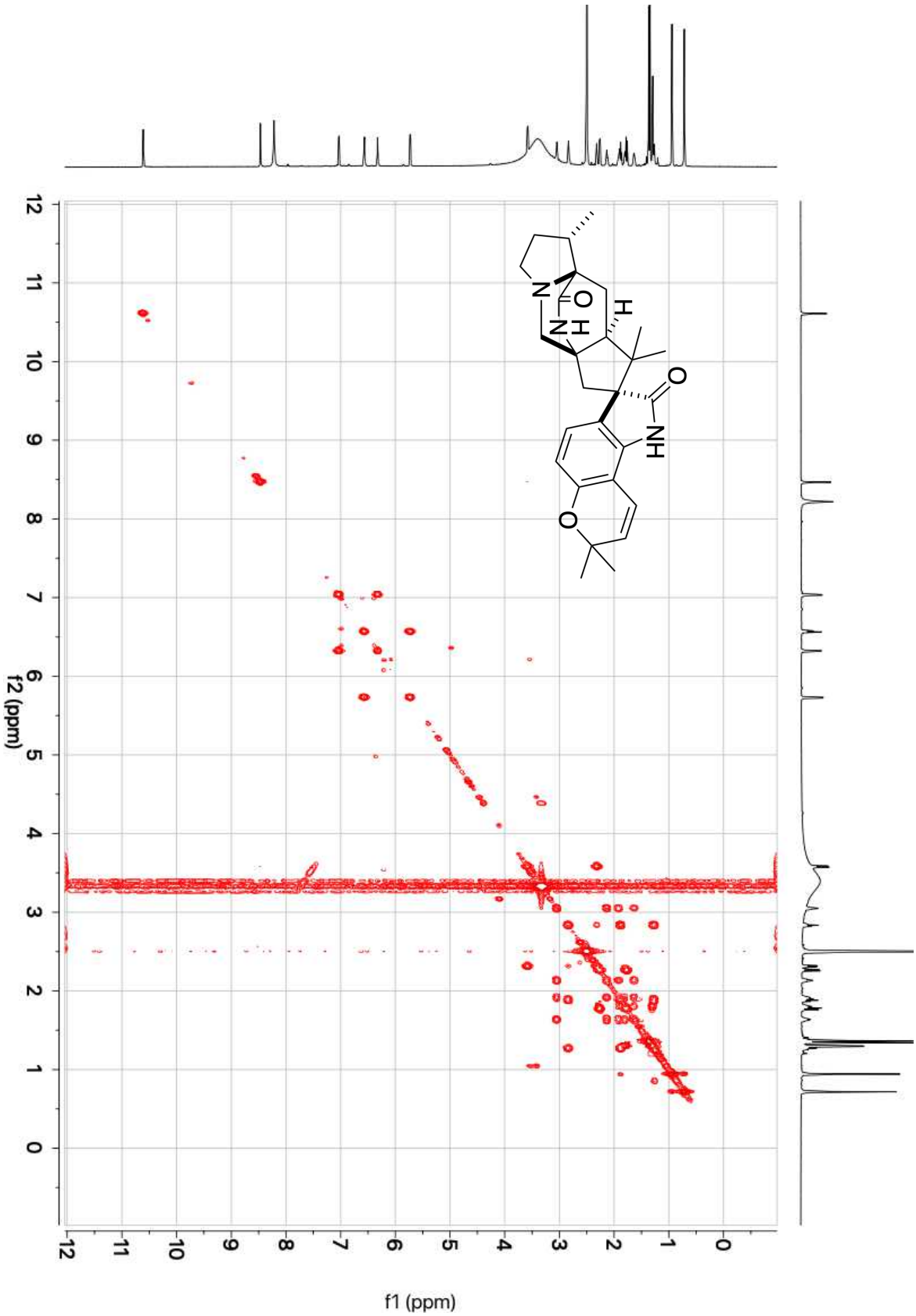

Figure 8.41 gCOSY correlations of paraherquamide M (**1.26**) (600 MHz, DMSO-d_6).

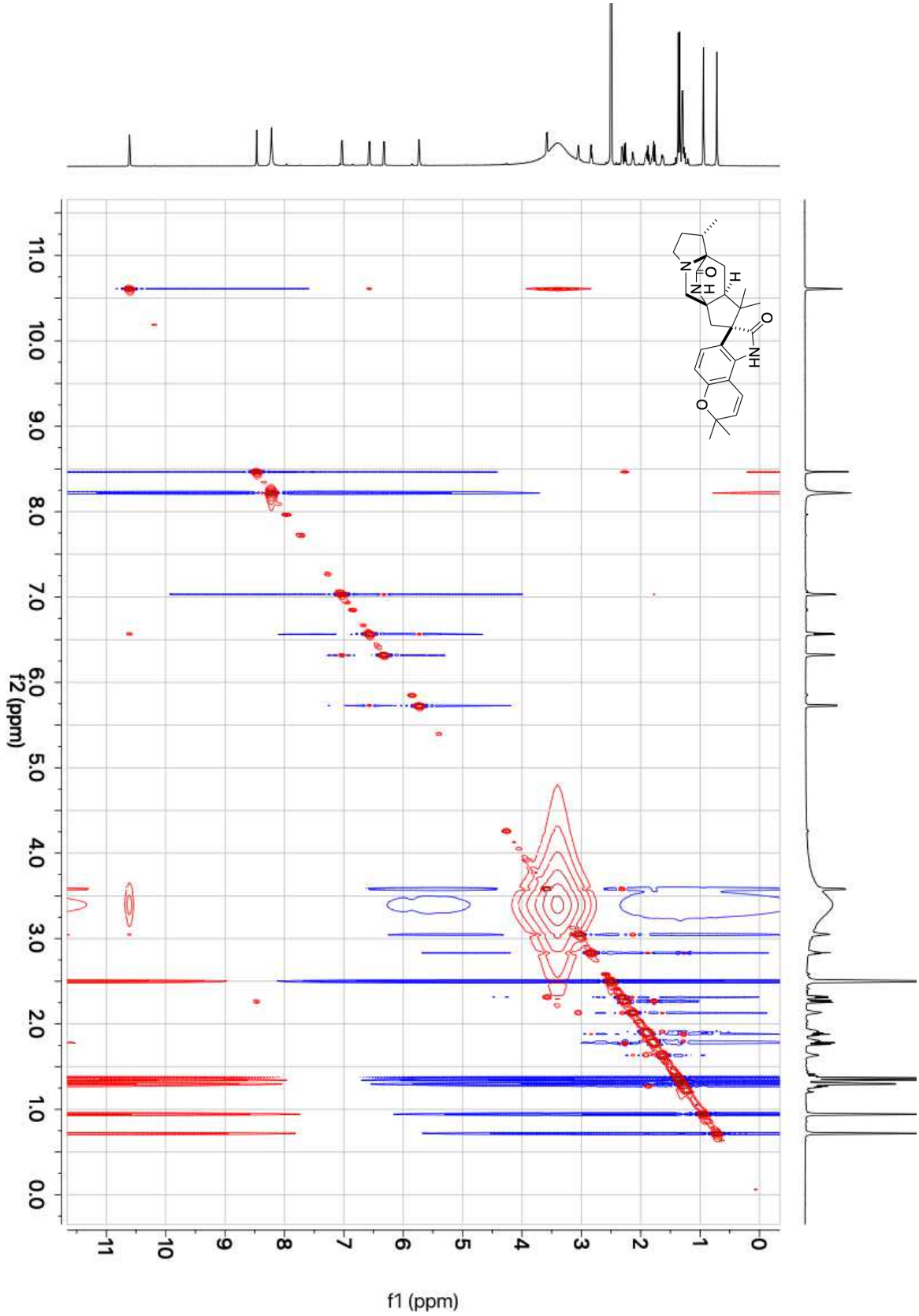

Figure 8.42 NOE correlations of paraherquamide M (**1.26**) (800 MHz, DMSO-d_6).

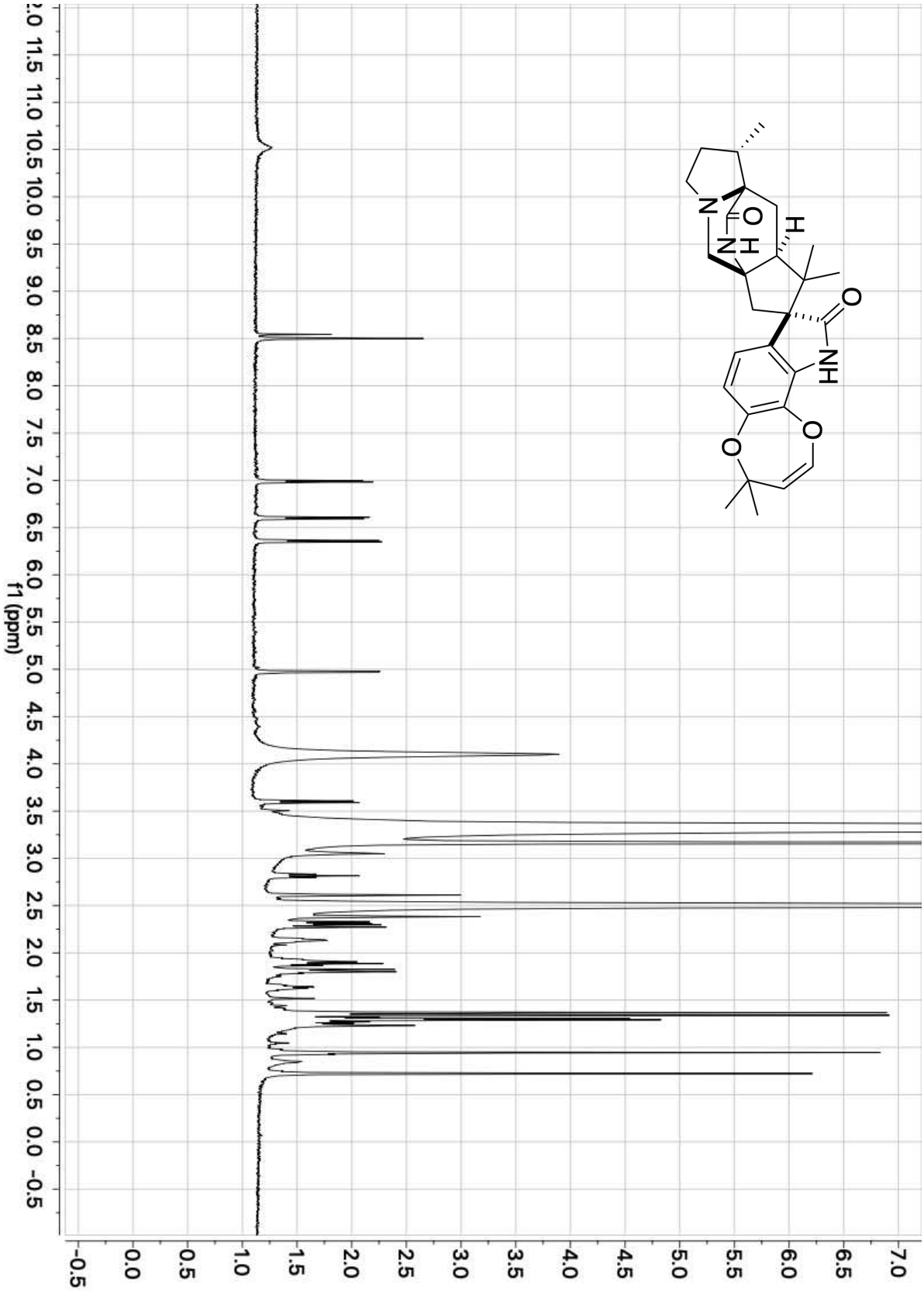

Figure 8.43 ^{1}H-NMR of paraherquamide N (**1.27**) (600 MHz, DMSO-d_6).

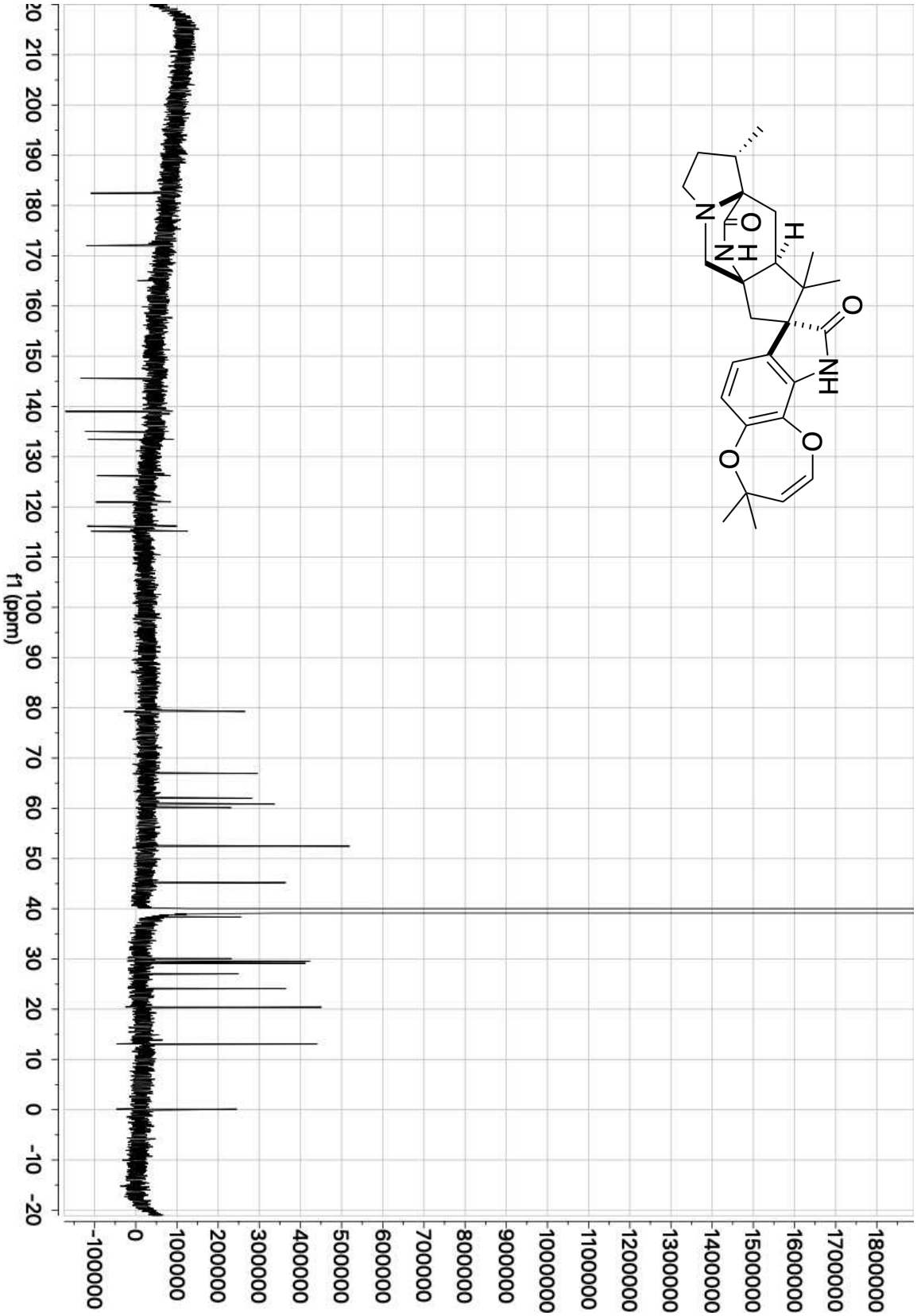

Figure 8.44 ^{13}C-NMR of paraherquamide N (**1.27**) (800 MHz, DMSO-d_6).

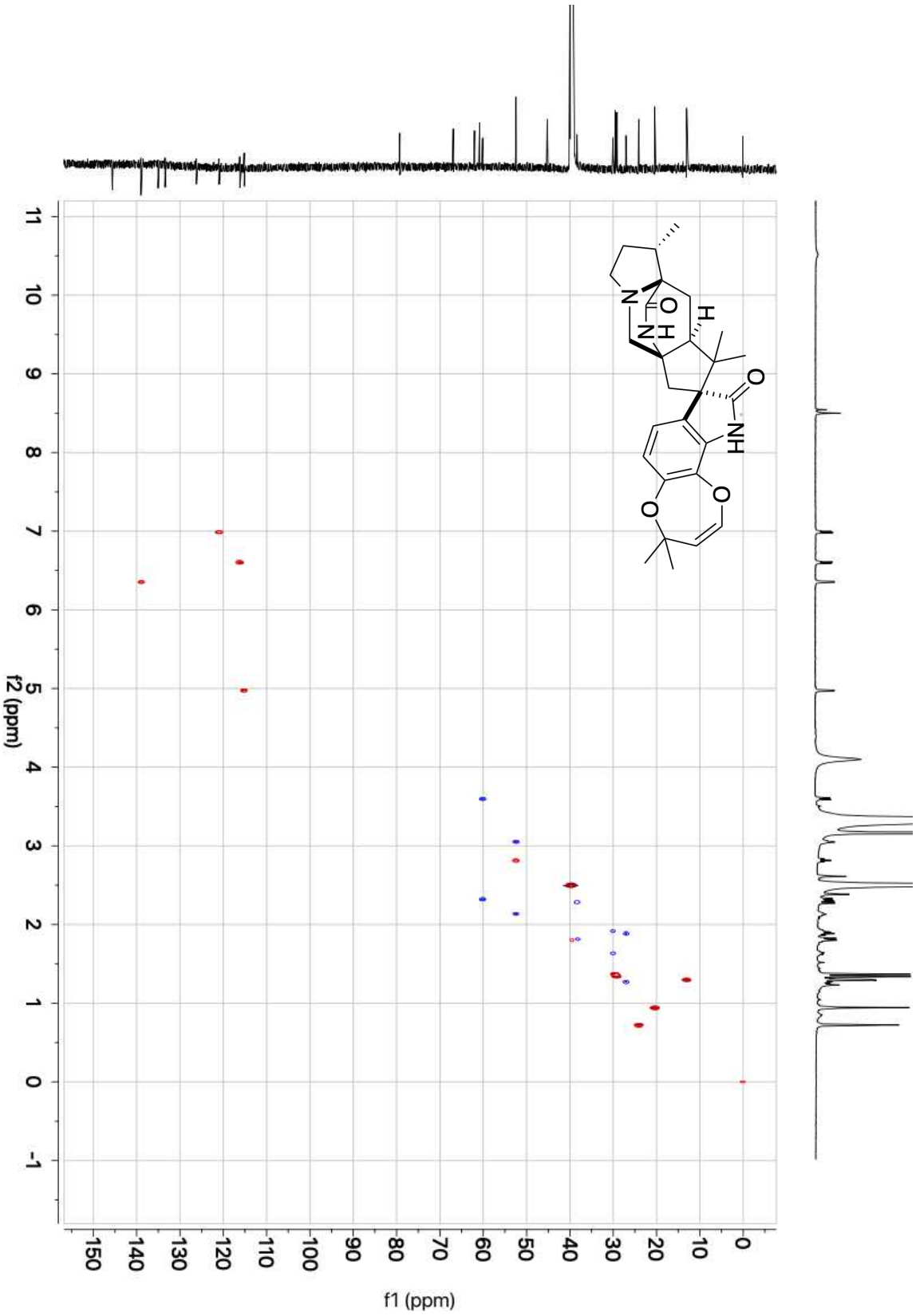

Figure 8.45 gHSQCAD correlations of paraherquamide N (**1.27**) (800 MHz, DMSO-d_6).

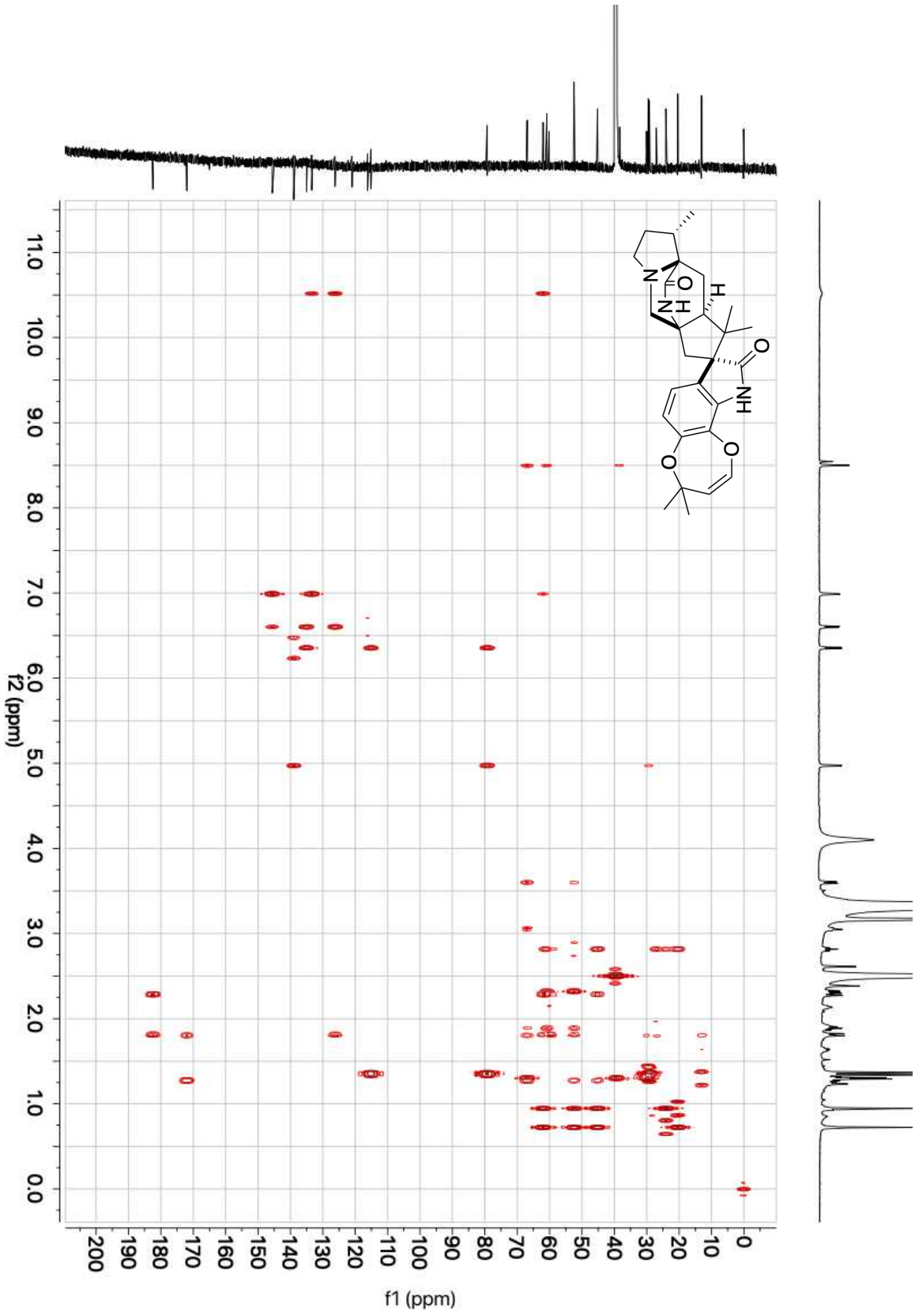

Figure 8.46 gHMBCAD correlations of paraherquamide N (**1.27**) (800 MHz, DMSO-d_6).

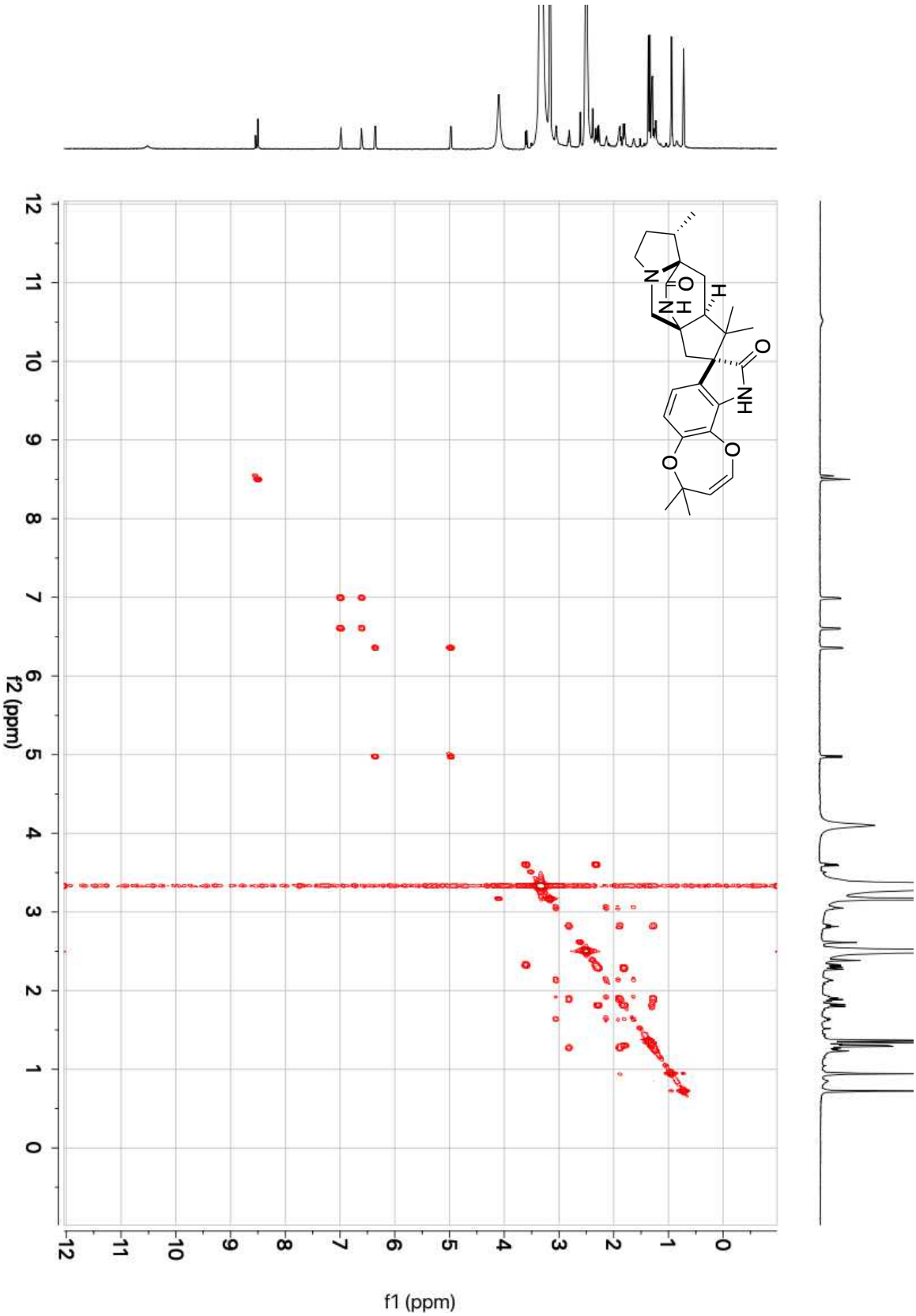

Figure 8.47 gCOSY correlations of paraherquamide N (**1.27**) (600 MHz, DMSO-d_6).

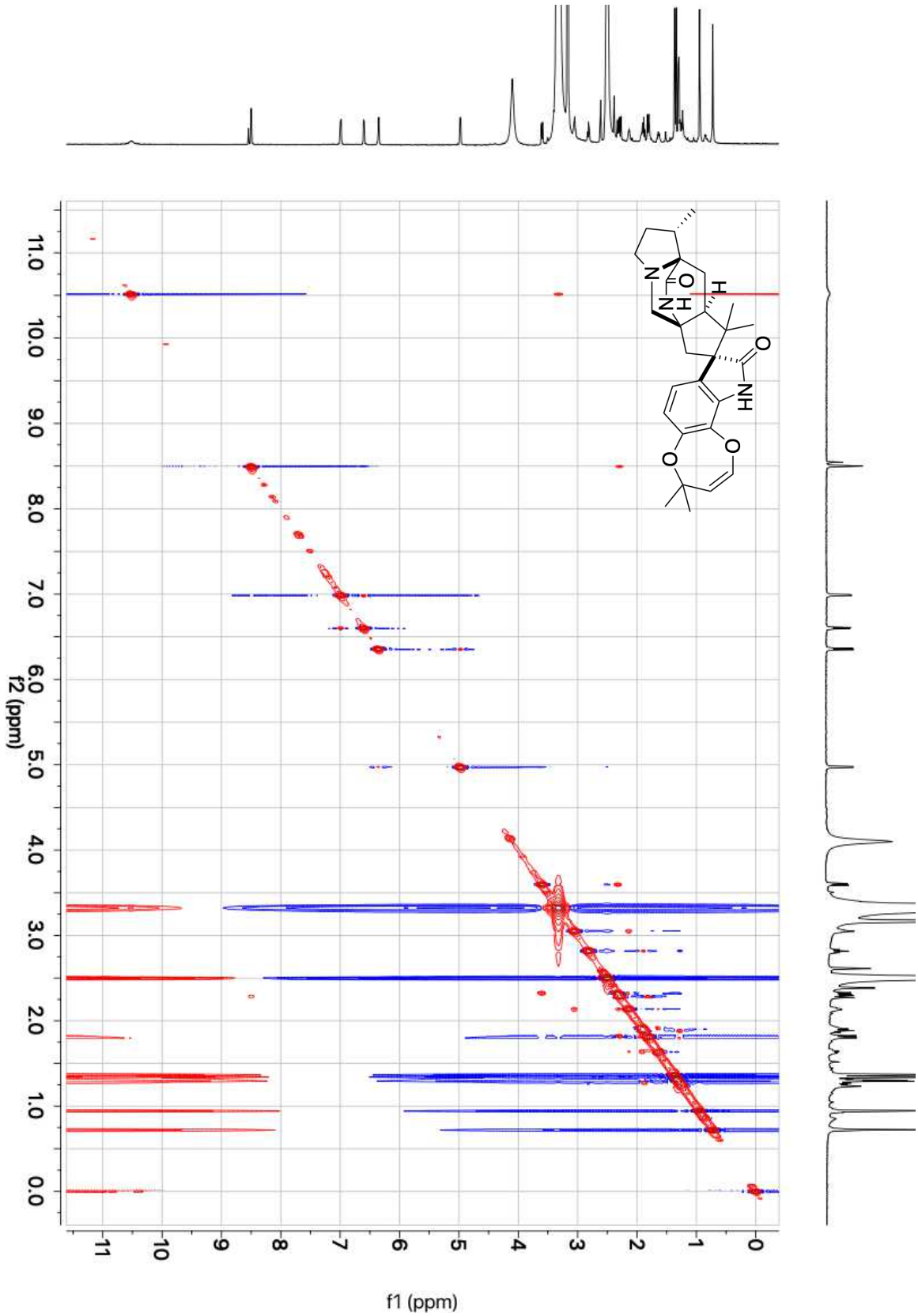

Figure 8.48 NOE correlations of paraherquamide N (**1.27**) (800 MHz, DMSO-d_6).

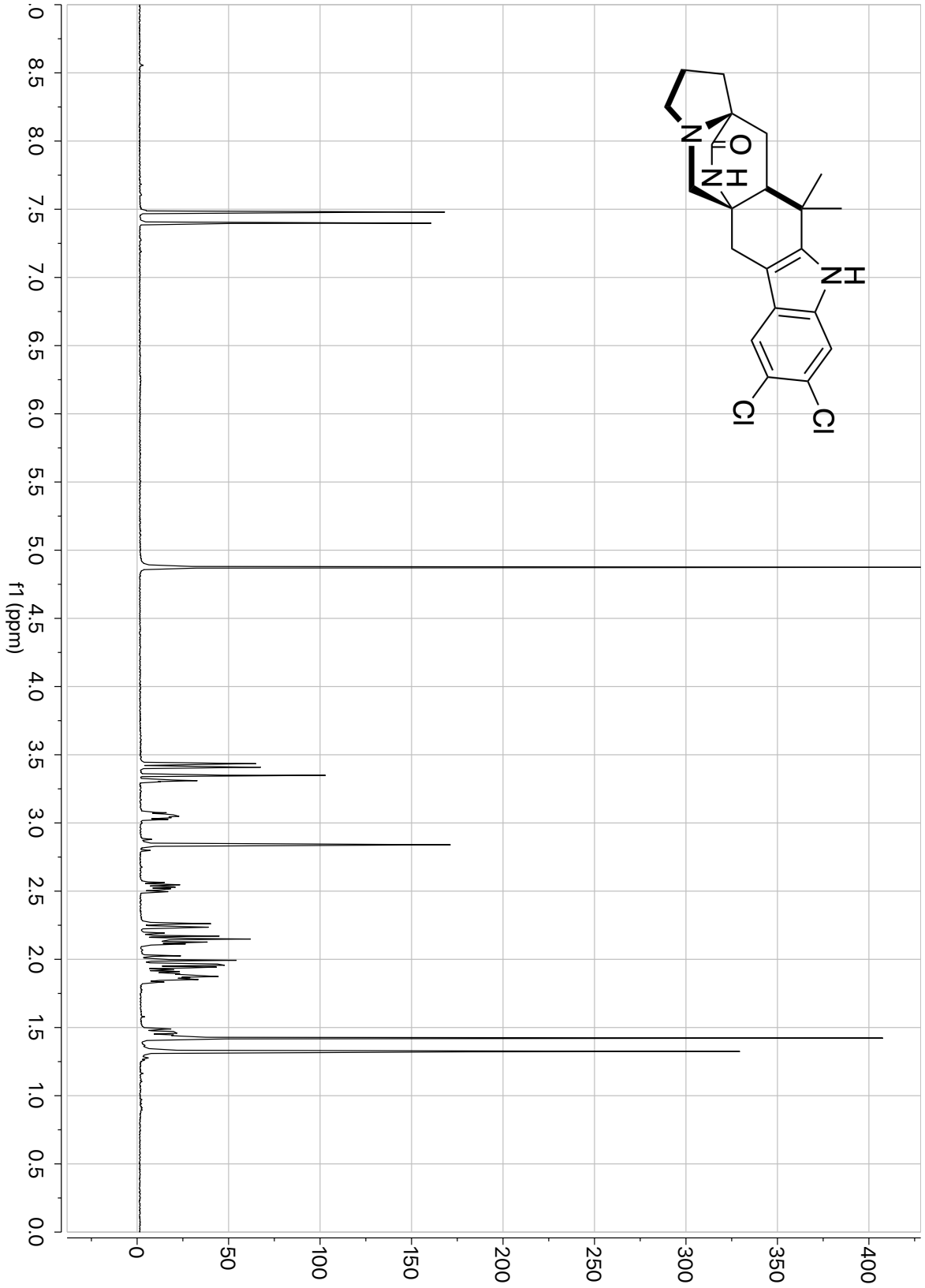

Figure 8.49 ^{1}H-NMR of fungal malbrancheamide (**1.17**) (600 MHz, CD_3OD).

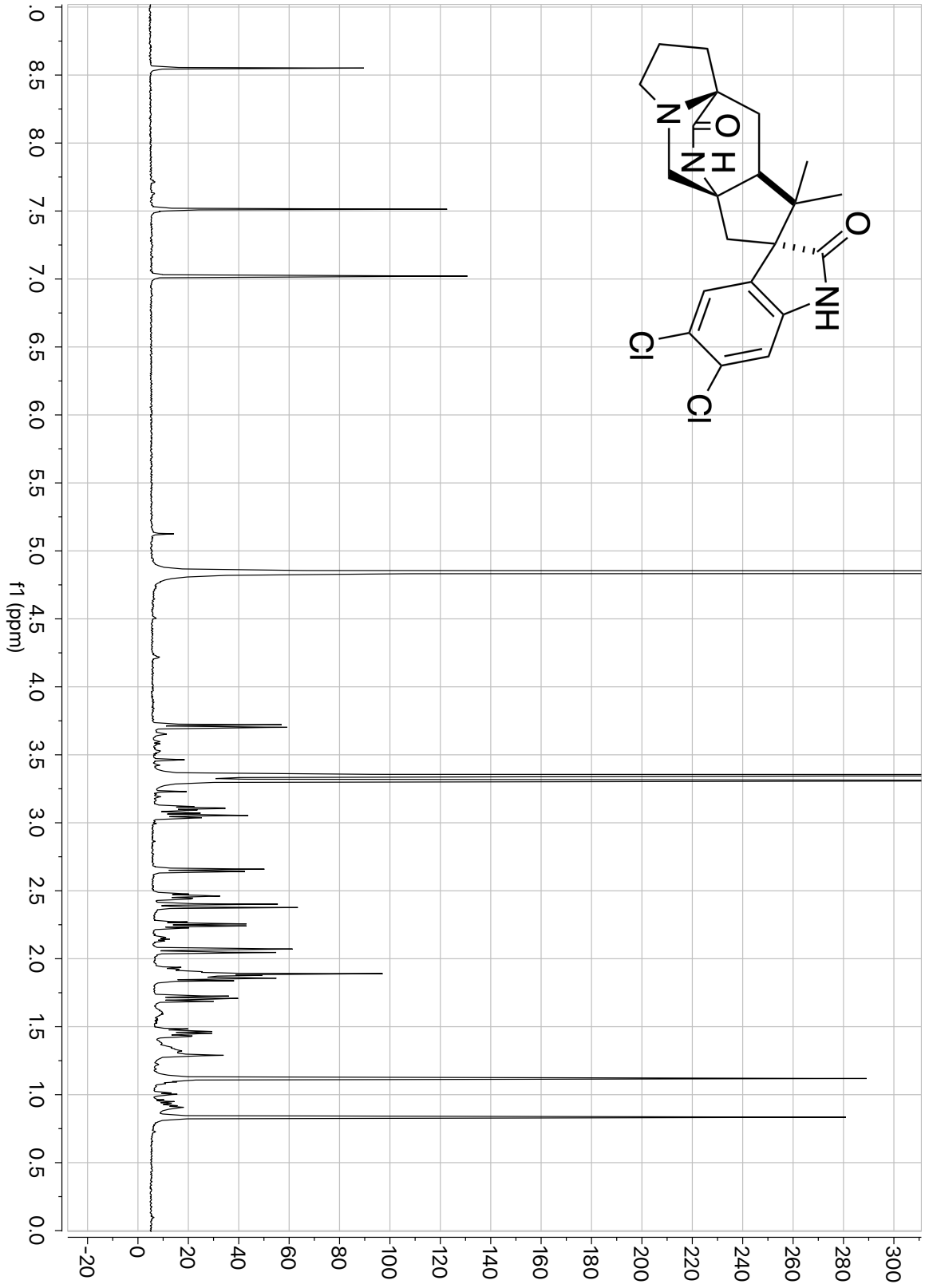

Figure 8.50 ^{1}H-NMR of spiromalbramide (**3.1**) (600 MHz, CD_3OD).

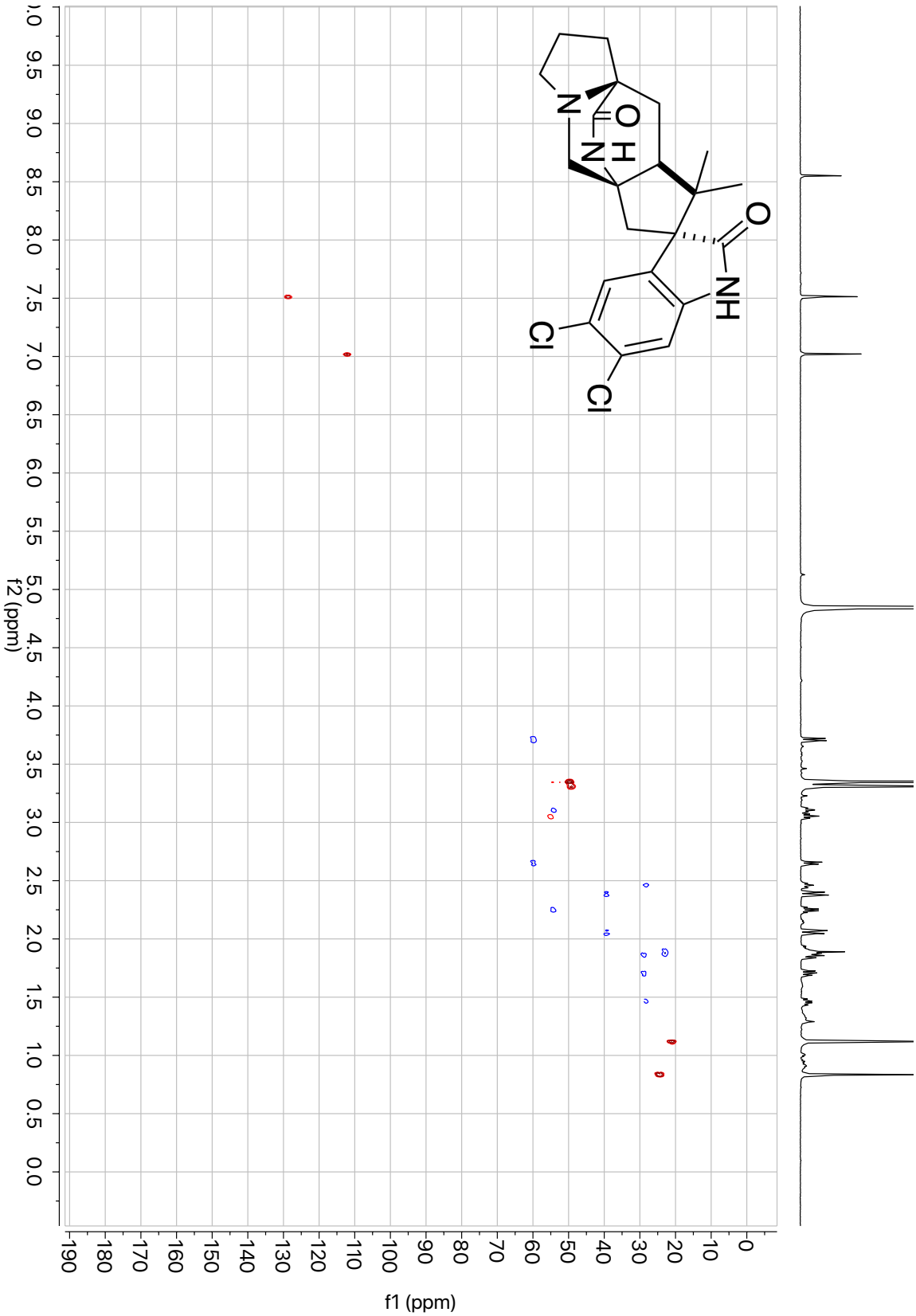

Figure 8.51 gHSQCAD correlations of spiromalbramide (**3.1**) (600 MHz, CD_3OD).

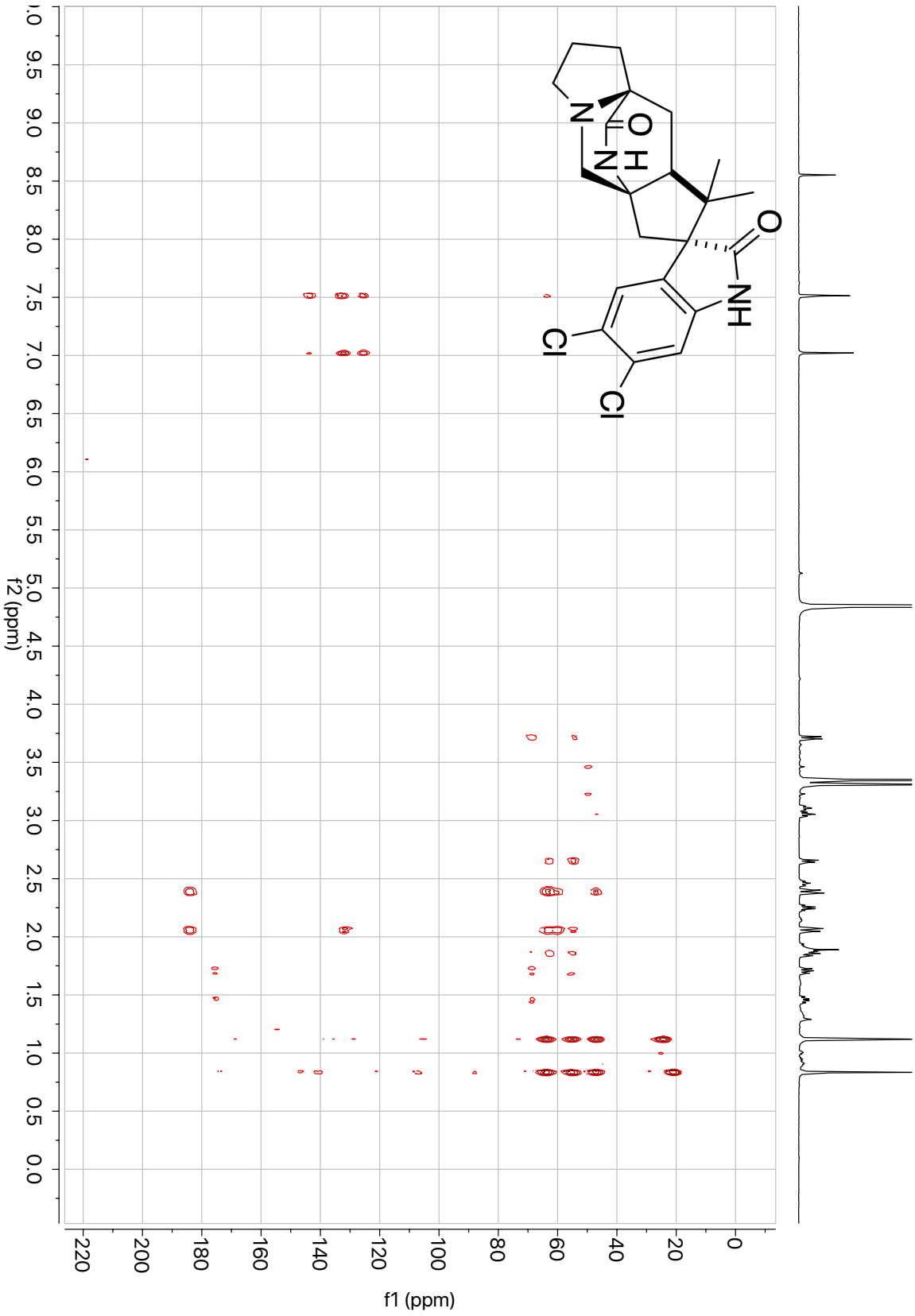

Figure 8.52 gHMBCAD correlations of spiromalbramide (**3.1**) (600 MHz, CD_3OD).

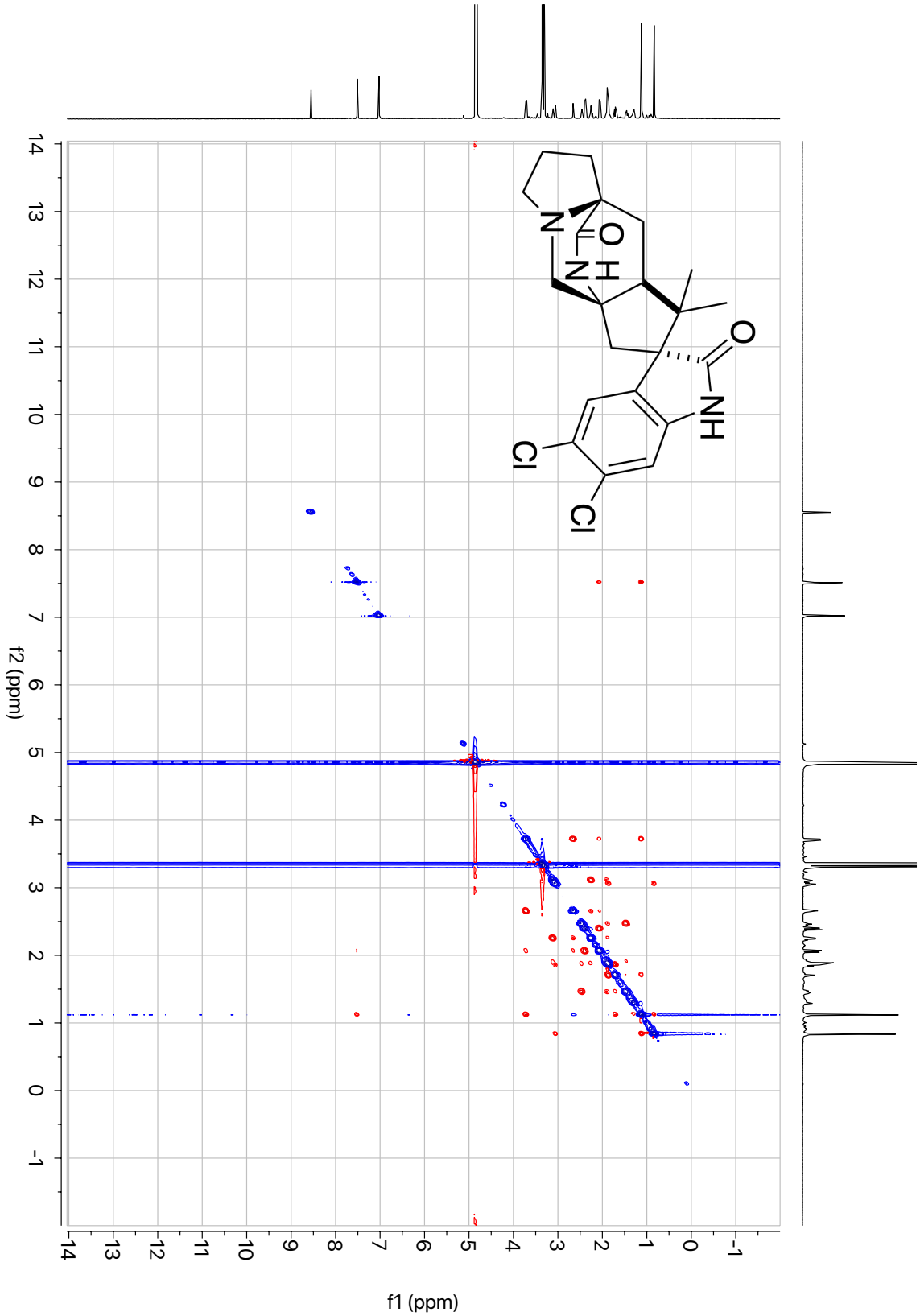

Figure 8.53 NOE correlations of spiromalbramide (**3.1**) (600 MHz, CD_3OD).

Chapter 9

Perturbation of the Interactions of Calmodulin with GRK5 using the Natural Product Malbrancheamide Experimental Section

9.1 Experimental Methods

9.1.1 Isolation of Malbrancheamide

The isolation and purification procedure was adapted from Martínez-Luis, *et al*. and Fraley, *et al.*[5, 72] Individual flasks of 75 mL potato dextrose broth were inoculated with 20 µL of *Malbranchea aurantiaca* spore stock and grown for 3 wk, or until a white fungal mat was produced. Prior to the noticeably orange sporulation, the cultures were pulverized and extracted with dichloromethane. The crude extract was acid-base purified first with 1 M HCl, then neutralized with 2 M ammonium hydroxide to pH 9, and back extracted with dichloromethane. The extract was then purified by chiral HPLC on a Lux 5 µm Cellulose-3 250 x 10 mm column (Phenomenex, Torrance, CA) using the following program: 50% acetonitrile for 18 min, gradient to 55% acetonitrile over 2 min, 55% acetonitrile for 2 min, gradient to 40% acetonitrile over 2 min, 40% acetonitrile for 5 min, at a flow rate of 4 mL min^{-1}. The mobile phase consisted of water and acetonitrile. From a 1.5 L growth of *M. aurantiaca* 5.8 mg L^{-1} malbrancheamide was obtained (^{1}H-NMR, 400 MHz, CD_3OD, ∂ 1.32 (s, 3H), 1.42 (s, 3H), 1.49 (m, 1H), 1.87 (m, 2H), 1.96 (dd, *J* = 13.1, 5.2 Hz, 1H), 2.03 (d, *J* = 13.1 Hz, 1H), 2.03 (m, 1H), 2.13 (m, 1H), 2.19 (m, 1H), 2.27 (dd, *J* = 10.3, 1.5 Hz, 1H), 2.56 (m, 1H), 2.84 (s, 2H), 3.43 (d, *J* = 10.2 Hz, 1H), 7.40 (s, 1H), 7.48 (s, 1H).

9.1.2 Production and Purification of Isomalbrancheamide D

Reactions were run in 1 mL aliquots with 40 µM MalA, 54 µM HpaC flavin reductase, 250 µM isomalbrancheamide B, 100 µM FAD, 50 mM NaBr, 5 mM NADH, and filled to the total volume with reaction buffer (50 mM NaH_2PO_4, 1 mM EDTA, 0.2 mM DTT, 10% glycerol, pH 7.3). Reactions were extracted after 12 hours with 2 mL ethyl acetate in triplicate, dried under nitrogen gas, and resuspended in methanol for HPLC purification. In a 2.3 mg reaction with isomalbrancheamide B, 1.8 mg isomalbrancheamide D were isolated. The product was purified using chiral HPLC with the previously mentioned semi-preparative cellulose column with the following HPLC time program: 70% acetonitrile for 14 min, gradient to 60% acetonitrile over 2

min at a flowrate of 4 mL min^{-1}. (^{1}H-NMR, 700 MHz, CD_3OD, ∂ 1.33 (s, 3H), 1.43 (s, 3H), 1.46 (m, 1H), 1.88 (m, 2H), 1.94 (m, 1H), 2.01 (m, 1H), 2.15 (m, 1H), 2.16 (q, 1H, J = 8.8 Hz), 2.26 (d, 1H, J = 10.4 Hz), 2.53 (ddd, 1H, J = 12.2, 9.1, 5.6 Hz), 2.85 (d, 2H, J = 4.8 Hz), 3.06 (m, 1H), 3.43 (d, 1H, J = 10.3 Hz, 1H), 7.51 (s, 1H), 7.57 (s, 1H).

9.1.3 Protein Expression and Purification

Human calmodulin (CaM) was inserted into *pMCSG7* containing a TEV-cleavable N-terminal hexahistidine tag using ligation-independent cloning, confirmed with Sanger sequencing, and transformed into *E. coli* BL21 DE3 pLysS cells. Cells were grown at 37 ˚C in terrific broth to an OD_{600} of 0.6-1.0, cooled to 20 ˚C, and induced with 0.5 mM IPTG overnight. CaM cell pellets were resuspended in lysis buffer composed of 20 mM HEPES pH 8.0, 200 mM NaCl, 40 mM imidazole, 5 mM $CaCl_2$, 1 mM dithiothreitol (DTT), leupeptin, 2 µg/mL soybean trypsin protease inhibitor, and 0.1 µM phenylmethylsulfonyl fluoride (PMSF) and lysed by sonication. Lysate was clarified by centrifugation for 30 min at 15,000xg. After centrifugation, the supernatant was glass filtered and slowly flowed through Ni-NTA resin. The resin was washed with lysis buffer and CaM eluted with lysis buffer supplemented with an additional 200 mM imidazole. TEV protease was added to the purified CaM at a final concentration of 10% w/v and dialyzed against 20 mM HEPES pH 8.0, 200 mM NaCl, 5 mM $CaCl_2$, and 1 mM DTT overnight to cleave the hexahistidine tag. Cleaved protein was flowed through Ni-NTA resin and the protein that flowed through was further purified via size exclusion chromatography (SEC) on an analytical S75 column in 20 mM HEPES pH 8.0, 200 mM NaCl, 5 mM $CaCl_2$, and 1 mM DTT. CaM of ≥95% purity by SDS-PAGE was aliquoted, flash frozen, and stored at -80 ºC. Calmodulin protein concentrations were determined by absorbance at 280 nm using a calculated molecular weight of 19,580 Da and extinction coefficient of 4,470 M^{-1} cm^{-1}. His-tagged N- or C-terminal lobes (residues 1-75 and 78-149, respectively) of CaM were also expressed and purified as described above for full-length CaM.

Human GRK5 with a C-terminal hexahistidine tag was cloned into a modified *pFastBac* HTB vector and verified by Sanger sequencing. High-titer recombinant baculovirus was prepared using the Bac-to-Bac protocol (Invitrogen/ThermoFisher, Carlsbad, CA) and used to infect Sf9 or Hi5 insect cells at a density of $2x10^6$ cells mL^{-1} for 48-60 h. GRK5 insect cell pellets were resuspended in lysis buffer containing 20 mM HEPES pH 8.0, 100 mM NaCl, 40 mM imidazole, 1 mM DTT, and 0.1 µM PMSF, 2 µg mL^{-1} leupeptin, and 2 µg mL^{-1} soybean trypsin protease inhibitor and briefly sonicated. Lysate was clarified by centrifugation for 1 h at >200,000xg. After

centrifugation, the supernatant was glass filtered and slowly flowed through Ni-NTA resin. The resin was washed with lysis buffer and GRK5 eluted with lysis buffer supplemented with an additional 200 mM imidazole. Eluted GRK5 was further purified via cation exchange chromatography on a HiTrap S column with a gradient of 0.0-1.0 M NaCl at pH 8.0. Fractions containing GRK5 were combined and run over an analytical S200 SEC column in 20 mM HEPES pH 8.0, 200 mM NaCl, and 1 mM DTT. GRK5 of ≥95% purity by SDS-PAGE was aliquoted, flash frozen, and stored at -80 ˚C. GRK5 protein concentrations were determined by absorbance at 280 nm using a calculated molecular weight of 70,660 Da and extinction coefficient of 60,280 M^{-1} cm^{-1}. Peptides encompassing the N (residues 2-31) or C (residues 546-565) were previously synthesized,[239] stored lyophilized in a desiccator at -20 ºC, and resuspended in DMSO prior to use in assays.

9.1.4 Determination of the Ca^{2+}·CaM·Malbrancheamide Crystal Structures

Ca^{2+}·CaM at 10-12 mg mL^{-1} was incubated at room temperature with 2 molar equivalents of malbrancheamide or isomalbrancheamide D in 20 mM HEPES pH 8.0, 200 mM NaCl, and 1 mM DTT supplemented with 5 mM $CaCl_2$ for 30 min. Sitting drop sparse-matrix screens with 0.5 µL well solution and 0.5 µL Ca^{2+}·CaM·malbrancheamide or isomalbrancheamide D were incubated at 20 ˚C. Small rod-like crystals appeared after 3-4 d in drops using well solution containing 0.1 M Tris pH 8.5, 0.2 M $MgCl_2$, and 20% (w/v) PEG 8,000. Crystals were harvested directly from the drop without cryoprotection, and diffraction data were collected at LS-CAT (Sector 21, Advanced Photon Source, Argonne National Lab) on an Eiger 9M detector (Dectris, Baden-Dättwil, Switzerland) at 100 K. Data were indexed, integrated, and scaled using xia2, DIALS, and Aimless.[240-242]

The diffraction data for crystals grown with either ligand were highly anisotropic with diffraction along the h axis extending to 2.7 Å, while diffraction in the k and l directions was observed to 1.8 Å in the case of Ca^{2+}·CaM ·malbrancheamide. The resulting datasets had large R_{meas} values overall and especially in the highest resolution shells, but $CC_{1/2}$ [243] and I/σ(I) strongly indicated meaningful data were present beyond 2.7 Å for the malbrancheamide data set. Ultimately, data were truncated at 1.96 Å for Ca^{2+}·CaM ·malbrancheamide and 1.89 Å for Ca^{2+}·CaM·isomalbrancheamide D yielding high resolution shells with I/σ(I)>2 and $CC_{1/2}$>0.9.

Molecular replacement was performed with Phaser[244] in Phenix[215] using one chain of PDB 4HEX.[245] Ligand restraints were prepared using eLBOW.[246] Reciprocal space refinement carried

out in Phenix Refine was alternated with real space refinement and model building in Coot.[216, 247] Ligand occupancy was set at 100% after allowing Phenix Refine to vary its occupancy automatically which returned an occupancy >90% across multiple rounds of refinement. Graphics were prepared with PyMol (version 2.1, Schrödinger LLC.). Structure factors and model coordinates have been deposited in the Protein Data Bank with the accession codes 6EEB and 6O5G.

9.1.5 Isothermal Titration Calorimetry (ITC)

ITC was performed with a NanoITC instrument (TA Instruments, New Castle, DE). Malbrancheamide or isomalbrancheamide D at 600 μM in 20 mM HEPES pH 8.0, 200 mM NaCl, 5 mM $CaCl_2$, and 5% DMSO was slowly titrated into a solution of 80 μM Ca^{2+}·CaM in an identical buffer. Although not ideal, the addition of DMSO to the buffers was required to obtain reasonable binding curves to the poor solubility of malbrancheamide at high concentrations in aqueous solution. The heat of binding was analyzed using Nano Analyze software (TA Instruments) and fit to a sigmoidal binding curve to obtain the binding affinity (K_d) and stoichiometry. ITC was repeated three times and statistical significance determined via Student's two-tailed T-test.

9.1.6 Radiometric Kinase Assays

Kinase assays were performed with 50 nM purified human GRK5 and either 5 μM light activated bovine rhodopsin in rod outer segment membranes, 10 μM porcine tubulin monomer (Cat. #T240, Cytoskeleton, Denver, CO), or 7 μM bovine myelin basic protein (MyBP, Cat. #13-104, EMD MilliporeSigma, Burlington, MA) in buffer containing 20 mM HEPES pH 8.0, 10 mM $MgCl_2$, 0.5 mM $CaCl_2$, and 1 mM DTT. CaM, CaM lobes, GRK5 terminal peptides, and/or malbrancheamide were added and the reactions initiated with 10 μM ATP spiked with [γ-^{32}P]-ATP (Perkin-Elmer, Waltham, MA) and allowed to proceed for 2 min at room temperature for tubulin and MyBP substrates and 5 min at room temperature for rhodopsin prior to quenching with SDS loading dye. Samples were separated on 4-15% polyacrylamide gels, dried, and exposed overnight on phosphor screens. Screens were imaged on a Typhoon imager (GE Healthcare, Chicago, IL), band intensities quantified using ImageQuant, and fit to a three parameter dose-response model in GraphPad Prism with the Hill slope constrained to 1 and the top and bottom plateaus unconstrained. The dose-response model equation is: Y=Bottom + (Top-Bottom)/(1+10^((LogEC50-X))). IC_{50} and EC_{50} values (average ± SD) are reported when the plateaus surrounding the dose-response curves were defined. All experiments were performed

three times and reported as mean ± SD. Reactions containing rhodopsin were incubated 5 min and tubulin and MyBP reactions were allowed to proceed for 2 min at room temperature. Data were normalized to either saturated substrate or GRK5 phosphorylation in the absence of small molecule inhibitor and/or Ca^{2+}·CaM (100%) and phosphor image plate background (0%) measurements after 5 min. For MyBP, 100% represents the maximum phosphorylation in the presence of 500 μM CaM.

9.1.7 Complex Formation and Light Scattering

Purified GRK5 and Ca^{2+}·CaM were mixed in a 1:3 molar ratio, supplemented with 5 mM $CaCl_2$, and incubated at 4 ˚C for 30 min prior to separation by size exclusion chromatography (SEC) using an analytical S200 10/300 column (GE Healthcare, Chicago, IL). Approximately 500 μg of Ca^{2+}·CaM–GRK5 complex, or 500 μg of GRK5 alone as a control, was then injected onto Shodex KW-804 liquid chromatography column coupled to a Dawn-Helios multi-angle light scattering (MALS) detector (Wyatt Technologies, Santa Barbara, CA) to determine the molecular weight and stoichiometry of the complex through interpolation of a standard calibration curve.

9.1.8 Small-Angle X-Ray Scattering (SAXS)

SAXS was performed at BioCAT (beamline 18ID at the Advanced Photon Source, Argonne National Laboratory) with in-line size exclusion chromatography (SEC-SAXS) to separate the sample from aggregates and other contaminants thus ensuring optimal sample quality. GRK5 and Ca^{2+}·CaM–GRK5 complex at 6 and 10 mg/mL were loaded onto a Superdex 200 Increase 10/300 GL column, which was run at 1.0 mL min^{-1} by an AKTA Pure FPLC (GE Healthcare Life Sciences, Chicago, IL). The eluate was passed through a UV monitor and flown through the SAXS flow cell, which consists of a 1.5 mm ID quartz capillary with 10 μm walls. Scattering intensity was recorded using a Pilatus3 1M detector (Dectris, Baden-Dättwil, Switzerland) which was placed 3.5 m from the sample giving access to a q-range of 0.004 $Å^{-1}$ to 0.4 $Å^{-1}$. Exposures of 0.5 s were acquired every 2 s during elution and the data were reduced using BioXTAS RAW 1.4.0.[248] Additional experimental parameters can be found in **Table 9.1**.

Buffer blanks were created by averaging regions flanking the elution peak and subtracted from exposures selected from the elution peak to create the I(q) vs q curves used for subsequent analyses. The ATSAS and ScÅtter software packages were used to further process data and generate data plots.[249-251] Porod exponents for the evaluation of compactness were calculated automatically by ScÅtter after defining the linear region of the Porod plot.

Electron density was reconstructed from the raw SAXS data using the program DENsity from Solution Scattering (DENSS).[252] The higher concentration samples produced the strongest signal and strongest density (judged by density at increasing σ and better quality of fits/correlation coefficients for R_g and D_{max}) and were used for modeling. The program dock_in_map as part of the Phenix software package was used to perform automatic, unbiased docking of the proteins into the reconstructed density using an automatically selected search order. GRK5 was fit to the density of the complex using a random starting position and the density occupied by GRK5 after automatic placement was omitted from a subsequent search for the placement of Ca^{2+}·CaM. GRK5 (PDB 4WNK) with a modeled N-terminus, AST loop, and C-terminus from GRK6 (PDB 3NYN), a GRK structure with all three features resolved, was used as the GRK5 model and Ca^{2+}·CaM (PDB 5J03) was chosen from a variety of different liganded states of Ca^{2+}·CaM for its quality of fit to the density. CRYSOL[253] as part of the ATSAS PyMol plugin SASpy[254] was used to score the model against the raw SAXS data. PyMol (version 2.1, Schrödinger LLC., New York City, NY) was used to generate figures.

9.1.9 Negative Stain EM

Purified Ca^{2+}·CaM–GRK5 complex was isolated by SEC as described under *Complex Formation and Light Scattering*. For negative stain imaging, protein samples were diluted with buffer (20 mM HEPES, 200 mM NaCl, 5 mM $CaCl_2$, 1 mM DTT) to 0.02-0.05 mg mL^{-1}. The samples were prepared using a conventional negative staining protocol,[255] and imaged at room temperature with a Technai T12 electron microscope operated at 120 kV using low dose procedures. Images were recorded at a magnification of 71,138x and a defocus value of ~ -1.4 µm on a Gatan US4000 CCD camera. All images were binned (2x2 pixels) to obtain a pixel size of 4.16 Å on the specimen level. Particles were manually picked using e2boxer.py (part of the EMAN2 software suite).[256] 2D reference-free alignment and classification of particle projections was performed using ISAC.[257]

9.1.10 Flow Cytometry Protein Interaction Assay (FCPIA)

FCPIA was performed as described previously.[258, 259] CaM was labeled with amine-reactive biotin at a 1:1 molar ratio, followed by its conjugation to SPHERO streptavidin-coated beads (Spherotech). Different amounts of GRK5, labeled with AlexaFluor-488 C_5-maleimide (AF488- GRK5) at 1:1 ratio, were incubated with CaM-beads in the buffer containing 20 mM HEPES pH 8.0, 100 mM NaCI, 2 mM DTT, 1% (w/v) bovine serum albumin and 0.1% (v/v) lubrol

containing either 2.5 mM EGTA or 2.5 mM $CaCl_2$ for 30 min at 20 ˚C. Then, the bead-associated fluorescence was measured using Accuri C6 Flow Cytometer. The fluorescence as a function of AF488-GRK5 concentration was plotted and fit to an equation for total binding in GraphPad Prism software: $Y=B_{max}*X/(Kd+X)+NS*X+Background$, where B_{max} is the maximum specific binding and NS is the slope of non-specific binding. For competition experiments, various concentrations of unlabeled GRK5 variants or peptides were incubated with 10 nM of CaM-conjugated beads and 100 nM of AF488-GRK5. Peptides that bind CaM were able to compete with fluorescent GRK5 leading to a decrease in bead-associated fluorescence compared to the samples in which no competitor was present. The binding affinity (K_i) of each peptide was calculated via the Cheng-Prusoff equation. Each peptide was tested three times in duplicate and the data reported as average ± SD normalized after baseline correction for non-specific binding.

9.1.11 GRK5 Nuclear Translocation Assay

Neonatal rat cardiac fibroblasts (NRCFs) were plated overnight in Dulbecco's Modified Eagle Medium (DMEM) supplemented with 10% fetal bovine serum (FBS) and 1% penicillin/streptomycin (pen/strep). On day 2, NRCFs were switched to base DMEM with no additives and either 0.1% DMSO (as a negative control) or 1 μM malbrancheamide (in DMSO) and incubated overnight. On Day 3, base DMEM was replaced for 2 h and then 5 μM of the hypertrophic agonist angiotensin II (AngII) was added (or vehicle – PBS as the non-stimulated control) and incubated for an additional 90 min. Nuclear fractions were then purified from cardiac fibroblast cell pellets as described[200] and GRK5 protein content was quantitated using western blotting (using GRK5 antibody SC-518005, Santa Cruz Biotechnology, Dallas, TX) and densitometry using levels of the nuclear protein fibrillarin as a normalization loading control. Statistical significance of n=3 independent experiments was determined via two-way ANOVA with Tukey's post hoc correction for multiple comparisons.

9.1.12 Hypertrophic Phenotypic Assay

AC16 human cardiomyocyte cells were plated overnight in DMEM supplemented with 10% FBS and 1% pen/strep. On day 2, cells were switched to base DMEM with no additives and either 0.1% DMSO or 1 μM malbrancheamide (in DMSO) and incubated overnight. On Day 3, the hypertrophic α-adrenergic agonist phenylephrine (PE)[200] was added to a final concentration of 50 μM (or vehicle (DMEM) was added for the non-stimulated control) and incubated for 48 h. Cells were then fixed with 3.7% formaldehyde, permeabilized in 0.2% NP-40, and stained for DAPI to visualize cell nuclei and F-actin (phalloidin-488) to identify cellular area. IMAGE-J software was

used to manually quantitate cell area of PE-treated cardiomyocytes versus vehicle-treated cells (±malbrancheamide) using F-actin staining. Statistical significance of 3 biological replicates (independent experiments with 50-100 cells measured per replicate) was determined via two-way ANOVA with Tukey's post hoc correction for multiple comparisons.

9.2 Tables

Table 9.1 SAXS data collection parameters.

SAXS data collection parameters	
Instrument	Bio-CAT facility at the Advanced Photon Source beamline 18ID with Pilatus3 1M (Dectris) detector
Wavelength (Å)	1.033
Beam size (μm^2)	150 (h) x 25 (v)
Camera length (m)	3.5
q-measurement range ($Å^{-1}$)	0.004-0.4
Absolute scaling method	N/A
Basis for normalization to constant counts	To incident intensity, by ion chamber counter
Method for monitoring radiation damage	Automated frame-by-frame comparison of relevant regions
Exposure time, number of exposures	0.5 s exposure time with a 2 s total exposure period (0.5 s on, 1.5 s off) of entire SEC elution
Sample configuration	SEC-SAXS. Size separation by an AKTA Pure with a Superdex 200 Increase 10/300 GL column. SAXS data measured in a 1.5 mm ID quartz capillary.
Sample temperature (ºC)	20
Software employed for SAS data reduction, analysis and interpretation	
SAXS data reduction	Radial averaging; frame comparison, averaging, and subtraction done using BioXTAS RAW 1.4.0. (11)
Basic analysis: Guinier, M.W., P(r)	Guinier fit and molecular weight using BioXTAS RAW 1.4.0, P(r) function using GNOM. (13)

Table 9.2 Data collection statistics for SEC-SAXS experiments.

	GRK5	Ca^{2+}·CaM–GRK5	GRK5	Ca^{2+}·CaM–GRK5
Concentration (mg/mL)	6	6	10	10
Guinier I(0)	27.4	17.2	26.7	30.8
Guinier R_g (Å)	31.8	37.3	29.6	35.3
Guinier Pearson CC	0.84	0.86	0.92	0.94
P(r) I(0)	27.0	15.2	30.0	32.9
P(r) R_g (Å)	31.2	32.2	30.0	34.0
P(r) Quality of Fit	0.81	0.83	0.90	0.94
D_{max} (Å)	94	108	97	109
Estimated MW (kDa)	68	85	73	95
Actual MW (kDa)	70.7	90.3	70.7	90.3

Data collection statistics for SEC-SAXS experiments. Zero angle intensity [I(0)], radius of gyration (R_g), and quality of fit/Pearson correlation coefficient derived from Guinier and Pair-distance [P(r)] analyses are displayed. The maximum particle size D_{max} was determined from the largest radius in the P(r) plot (Supplemental Figure 1). Estimated molecular weight (MW) was calculated by dividing the Porod volume by 1.7.[260]

Table 9.3 Crystallographic data collection for the Ca^{2+}·CaM complexes.

Ligand	Malbrancheamide	Isomalbrancheamide D
Wavelength (Å)	1.0332	0.9839
Resolution (Å)	35 – 1.96 (2.03 – 1.96)*	38 – 1.89 (1.96 – 1.89)*
Space group	*C* 2 2 2_1	*C* 2 2 2_1
Unit cell constants (Å, º)	49.1 56.9 116.8 90 90 90	50.9 56.8 117.2 90 90 90
Total reflections	158,616 (16,218)	181,440 (18,251)
Unique reflections	12,096 (1,184)	13,910 (1,356)
Multiplicity	13.1 (13.7)	13.0 (13.5)
Completeness (%)	99.8 (99.8)	99.7 (99.9)
Mean I/σ(I)	7.5 (2.6)	19.8 (4.5)
Wilson B-factor	29.7	24.1
R_{meas}	0.200 (0.831)	0.083 (0.606)
R_{pim}	0.055 (0.223)	0.023 (0.166)
$CC_{1/2}$	0.995 (0.944)	0.999 (0.957)
Reflections used in refinement	12,080 (1,181)	13,896 (1,356)
Reflections used for R_{free}	1,207 (118)	1,391 (136)
R_{work} / R_{free}	0.212/0.260 (0.351/0.402)	0.190/0.238 (0.236/0.316)
Number of non-hydrogen atoms	1,212	1,253
Protein	1,129	1,129
Ligand	32	32
Solvent	51	92
RMS bonds (Å)	0.007	0.005
RMS angles (º)	0.88	0.72
Ramachandran favored (%)	98.6	100.0
Ramachandran allowed (%)	1.4	0.0
Ramachandran outliers (%)	0.0	0.0
Rotamer outliers (%)	0.0	1.6
Clashscore	11.7	1.8
Average B-factor	55.2	38.6
Protein	54.7	38.0
Ligand	90.7	59.3
Solvent	44.0	40.1
PDB Accession	6EEB	6O5G

*Statistics for the highest-resolution shell are shown in parentheses

9.3 Figures

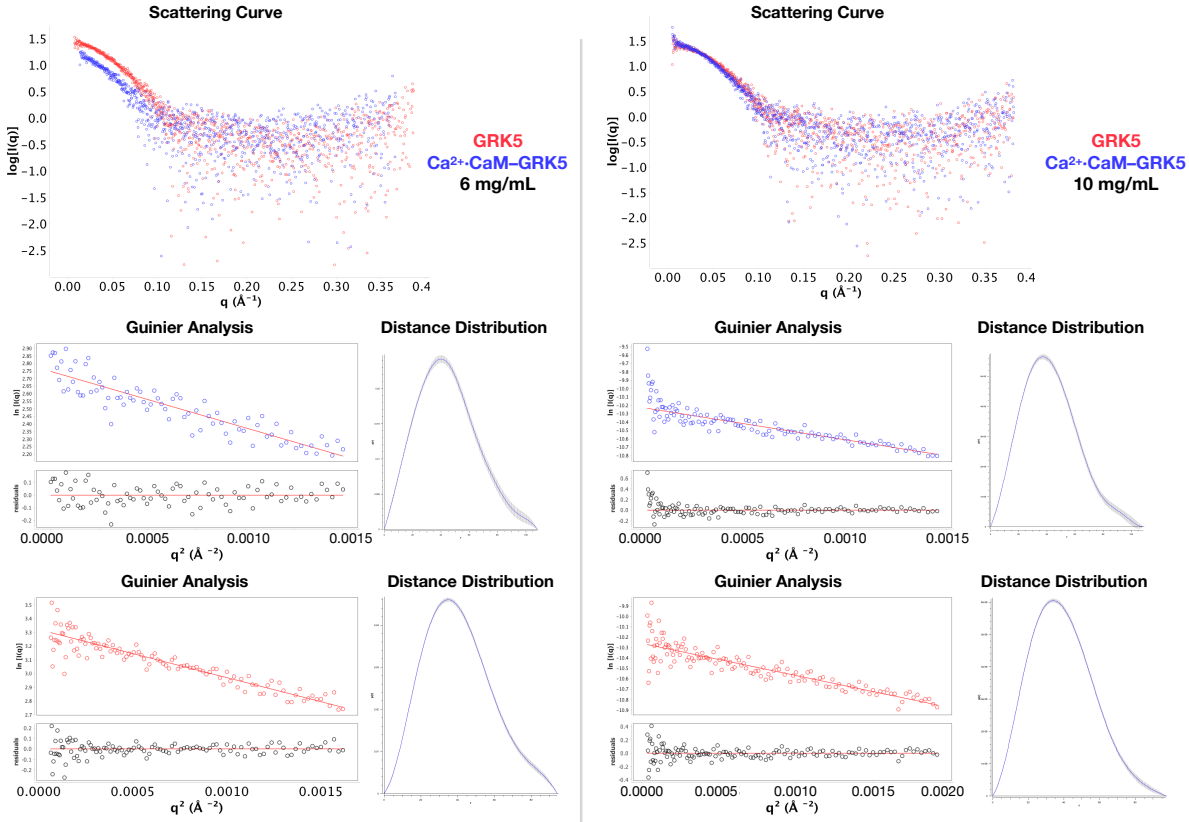

Figure 9.1 SAXS data for GRK5 and the Ca^{2+}·CaM–GRK5 complex. Data are from from 6 and 10 mg mL^{-1} samples. Shown are the raw scattering curves (10 mg mL^{-1} scattering scaled to GRK5 from the 6 mg mL^{-1} data set in ScÅtter for comparison purposes), Guinier plots for the $qR_g<1.3$ regions, and the corresponding pair-distance distribution [P(r)]. The best-fit line used to calculate I(0) through extrapolation is shown on the Guinier plots. The maximum particle dimension (D_{max}) reported in Supplemental Table 2 was determined from the largest X-intercept on the pair-distance distributions.

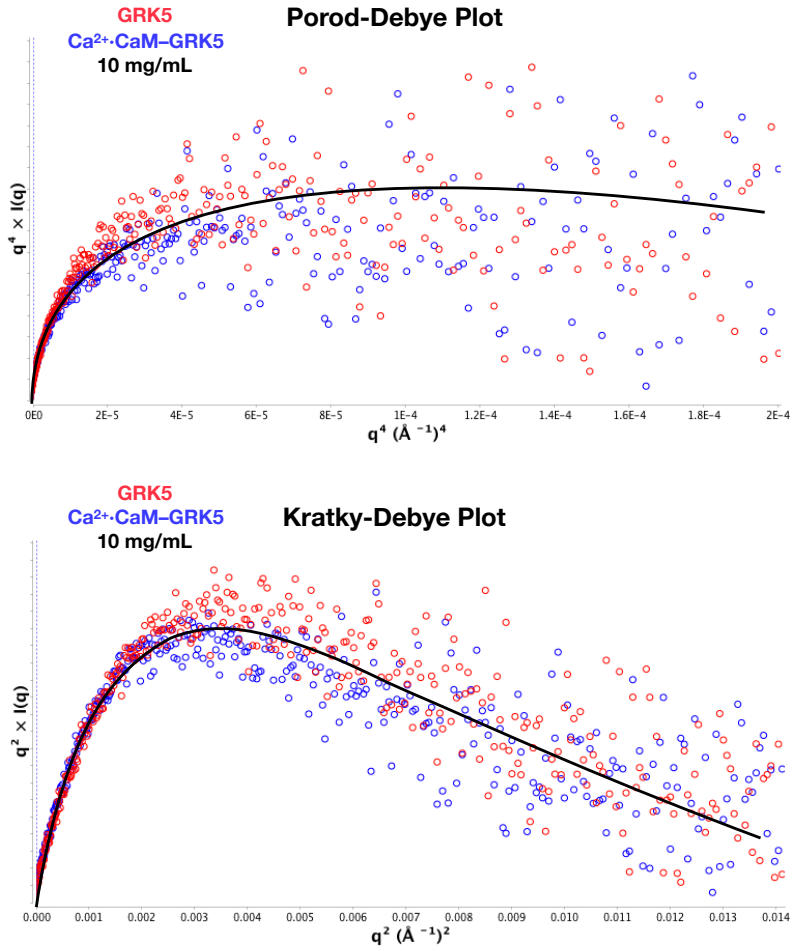

Figure 9.2 Flexibility analysis of GRK5 and the Ca^{2+}·CaM–GRK5 complex. Data from 10 mg mL^{-1} SEC-SAXS experiments. Both samples display a plateau in their Porod-Debye plots at q_{max}=0.12 $Å^{-1}$ whereas their respective Kratky-Debye plots are decreasing indicating the particles do not display a high degree of flexibility. Plots were prepared in ScÅtter.

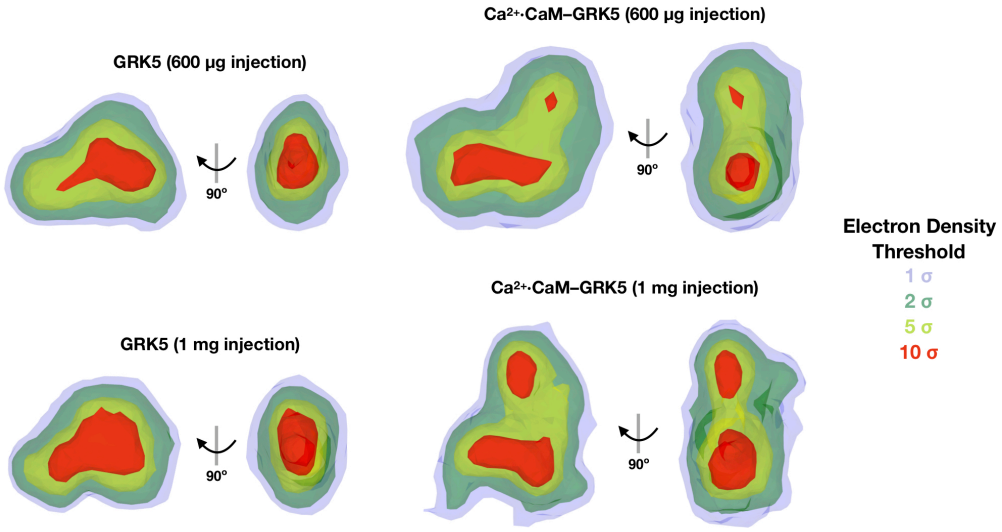

Figure 9.3 Reconstructed electron densities from SEC-SAXS experiments using DENSS.

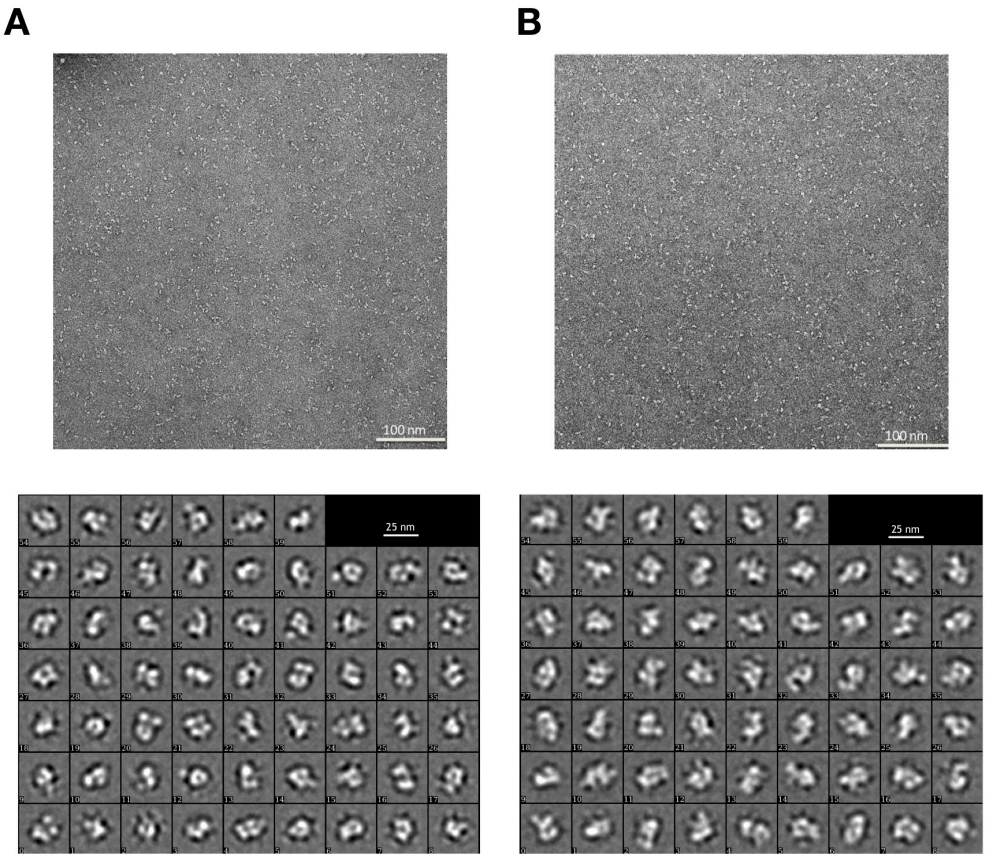

Figure 9.4 Representative negative stain micrographs. **A)** GRK5 and **B)** the Ca^{2+}·CaM–GRK5 complex. Data were collected on a Technai T12 electron microscope operated at 120 kV using low dose procedures. Images were recorded at a magnification of 71,138x and a defocus value of ~ -1.4 µm on a Gatan US4000 CCD camera.

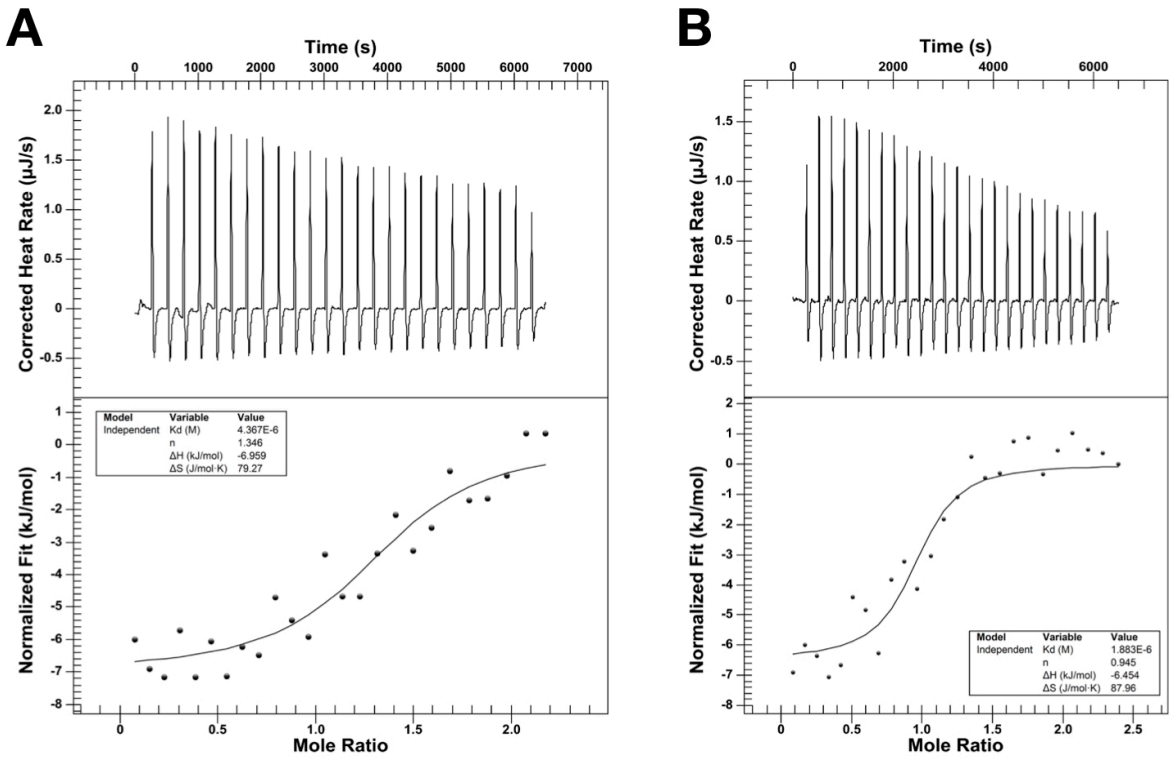

Figure 9.5 Representative ITC curves **A)** malbrancheamide and **B)** isomalbrancheamide D binding to Ca^{2+}·CaM.

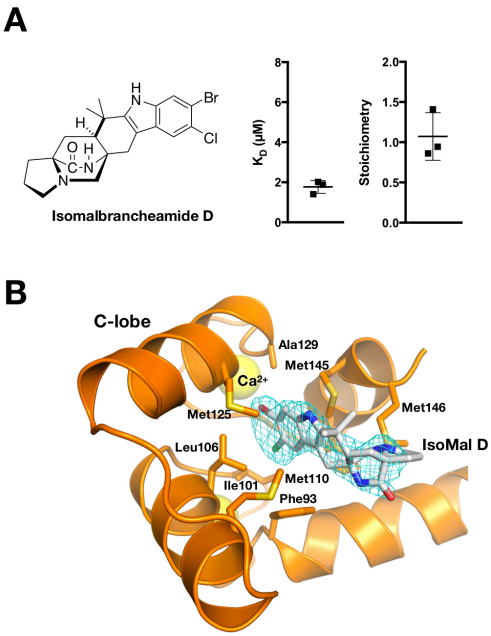

Figure 9.6 Ca^{2+}·CaM complex with isomalbrancheamide D. Isomalbrancheamide D also binds to the C-lobe of Ca^{2+}·CaM. **A)** Chemical structure of isomalbrancheamide D and ITC binding results (average ± S.D., N=3). **B)** C-lobe hydrophobic pocket with isomalbrancheamide D (IsoMal D) bound. Cyan mesh represents refined $|2\boldsymbol{F_o}| - |\boldsymbol{F_c}|$ density

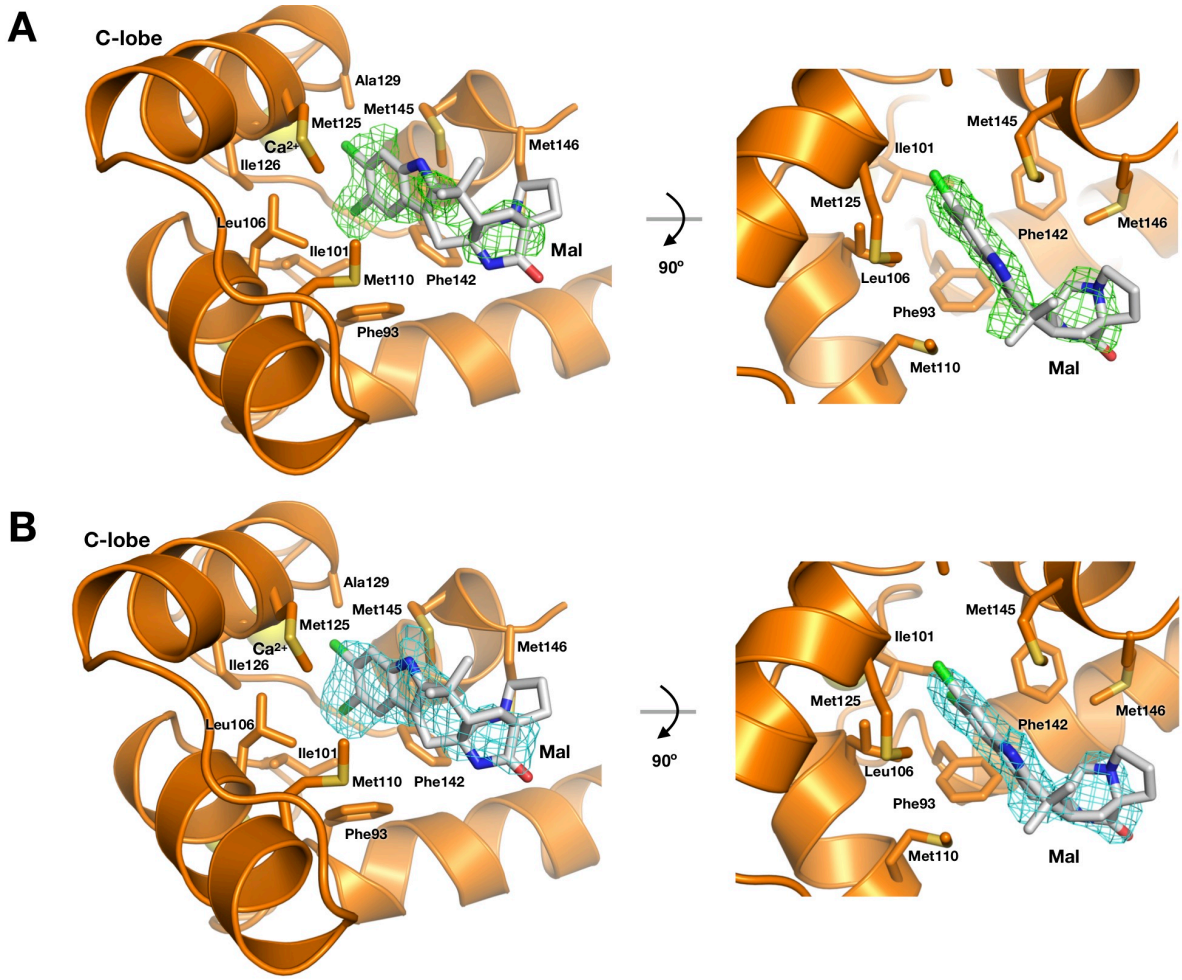

Figure 9.7 Electron density for malbrancheamide (Mal) bound to Ca^{2+}·CaM. **A)** Green mesh represents positive $|\boldsymbol{F_o}| - |\boldsymbol{F_c}|$ omit density contoured at 2.5 σ. **B)** Cyan mesh represents refined $|\boldsymbol{2F_o}| - |\boldsymbol{F_c}|$ density contoured at 1.0 σ.

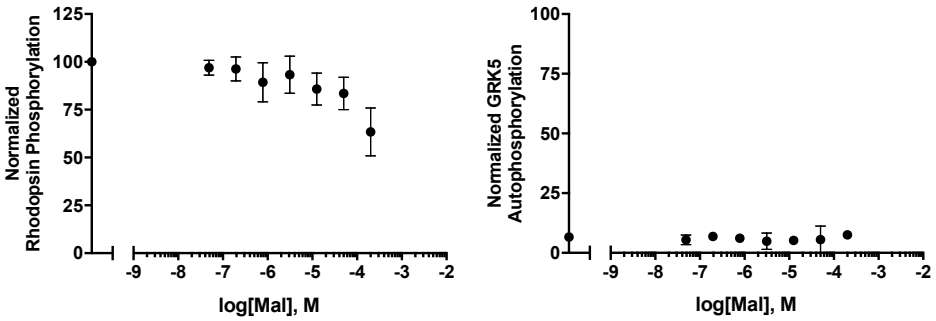

Figure 9.8 Effect of malbrancheamide on GRK5 activities in the absence of Ca^{2+}·CaM. Addition of malbrancheamide (Mal) does not affect phosphorylation of rhodopsin or GRK5 autophosphorylation. Experiments were performed three times and shown here as mean ± SD. Data were normalized to either saturated substrate or GRK5 phosphorylation in the absence of small molecule inhibitor and/or Ca^{2+}·CaM (100%) and phosphor image background (0%) measurements after 5 min.

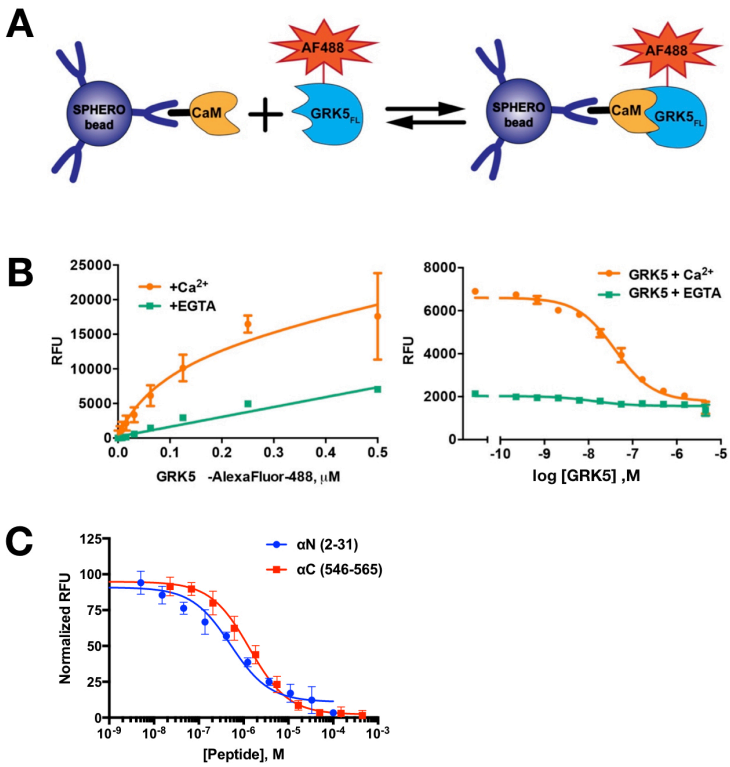

Figure 9.9 Determination of terminal peptide binding affinities by flow cytometry protein interaction assay (FCPIA). **A)** Schematic of the FCPIA assay. Interaction between Ca^{2+}·CaM and GRK5 leads to an increase in fluorescence from the conjugated AlexaFluor-488 (AF488). **B)** Control binding experiments assessing binding of CaM in the presence of Ca^{2+} or EGTA and competition between unlabeled GRK5 and AlexaFluor-488-labeled GRK5 for CaM binding in the presence of Ca^{2+} or EGTA. **C)** Displacement of labeled GRK5 by peptides encompassing the N (residues 2-31) or C (residues 546-565) terminal region of GRK5. Binding affinities (K_i) calculated via the Cheng-Prusoff equation after correcting for non-specific binding are 250 ± 10 and 670 ± 14 nM for the N and C terminal peptides, respectively. Data are reported as average ± SD (n=3 in duplicate).

References

1. Kelley, L. A.; Mezulis, S.; Yates, C. M.; Wass, M. N.; Sternberg, M. J., The Phyre2 web portal for protein modelling, prediction and analysis. *Nat. Protoc.* **2015,** *10* (6), 845-858
.
2. Li, S. Y.; Srinivasan, K.; Tran, H.; Yu, F. A.; Finefield, J. M.; Sunderhaus, J. D.; McAfoos, T. J.; Tsukamoto, S.; Williams, R. M.; Sherman, D. H., Comparative analysis of the biosynthetic systems for fungal bicyclo[2.2.2]diazaoctane indole alkaloids: the (+)/(-)-notoamide, paraherquamide and malbrancheamide pathways. *Medchemcomm* **2012,** *3* (8), 987-996.
3. Yamazaki, M.; Okuyama, E.; Kobayashi, M.; Inoue, H., The structure of paraherquamide, a toxic metabolite from *Penicillium paraherquei*. *Tetrahedron Lett* **1981,** *22* (2), 135-136.
4. Lopez-Gresa, M. P.; Gonzalez, M. C.; Ciavatta, L.; Ayala, I.; Moya, P.; Primo, J., Insecticidal activity of paraherquamides, including paraherquamide H and paraherquamide I, two new alkaloids isolated from *Penicillium cluniae*. *J Agr Food Chem* **2006,** *54* (8), 2921-2925.
5. Martinez-Luis, S.; Rodriguez, R.; Acevedo, L.; Gonzalez, M. C.; Lira-Rocha, A.; Mata, R., Malbrancheamide, a new calmodulin inhibitor from the fungus *Malbranchea aurantiaca*. *Tetrahedron* **2006,** *62* (8), 1817-1822.
6. Qian-Cutrone, J. F.; Huang, S.; Shu, Y. Z.; Vyas, D.; Fairchild, C.; Menendez, A.; Krampitz, K.; Dalterio, R.; Klohr, S. E.; Gao, Q., Stephacidin A and B: Two structurally novel, selective inhibitors of the testosterone-dependent prostate LNCaP cells. *J Am Chem Soc* **2002,** *124* (49), 14556-14557.
7. Kato, H.; Yoshida, T.; Tokue, T.; Nojiri, Y.; Hirota, H.; Ohta, T.; Williams, R. M.; Tsukamoto, S., Notoamides A-D: Prenylated indole alkaloids isolated from a marine-derived fungus, *Aspergillus* sp. *Angew Chem Int Edit* **2007,** *46* (13), 2254-2256.
8. Grubbs, A. W.; Artman, G. D.; Tsukamoto, S.; Williams, R. M., A concise total synthesis of the notoamides C and D. *Angew Chem Int Edit* **2007,** *46* (13), 2257-2261.
9. Tsukamoto, S.; Kato, H.; Samizo, M.; Nojiri, Y.; Onuki, H.; Hirota, H.; Ohta, T., Notoamides F-K, Prenylated Indole Alkaloids isolated from a marine-derived *Aspergillus* sp. *J Nat Prod* **2008,** *71* (12), 2064-2067.
10. Birch, A. J.; Wright, J. J., Brevianamides - a new class of fungal alkaloid. *J Chem Soc Chem Comm* **1969,** (12), 644-&.
11. Blizzard, T. A.; Marino, G.; Mrozik, H.; Fisher, M. H.; Hoogsteen, K.; Springer, J. P., Chemical modification of paraherquamide. 1. Unusual reactions and absolute stereochemistry. *Abstr Pap Am Chem S* **1989,** *197*, 26-Orgn.
12. Blizzard, T. A.; Mrozik, H.; Fisher, M. H.; Schaeffer, J. M., Chemical modification of paraherquamide. 2. Replacement of the C-14 methyl group. *J Org Chem* **1990,** *55* (7), 2256-2259.
13. Blizzard, T. A.; Marino, G.; Mrozik, H.; Schaeffer, J. M.; Fisher, M. H., Chemical modification of paraherquamide. 3. Vinyl ether modified analogs. *Abstr Pap Am Chem S* **1989,** *198*, 42-Orgn.
14. Blizzard, T. A.; Margiatto, G.; Mrozik, H.; Schaeffer, J. M.; Fisher, M. H., Chemical modification of paraherquamide. 4. 1-N-substituted analogs. *Tetrahedron Lett* **1991,** *32* (22), 2441-2444.

15. Madariaga-Mazon, A.; Hernandez-Abreu, O.; Estrada-Soto, S.; Mata, R., Insights on the vasorelaxant mode of action of malbrancheamide. *J Pharm Pharmacol* **2015,** *67* (4), 551-558.
16. Artman, G. D.; Grubbs, A. W.; Williams, R. M., Concise, asymmetric, stereocontrolled total synthesis of stephacidins A, B and notoamide B. *J Am Chem Soc* **2007,** *129* (19), 6336-6342.
17. Maiya, S.; Grundmann, A.; Li, S. M.; Turner, G., The fumitremorgin gene cluster of *Aspergillus fumigatus*: Identification of a gene encoding brevianamide F synthetase. *Chembiochem* **2006,** *7* (7), 1062-1069.
18. Grundmann, A.; Li, S. M., Overproduction, purification and characterization of FtmPT1, a brevianamide F prenyltransferase from *Aspergillus fumigatus*. *Microbiol-Sgm* **2005,** *151*, 2199-2207.
19. Tsunematsu, Y.; Ishikawa, N.; Wakana, D.; Goda, Y.; Noguchi, H.; Moriya, H.; Hotta, K.; Watanabe, K., Distinct mechanisms for spiro-carbon formation reveal biosynthetic pathway crosstalk. *Nat Chem Biol* **2013,** *9* (12), 818.
20. Pistorius, D.; Li, Y. Y.; Sandmanny, A.; Muller, R., Completing the puzzle of aurachin biosynthesis in *Stigmatella aurantiaca* Sg a15. *Mol Biosyst* **2011,** *7* (12), 3308-3315.
21. Katsuyama, Y.; Harmrolfs, K.; Pistorius, D.; Li, Y. Y.; Muller, R., A semipinacol rearrangement directed by an enzymatic system featuring dual-function FAD-dependent monooxygenase. *Angew Chem Int Edit* **2012,** *51* (37), 9437-9440.
22. Ding, Y. S.; de Wet, J. R.; Cavalcoli, J.; Li, S. Y.; Greshock, T. J.; Miller, K. A.; Finefield, J. M.; Sunderhaus, J. D.; McAfoos, T. J.; Tsukamoto, S.; Williams, R. M.; Sherman, D. H., Genome-based characterization of two prenylation steps in the assembly of the stephacidin and notoamide anticancer agents in a marine-derived *Aspergillus* sp. *J Am Chem Soc* **2010,** *132* (36), 12733-12740.
23. Dan, Q.; Newmister, S. A.; Klas, K. R.; Fraley, A. E.; A., M. T.; Somoza, A. D.; Sunderhaus, J. D.; Ye, Y.; Shende, V. V.; Yu, F.; Sander, J. N.; Brown, W. C.; Zhao, L.; Paton, R. S.; Houk, K. N.; Smith, J. L.; Sherman, D. H.; Williams, R. M., Fungal indole alkaloid biogenesis through evolution of a bifunctional reductase/Diels-Alderase. *ChemRxiv Preprint.* **2019**.
24. Stocking, E. M.; SanzCervera, J. F.; Williams, R. M.; Unkefer, C. J., Studies on the biosynthesis of paraherquamide A. Origin of the beta-methylproline ring. *J Am Chem Soc* **1996,** *118* (29), 7008-7009.
25. Stocking, E. M.; Sanz-Cervera, J. F.; Unkefer, C. J.; Williams, R. M., Studies on the biosynthesis of paraherquamide. Construction of the amino acid framework. *Tetrahedron* **2001,** *57* (25), 5303-5320.
26. Stocking, E. M.; Martinez, R. A.; Silks, L. A.; Sanz-Cervera, J. F.; Williams, R. M., Studies on the biosynthesis of paraherquamide: Concerning the mechanism of the oxidative cyclization of l-isoleucine to beta-methylproline. *J Am Chem Soc* **2001,** *123* (14), 3391-3392.
27. Stocking, E. M.; Sanz-Cervera, J. F.; Williams, R. M., Studies on the biosynthesis of paraherquamide: Synthesis and incorporation of a hexacyclic indole derivative as an advanced metabolite. *Angew Chem Int Edit* **2001,** *40* (7), 1296.
28. Blanchflower, S. E.; Banks, R. M.; Everett, J. R.; Reading, C., Further novel metabolites of the paraherquamide family. *J Antibiot* **1993,** *46* (9), 1355-1363.
29. Yang, B.; Dong, J. D.; Lin, X. P.; Zhou, X. F.; Zhang, Y. Y.; Liu, Y. H., New prenylated indole alkaloids from fungus *Penicillium* sp derived of mangrove soil sample. *Tetrahedron* **2014,** *70* (25), 3859-3863.

30. Jiang, W.; Cacho, R. A.; Chiou, G.; Garg, N. K.; Tang, Y.; Walsh, C. T., EcdGHK are three tailoring iron oxygenases for amino acid building blocks of the echinocandin scaffold. *J Am Chem Soc* **2013,** *135* (11), 4457-4466.
31. Stocking, E. M.; Williams, R. M.; Sanz-Cervera, J. F., Reverse prenyl transferases exhibit poor facial discrimination in the biosynthesis of paraherquamide A, brevianamide A, and austamide. *J Am Chem Soc* **2000,** *122* (38), 9089-9098.
32. Tsukamoto, S.; Kawabata, T.; Kato, H.; Greshock, T. J.; Hirota, H.; Ohta, T.; Williams, R. M., Isolation of antipodal (-)-versicolamide B and notoamides L-N from a marine-derived *Aspergillus* sp. *Org Lett* **2009,** *11* (6), 1297-1300.
33. Tsukamoto, S.; Kato, H.; Greshock, T. J.; Hirota, H.; Ohta, T.; Williams, R. M., Isolation of notoamide E, a key precursor in the biosynthesis of prenylated indole alkaloids in a marine-derived fungus, *Aspergillus* sp. *J Am Chem Soc* **2009,** *131* (11), 3834.
34. Yin, S. Q.; Yu, X.; Wang, Q.; Liu, X. Q.; Li, S. M., Identification of a brevianamide F reverse prenyltransferase BrePT from *Aspergillus versicolor* with a broad substrate specificity towards tryptophan-containing cyclic dipeptides. *Appl Microbiol Biot* **2013,** *97* (4), 1649-1660.
35. Porter, A. E. A.; Sammes, P. G., A Diels-Alder Reaction of possible biosynthetic importance. *J Chem Soc Chem Comm* **1970,** (17), 1103.
36. Kim, H. J.; Ruszczycky, M. W.; Choi, S. H.; Liu, Y. N.; Liu, H. W., Enzyme catalysed [4+2] cycloaddition is a key step in the biosynthesis of spinosyn A. *Nature* **2011,** *473*, 109-112.
37. Hudson, G. A.; Zhang, Z. G.; Tietz, J. I.; Mitchell, D. A.; van der Donk, W. A., *In vitro* biosynthesis of the core scaffold of the thiopeptide thiomuracin. *J. Am. Chem. Soc.* **2015,** *137*, 16012-16015.
38. Wever, W. J.; Bogart, J. W.; Baccile, J. A.; Chan, A. N.; Schroeder, F. C.; Bowers, A. A., Chemoenzymatic synthesis of thiazolyl peptide natural products featuring an enzyme-catalyzed formal [4+2] cycloaddition. *J Am Chem Soc* **2015,** *137* (10), 3494-3497.
39. Tian, Z. H.; Sun, P.; Yan, Y.; Wu, Z. H.; Zheng, Q. F.; Zhou, S. X.; Zhang, H.; Yu, F. T.; Jia, X. Y.; Chen, D. D.; Mandi, A.; Kurtan, T.; Liu, W., An enzymatic [4+2] cyclization cascade creates the pentacyclic core of pyrroindomycins. *Nat Chem Biol* **2015,** *11* (4), 259-U91.
40. Ohashi, M.; Liu, F.; Hai, Y.; Chen, M. B.; Tang, M. C.; Yang, Z. Y.; Sato, M.; Watanabe, K.; Houk, K. N.; Tang, Y., SAM-dependent enzyme-catalysed pericyclic reactions in natural product biosynthesis. *Nature* **2017,** *549* (7673), 502.
41. Li, L.; Tang, M. C.; Tang, S. B.; Gao, S.; Soliman, S.; Hang, L.; Xu, W.; Ye, T.; Watanabe, K.; Tang, Y., Genome mining and assembly-line biosynthesis of the UCS1025A pyrrolizidinone family of fungal alkaloids. *J Am Chem Soc* **2018,** *140* (6), 2067-2071.
42. Kato, N.; Nogawa, T.; Takita, R.; Kinugasa, K.; Kanai, M.; Uchiyama, M.; Osada, H.; Takahashi, S., Control of the stereochemical course of [4+2] cycloaddition during trans-decalin formation by Fsa2-family enzymes. *Angew Chem Int Edit* **2018,** *57* (31), 9754-9758.
43. Li, H. Q.; Sun, W. G.; Deng, M. Y.; Zhou, Q.; Wang, J. P.; Liu, J. J.; Chen, C. M.; Qi, C. X.; Luo, Z. W.; Xue, Y. B.; Zhu, H. C.; Zhang, Y. H., Asperversiamides, linearly fused prenylated indole alkaloids from the marine-derived fungus *Aspergillus versicolor*. *J Org Chem* **2018,** *83* (15), 8483-8492.
44. Greshock, T. J.; Grubbs, A. W.; Jiao, P.; Wicklow, D. T.; Gloer, J. B.; Williams, R. M., Isolation, structure elucidation, and biomimetic total synthesis of versicolamide B, and the isolation of antipodal (-)-stephacidin A and (+)-notoamide B from *Aspergillus versicolor* NRRL 35600. *Angew Chem Int Edit* **2008,** *47* (19), 3573-3577.

45. Kato, H.; Nakahara, T.; Sugimoto, K.; Matsuo, K.; Kagiyama, I.; Frisvad, J. C.; Sherman, D. H.; Williams, R. M.; Tsukamoto, S., Isolation of notoamide S and enantiomeric 6-*epi*-stephacidin A from the fungus *Aspergillus amoenus*: Biogenetic implications. *Org Lett* **2015,** *17* (3), 700-703.
46. Sanz-Cervera, J. F.; Glinka, T.; Williams, R. M., Biosynthesis of the brevianamides - quest for a biosynthetic Diels-Alder cyclization. *J Am Chem Soc* **1993,** *115* (1), 347-348.
47. Finefield, J. M.; Greshock, T. J.; Sherman, D. H.; Tsukamoto, S.; Williams, R. M., Notoamide E: biosynthetic incorporation into notoamides C and D in cultures of *Aspergillus versicolor* NRRL 35600. *Tetrahedron Lett* **2011,** *52* (16), 1987-1989.
48. Williams, R. M.; Sanz-Cervera, J. F.; Sancenon, F.; Marco, J. A.; Halligan, K. M., Biomimetic Diels-Alder cyclizations for the construction of the brevianamide, paraherquamide, sclerotamide, asperparaline and VM55599 ring systems. *Bioorgan Med Chem* **1998,** *6* (8), 1233-1241.
49. Jornvall, H.; Persson, B.; Krook, M.; Atrian, S.; Gonzalezduarte, R.; Jeffery, J.; Ghosh, D., Short-chain dehydrogenases reductases (Sdr). *Biochemistry* **1995,** *34* (18), 6003-6013.
50. Polonsky, J.; Merrien, M. A.; Prange, T.; Pascard, C.; Moreau, S., Isolation and structure (X-ray-analysis) of marcfortine A, a new alkaloid from *Penicillium roqueforti*. *J Cheml Soc Chem Commun* **1980,** (13), 601-602.
51. Prange, T.; Billion, M. A.; Vuilhorgne, M.; Pascard, C.; Polonsky, J.; Moreau, S., Structures of marcfortine B and marcfortine C (X-ray analysis), alkaloids from *Penicillium roqueforti*. *Tetrahedron Lett* **1981,** *22* (21), 1977-1980.
52. Whyte, A. C.; Gloer, J. B.; Wicklow, D. T.; Dowdw, P. F., Sclerotiamide: a new member of the paraherquamide class with potent antiinsectan activity from the sclerotia of *Aspergillus sclerotiorum*. *J Nat Prod* **1996,** *59* (11), 1093-5.
53. Hayashi, H.; Nishimoto, Y.; Nozaki, H., Asperparaline A, a new paralytic alkaloid from *Aspergillus japonicus* JV-23. *Tetrahedron Lett* **1997,** *38* (32), 5655-5658.
54. Greshock, T. J.; Grubbs, A. W.; Tsukamoto, S.; Williams, R. M., A concise, biomimetic total synthesis of stephacidin A and notoamide B. *Angew Chem Int Edit* **2007,** *46* (13), 2262-2265.
55. Sommer, K.; Williams, R. M., Studies on paraherquamide biosynthesis: synthesis of deuterium-labeled 7-hydroxy-pre-paraherquamide, a putative precursor of paraherquamides A, E, and F. *Tetrahedron* **2009,** *65* (16), 3246-3260.
56. Li, S. Y.; Finefield, J. M.; Sunderhaus, J. D.; McAfoos, T. J.; Williams, R. M.; Sherman, D. H., Biochemical characterization of NotB as an FAD-Dependent oxidase in the biosynthesis of notoamide indole alkaloids. *J Am Chem Soc* **2012,** *134* (2), 788-791.
57. Finefield, J. M.; Kato, H.; Greshook, T. J.; Sherman, D. H.; Tsukamoto, S.; Williams, R. M., Biosynthetic studies of the notoamides: Isotopic synthesis of stephacidin A and incorporation into notoamide B and sclerotiamide. *Org Lett* **2011,** *13* (15), 3802-3805.
58. Sunderhaus, J. D.; McAfoos, T. J.; Finefield, J. M.; Kato, H.; Li, S. Y.; Tsukamoto, S.; Sherman, D. H.; Williams, R. M., Synthesis and bioconversions of notoamide T: A biosynthetic precursor to stephacidin A and notoamide B. *Org Lett* **2013,** *15* (1), 22-25.
59. McAfoos, T. J.; Li, S. Y.; Tsukamoto, S.; Sherman, D. H.; Williams, R. M., Studies on the biosynthesis of the stephacidins and notoamides. Total synthesis of notoamide S. *Heterocycles* **2010,** *82* (1), 461-472.
60. Li, S. Y.; Finefield, J. M.; Sunderhaus, J. D.; McAfoos, T. J.; Williams, R. M.; Sherman, D. H., Biochemical characterization of NotB as an FAD-dependent oxidase in the biosynthesis of notoamide indole alkaloids. *J Am Chem Soc* **2012,** *134* (50), 20565-20565.

61. Kagiyama, I.; Kato, H.; Nehira, T.; Frisvad, J. C.; Sherman, D. H.; Williams, R. M.; Tsukamoto, S., Taichunamides: Prenylated indole alkaloids from *Aspergillus taichungensis* (IBT 19404). *Angew Chem Int Edit* **2016,** *55* (3), 1128-1132.
62. Li, F.; Zhang, Z. Z.; Zhang, G. J.; Che, Q.; Zhu, T. J.; Gu, Q. Q.; Li, D. H., Determination of taichunamide H and structural revision of taichunamide A. *Org Lett* **2018,** *20* (4), 1138-1141.
63. Cai, S. X.; Luan, Y. P.; Kong, X. L.; Zhu, T. J.; Gu, Q. Q.; Li, D. H., Isolation and photoinduced conversion of 6-*epi*-stephacidins from *Aspergillus taichungensis*. *Org Lett* **2013,** *15* (9), 2168-2171.
64. Domingo, L. R.; Zaragoza, R. J.; Williams, R. M., Studies on the biosynthesis of paraherquamide A and VM99955. A theoretical study of intramolecular Diels-Alder cycloaddition. *J Org Chem* **2003,** *68* (7), 2895-2902.
65. Hu, X. L.; Bian, X. Q.; Wu, X.; Li, J. Y.; Hua, H. M.; Pei, Y. H.; Han, A. H.; Bai, J., Penioxalamine A, a novel prenylated spiro-oxindole alkaloid from *Penicillium oxalicum* TW01-1. *Tetrahedron Lett* **2014,** *55* (29), 3864-3867.
66. Lin, Z. J.; Wen, J. N.; Zhu, T. J.; Fang, Y. C.; Gu, Q. Q.; Zhu, W. M., Chrysogenamide a from an endophytic fungus associated with *Cistanche deserticola* and its neuroprotective effect on SH-SY5Y cells. *J Antibiot* **2008,** *61* (2), 81-85.
67. Li, C. W.; Wu, C. J.; Cui, C. B.; Xu, L. L.; Cao, F.; Zhu, H. J., Penicimutamides A-C: Rare carbamate-containing alkaloids from a mutant of the marine-derived *Penicillium purpurogenum* G59. *Rsc Adv* **2016,** *6* (77), 73383-73387.
68. Mascotti, M. L.; Ayub, M. J.; Furnham, N.; Thornton, J. M.; Laskowski, R. A., Chopping and changing: The evolution of the flavin-dependent monooxygenases. *J Mol Biol* **2016,** *428* (15), 3131-3146.
69. Bhandari, P.; Crombie, L.; Harper, M. F.; Rossiter, J. T.; Sanders, M.; Whiting, D. A., Mechanism and stereochemistry of the enzyme-catalyzed formation of a 2,2-dimethylchromene ring from a prenylated phenol - Conversion of rot-2'-enonic acid into deguelin by deguelin cyclase. *J Chem Soc Perk T 1* **1992,** (13), 1685-1697.
70. Crombie, L.; Rossiter, J. T.; Vanbruggen, N.; Whiting, D. A., Deguelin cyclase, a prenyl to chromen transforming enzyme from *Tephrosia vogellii*. *Phytochemistry* **1992,** *31* (2), 451-461.
71. Watts, K. R.; Loveridge, S. T.; Tenney, K.; Media, J.; Valeriote, F. A.; Crews, P., Utilizing DART mass spectrometry to pinpoint halogenated metabolites from a marine invertebrate-derived fungus. *J Org Chem* **2011,** *76* (15), 6201-6208.
72. Fraley, A. E.; Garcia-Borras, M.; Tripathi, A.; Khare, D.; Mercado-Marin, E. V.; Tran, H.; Dan, Q.; Webb, G. P.; Watts, K. R.; Crews, P.; Sarpong, R.; Williams, R. M.; Smith, J. L.; Houk, K. N.; Sherman, D. H., Function and structure of MalA/MalA', iterative halogenases for late-stage C-H functionalization of indole alkaloids. *J Am Chem Soc* **2017,** *139* (34), 12060-12068.
73. Zheng, Q. F.; Gong, Y. K.; Guo, Y. J.; Zhao, Z. X.; Wu, Z. H.; Zhou, Z. X.; Chen, D. D.; Pan, L. F.; Liu, W., Structural insights into a flavin-dependent [4+2] cyclase that catalyzes trans-decalin formation in pyrroindomycin biosynthesis. *Cell Chem Biol* **2018,** *25* (6), 718.
74. Fage, C. D.; Isiorho, E. A.; Liu, Y. N.; Wagner, D. T.; Liu, H. W.; Keatinge-Clay, A. T., The structure of SpnF, a standalone enzyme that catalyzes [4+2] cycloaddition. *Nat Chem Biol* **2015,** *11* (4), 256.
75. Cai, Y.; Hai, Y.; Ohashi, M.; Jamieson, C.; Garcia-Borràs, M.; Houk, K. N.; Zhou, J.; Tang, Y., Structural basis for stereoselective dehydration and hydrogen-bonding catalysis by the SAM-dependent pericyclase LepI. *bioRxiv* **2018**.

76. Zheng, Q. F.; Guo, Y. J.; Yang, L. L.; Zhao, Z. X.; Wu, Z. H.; Zhang, H.; Liu, J. P.; Cheng, X. F.; Wu, J. Q.; Yang, H. Y.; Jiang, H. L.; Pan, L. F.; Liu, W., Enzyme-dependent [4+2] cycloaddition depends on lid-like interaction of the N-terminal sequence with the catalytic core in PyrI4. *Cell Chem Biol* **2016,** *23* (3), 352-360.
77. Byrne, M. J.; Lees, N. R.; Han, L. C.; van der Kamp, M. W.; Mulholland, A. J.; Stach, J. E. M.; Willis, C. L.; Race, P. R., The catalytic mechanism of a natural Diels-Alderase revealed in molecular detail. *J Am Chem Soc* **2016,** *138* (19), 6095-6098.
78. Filling, C.; Berndt, K. D.; Benach, J.; Knapp, S.; Prozorovski, T.; Nordling, E.; Ladenstein, R.; Jornvall, H.; Oppermann, U., Critical residues for structure and catalysis in short-chain dehydrogenases/reductases. *J Biol Chem* **2002,** *277* (28), 25677-25684.
79. Oppermann, U.; Filling, C.; Hult, M.; Shafqat, N.; Wu, X. Q.; Lindh, M.; Shafqat, J.; Nordling, E.; Kallberg, Y.; Persson, B.; Jornvall, H., Short-chain dehydrogenases/reductases (SDR): the 2002 update. *Chem-Biol Interact* **2003,** *143*, 247-253.
80. Birch, A. J.; Wright, J. J., Studies in relation to biosynthesis. XLII. Structural elucidation and some aspects of biosynthesis of brevianamides A and E. *Tetrahedron* **1970,** *26* (10), 2329-&.
81. Latham, J.; Brandenburger, E.; Shepherd, S. A.; Menon, B. R. K.; Micklefield, J., Development of halogenase enzymes for use in synthesis. *Chem Rev* **2018,** *118* (1), 232-269.
82. Agarwal, V.; Miles, Z. D.; Winter, J. M.; Eustaquio, A. S.; El Gamal, A. A.; Moore, B. S., Enzymatic halogenation and dehalogenation reactions: pervasive and mechanistically diverse. *Chem Rev* **2017,** *117* (8), 5619-5674.
83. Schnepel, C.; Sewald, N., Enzymatic halogenation: A timely strategy for regioselective C-H activation. *Chem-Eur J* **2017,** *23* (50), 12064-12086.
84. Weichold, V.; Milbredt, D.; van Pee, K. H., Specific enzymatic halogenation-from the discovery of halogenated enzymes to their applications *in vitro* and *in vivo*. *Angew Chem Int Edit* **2016,** *55* (22), 6374-6389.
85. Shepherd, S. A.; Menon, B. R. K.; Fisk, H.; Struck, A. W.; Levy, C.; Leys, D.; Micklefield, J., A Structure-guided switch in the regioselectivity of a tryptophan halogenase. *Chembiochem* **2016,** *17* (9), 821-824.
86. Lang, A.; Polnick, S.; Nicke, T.; William, P.; Patallo, E. P.; Naismith, J. H.; van Pee, K. H., Changing the regioselectivity of the tryptophan 7-halogenase PrnA by site-directed mutagenesis. *Angew Chem Int Edit* **2011,** *50* (13), 2951-2953.
87. Andorfer, M. C.; Park, H. J.; Vergara-Coll, J.; Lewis, J. C., Directed evolution of RebH for catalyst-controlled halogenation of indole C-H bonds. *Chem Sci* **2016,** *7* (6), 3720-3729.
88. Frese, M.; Sewald, N., Enzymatic halogenation of tryptophan on a gram scale. *Angew Chem Int Edit* **2015,** *54* (1), 298-301.
89. Yeh, E.; Blasiak, L. C.; Koglin, A.; Drennan, C. L.; Walsh, C. T., Chlorination by a long-lived intermediate in the mechanism of flavin-dependent halogenases. *Biochemistry* **2007,** *46* (5), 1284-1292.
90. Prudhomme, M., Recent developments of rebeccamycin analogues as topoisomerase I inhibitors and antitumor agents. *Curr Med Chem* **2000,** *7* (12), 1189-1212.
91. Nitanai, Y.; Kikuchi, T.; Kakoi, K.; Hanmaki, S.; Fujisawa, I.; Aoki, K., Crystal structures of the complexes between vancomycin and cell-wall precursor analogs. *J Mol Biol* **2009,** *385* (5), 1422-1432.
92. Yim, G.; Thaker, M. N.; Koteva, K.; Wright, G., Glycopeptide antibiotic biosynthesis. *J Antibiot* **2014,** *67* (1), 31-41.

93. Yeh, E.; Garneau, S.; Walsh, C. T., Robust in vitro activity of RebF and RebH, a two-component reductase/halogenase, generating 7-chlorotryptophan during rebeccamycin biosynthesis. *P Natl Acad Sci USA* **2005,** *102* (11), 3960-3965.
94. Bitto, E.; Huang, Y.; Bingman, C. A.; Singh, S.; Thorson, J. S.; Phillips, G. N., The structure of flavin-dependent tryptophan 7-halogenase RebH. *Proteins* **2008,** *70* (1), 289-293.
95. Schmartz, P. C.; Zerbe, K.; Abou-Hadeed, K.; Robinson, J. A., Bis-chlorination of a hexapeptide-PCP conjugate by the halogenase involved in vancomycin biosynthesis. *Org Biomol Chem* **2014,** *12* (30), 5574-5577.
96. Cacho, R. A.; Chooi, Y. H.; Zhou, H.; Tang, Y., Complexity generation in fungal polyketide biosynthesis: A spirocycle-forming P450 in the concise pathway to the antifungal drug griseofulvin. *Acs Chem Biol* **2013,** *8* (10), 2322-2330.
97. Chankhamjon, P.; Tsunematsu, Y.; Ishida-Ito, M.; Sasa, Y.; Meyer, F.; Boettger-Schmidt, D.; Urbansky, B.; Menzel, K. D.; Scherlach, K.; Watanabe, K.; Hertweck, C., Regioselective dichlorination of a non-activated aliphatic carbon atom and phenolic bismethylation by a multifunctional fungal flavoenzyme. *Angew Chem Int Edit* **2016,** *55* (39), 11955-11959.
98. Ferrara, M.; Perrone, G.; Gambacorta, L.; Epifani, F.; Solfrizzo, M.; Gallo, A., Identification of a halogenase involved in the biosynthesis of ochratoxin A in *Aspergillus carbonarius*. *Appl Environ Microb* **2016,** *82* (18), 5631-5641.
99. Menon, B. R. K.; Brandenburger, E.; Sharif, H. H.; Klemstein, U.; Shepherd, S. A.; Greaney, M. F.; Micklefield, J., RadH: A versatile halogenase for integration into synthetic pathways. *Angew Chem Int Edit* **2017,** *56* (39), 11841-11845.
100. Wick, J.; Heine, D.; Lackner, G.; Misiek, M.; Tauber, J.; Jagusch, H.; Hertweck, C.; Hoffmeister, D., A fivefold parallelized biosynthetic process secures chlorination of *Armillaria mellea* (honey mushroom) toxins. *Appl Environ Microb* **2016,** *82* (4), 1196-1204.
101. Zeng, J.; Zhan, J. X., A novel fungal flavin-dependent halogenase for natural product biosynthesis. *Chembiochem* **2010,** *11* (15), 2119-2123.
102. Suzuki, T.; Honda, H.; Katsumata, R., Production of antibacterial compounds analogous to chloramphenicol B a paraffin-grown bacterium. *Agr Biol Chem Tokyo* **1972,** *36* (12), 2223-2228.
103. Schlunzen, F.; Zarivach, R.; Harms, J.; Bashan, A.; Tocilj, A.; Albrecht, R.; Yonath, A.; Franceschi, F., Structural basis for the interaction of antibiotics with the peptidyl transferase centre in eubacteria. *Nature* **2001,** *413* (6858), 814-821.
104. Piraee, M.; White, R. L.; Vining, L. C., Biosynthesis of the dichloroacetyl component of chloramphenicol in *Streptomyces venezuelae* ISP5230: genes required for halogenation. *Microbiol-Sgm* **2004,** *150*, 85-94.
105. Podzelinska, K.; Latimer, R.; Bhattacharya, A.; Vining, L. C.; Zechel, D. L.; Jia, Z. C., Chloramphenicol biosynthesis: The structure of CmIS, a flavin-dependent halogenase showing a covalent flavin-aspartate bond. *J Mol Biol* **2010,** *397* (1), 316-331.
106. Shah, M. B.; Liu, J. B.; Zhang, Q. H.; Stout, C. D.; Halpert, J. R., Halogen-pi interactions in the cytochrome P450 active site: structural insights into human P450 2B6 substrate selectivity. *Faseb J* **2017,** *31*.
107. Imai, Y. N.; Inoue, Y.; Nakanishi, I.; Kitaura, K., Cl-pi interactions in protein-ligand complexes. *Protein Sci* **2008,** *17* (7), 1129-1137.
108. Politzer, P.; Murray, J. S.; Clark, T., Halogen bonding: an electrostatically-driven highly directional noncovalent interaction. *Phys Chem Chem Phys* **2010,** *12* (28), 7748-7757.

109. Xu, Z. J.; Yang, Z.; Liu, Y. T.; Lu, Y. X.; Chen, K. X.; Zhu, W. L., Halogen bond: Its role beyond drug-target binding affinity for drug discovery and development. *J Chem Inf Model* **2014,** *54* (1), 69-78.
110. Bissantz, C.; Kuhn, B.; Stahl, M., A medicinal chemist's guide to molecular interactions. *J Med Chem* **2010,** *53* (14), 5061-5084.
111. Gillis, E. P.; Eastman, K. J.; Hill, M. D.; Donnelly, D. J.; Meanwell, N. A., Applications of fluorine in medicinal chemistry. *J Med Chem* **2015,** *58* (21), 8315-8359.
112. Renata, H.; Wang, Z. J.; Arnold, F. H., Expanding the enzyme universe: Accessing non-natural reactions by mechanism-guided directed evolution. *Angew Chem Int Edit* **2015,** *54* (11), 3351-3367.
113. Poor, C. B.; Andorfer, M. C.; Lewis, J. C., Improving the stability and catalyst lifetime of the halogenase RebH by directed evolution. *Chembiochem* **2014,** *15* (9), 1286-1289.
114. Payne, J. T.; Poor, C. B.; Lewis, J. C., Directed evolution of RebH for site-selective halogenation of large biologically active molecules. *Angew Chem Int Edit* **2015,** *54* (14), 4226-4230.
115. Shepherd, S. A.; Karthikeyan, C.; Latham, J.; Struck, A. W.; Thompson, M. L.; Menon, B. R. K.; Styles, M. Q.; Levy, C.; Leys, D.; Micklefield, J., Extending the biocatalytic scope of regiocomplementary flavin-dependent halogenase enzymes. *Chem Sci* **2015,** *6* (6), 3454-3460.
116. Payne, J. T.; Andorfer, M. C.; Lewis, J. C., Regioselective arene halogenation using the FAD-dependent halogenase RebH. *Angew Chem Int Edit* **2013,** *52* (20), 5271-5274.
117. Andorfer, M. C.; Belsare, K. D.; Girlich, A. M.; Lewis, J. C., Aromatic halogenation by using bifunctional flavin reductase-halogenase fusion enzymes. *Chembiochem* **2017,** *18* (21), 2099-2103.
118. Li, S. Y.; Podust, L. M.; Sherman, D. H., Engineering and analysis of a self-sufficient biosynthetic cytochrome P450 PikC fused to the RhFRED reductase domain. *J Am Chem Soc* **2007,** *129* (43), 12940.
119. Zehner, S.; Kotzsch, A.; Bister, B.; Sussmuth, R. D.; Mendez, C.; Salas, J. A.; van Pee, K. H., A regioselective tryptophan 5-halogenase is involved in pyrroindomycin biosynthesis in *Streptomyces rugosporus* LL-42D005. *Chem Biol* **2005,** *12* (4), 445-452.
120. Runguphan, W.; Qu, X. D.; O'Connor, S. E., Integrating carbon-halogen bond formation into medicinal plant metabolism. *Nature* **2010,** *468* (7322), 461-U294.
121. Zeng, J.; Zhan, J. X., Characterization of a tryptophan 6-halogenase from *Streptomyces toxytricini*. *Biotechnol Lett* **2011,** *33* (8), 1607-1613.
122. Frabel, S.; Krischke, M.; Staniek, A.; Warzecha, H., Recombinant flavin-dependent halogenases are functional in tobacco chloroplasts without co-expression of flavin reductase genes. *Biotechnol J* **2016,** *11* (12), 1586-1594.
123. Sandoval, F. J.; Zhang, Y.; Roje, S., Flavin nucleotide metabolism in plants: Monofunctional enzymes synthesize FAD in plastids. *J Biol Chem* **2008,** *283* (45), 30890-30900.
124. Dong, C. J.; Flecks, S.; Unversucht, S.; Haupt, C.; van Pee, K. H.; Naismith, J. H., Tryptophan 7-halogenase (PrnA) structure suggests a mechanism for regioselective chlorination. *Science* **2005,** *309* (5744), 2216-2219.
125. Glenn, W. S.; Nims, E.; O'Connor, S. E., Reengineering a tryptophan halogenase to preferentially chlorinate a direct alkaloid precursor. *J Am Chem Soc* **2011,** *133* (48), 19346-19349.
126. El Gamal, A.; Agarwal, V.; Diethelm, S.; Rahman, I.; Schorn, M. A.; Sneed, J. M.; Louie, G. V.; Whalen, K. E.; Mincer, T. J.; Noel, J. P.; Paul, V. J.; Moore, B. S., Biosynthesis

of coral settlement cue tetrabromopyrrole in marine bacteria by a uniquely adapted brominase-thioesterase enzyme pair. *P Natl Acad Sci USA* **2016,** *113* (14), 3797-3802.
127. Mitchell, A. J.; Dunham, N. P.; Bergman, J. A.; Wang, B.; Zhu, Q.; Chang, W. C.; Liu, X. Y.; Boal, A. K., Structure-guided reprogramming of a hydroxylase to halogenate its small molecule substrate. *Biochemistry* **2017,** *56* (3), 441-444.
128. Hillwig, M. L.; Liu, X. Y., A new family of iron-dependent halogenases acts on freestanding substrates. *Nat Chem Biol* **2014,** *10* (11), 921-923.
129. Mitchell, A. J.; Zhu, Q.; Maggiolo, A. O.; Ananth, N. R.; Hillwig, M. L.; Liu, X. Y.; Boal, A. K., Structural basis for halogenation by iron- and 2-oxo-glutarate-dependent enzyme WelO5. *Nat Chem Biol* **2016,** *12* (8), 636-+.
130. Andorfer, M. C.; Grob, J. E.; Hajdin, C. E.; Chael, J. R.; Siuti, P.; Lilly, J.; Tan, K. L.; Lewis, J. C., Understanding flavin-dependent halogenase reactivity via substrate activity profiling. *Acs Catal* **2017,** *7* (3), 1897-1904.
131. Weeks, A. M.; Coyle, S. M.; Jinek, M.; Doudna, J. A.; Chang, M. C. Y., Structural and biochemical studies of a fluoroacetyl-CoA-specific thioesterase reveal a molecular basis for fluorine selectivity. *Biochemistry* **2010,** *49* (43), 9269-9279.
132. Walker, M. C.; Thuronyi, B. W.; Charkoudian, L. K.; Lowry, B.; Khosla, C.; Chang, M. C. Y., Expanding the fluorine chemistry of living systems using engineered polyketide synthase pathways. *Science* **2013,** *341* (6150), 1089-1094.
133. Deng, H.; O'Hagan, D., The fluorinase, the chlorinase and the duf-62 enzymes. *Curr Opin Chem Biol* **2008,** *12* (5), 582-592.
134. Deng, H.; Cobb, S. L.; McEwan, A. R.; McGlinchey, R. P.; Naismith, J. H.; O'Hagan, D.; Robinson, D. A.; Spencer, J. B., The fluorinase from *Streptomyces cattleya* is also a chlorinase. *Angew Chem Int Edit* **2006,** *45* (5), 759-762.
135. Zhu, X. F.; Robinson, D. A.; McEwan, A. R.; O'Hagan, D.; Naismith, J. H., Mechanism of enzymatic fluorination in *Streptomyces cattleya*. *J Am Chem Soc* **2007,** *129* (47), 14597-14604.
136. Eustaquio, A. S.; O'Hagan, D.; Moore, B. S., Engineering fluorometabolite production: Fluorinase expression in *Salinispora tropica* yields fluorosalinosporamide. *J Nat Prod* **2010,** *73* (3), 378-382.
137. Williams, P. G.; Buchanan, G. O.; Feling, R. H.; Kauffman, C. A.; Jensen, P. R.; Fenical, W., New cytotoxic salinosporamides from the marine actinomycete *Salinispora tropica*. *J Org Chem* **2005,** *70* (16), 6196-6203.
138. Deng, H.; Ma, L.; Bandaranayaka, N.; Qin, Z. W.; Mann, G.; Kyeremeh, K.; Yu, Y.; Shepherd, T.; Naismith, J. H.; O'Hagan, D., Identification of fluorinases from *Streptomyces* sp MA37, *Norcardia brasiliensis*, and *Actinoplanes* sp N902-109 by genome mining. *ChemBioChem* **2014,** *15* (3), 364-368.
139. O'Hagan, D.; Deng, H., Enzymatic fluorination and biotechnological developments of the fluorinase. *Chem Rev* **2015,** *115* (2), 634-649.
140. Dall'Angelo, S.; Bandaranayaka, N.; Windhorst, A. D.; Vugts, D. J.; van der Born, D.; Onega, M.; Schweiger, L. F.; Zanda, M.; O'Hagan, D., Tumour imaging by positron emission tomography using fluorinase generated 5-[F-18]fluoro-5-deoxyribose as a novel tracer. *Nucl Med Biol* **2013,** *40* (4), 464-470.
141. Thompson, S.; Onega, M.; Ashworth, S.; Fleming, I. N.; Passchier, J.; O'Hagan, D., A two-step fluorinase enzyme mediated F-18 labelling of an RGD peptide for positron emission tomography. *Chem Commun* **2015,** *51* (70), 13542-13545.

142. Thompson, S.; Fleming, I. N.; O'Hagan, D., Enzymatic transhalogenation of dendritic RGD peptide constructs with the fluorinase. *Org Biomol Chem* **2016,** *14* (11), 3120-3129.
143. Yeo, W. L.; Chew, X.; Smith, D. J.; Chan, K. P.; Sun, H.; Zhao, H. M.; Lim, Y. H.; Ang, E. L., Probing the molecular determinants of fluorinase specificity. *Chem Commun* **2017,** *53* (17), 2559-2562.
144. Dong, C. J.; Huang, F. L.; Deng, H.; Schaffrath, C.; Spencer, J. B.; O'Hagan, D.; Naismith, J. H., Crystal structure and mechanism of a bacterial fluorinating enzyme. *Nature* **2004,** *427* (6974), 561-565.
145. Senn, H. M., Insights into enzymatic halogenation from computational studies. *Front Chem* **2014,** *2*.
146. Sun, H. H.; Yeo, W. L.; Lim, Y. H.; Chew, X. Y.; Smith, D. J.; Xue, B.; Chan, K. P.; Robinson, R. C.; Robins, E. G.; Zhao, H. M.; Ang, E. L., Directed evolution of a fluorinase for improved fluorination efficiency with a non-native substrate. *Angew Chem Int Edit* **2016,** *55* (46), 14275-14278.
147. Neumann, C. S.; Walsh, C. T.; Kay, R. R., A flavin-dependent halogenase catalyzes the chlorination step in the biosynthesis of *Dictyostelium* differentiation-inducing factor 1. *P Natl Acad Sci USA* **2010,** *107* (13), 5798-5803.
148. Nielsen, M. T.; Nielsen, J. B.; Anyaogu, D. C.; Holm, D. K.; Nielsen, K. F.; Larsen, T. O.; Mortensen, U. H., Heterologous reconstitution of the intact geodin gene cluster in *Aspergillus nidulans* through a simple and versatile PCR-based approach. *Plos One* **2013,** *8* (8).
149. Chankhamjon, P.; Boettger-Schmidt, D.; Scherlach, K.; Urbansky, B.; Lackner, G.; Kalb, D.; Dahse, H. M.; Hoffmeister, D.; Hertweck, C., Biosynthesis of the halogenated mycotoxin aspirochlorine in koji mold involves a cryptic amino acid conversion. *Angew Chem Int Edit* **2014,** *53* (49), 13409-13413.
150. Sato, M.; Winter, J. M.; Kishimoto, S.; Noguchi, H.; Tang, Y.; Watanabe, K., Combinatorial generation of chemical diversity by redox enzymes in chaetoviridin biosynthesis. *Org Lett* **2016,** *18* (6), 1446-1449.
151. Seibold, C.; Schnerr, H.; Rumpf, J.; Kunzendorf, A.; Hatscher, C.; Wage, T.; Ernyei, A. J.; Dong, C. J.; Naismith, J. H.; van Pee, K. H., A flavin-dependent tryptophan 6-halogenase and its use in modification of pyrrolnitrin biosynthesis. *Biocatal Biotransfor* **2006,** *24* (6), 401-408.
152. Dorrestein, P. C.; Yeh, E.; Garneau-Tsodikova, S.; Kelleher, N. L.; Walsh, C. T., Dichlorination of a pyrrolyl-S-carrier protein by FADH(2)-dependent halogenase PltA during pyoluteorin biosynthesis. *P Natl Acad Sci USA* **2005,** *102* (39), 13843-13848.
153. Figueroa, M.; Gonzalez-Andrade, M.; Sosa-Peinado, A.; Madariaga-Mazon, A.; Del Rio-Portilla, F.; Gonzalez, M. D.; Mata, R., Fluorescence, circular dichroism, NMR, and docking studies of the interaction of the alkaloid malbrancheamide with calmodulin. *J Enzym Inhib Med Ch* **2011,** *26* (3), 378-385.
154. Klas, K.; Tsukamoto, S.; Sherman, D. H.; Williams, R. M., Natural Diels-Alderases: Elusive and irresistable. *J Org Chem* **2015,** *80* (23), 11672-11685.
155. Stocking, E. M.; Williams, R. M., Chemistry and biology of biosynthetic Diels-Alder reactions. *Angew Chem Int Edit* **2003,** *42* (27), 3078-3115.
156. Finefield, J. M.; Frisvad, J. C.; Sherman, D. H.; Williams, R. M., Fungal origins of the bicyclo[2.2.2]diazaoctane ring system of prenylated indole alkaloids. *J Nat Prod* **2012,** *75* (4), 812-833.

157. Ding, Y.; Greshock, T. J.; Miller, K. A.; Sherman, D. H.; Williams, R. M., Premalbrancheamide: synthesis, isotopic labeling, biosynthetic incorporation, and detection in cultures of Malbranchea aurantiaca. *Org Lett* **2008,** *10* (21), 4863-6.
158. Buedenbender, S.; Rachid, S.; Muller, R.; Schulz, G. E., Structure and action of the myxobacterial chondrochloren halogenase CndH: A new variant of FAD-dependent halogenases. *J Mol Biol* **2009,** *385* (2), 520-530.
159. Gutekunst, W. R.; Baran, P. S., C-H functionalization logic in total synthesis. *Chem Soc Rev* **2011,** *40* (4), 1976-1991.
160. Chung, W. J.; Vanderwal, C. D., Stereoselective halogenation in natural product synthesis. *Angew Chem Int Edit* **2016,** *55* (14), 4396-4434.
161. MegAlign Pro. Version 12.0. DNASTAR. Madison, WI.
162. Ondeyka, J. G.; Goegelman, R. T.; Schaeffer, J. M.; Kelemen, L.; Zitano, L., Novel antinematodal and antiparasitic agents from *Penicillium charlesii*. 1. Fermentation, isolation and biological activity. *J Antibiot* **1990,** *43* (11), 1375-1379.
163. Blizzard, T. A.; Margiatto, G.; Mrozik, H.; Schaeffer, J. M.; Fisher, M. H., Chemical modification of paraherquamide. 3. Vinyl ether modified analogs. *Tetrahedron Lett* **1991,** *32* (22), 2437-2440.
164. Blizzard, T. A.; Marino, G.; Mrozik, H.; Fisher, M. H.; Hoogsteen, K.; Springer, J. P., Chemical modification of paraherquamide. 1. Unusual reactions and absolute stereochemistry. *J Org Chem* **1989,** *54* (11), 2657-2663.
165. Little, P. R.; Hodge, A.; Watson, T. G.; Seed, J. A.; Maeder, S. J., Field efficacy and safety of an oral formulation of the novel combination anthelmintic, derquantel-abamectin, in sheep in New Zealand. *New Zeal Vet J* **2010,** *58* (3), 121-129.
166. Tsuda, M.; Kasai, Y.; Komatsu, K.; Sone, T.; Tanaka, M.; Mikami, Y.; Kobayashi, J., Citrinadin A, a novel pentacyclic alkaloid from marine-derived fungus *Penicillium citrinum*. *Org Lett* **2004,** *6* (18), 3087-3089.
167. Huang, K. X.; Fujii, I.; Ebizuka, Y.; Gomi, K.; Sankawa, U., Molecular cloning and heterologous expression of the gene encoding dihydrogeodin oxidase, a multicopper blue enzyme from *Aspergillus terreus*. *J Biol Chem* **1995,** *270* (37), 21495-21502.
168. Ames, B. D.; Haynes, S. W.; Gao, X.; Evans, B. S.; Kelleher, N. L.; Tang, Y.; Walsh, C. T., Complexity generation in fungal peptidyl alkaloid biosynthesis: Oxidation of fumiquinazoline A to the heptacyclic hemiaminal fumiquinazoline C by the flavoenzyme Af12070 from *Aspergillus fumigatus*. *Biochemistry* **2011,** *50* (40), 8756-8769.
169. Gao, X.; Chooi, Y. H.; Ames, B. D.; Wang, P.; Walsh, C. T.; Tang, Y., Fungal indole alkaloid biosynthesis: Genetic and biochemical investigation of the tryptoquialanine pathway in *Penicillium aethiopicum*. *J Am Chem Soc* **2011,** *133* (8), 2729-2741.
170. Ballou, D. P.; Entsch, B.; Cole, L. J., Dynamics involved in catalysis by single-component and two-component flavin-dependent aromatic hydroxylases. *Biochem Bioph Res Co* **2005,** *338* (1), 590-598.
171. Hicks, K. A.; O'Leary, S. E.; Begley, T. P.; Ealick, S. E., Structural and mechanistic studies of HpxO, a novel flavin adenine dinucleotide-dependent urate oxidase from *Klebsiella pneumoniae*. *Biochemistry* **2013,** *52* (3), 477-487.
172. Zheng, Y. J.; Tice, C. M.; Singh, S. B., The use of spirocyclic scaffolds in drug discovery. *Bioorganic & Medicinal Chemistry Letters* **2014,** *24* (16), 3673-3682.
173. Gonzalez-Andrade, M.; Mata, R.; Madariaga-Mazon, A.; Rodriguez-Sotres, R.; Del Pozo-Yauner, L.; Sosa-Peinado, A., Importance of the interaction protein-protein of the CaM-

PDE1A and CaM-MLCK complexes in the development of new anti-CaM drugs. *J Mol Recognit* **2013,** *26* (4), 165-74.
174. Biochemicals, C. CaM Inhibitors. http://www.scbt.com/chemicals-table-cam_inhibitors.html
175. Cook, W. J.; Walter, L. J.; Walter, M. R., Drug-binding by calmodulin - crystal structure of a calmodulin trifluoperazine complex. *Biochemistry* **1994,** *33* (51), 15259-15265.
176. Vandonselaar, M.; Hickie, R. A.; Quail, J. W.; Delbaere, L. T. J., Trifluoperazine-induced conformational change in Ca^{2+}-calmodulin. *Nat Struct Biol* **1994,** *1* (11), 795-801.
177. Osawa, M.; Swindells, M. B.; Tanikawa, J.; Tanaka, T.; Mase, T.; Furuya, T.; Ikura, M., Solution structure of calmodulin-W-7 complex: The basis of diversity in molecular recognition. *J Mol Biol* **1998,** *276* (1), 165-176.
178. Drugbank. http://www.drugbank.ca/drugs/DB00831 (accessed Apr 20, 2019).
179. Tesmer, J. J. G., Hitchhiking on the heptahelical highway: structure and function of 7TM receptor complexes. *Nat Rev Mol Cell Bio* **2016,** *17* (7), 439-450.
180. Komolov, K. E.; Benovic, J. L., G protein-coupled receptor kinases: Past, present and future. *Cell Signal* **2018,** *41*, 17-24.
181. Chuang, T. T.; Paolucci, L.; DeBlasi, A., Inhibition of G protein-coupled receptor kinase subtypes by Ca^{2+}/calmodulin. *J Biol Chem* **1996,** *271* (45), 28691-28696.
182. Pronin, A. N.; Satpaev, D. K.; Slepak, V. Z.; Benovic, J. L., Regulation of G protein-coupled receptor kinases by calmodulin and localization of the calmodulin binding domain. *J Biol Chem* **1997,** *272* (29), 18273-18280.
183. Levay, K.; Satpaev, D. K.; Pronin, A. N.; Benovic, J. L.; Slepak, V. Z., Localization of the sites for Ca^{2+}-binding proteins on G protein-coupled receptor kinases. *Biochemistry* **1998,** *37* (39), 13650-13659.
184. Pronin, A. N.; Satpaev, D. K.; Slepak, V. Z.; Benovic, J. L., Regulation of G protein-coupled receptor kinases by calmodulin and localization of the calmodulin binding domain. *Faseb J* **1997,** *11* (9), A1161-A1161.
185. Iacovelli, L.; Sallese, M.; Mariggio, S.; De Blasi, A., Regulation of G-protein-coupled receptor kinase subtypes by calcium sensor proteins. *Faseb J* **1999,** *13* (1), 1-8.
186. Cuspidi, C.; Sala, C.; Negri, F.; Mancia, G.; Morganti, A.; Hypertension, I. S., Prevalence of left-ventricular hypertrophy in hypertension: an updated review of echocardiographic studies. *J Hum Hypertens* **2012,** *26* (6), 343-349.
187. Martini, J. S.; Raake, P.; Vinge, L. E.; DeGeorge, B.; Chuprun, J. K.; Harris, D. M.; Gao, E.; Eckhart, A. D.; Pitcher, J. A.; Koch, W. J., Uncovering G protein-coupled receptor kinase-5 as a histone deacetylase kinase in the nucleus of cardiomyocytes. *P Natl Acad Sci USA* **2008,** *105* (34), 12457-12462.
188. Hullmann, J. E.; Grisanti, L. A.; Makarewich, C. A.; Gao, E.; Gold, J. I.; Chuprun, J. K.; Tilley, D. G.; Houser, S. R.; Koch, W. J., GRK5-mediated exacerbation of pathological cardiac hypertrophy involves facilitation of nuclear NFAT activity. *Circ Res* **2014,** *115* (12), 976-U128.
189. Sorriento, D.; Santulli, G.; Ciccarelli, M.; Maione, A. S.; Illario, M.; Trimarco, B.; Iaccarino, G., The amino-terminal domain of GRK5 inhibits cardiac hypertrophy through the regulation of calcium-calmodulin dependent transcription factors. *Int J Mol Sci* **2018,** *19* (3).
190. Sato, P. Y.; Chuprun, J. K.; Schwartz, M.; Koch, W. J., The evolving impact of G protein-coupled receptor kinases in cardiac health and disease. *Physiol Rev* **2015,** *95* (2), 377-404.

191. Beyett, T. S.; Bandekar, S. J.; Tesmer, J. J. G., Molecular basis for targeting, inhibition, and receptor phosphorylation in the G protein-coupled receptor kinase 4 subfamily. *Method Pharmacol Tox* **2016**, 59-74.
192. Komolov, K. E.; Bhardwaj, A.; Benovic, J. L., Atomic structure of GRK5 reveals distinct structural features novel for G protein-coupled receptor kinases. *J Biol Chem* **2015,** *290* (34), 20629-20647.
193. Homan, K. T.; Waldschmidt, H. V.; Glukhova, A.; Cannavo, A.; Song, J. L.; Cheung, J. Y.; Koch, W. J.; Larsen, S. D.; Tesmer, J. J. G., Crystal structure of G protein-coupled receptor kinase 5 in complex with a rationally designed inhibitor. *J Biol Chem* **2015,** *290* (34), 20649-20659.
194. Gonzalez-Andrade, M.; Rodriguez-Sotres, R.; Madariaga-Mazon, A.; Rivera-Chavez, J.; Mata, R.; Sosa-Peinado, A.; del Pozo-Yauner, L.; Arias-Olguin, I. I., Insights into molecular interactions between CaM and its inhibitors from molecular dynamics simulations and experimental data. *J Biomol Struct Dyn* **2016,** *34* (1), 78-91.
195. Boguth, C. A.; Singh, P.; Huang, C. C.; Tesmer, J. J. G., Molecular basis for activation of G protein-coupled receptor kinases. *Embo J* **2010,** *29* (19), 3249-3259.
196. Pitcher, J. A.; Fredericks, Z. L.; Stone, W. C.; Premont, R. T.; Stoffel, R. H.; Koch, W. J.; Lefkowitz, R. J., Phosphatidylinositol 4,5-bisphosphate (PIP2)-enhanced G protein-coupled receptor kinase (GRK) activity - location, structure, and regulation of the PIP2 binding site distinguishes the GRK subfamilies. *J Biol Chem* **1996,** *271* (40), 24907-24913.
197. Pronin, A. N.; Morris, A. J.; Surguchov, A.; Benovic, J. L., Synucleins are a novel class of substrates for G protein-coupled receptor kinases. *J Biol Chem* **2000,** *275* (34), 26515-26522.
198. Waldschmidt, H. V.; Homan, K. T.; Cruz-Rodriez, O.; Cato, M. C.; Waninger-Saroni, J.; Larimore, K. M.; Cannavo, A.; Song, J.; Cheung, J. Y.; Kirchhoff, P. D.; Koch, W. J.; Tesmer, J. J. G.; Larsen, S. D., Structure-based design, synthesis, and biological evaluation of highly selective and potent G protein-coupled receptor kinase 2 inhibitors. *J Med Chem* **2016,** *59* (8), 3793-3807.
199. Krissinel, E.; Henrick, K., Inference of macromolecular assemblies from crystalline state. *J Mol Biol* **2007,** *372* (3), 774-797.
200. Gold, J. I.; Martini, J. S.; Hullmann, J.; Gao, E.; Chuprun, J. K.; Lee, L.; Tilley, D. G.; Rabinowitz, J. E.; Bossuyt, J.; Bers, D. M.; Koch, W. J., Nuclear translocation of cardiac G protein-coupled receptor kinase 5 downstream of select Gq-activating hypertrophic ligands is a calmodulin-dependent process. *Plos One* **2013,** *8* (3).
201. Kursula, P., The many structural faces of calmodulin: a multitasking molecular jackknife. *Amino Acids* **2014,** *46* (10), 2295-2304.
202. Bhattacharya, S.; Bunick, C. G.; Chazin, W. J., Target selectivity in EF-hand calcium binding proteins. *Bba-Mol Cell Res* **2004,** *1742* (1-3), 69-79.
203. Huang, C. C.; Tesmer, J. J. G., Recognition in the face of diversity: Interactions of heterotrimeric G proteins and G protein-coupled receptor (GPCR) kinases with activated GPCRs. *J Biol Chem* **2011,** *286* (10), 7715-7721.
204. Pao, C. S.; Barker, B. L.; Benovic, J. L., Role of the amino terminus of G protein-coupled receptor kinase 2 in receptor phosphorylation. *Biochemistry* **2009,** *48* (30), 7325-7333.
205. Thiyagarajan, M. M.; Stracquatanio, R. P.; Pronin, A. N.; Evanko, D. S.; Benovic, J. L.; Wedegaertner, P. B., A predicted amphipathic helix mediates plasma membrane localization of GRK5. *J Biol Chem* **2004,** *279* (17), 17989-17995.

206. Pronin, A. N.; Carman, C. V.; Benovic, J. L., Structure-function analysis of G protein-coupled receptor kinase-5 - role of the carboxyl terminus in kinase regulation. *J Biol Chem* **1998,** *273* (47), 31510-31518.
207. Yang, P.; Glukhova, A.; Tesmer, J. J. G.; Chen, Z., Membrane orientation and binding determinants of G protein-coupled receptor kinase 5 as assessed by combined vibrational spectroscopic studies. *Plos One* **2013,** *8* (11).
208. Pronin, A. N.; Benovic, J. L., Regulation of the G protein-coupled receptor kinase GRK5 by protein kinase C. *J Biol Chem* **1997,** *272* (6), 3806-3812.
209. Penn, R. B.; Pronin, A. N.; Benovic, J. L., Regulation of G protein-coupled receptor kinases. *Trends Cardiovas Med* **2000,** *10* (2), 81-89.
210. Palczewski, K.; Buczylko, J.; Lebioda, L.; Crabb, J. W.; Polans, A. S., Identification of the N-Terminal Region in Rhodopsin kinase involved in its interaction with rhodopsin. *J Biol Chem* **1993,** *268* (8), 6004-6013.
211. Johnson, L. R.; Scott, M. G. H.; Pitcher, J. A., G protein-coupled receptor kinase 5 contains a DNA-binding nuclear localization sequence. *Mol Cell Biol* **2004,** *24* (23), 10169-10179.
212. Stols, L.; Gu, M. Y.; Dieckman, L.; Raffen, R.; Collart, F. R.; Donnelly, M. I., A new vector for high-throughput, ligation-independent cloning encoding a tobacco etch virus protease cleavage site. *Protein Expres Purif* **2002,** *25* (1), 8-15.
213. Chakraborty, S.; Ortiz-Maldonado, M.; Entsch, B.; Ballou, D. P., Studies on the mechanism of *p*-hydroxyphenyl acetate 3-hydroxylase from *Pseudomonas aeruginosa*: A system composed of a small flavin reductase and a large flavin-dependent oxygenase. *Biochemistry* **2010,** *49* (2), 372-385.
214. Kabsch, W., Xds. *Acta Crystallogr D* **2010,** *66*, 125-132.
215. Adams, P. D.; Afonine, P. V.; Bunkoczi, G.; Chen, V. B.; Davis, I. W.; Echols, N.; Headd, J. J.; Hung, L. W.; Kapral, G. J.; Grosse-Kunstleve, R. W.; McCoy, A. J.; Moriarty, N. W.; Oeffner, R.; Read, R. J.; Richardson, D. C.; Richardson, J. S.; Terwilliger, T. C.; Zwart, P. H., PHENIX: a comprehensive Python-based system for macromolecular structure solution. *Acta Crystallogr D* **2010,** *66*, 213-221.
216. Emsley, P.; Cowtan, K., Coot: model-building tools for molecular graphics. *Acta Crystallogr D* **2004,** *60*, 2126-2132.
217. Frisch, M. J.; Trucks, G. W.; Schlegel, H. B.; Scuseria, G. E.; Robb, M. A.; Cheeseman, J. R.; Scalmani, G.; Barone, V.; Mennucci, B.; Petersson, G. A.; Nakatsuji, H.; Caricato, M.; Li, X.; Hratchian, H. P.; Izmaylov, A. F.; Bloino, J.; Zheng, G.; Sonnenberg, J. L.; Hada, M.; Ehara, M.; Toyota, K.; Fukuda, R.; Hasegawa, J.; Ishida, M.; Nakajima, T.; Honda, Y.; Kitao, O.; Nakai, H.; Vreven, T.; Montgomery, J. A., Jr.; Peralta, J. E.; Ogliaro, F.; Bearpark, M.; Heyd, J. J.; Brothers, E.; Kudin, K. N.; Staroverov, V. N.; Kobayashi, R.; Normand, J.; Raghavachari, K.; Rendell, A.; Burant, J. C.; yengar, S. S.; Tomasi, J.; Cossi, M.; Rega, N.; Millam, M. J.; Klene, M.; Knox, J. E.; Cross, J. B.; Bakken, V.; Adamo, C.; Jaramillo, J.; Gomperts, R.; Stratmann, R. E.; Yazyev, O.; Austin, A. J.; Cammi, R.; Pomelli, C.; Ochterski, J. W.; Martin, R. L.; Morokuma, K.; Zakrzewski, V. G.; Voth, G. A.; Salvador, P.; Dannenberg, J. J.; Dapprich, S.; Daniels, A. D.; Farkas, Ö.; Foresman, J. B.; Ortiz, J. V.; Cioslowski, J.; Fox, D. J. *Gaussian 09, Revision D.01*, Gaussian Inc: 2013.
218. Zhao, Y.; Truhlar, D. G., The M06 suite of density functionals for main group thermochemistry, thermochemical kinetics, noncovalent interactions, excited states, and transition elements: two new functionals and systematic testing of four M06-class functionals and 12 other functionals. *Theor Chem Acc* **2008,** *120* (1-3), 215-241.

219. Barone, V.; Cossi, M., Quantum calculation of molecular energies and energy gradients in solution by a conductor solvent model. *J Phys Chem A* **1998,** *102* (11), 1995-2001.
220. Cossi, M.; Rega, N.; Scalmani, G.; Barone, V., Energies, structures, and electronic properties of molecules in solution with the C-PCM solvation model. *J Comput Chem* **2003,** *24* (6), 669-681.
221. Simon, L.; Goodman, J. M., How reliable are DFT transition structures? Comparison of GGA, hybrid-meta-GGA and meta-GGA functionals. *Org Biomol Chem* **2011,** *9* (3), 689-700.
222. Schutz, C. N.; Warshel, A., What are the dielectric "constants" of proteins and how to validate electrostatic models? *Proteins* **2001,** *44* (4), 400-417.
223. Li, L.; Li, C.; Zhang, Z.; Alexov, E., On the 'Dielectric "constant" of proteins: Smooth dielectric function for macromolecular modeling and its implementation in DelPhi. *J Chem Theory Comput* **2013,** *9* (4), 2126-2136.
224. Legault, C., CYLview, version 1.0 b, Université de Sherbrooke **2009**.
225. Salomon-Ferrer, R.; Gotz, A. W.; Poole, D.; Le Grand, S.; Walker, R. C., Routine microsecond molecular dynamics simulations with AMBER on GPUs. 2. Explicit solvent particle mesh Ewald. *J Chem Theory Comput* **2013,** *9* (9), 3878-3888.
226. Case, D. S.; Cerutti, T. E.; Cheatham, I., T. E.; Darden, T. A.; Duke, R. E.; Giese, T. J.; Gohlke, H.; Goetz, A. W.; Greene, D.; Homeyer, N.; Izadi, S.; Kovalenko, A.; Lee, T. S.; LeGrand, S.; Li, P.; Lin, C.; Liu, J.; Luchko, T.; Luo, R.; Mermelstein, D.; Merz, K. M.; Monard, G.; Nguyen, H.; Omelyan, I.; Onufriev, A.; Pan, F.; Qi, R.; Roe, D. R.; Roitberg, A.; Sagui, C.; Simmerling, C. L.; Botello-Smith, W. M.; Swails, J.; Walker, R. C.; Wang, J.; Wolf, R. M.; Wu, X.; Xiao, L.; M., Y. D.; Kollman, P. A., *AMBER 2017*. University of California, San Francisco, **2017**.
227. Wang, J. M.; Wolf, R. M.; Caldwell, J. W.; Kollman, P. A.; Case, D. A., Development and testing of a general AMBER force field. *J Comput Chem* **2004,** *25* (9), 1157-1174.
228. Bayly, C. I.; Cieplak, P.; Cornell, W. D.; Kollman, P. A., A Well-behaved electrostatic potential based method using charge restraints for deriving atomic charges - the Resp Model. *J Phys Chem-Us* **1993,** *97* (40), 10269-10280.
229. Besler, B. H.; Merz, K. M.; Kollman, P. A., Atomic charges derived from semiempirical methods. *J Comput Chem* **1990,** *11* (4), 431-439.
230. Singh, U. C.; Kollman, P. A., An approach to computing electrostatic charges for molecules. *J Comput Chem* **1984,** *5* (2), 129-145.
231. Jorgensen, W. L.; Chandrasekhar, J.; Madura, J. D.; Impey, R. W.; Klein, M. L., Comparison of simple potential functions for simulating liquid water. *Journal of Chemical Physics* **1983,** *79* (2), 926-935.
232. Wang, J. M.; Cieplak, P.; Kollman, P. A., How well does a restrained electrostatic potential (RESP) model perform in calculating conformational energies of organic and biological molecules? *J Comput Chem* **2000,** *21* (12), 1049-1074.
233. Darden, T.; York, D.; Pedersen, L., Particle Mesh Ewald - an N.Log(N) Method for Ewald sums in large systems. *Journal of Chemical Physics* **1993,** *98* (12), 10089-10092.
234. Sondergaard, C. R.; Olsson, M. H. M.; Rostkowski, M.; Jensen, J. H., Improved treatment of ligands and coupling effects in empirical calculation and rationalization of pK(a) values. *J Chem Theory Comput* **2011,** *7* (7), 2284-2295.
235. Olsson, M. H. M.; Sondergaard, C. R.; Rostkowski, M.; Jensen, J. H., PROPKA3: Consistent treatment of internal and surface residues in empirical pK(a) predictions. *J Chem Theory Comput* **2011,** *7* (2), 525-537.

236. Kabsch, W., *Acta. Crystallogr. D. Biol. Crystallogr.* **2010,** *66*, 125-132.
237. Adams, P. D.; Afonine, P. V.; BUnkoczi, G.; Chen, V. B.; Davis, I. W.; Echols, N.; Headd, J. J.; Hung, L. W.; Kapral, G. J.; Grosse-Kunstleve, R. W.; McCoy, A. J.; Moriarty, N. W.; Oeffner, R.; Read, R. J.; Richardson, D. C.; Richardson, J. S.; Terwilliger, T. C.; Zwart, P. H., *Acta. Crystallogr. D. Biol. Crystallogr.* **2010,** *66*, 213-221.
238. Emsley, P.; Cowtan, K., *Acta. Crystallogr. D. Biol. Crystallogr.* **2004,** *60*, 2126-2132.
239. Ding, B.; Glukhova, A.; Sobczyk-Kojiro, K.; Mosberg, H. I.; Tesmer, J. J. G.; Chen, Z., Unveiling the membrane-binding properties of N-terminal and C-terminal regions of G protein-coupled receptor kinase 5 by combined optical spectroscopies. *Langmuir* **2014,** *30* (3), 823-831.
240. Winn, M. D.; Ballard, C. C.; Cowtan, K. D.; Dodson, E. J.; Emsley, P.; Evans, P. R.; Keegan, R. M.; Krissinel, E. B.; Leslie, A. G. W.; McCoy, A.; McNicholas, S. J.; Murshudov, G. N.; Pannu, N. S.; Potterton, E. A.; Powell, H. R.; Read, R. J.; Vagin, A.; Wilson, K. S., Overview of the CCP4 suite and current developments. *Acta Crystallogr D* **2011,** *67*, 235-242.
241. Winter, G.; Waterman, D. G.; Parkhurst, J. M.; Brewster, A. S.; Gildea, R. J.; Gerstel, M.; Fuentes-Montero, L.; Vollmar, M.; Michels-Clark, T.; Young, I. D.; Sauter, N. K.; Evans, G., DIALS: implementation and evaluation of a new integration package. *Acta Crystallographica Section D-Structural Biology* **2018,** *74*, 85-97.
242. Winter, G., xia2: an expert system for macromolecular crystallography data reduction. *J Appl Crystallogr* **2010,** *43*, 186-190.
243. Karplus, P. A.; Diederichs, K., Linking crystallographic model and data quality. *Science* **2012,** *336* (6084), 1030-1033.
244. Mccoy, A. J.; Grosse-Kunstleve, R. W.; Adams, P. D.; Winn, M. D.; Storoni, L. C.; Read, R. J., Phaser crystallographic software. *J Appl Crystallogr* **2007,** *40*, 658-674.
245. Kumar, V.; Chichili, V. P. R.; Tang, X. H.; Sivaraman, J., A novel trans conformation of ligand-free calmodulin. *Plos One* **2013,** *8* (1).
246. Moriarty, N. W.; Grosse-Kunstleve, R. W.; Adams, P. D., Electronic ligand builder and optimization workbench (eLBOW): a tool for ligand coordinate and restraint generation. *Acta Crystallogr D* **2009,** *65*, 1074-1080.
247. Emsley, P.; Lohkamp, B.; Scott, W. G.; Cowtan, K., Features and development of Coot. *Acta Crystallogr D* **2010,** *66*, 486-501.
248. Hopkins, J. B.; Gillilan, R. E.; Skou, S., BioXTAS RAW: Improvements to a free open-source program for small-angle X-ray scattering data reduction and analysis. *J Appl Crystallogr* **2017,** *50*, 1545-1553.
249. Franke, D.; Petoukhov, M. V.; Konarev, P. V.; Panjkovich, A.; Tuukkanen, A.; Mertens, H. D. T.; Kikhney, A. G.; Hajizadeh, N. R.; Franklin, J. M.; Jeffries, C. M.; Svergun, D. I., ATSAS 2.8: A comprehensive data analysis suite for small-angle scattering from macromolecular solutions. *J Appl Crystallogr* **2017,** *50*, 1212-1225.
250. Svergun, D. I., Determination of the Regularization parameter in indirect-transform methods using perceptual criteria. *J Appl Crystallogr* **1992,** *25*, 495-503.
251. Rambo, R. P.; Tainer, J. A., Characterizing flexible and intrinsically unstructured biological macromolecules by SAS using the Porod-Debye law. *Biopolymers* **2011,** *95* (8), 559-571.
252. Grant, T. D., *Ab initio* electron density determination directly from solution scattering data. *Nat Methods* **2018,** *15* (3), 191-+.

253. Svergun, D.; Barberato, C.; Koch, M. H. J., CRYSOL - A program to evaluate X-ray solution scattering of biological macromolecules from atomic coordinates. *J Appl Crystallogr* **1995,** *28*, 768-773.
254. Panjkovich, A.; Svergun, D. I., SASpy: A PyMOL plugin for manipulation and refinement of hybrid models against small angle X-ray scattering data. *Bioinformatics* **2016,** *32* (13), 2062-2064.
255. Peisley, A.; Skiniotis, G., 2D projection analysis of GPCR complexes by negative stain electron microscopy. *Methods Mol Biol* **2015,** *1335*, 29-38.
256. Tang, G.; Peng, L.; Baldwin, P. R.; Mann, D. S.; Jiang, W.; Rees, I.; Ludtke, S. J., EMAN2: An extensible image processing suite for electron microscopy. *J Struct Biol* **2007,** *157* (1), 38-46.
257. Yang, Z. F.; Fang, J.; Chittuluru, J.; Asturias, F. J.; Penczek, P. A., Iterative stable alignment and clustering of 2D transmission electron microscope images. *Structure* **2012,** *20* (2), 237-247.
258. Roman, D. L.; Ota, S.; Neubig, R. R., Polyplexed flow cytometry protein interaction assay: A novel high-throughput screening paradigm for RGS protein inhibitors. *J Biomol Screen* **2009,** *14* (6), 610-619.
259. Shankaranarayanan, A.; Thal, D. M.; Tesmer, V. M.; Roman, D. L.; Neubig, R. R.; Kozasa, T.; Tesmer, J. J. G., Assembly of high order G alpha(q)-effector complexes with RGS proteins. *J Biol Chem* **2008,** *283* (50), 34923-34934.
260. Petoukhov, M. V.; Franke, D.; Shkumatov, A. V.; Tria, G.; Kikhney, A. G.; Gajda, M.; Gorba, C.; Mertens, H. D. T.; Konarev, P. V.; Svergun, D. I., New developments in the ATSAS program package for small-angle scattering data analysis. *J Appl Crystallogr* **2012,** *45*, 342-350.